SYNTHESIS AND CHARACTERIZATION OF POLY(9,9-DIHEXYLFLUORENE-*MB*-METHYLENE)S

by

James Edward Copenhafer

B.S. Chemistry, University of Richmond, 2000

Submitted to the Graduate Faculty of

Arts and Sciences in partial fulfillment

of the requirements for the degree of

Doctor of Philosophy

University of Pittsburgh

2006

UNIVERSITY OF PITTSBURGH

FACULTY OF ARTS AND SCIENCES

This dissertation was presented

by

James Edward Copenhafer

It was defended on

November 6, 2006

and approved by

Dr. Eric Beckman, Associate Professor, Department of Engineering

Dr. Toby M Chapman, Associate Professor, Department of Chemistry

Dr. Tara Y. Meyer, Associate Professor, Department of Chemistry

Dr. Stephane Petoud, Assistant Professor, Department of Chemistry

Dr. Tara Y. Meyer
Dissertation Director

SYNTHESIS AND CHARACTERIZATION OF POLY(9,9-DIHEXYLFLUORENE-*MB*-METHYLENE)S

James Edward Copenhafer, Ph.D.

University of Pittsburgh, 2006

The synthesis and characterization of copolymers possessing *exact* repeating sequences of 9,9-dihexylfluorene and methylene repeat units are described. Each poly(9,9-dihexylfluorene-*mb*-methylene) (PFM, *mb* = multiblock) was synthesized following the assembly of a symmetrically disubstituted monodisperse oligofluorene. Alkyl segments possessing terminal alkene functionality were then coupled at both of the substituted positions on the oligofluorene to give a macromolecular "segmer" compound. Each segmer was polymerized using Acyclic Diene Metathesis (ADMET) and, following post-polymerization hydrogenation, a PFM with an entirely repeating diblock sequence was produced. PFMs possessing 9,9-dihexylfluorene segment lengths of x = 1, 2, 3, 4, 7, or 8 units and methylene segment lengths of y = 10 or 18 units were prepared to give a ten member PFM library.

As PFMs have exact chemical compositions and monomer unit sequencing, studies aimed at elucidating solution and bulk phase trends were performed. Spectroscopic characteristics that make polyfluorene-type materials attractive include their generally efficient blue light emission (λ_{max} ~ 448 nm). Successful investigations into the optical tuning of PFMs in solution and in the bulk are described. Additionally, thermal- and photostabilities of PFMs under a variety of conditions are reported and compared to the related homopolymer, poly(9,9-dihexylfluorene) [PDHF]. Compared to PDHF, PFMs display similar, and in some cases superior resistance to photobleaching processes. Additionally, thermal and photostability investigations into keto-

induced degradation processes of PFMs suggest that interruption of the fluorene segments with alkyl spacers effectively suppresses intrachain charge migration and interchain Förster energy transfer in the bulk. The rate of PFM, and likewise PDHF degradation was found to be at least partially dependent on the initial state of the sample.

Efforts toward the transition metal-catalyzed production of cyclic oligomers are described. Two rigid bifunctional molecules bearing both transition-metal metathesis initiating and terminating groups were prepared. The synthesis and metathesis activity of these compounds are reported.

TABLE OF CONTENTS

LIST OF TABLES

LIST OF FIGURES

LIST OF SCHEMES

SYMBOLS AND ABBREVIATIONS

AFM	atomic force microscopy
alt	alternating
b	block
b	broad
BDOH-PF	poly[9,9-bis(dioxaheptyl)fluorene]
bipy	2,2'-bipyridine
COD	1,5-cyclooctadiene
CP	conjugated polymer
d	day
d	doublet
DMF	dimethylformamide
DP	degree of polymerization
EL	electroluminescence
eq	equivalent
GPC	gel permeation chromatography
LC	liquid crystalline
m	multiplet
NBS	*N*-bromosuccinimide
PA	polyacetylene
PANI	polyaniline
PBLG	poly(γ-benzyl-L-glutamate)
PC	polycarbazole

pd	pseudo doublet
PDHF	poly(9,9-di-*n*-hexylfluorene)
PDI	polydispersity index
PDOF	poly(9,9-di-*n*-octylfluorene)
PE	polyethylene
PF	polyfluorene
PFcE	poly(fluorene-*co*-polyether)
PFcM	poly(fluorene-*co*-polymethylene)
PFE	poly(9,9-dialkylfluorene-*alt*-ethynylene)
PFV	poly(9,9-dialkylfluorene-*alt*-vinylene)
PhMe	toluene
PL	photoluminescence
PLED	polymeric light emitting device
PNB	polynorbornene
PPP	poly(para-phenylene)
PPV	poly(*para*-phenylene vinylene)
PPE	poly(*para*-phenylene ethynylene)
PS	polystyrene
PT	polythiophene
PU	polyurethane/urea
q	quartet
s	singlet
t	triplet

TFA	trifluoroacetic acid
T_g	glass transition temperature
T_m	melting temperature
tosyl	toluenesulfonyl

PREFACE

My time at Pitt has been a formative experience. Every once in a while I think back all the way to the Summer of 2000, which marked the beginning of my graduate education in the Department of Chemistry, and I smile when I think of just how far I have come. There are so many people who helped me get to the point I am at now. I thank Dr. Tara Y. Meyer for instilling in me a deep-seated passion for interdisciplinary chemistry while guiding me through my research. I feel privileged to have been advised by someone as knowledgeable and as dedicated to graduate education as she is. I thank her for pushing me to excel and I hope to repay her for her commitment. My fellow Meyer Group members are also owed a debt of gratitude for helping me "re-wire" my brain so I could progress in the lab. I thank them all collectively, and in particular I thank Steve Bell, Rachel Ward, Pat Riley, Robbyn Berenda, Ken Cutler, Ryan Stayshich, and Ben Norris. Most especially I thank Daniel Knapton for being a great friend and for setting a truly excellent example as a lab mate.

The Chemistry Department at Pitt treated me much better than I had any right to expect. I thank Dr. Steven Geib for teaching me remarkable skills and for the extended stay as his X-Ray Lab teaching assistant. I thank George Bandik and Len Kogut for their perpetual good cheer and encouragement, Fran Nagy for her attentiveness, and Margarete Bower for not revoking my library privileges when she caught me stealing an issue of *Angewandte Chemie* that one time.

I thank Prof. Eric Beckman, Prof. Toby Chapman, and Prof. Stéphane Petoud for serving on my Dissertation Committee, Prof. Chapman, Prof. Alexander Star, and Prof. David Waldeck for serving on my Proposal Committee, and Prof. Petoud and the late Prof. Rex Shepherd for serving on my Comprehensive Committee. I hold your attention, advice, and constructive criticism in deep regard.

Nothing I could write would convey how much I wish to thank my girlfriend, Carrie Dougherty, for everything she has done for me the past few years. I am grateful to her for urging me onward and for making me a part of her family. I thank my family as well–Paul, Mom, and Dad, for their unwavering support and their interest in my doings in Pittsburgh. Though communication has at times been one-sided I am always thinking of you. Thanks for always being there.

1. Introduction

1.1. Repeating Sequence Copolymers: Inspiration from Nature

Nature is the ultimate inspiration for the development of polymers with controlled sequence. Biopolymers that combine sequence and a multiblock architecture have enviable mechanical properties that are difficult to duplicate. This is the case in spider silks, which combine strength, elasticity, light weight and adhesive properties and have been much studied.[1, 2] It has been found that naturally occurring silks consist of crystalline segments such as $(GlyAlaGlyAlaGlySer)_n$ that alternate with amorphous segments. These amorphous segments often contain amino acids with bulky side groups.[3] The ordered sequences are believed to be key in the formation of anti-parallel β-sheets that act as temporary cross-links. Attempts to prepare synthetic polymers with similar properties have been undertaken by several groups. Rathore and Sogah reported that multiblock copolymers with $(Ala)_{4,6}$ or (AlaGlyAlaGly) alternating with short PEG oligomers ($n \sim 13$) gave the desired β-sheet structures (Figure 1.1).[2] Zhou reported similar ordering in copolymers possessing $(Ala)_5$ and isoprene blocks.[4] Tirrell and coworkers prepared related "periodic polypeptides".[5] Keratin, fibronectin, elastin, and collagen are other examples of biopolymers whose properties can be traced to specific sequences.[6-11] Termonia has modeled this class of multiblock copolymer.[12]

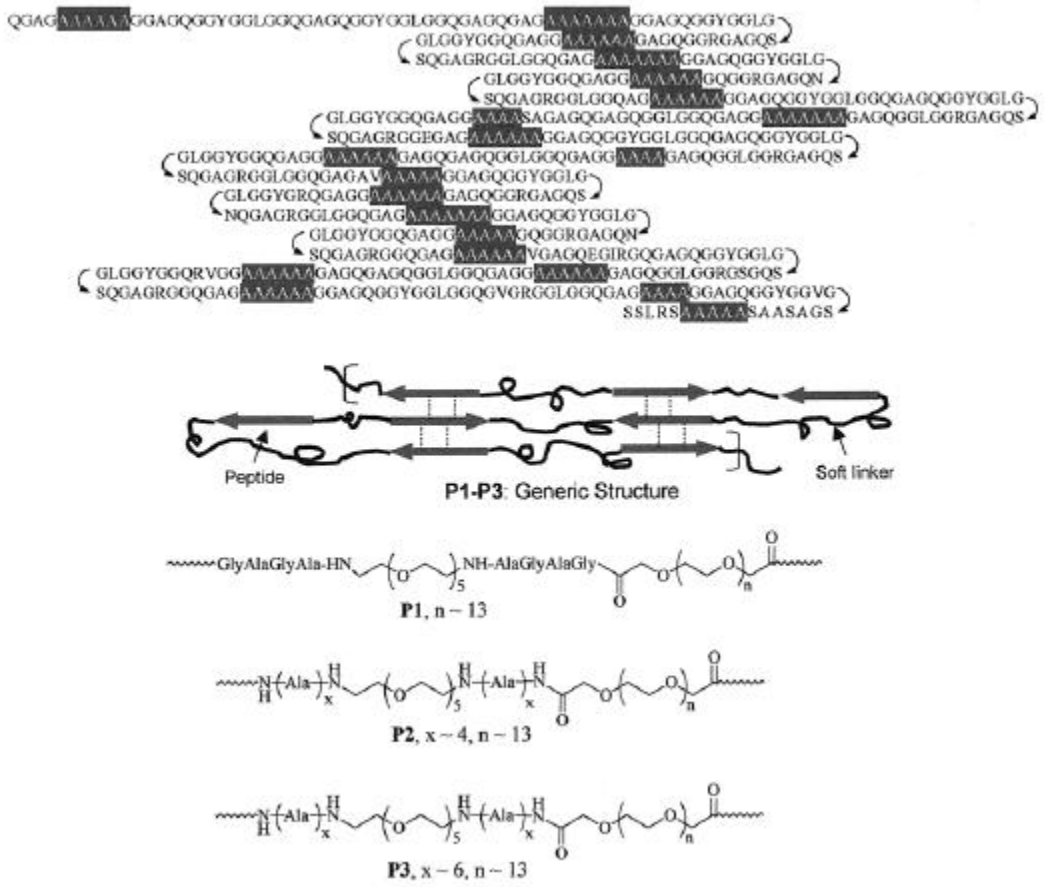

Figure 1.1. Top: alanine segments present in silk of *N. clavipes* order into β-sheet regions. Middle: Rathore's conceptual rendering of PEG-poly(alanine) segmented copolymers. Bottom: Chemical compositions of polymers Rathore used to construct self assembled β-sheets. This figure is taken from Rathore and Sogah, *J. Am. Chem. Soc.*, **2001**, *123*, 5231-5239.

Though they are not technically RSCs (because biomolecules rarely have an exact repeating motif throughout), polypeptides represent an extremely important class of highly sequenced macromolecules that are routinely prepared in the laboratory. The solid phase synthesis used in their preparation is not practical for routine materials preparation, however. The method suffers from significant limitations in scale–milligram quantities are considered large preps, as well as practical lengths of chains (DP < 50) that can be prepared.[13] Moreover, since the scale-up necessarily involves co-opting the synthetic machine of natural organisms, there is a severe restriction on the types of polymers that can be produced.[14-16] Despite these

limitations, the effect of sequence on solution interactions has been exhaustively studied for polypeptides, both synthetic and natural. Protein conformation, which determines function, is one of the most dramatic justifications for the development of synthetic materials with complex sequencing.

1.2. Repeating Sequence Copolymers: Precedence

1.2.1. Polyurethanes

The foremost model of synthetic RSCs comes in the form of the amazingly versatile polyurethanes/polyureas (PUs) which are the best understood and most economically important segmented multiblock copolymers. Consumed at a rate of greater than 9 million tons per year worldwide, polyurethane foams, coatings, adhesives, and elastomers are utilized in a variety of applications.[17] The most common synthesis of segmented PUs involves the combination of a poly(ether glycol) with an excess of diisocyanate to form an isocyanate-functionalized prepolymer (Scheme 1.1). Reaction of this prepolymer with a short chain diamine or diol chain extender gives high molecular weight PU. This 2-step synthesis gives a highly segmented polymer with soft blocks, dominated by the diol chains, and hard blocks comprising the hydrogen-bonded urea/urethane chains connected by chain extenders. Although there is much to learn from structure/function studies of PUs, the inherent polydispersity in their segments disrupts long range order.[18-20]

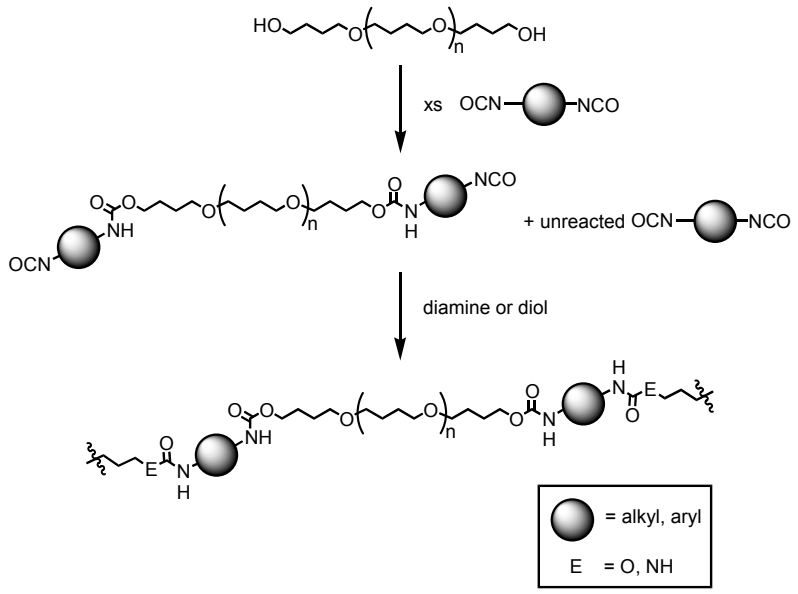

Scheme 1.1. The conventional preparation of segmented PUs.

Well-defined polyurethane/polyureas RSCs have been occasionally prepared and their properties have been found to differ from the less uniform multiblock PUs prepared by the conventional synthetic approach described above. In particular, an effort has been made to define the number of urethane/urea groups in the hard block. Sijbesma and coworkers prepared a series of PUs wherein the number of urea groups between THF-derived polyether softblocks ranged from 1-4 (Figure 1.2).[21] They found that hydrogen bonding was significantly greater and increased with the number of urea groups in the hard block. Not surprisingly, flow temperatures were also dependent, ranging from < 20 °C for one urea group to > 200 °C for four. Even more interesting was the comparison of the polymers with two urea groups per hard block with a conventionally prepared polyurea that had the same ratio of urea groups to soft block groups, but did not have the same uniformity. The conventionally prepared polymer showed less effective hydrogen bonding and a lower flow temperature than the RSC polyurea. The length and polydispersity of the soft block also affects PU properties.

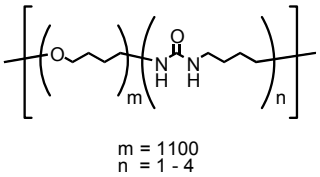

Figure 1.2. Poly(ether-*b*-polyurea)s prepared by Sibesjma and coworkers.

1.2.2. Main Chain Liquid Crystalline Polymers

Main chain liquid crystalline (LC) polymers are the most common class of polymers that have been prepared as RSCs.[22, 23] These polymers typically consist of rigid backbone groups and flexible spacer units and are most often assembled by the condensation of the preformed segments; ester linkages predominate. Sequence has been shown to be crucial in these systems. The rigid groups are predisposed to form ordered phases in the melt (or solution). As an example, changing the mesogen from biphenyl (a = 2) to terphenyl (a = 3) in the polymer in Figure 1.3 increases the T_i, the temperature which the polymer loses its liquid crystalline characteristics and becomes isotropic.[24] Changing the length of the alkyl spacer by one unit from b = 5 to b = 6 changes the liquid crystalline phase from smectic C to smectic A.[25] In another study, an RSC comprising regularly alternating poly(*p*-oxybenzoate-*co*-*p*-phenylene isophthalate) was compared with a copolymer formed by a random copolymerization of the three components: *p*-hydrobenzoic acid, isophthalic acid, and hydroquinone diacetate. The RSC exhibited a higher T_g and exhibited two sharp nematic transitions; the random copolymer had a lower T_g and exhibited only one broad crystalline-to-nematic transition.[26]

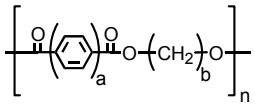

Figure 1.3. A liquid crystalline RSC.[27, 28]

Although many RSCs have been prepared in an effort to yield good main chain liquid crystalline materials,[22, 25, 29-32]the research has been driven by application and, with only a few exceptions, little effort has been put into a holistic evaluation of the structure/function relationships of these polymers.[33-35]

1.3. Polyfluorene: A Main Chain LC Homopolymer

Polyfluorene (PF, Figure 1.4) is a member of the conjugated homopolymer class of materials. A conjugated polymer (CP) is polyunsaturated and features complete π–electron delocalization along its backbone. This extended delocalization translates into an electronic band structure that is reminiscent of silicon, and as such organic CPs are sometimes thought to be "synthetic metals." CPs first came to prominence in 1977 when Shirakawa showed that polyacetylene (PA, Figure 1.5), normally considered a semiconducting material, exhibited a significant increase in conductivity upon doping with electron donors or acceptors.[36-38] These materials received more attention in 2000 when Shirakawa, Heeger, and MacDiarmid were recognized with the Nobel Prize in Chemistry for their work on CPs.[39] The electronic properties of CPs remain the subject of intense investigation, with applications in organic lasers,[40, 41] field effect transistors,[42-44] polymeric light emitting devices (PLEDs),[45] and non-linear optical devices[46, 47] being pursued.

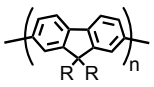

Figure 1.4. The general structure of polyfluorene (PF).

In addition to PF and PA, other examples of conjugated polymers with all-carbon skeletons include poly(*para*-phenylene) (PPP), poly(*para*-phenylene vinylene) (PPV), and poly(*para*-phenylene ethynylene) (PPE). Conjugated polymers incorporating heteroatoms are numerous as well; examples of this include polypyrrole (PPy), poly(*p*-aniline) (PANI, shown in emeraldine base form), poly(3,6-carbazole) (PC), and poly(2,5-thiophene) (PT).

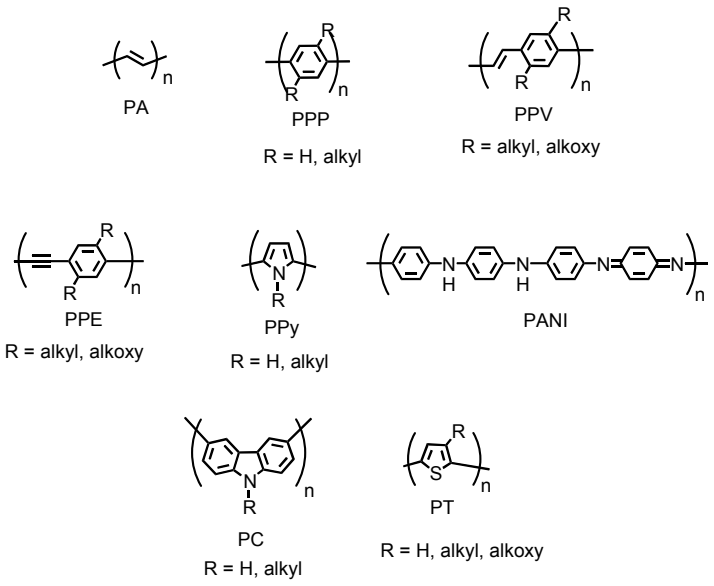

Figure 1.5. Other examples of conjugated polymers.

Any discussion of the attractive features of PF should first begin by introducing the numbering convention along the fluorene moiety. This is illustrated in Figure 1.6. There are three common sites of reactivity along the fluorene moiety- these are denoted as carbons 2, 7, and 9. From a reactivity standpoint, C2 and C7 are sites for substitution by the presence of an

electrophile, while C9 is subject to deprotonation-substitution as well as radical-pathway reactions. The vast majority of chemical transformations on the fluorene backbone occur at these three sites. Because connectivity along PF occurs at C2 and C7, substitution at C9 is the main distinguishing characteristic of PF homopolymers and fluorene-containing copolymers. This subject is treated in Section 1.4.

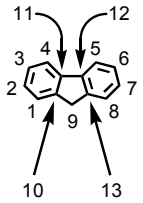

Figure 1.6. Numbering convention on the fluorene moiety.

The motivation for polymerizing 9,9-disubstituted fluorene first arose due to drawbacks associated with the structurally similar homopolymer PPP. The unsubstituted form of PPP is rendered insoluble at relatively low molecular weight. Since polymer processing is typically performed from a concentrated solution of the polymer, the inability to solubilize PPP makes it difficult to cast it into a film for transistor applications, for example. Additionally, in order to relieve steric strain, PPP adopts a dihedral angle of 23° between phenylene units on average.[48] Dihedral twisting is undesirable because it reduces the polymer's effective conjugation length, which is defined as the number of bonded aromatic rings at which the optical and electronic properties of a conjugated polymer become saturated. Inter-ring phenylene torsion thus directly impacts the polymer's conductivity. Müllen and Berresheim synthesized more soluble, higher molecular weight PPP by introducing alkyl or alkoxy groups on the arylene repeat unit, but this

modification was found to exacerbate inter-ring torsion–the dihedral angle of poly(*para*-2,5-dialkyl phyenylene) increased to 45°.[49]

PF is a formal analogue of PPP. The biphenyl repeat unit in PF serves to incorporate the PPP motif, with the added benefit of planarity of the two phenyl rings within the fluorene repeat unit. It should be noted that, like PPP, PFs do have an inter-fluorene dihedral angle; this is found to be between 15° and 24°.[50] Additionally, though the fluorene moiety is "planarized" by C9 there remains a small deviation from collinearity of the phenylene rings. An angle of 19° was calculated to be the angle at which the para axes in fluorene (defined by lines connecting C2-C11 and C7-C12) deviated from strict linearity.[51]

The structural differences between PF and PPP affect the properties they display in the bulk, as evidenced by the effective conjugation lengths of each. Studies of low molecular weight PPP revealed an effective conjugation length of 11 phenylene units,[52, 53] while PF was reported to reach effective conjugation at 10-12 units, or 20-24 aromatic rings.[48] This contrasts greatly with PT, where extended coplanarity of the thiophenyl moieties results in an effective conjugation length upwards of 96 repeat units.[54] Longer effective conjugation lengths allow for greater resistance against oxidative doping, higher ionization potential, and smaller electronic band gaps.[55] CPs with small band gaps at short effective conjugation lengths are highly desirable because light emission from a conjugated polymer shifts bathochromically with increasing effective conjugation length. The band gap for PF is typically ~2.8 eV,[56] which is lower than the band gap of 3.4 eV reported for poly(*para*-2-decyloxy phenylene).[57] This decreased band gap can be attributed to increased planarity of the fluorene unit relative to a biphenyl unit. Optical properties of CPs, and PF in particular, are described in more detail in Section 1.6 and Section 1.10.1.

1.4. C9 Substitution

The vast majority of fluorene-containing polymers are substituted at C9, though isolated reports on the incorporation of 9,9-unsubstituted fluorene into a polymer[58] as well as its use in end capping 9,9-dialkyl PFs[59] are known. Substitution at C9 is routinely performed prior to polymerization and is facilitated using standard S_N2 chemistry, which allows for the attachment of a variety of groups. A representative sample of these groups is shown in Figure 1.7 and includes *n*- (A),[60, 61] branched (B),[62] chiral (C)[60, 61], and spirocyclo alkyls (D);[63] oligoether (E);[60, 64] phenol (F);[65] ester (G);[58] alkyl(trialkylamine) (H) and alkyl(tetraalkylammonium) (I);[66-68] spirofluorenyl (J);[69] spiro(bis-styrylamino)fluorenyl (K);[70] triarylamine(L);[71] and phenylene[72] (M) and benzyl ether[73] dendron (N) groups. Careful control of nucleophile stoichiometry and relative ease of purification away from byproducts allows for monosubstitution at C9, and as such fluorene moieties bearing one *n*-hexyl (O) and one ethyl ester substituent (P) have been reported.[58] Polymeric fluorene moieties with ternary C9 functionality such as alkylidene (Q) have also been reported.[44]

Key to these modifications is the finding that the electronic character about the fluorene moiety is not changed appreciably by substitution at C9.[74] Thus, C9 substituents have been chosen to render PFs soluble in organic and/or aqueous solvents,[68, 75] to facilitate Förster energy transfer behavior,[70, 76] to enforce particular phase ordering in the bulk,[77] and to inhibit polymer degradation,[72] for example.

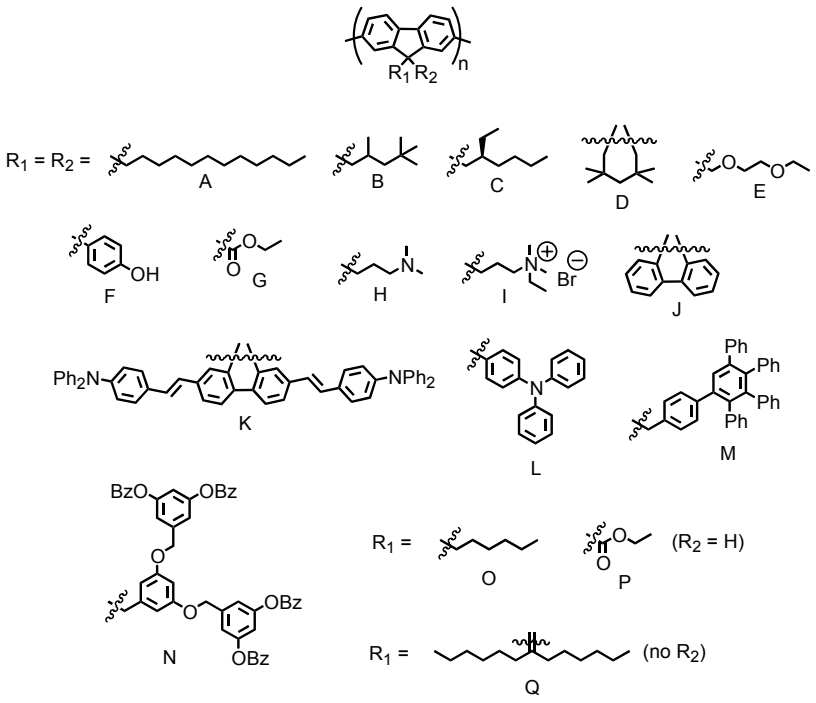

Figure 1.7. Illustration of various groups substituted at C9 on fluorene-containing polymers.

1.5. PF Conductivity

Ranger prepared PF copolymers P9EF, P9KF, P9BF, and P9BFP (Figure 1.8) in an effort to gauge the ability of PFs to conduct electrons.[58, 78, 79] The polymers were prepared such that the repeat unit was a perfectly alternating bifluorene wherein one fluorene was 9,9-dialkyl or, in the case of P9BFP, alkylidene substituted. The other fluorene moiety was monosubstituted with an electron withdrawing functionality.

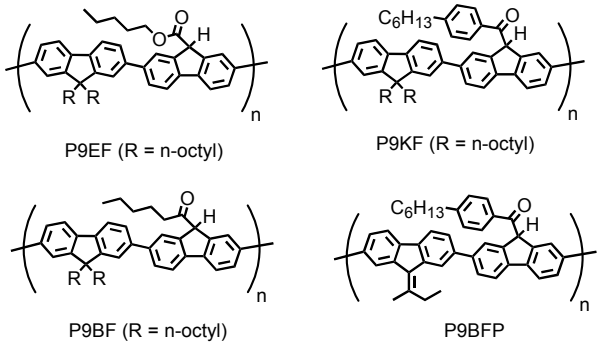

Figure 1.8. Base-dopable PF copolymers prepared by Ranger and coworkers.

The addition of ^{t}BuOK to a solution of the polymer in THF served to dope the polymer backbone (shown for P9KF, Scheme 1.2). Ranger reported stabilized conductivities of $\sigma \sim 10^{-9}$ S/cm for undoped PF copolymers. When doped with base the polymers were much more conductive, with $\sigma = 10^{-6}$ for the ester-containing P9EF, and $\sigma \sim 10^{-4}$ -10^{-3} S/cm for the ketone-functionalized copolymers P9KF, P9BF, and P9BFP. These conductivities are respectable for organic conductors but do not yet approach the conductivity, $\sigma \sim 10^{1}$ S/cm, of polished, prime silicon.[80]

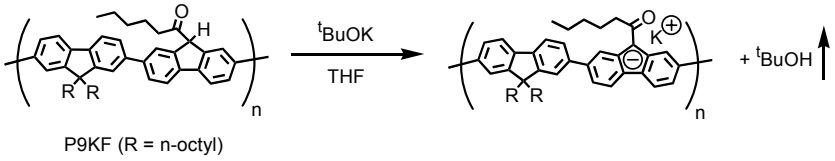

Scheme 1.2. Method of doping employed by Ranger.

1.6. Light Emission Characteristics of PF Homopolymers

A major source of interest in fluorene-containing polymers stems from their attractive light emission characteristics. As can be seen in the case of poly(9,9-di-*n*-hexylfluorene) (PDHF)

in Figure 1.9, the absorption spectrum of a pristine polyfluorene in $CHCl_3$ consists of a featureless π-π* transition at 380 nm. Any vibronic fine-structure is obscured by the presence of a range of conjugation lengths in the polymer. The solution-phase emission, in contrast, exhibits three well-resolved bands at 420, 448, and 472 nm, assigned to the 0-0, 0-1, and 0-2 transitions, respectively.[81] PF has a high quantum efficiency (50-70%) and emits an intense sky blue color under UV light.[64, 82] As PF is processible under a variety of C9 substitutions and as it is readily accessed (see Section 1.8) it is very attractive for light emitting applications.

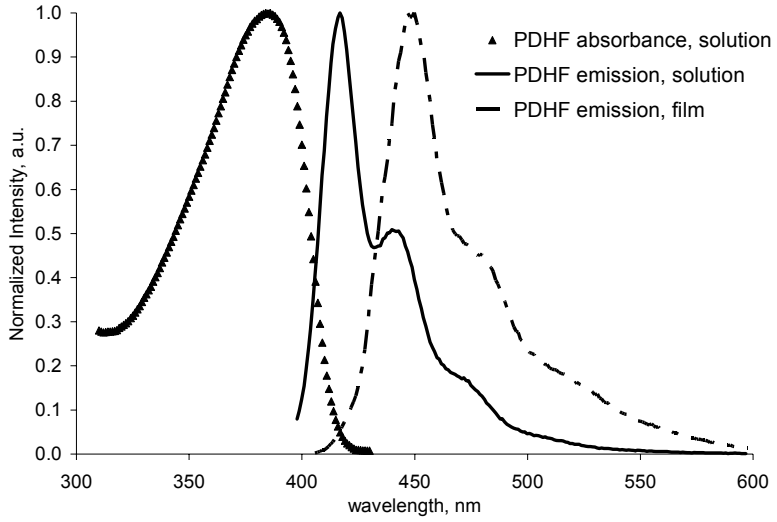

Figure 1.9. The absorption and emission spectra of PDHF in $CHCl_3$, and the emission spectrum of a pristine film of PDHF.

The emission spectra of solid state PF films have characteristics similar to the polymers in solution although the maxima are shifted bathochromically by 30-40 nm and the quantum yields decrease to ~16%.[82] The emission maximum for a pristine film of PDHF, then, occurs at 450 nm, and vibronic coupling is denoted by shoulders at 480 and 535 nm.

PF emission properties are currently the subject of much discussion, as the stability of these polymers when cast as films does not meet performance criteria for commercialization. Specifically, upon heating (or exposure to UV-light or current), the PF spectrum undergoes a dramatic transformation.[74] The blue emission decreases and a weak band at ca. 535 nm (2.3 eV) appears and becomes intense, resulting in an undesired dominant green emission. Efforts aimed at understanding the origin of this emission and at establishing the increased stability of our fluorene-containing RSC polymers are described in Chapter 3.

1.7. Bulk Phase Morphology and Liquid Crystallinity

The bulk morphology of *n*-alkyl derivatives of PF has been studied. Two distinct phases have been identified, a glassy α-phase and a more highly ordered β-phase.[51] The β-phase spectrum is analogous to that of the α-phase except for a small bathochromic shift in both absorption and emission. The formation of this phase, which occurs upon exposure of α-phase films to thermal cycling and certain solvents, is attributed to side-chain crystallization. The extended correlation length, 22 nm for the β-phase vs. 15 nm for the α-phase of PFO, is said to result from more efficient packing of the alkyl chains in the bulk. These chains are hence prone to crystallization and promote the onset of the α-phase.[77] The substitution of branched side-chains suppresses the formation of the β-phase.[83]

As mentioned in Section 1.3, PFs are known to exhibit LC behavior. The first report of this phenomenon by Bradley and coworkers who observed the formation of an LC phase by DSC.[84] Transition temperatures from semi-crystalline to LC phases occur from 60-160 °C, depending on the length and branching of the side-chains.[74, 82] The birefringent phases for dialkyl

polyfluorenes exhibit Schlieren textures that are consistent with nematic organization.[82] The clearing point (the transition from the LC state to the isotropic state) is quite high (>250 °C) and is difficult to detect as thermal decomposition begins in the same temperature range.[74]

The ability of poly(9,9-di-*n*-octylfluorene) (PDOF) to align in the bulk into an LC monodomain was demonstrated by Grell and Bradley in 1997.[84] This was the first report of the alignment of a conjugated polymer in its LC state, which was accomplished by spin-coating the film onto a rubbed polyimide substrate. Alignment occurred after heating the film above its melting temperature, T_m = 170° C, and cooling the film slowly. Two ordered, aligned states for PDOF were produced. First, cooling slowly from T_m to room temperature oriented PDOF into a crystalline film. However, by cooling slowly from 200° C to the T_m and then rapidly quenching the film to room temperature, PDOF was found to bypass crystallization and was obtained as an oriented LC glass. Monodisperse oligofluorenes have also been found to exhibit liquid crystalline behavior and have similarly been trapped in their LC states by bulk processing methods.[85] Monodisperse oligofluorenes are described in greater detail in Section 1.9.

1.8. Polyfluorene Synthesis

The first synthesis of PF was reported by Fukuda in 1989.[86] In this report, PDHF was produced by the oxidative coupling of 9,9-dihexylfluorene using $FeCl_3$ (Scheme 1.3). The polymer recovered was found to have low molecular weight (M_n = <5000 as determined by GPC relative to PS standards) and suffered from lack of complete regioselectivity in that coupling at carbons other than C2 and C7 occurred, leading to structural defects in the polymer. The substituional irregularity led to poor quality films. Removal of metallic impurities was also

problematic and posed problems for potential device incorporation. Fukuda did, however, report the important observation that as the length of the straight chain alkyl substituents on C9 increased the T_g of the polymer decreased.

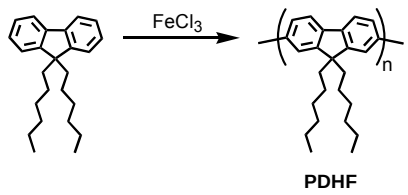

Scheme 1.3. Fukuda's approach to PF.

With the development of improved aryl-aryl coupling methodologies came improved syntheses of PF. Pei published the first transition metal-catalyzed synthesis of PF in 1996, accomplishing the regioregular polymerization of dibromofluorene using Ni^0 generated *in situ* from $NiCl_2$ and Zn. The resultant poly[9,9-bis(dioxaheptyl)fluorene] (BDOH-PF) exhibited a dramatic increase in MW (M_n = 94,000 and M_w = 215,000, GPC relative to PS) relative to previous preparations (Scheme 1.4).[64] Additionally, Pei noted the strikingly small solvatochromic effect present in samples of BDOH-PF: whereas poly(3-*n*-hexylthiophene) exhibited absorbance maxima of λ = 425 in a dilute solution of $CHCl_3$ and λ = 405 when cast as a film,[87] BDOH-PF gave absorbance maxima of λ = 385 nm as a film and λ = 378 nm as a dilute solution in THF. This very minor difference in maxima was attributed to the relief of inter-ring torsion associated with PF.

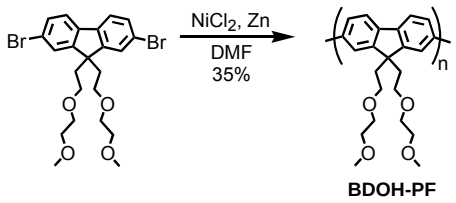

Scheme 1.4. Pei's Ni^0-catalyzed route to PF.

Ranger[58] and Woo[88] synthesized 9,9-dialkyl PFs *via* the Suzuki cross-coupling methodology in 1997. This reaction is catalyzed by Pd^0 and couples a 2,7-dihalo-9,9-dialkylfluorene and a 9,9-dialkylfluorene-2,7-bisboronic ester or acid. Ranger used derivatized 9,9-dioctylfluorenes to yield PDOF with molecular weights of M_n = 24,000 and M_w = 40,000 (Scheme 1.5).

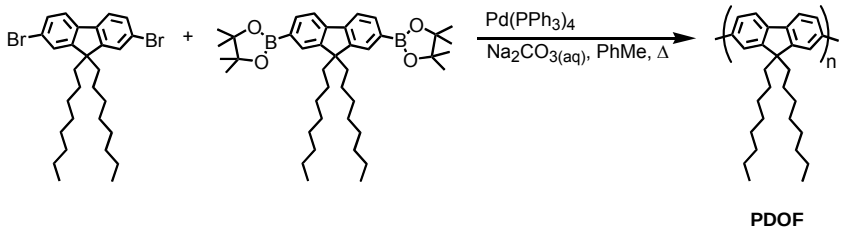

Scheme 1.5. The Pd^0-catalyzed route to PF from a dibromofluorene and a fluorene-bis(boronic ester).

In 1998, Kreyenschmidt[89] reported the synthesis of PDHF *via* the simplified, Zn-free Yamamoto homocoupling methodology. This route uses stoichiometric quantities of $Ni(COD)_2$ as a coupling agent to polymerize a 2,7-bromo-9,9-dialkylfluorene. In this fashion PDHF with a degree of polymerization, DP = 54 was prepared (Scheme 1.6).

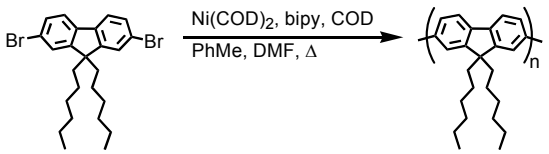

Scheme 1.6. Kreyenschmidt's synthesis of PDHF using the Yamamoto homocoupling strategy.

1.9. Monodisperse Oligofluorenes

Kreyenschmidt's report of the synthesis of PDHF coincided with a report by Klaerner on oligomeric 9,9-dihexylfluorenes.[48] This was the first instance of the synthesis and characterization of fluorenes of low DP (n = 3-10). Oligomer compounds are useful for the modelling of analogous polymers and for the elucidation of structure-property relationships.[90] Indeed, Klaerner's motivation for preparing oligofluorenes was for the unambiguous determination of the effective conjugation length of PDHF. An oligofluorene series was prepared in one pot by optimizing the homocoupling conditions shown in Scheme 1.6 to yield statistical mixtures of oligomeric product. After end-capping with 9,9-dihydrofluorene and removing high molecular weight polymer by precipitation, oligomers from terfluorene (n = 3) up to decafluorene (n = 10) were separated by HPLC for subsequent characterization. The plot of the absorption energy, λ_{max}, of each oligomer versus $1/n$ revealed the effective conjugation length of PDHF to be 12 fluorene units, or 24 aryl rings upon linear extrapolation of $1/n$ to zero (Figure 1.10).

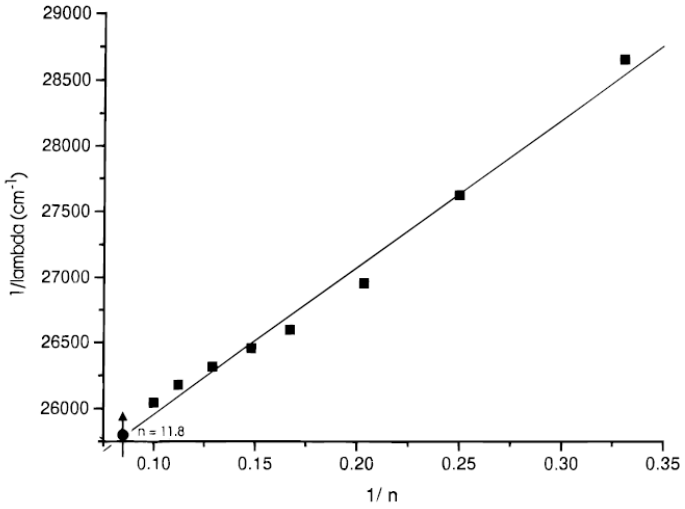

Figure 1.10. Klaerner's plot of λ_{max} vs. 1/*n* for oligofluorenes of *n* = 3 - 10. This figure is from Klaerner, G.; and Miller, R.D. *Macromolecules* **1998**, *31*, 2007-2009.

In 2000, Lee and Tsutsui reported the use of an iterative synthetic strategy to arrive at oligofluorenes using controlled chemical means.[91] This approach is depicted in Figure 1.11. Iterative oligomer assembly is an attractive strategy because, by design, it requires the preparation of few reactive intermediates and because growth of suitably long oligomers is achieved using a limited variety of reaction conditions. Lee's strategy began with the preparation of 2-bromo-9,9-dihexylfluorene, which was then homocoupled using Yamamoto conditions to produce the bifluorene (A, Scheme 1.7). This bifluorene was then "reactivated" by bromination at C2 and C2' to give the dibromobifluorene (B). At this point, Lee employed the Suzuki coupling of B with two equivalents of 9,9-dihexylfluorenyl boronic ester to yield the quaterfluorene (C). Though it was not performed, the synthetic cycle could conceivably begin anew, with a "reactivating" bromination of the quaterfluorene and subsequent Suzuki reaction to yield a hexafluorene, and so on to give even-numbered oligofluorenes. A similar cycle was described to allow for the preparation of oligofluorenes with odd-numbered segment lengths.

The iterative 2*n* growth described was advantageous in that it avoided the complex separation of oligomers Klaerner had performed. On the other hand, Klaerner had arrived at a library of oligofluorenes in one synthetic step, whereas Lee had run multiple reactions and obtained a smaller library. Regardless, both studies found that as the length of the oligofluorene increased, optical absorption and emission maxima shifted to longer wavelengths.

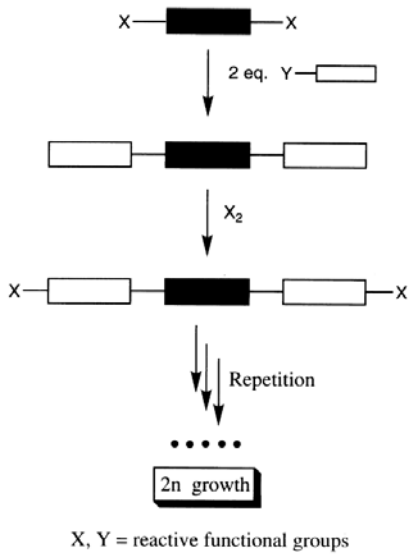

Figure 1.11. Conceptual representation of iterative oligomer assembly. This figure is from Lee, S.H.; and Tsutsui, T. *Thin Solid Films*, **2000**, *363*, 76-80.

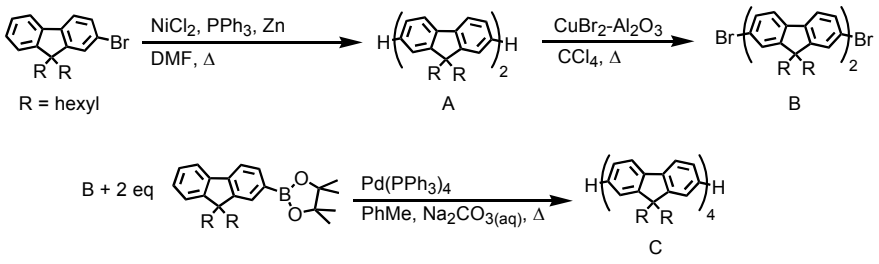

Scheme 1.7. Lee's iterative approach to oligofluorene assembly.

A third strategy to the synthesis of monodisperse oligofluorenes was published by Geng in 2002.[85] This approach was modular in nature, using multiple combinations of relatively few fluorenyl intermediates to assemble oligofluorene products. An example from Geng's report is reproduced in Scheme 1.8, where 2,7''-diiodoterfluorene (A) is used as a core module. Fluorene A was employed in three separate Suzuki reactions where the coupling partner was bifluorenyl (*n* = 2), terfluorenyl (*n* = 3) or quaterfluorenyl (*n* = 4). The products of these reactions were oligofluorenes with fluorene segment lengths of *n* = 7, 9, and 11, respectively. In this fashion oligofluorenes with segment lengths from two up to sixteen units were rapidly accessed. Geng went on to show that oligofluorenes exhibited T_gs that increased with increasing fluorene segment length (as observed by DSC according to first cooling scans). Furthermore, when cooling, the oligofluorenes retained their oriented, glassy nematic state while resisting crystallization as described in Section 1.7. Also, because the oligofluorenes were peralkylated at C9 with chiral 2-(*S*)-methylbutyl groups, they exhibited polarized fluorescence. This resulted from the arrangement of oligomers into left-handed helices in the bulk as revealed by molecular dynamics simulations. Culligan then incorporated closely related monodisperse chiral oligofluorenes into a device for polarized electroluminescence.[92]

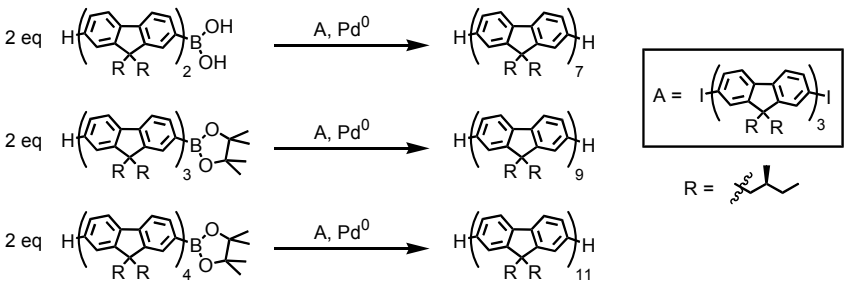

Scheme 1.8. Geng's modular approach to oligofluorene assembly.

1.10. Fluorene Copolymers

Fluorene monomer compounds are frequently employed in the synthesis of functional copolymers. Copolymerization with other monomer units can be performed in order to maintain conjugation or rigidity throughout the polymer backbone (Sections 1.10.1 and 1.10.2), or it can be performed such that conjugation is interrupted by a flexible spacer unit (Section 1.10.3). The polymers produced then fall into two general categories: if rigidity is maintained throughout the backbone the polymer is a rod-rod copolymer, and if fluorene segments are broken by segments with significant conformational freedom (i.e. *n*-alkyl groups) the polymer is a rod-coil copolymer.

1.10.1. Rod-Rod Copolyfluorenes: Scope and Light Emission Characteristics

A wide variety of rod-rod copolymers incorporating a fluorene repeat unit have been prepared. In 2000, Leclere described the variety of repeat units used for random, alternating, and block copolymers (Figure 1.12).[93] The ensuing six years have seen further elaboration on the type of conjugated monomer used in copolyfluorene synthesis; a representative selection of these examples follows in Figure 1.13. The copolymerization of fluorene monomer units with other aryl units produces polymers in which each monomer unit contributes rigid rod-like packing forces. So-called rod-rod copolymers containing fluorene units are of interest for a number of reasons. First, the solubilizing effect of, for example, 9,9-di-*n*-alkyl fluorenes is very attractive when paired with other repeat units lacking such character, or upon which substitution would significantly alter its electronic properties. Because processing a polymer frequently involves handling it in solution, the ability to dissolve a polymer is an important design criterion. Schmitt

used fluorene prepolymers to enable the selective dissolution of a PF-PANI block copolymer away from insoluble PANI homopolymeric material. The PF-PANI copolymer was thereafter shown to be processible in toluene.[94] The synthesis of this copolymer is described in Section 1.10.2.

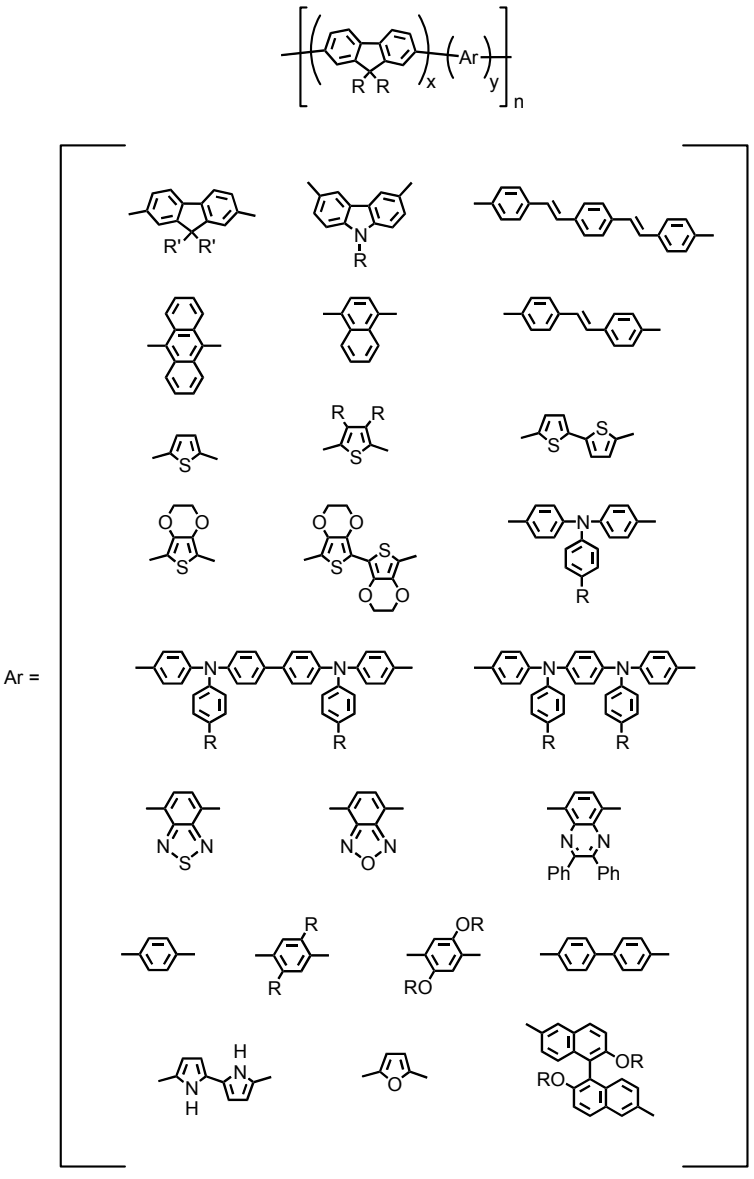

Figure 1.12. Fluorene-containing rod-rod copolymers. This figure is reproduced from Leclerc, M., *J. Polym. Sci. Pt. A: Polym. Chem.* **2001**, *39*, 2867-2873.

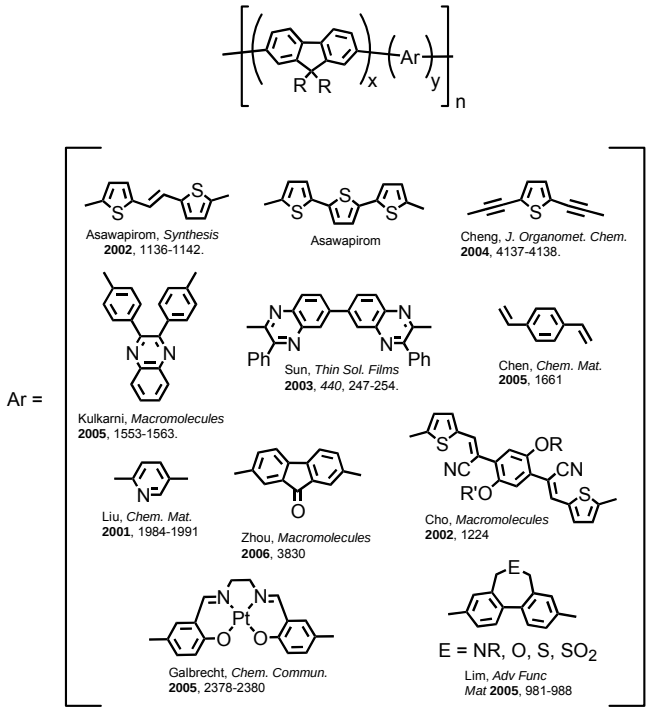

Figure 1.13. New rod-rod copolyfluorenes.[56, 65, 95-103]

A second motivation for the preparation of rod-rod copolyfluorenes lies in the attractive light emission properties the materials have been found to exhibit. The shifting of absorption and emission maxima by copolymerization with other conjugated moieties offers a simple but powerful method of tuning optics properties. Light emission is readily tuned by adjusting effective conjugation lengths on the polymer backbone. As such, the longer the effective conjugation is, the greater the wavelength of maximum emission will be. Fluorene-containing copolymers with photoexcitation maxima in the violet (380-420 nm), blue (440-500 nm), green (520-565 nm), yellow (565-590 nm), orange (590-625 nm), and red (625-740 nm) sectors of the visible region have been produced (Figure 1.14). Additionally, a fluorene-containing random copolymer emitting white light as a combination of intense red, green, and blue emission (400 – 800 nm) under electroluminescence has been produced (Figure 1.15).

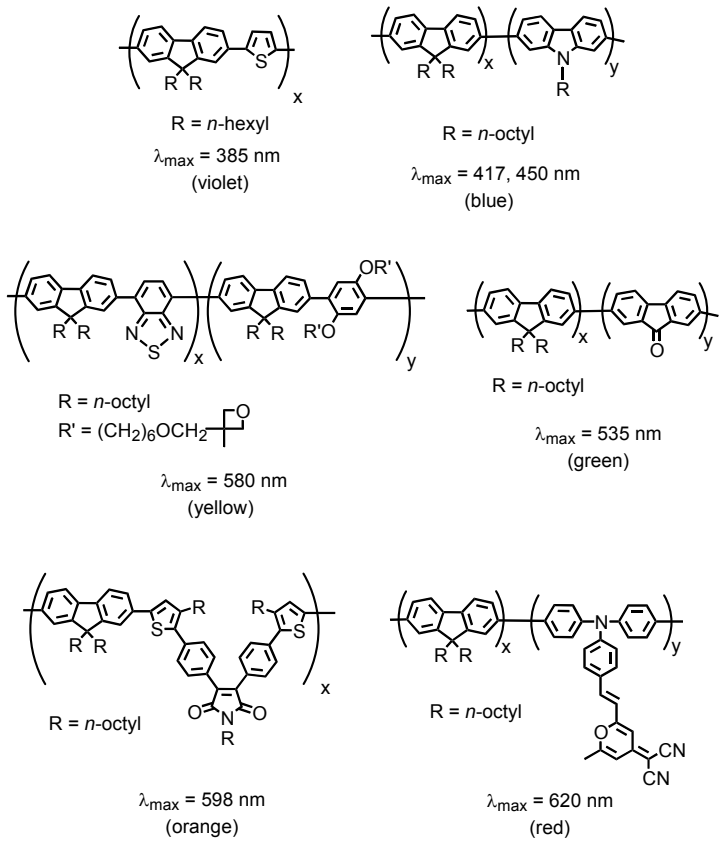

Figure 1.14. Examples of the array of colors emitted by fluorene-containing copolymers in solution upon photoexcitation. Shown are violet,[104] blue, [105] yellow,[106] green, [100] orange, [107] and red.[56]

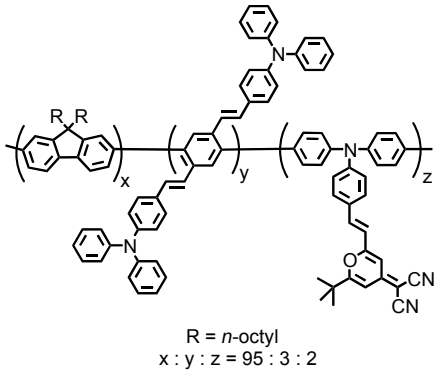

Figure 1.15. An example of a copolymer which exhibits white light emission upon electrostimulation.[108]

1.10.2. Rod-Rod Copolyfluorenes: Synthesis

In addition to facilitating the regioregular homopolymerization of 2,7-substituted fluorenes, the development of well-defined transition metal-catalyzed reactions has greatly enabled the synthesis of new and useful rigid rod copolyfluorenes. The majority of these copolymers are prepared using Suzuki and Yamamoto reactions (see Section 1.8). Polymerization *via* the Suzuki reaction can yield alternating copolyfluorenes, as the fluorene monomer possesses 2, 7-diboronate or boronic acid substitution while the comonomer is bromo-, iodo- or tosyl-substituted. An example in which the Suzuki reaction has been employed for this purpose is the preparation by Vamvounis[104] of poly(9,9-dihexylfluorene-*alt*-thiophene), shown in Scheme 1.9.

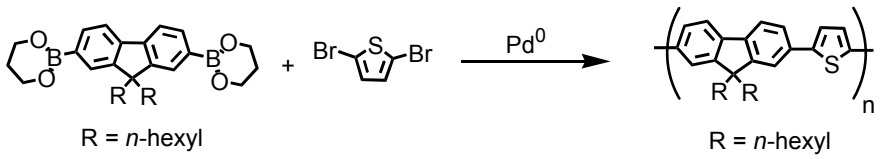

Scheme 1.9. The preparation of poly(9,9-dihexylfluorene-*alt*-thiophene) *via* the Suzuki reaction.

Copolymers produced using the Yamamoto reaction are random, as coupling of halogen-terminated aryl monomers occurs without control over monomer sequence. An example of this approach is the copolymerization by Galbrecht[102] of 2,7-dibromo-9,9-dioctylfluorene with a dichloro-substituted Pt-salen complex, shown in Scheme 1.10.

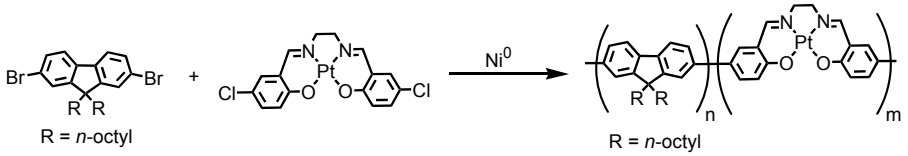

Scheme 1.10. The preparation of poly[9,9-dioctylfluorene-*co*-(Pt-salen)] *via* the Yamamoto reaction.

Poly(9,9-dialkylfluorene-*alt*-vinylene) (PFV), a rigid rod CP which can be considered an alternating copolymer of a 9,9-dialkylfluorene and acetylene, has been produced using several less commonly employed routes. These routes are depicted in Scheme 1.11 and include implementations of Heck,[109] Horner-Emmons,[110] and Acyclic Diene Metathesis (ADMET)[111] polymerization reactions. The Horner-Emmons polymerization is noteworthy as it is transition metal free, though these reaction conditions call for the use of excess base. Use of Horner-Emmons conditions generate PFV with monomodal size distribution with molecular weights M_w = 94,000 and M_n = 27,000 (PDI = 2.7) relative to PS standards. PFV was also prepared from 2,7-divinyl-9,9-di-octylfluorene using the ADMET polymerization reaction. The metathesis catalyst used in this instance was the air sensitive Schrock alkylidene (Scheme 1.11, inset) and molecular weights of M_w = 14,000 – 58,000 and M_n = 8,900 – 31,600 (PDI = 1.61 – 1.92) were reported. The use of ADMET is treated in greater detail in Section 2.3.2. Curiously, no molecular weights were reported for the synthesis of PFV by the Heck reaction.

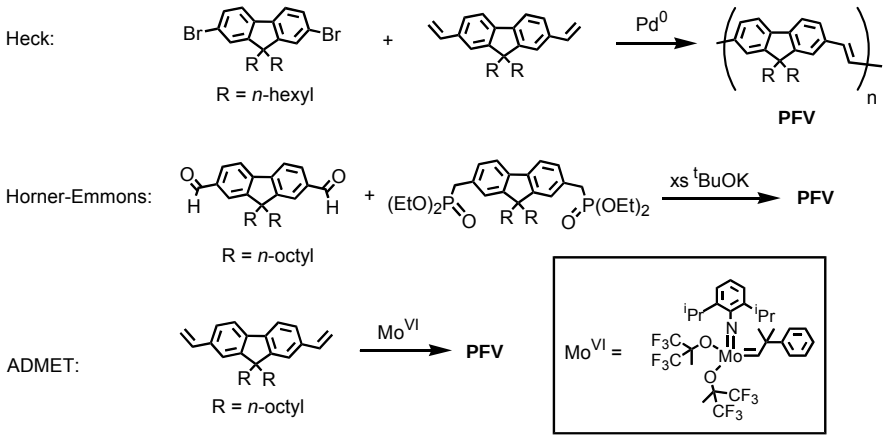

Scheme 1.11. The preparation of PFV *via* the Heck, Horner-Emmons, and ADMET polymerization reactions. Inset: Schrock's Mo^{VI} catalyst used in the making of PFV by ADMET.

Lastly, Pschirer[112] and Brizius[113] reported the acyclic diyne metathesis (ADIMET) polymerization of 2,7-di(prop-2-ynyl) fluorenes to yield the corresponding poly(9,9-dialkylfluorene-*alt*-ethynylene)s (PFEs, Scheme 1.12). This reaction uses a $Mo(CO)_6$/4-chlorophenol precatalyst system to generate PFEs, which were produced with degrees of polymerization ranging from DP = ~ 20 to 82 . Polydispersity indices (PDIs) ranged from 3.6 to 5.8. Substrates with *n*- and branched alkyl substituents at C9 were polymerized by ADIMET, as was a 9,9-di-ω-alkenyl fluorene (R = (*S*)-(+)-citronellyl, shown) indicating that ADIMET polymerization tolerated alkenes. PFEs in chloroform were found to exhibit aggregation behavior consistent with that observed for PPE upon addition MeOH, while their emission spectra were more consistent with PF.

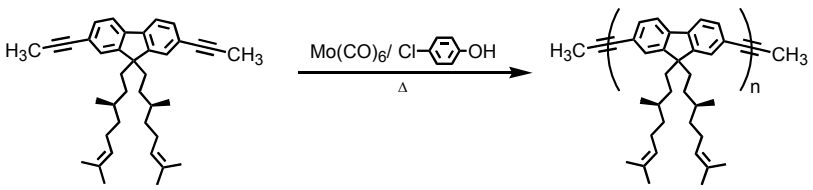

Scheme 1.12. The preparation of PFEs *via* the ADIMET polymerization reaction.

Block copolymers have also been prepared using transition metal-catalyzed reactions. Asawapirom prepared poly(9,9-diethylhexylfluorene-*b*-poly-2-undecyl aniline) by first synthesizing the fluorene block under Ni^0-catalyzed Yamamoto conditions and endcapping with *p*-bromoaniline (A, Scheme 1.13).[114] 2-Undecyl aniline was then polymerized under standard PANI oxidative coupling conditions ($NH_4S_2O_3/H^+$) to give tri-block PANI-PF-PANI (B). Asawapirom's interest in producing PF-PANI stemmed from the likelihood that it would self assemble in the bulk phase. Self assembly was indeed observed–cylindrical domains 50-300 nm in diameter were noted. This feature is expected to directly impact the material's charge separation properties because PF and PANI have different oxidation and reduction potentials. The identification of phase separation in PF-PANI has implications for photovoltaic devices, where charge injection from an electron donating component to an acceptor component is made more efficient when the material is a single, microphase-structured entity. Asawapirom also reported the synthesis of a PT-PF-PT triblock copolymer which exhibited interesting morphological properties.[114]

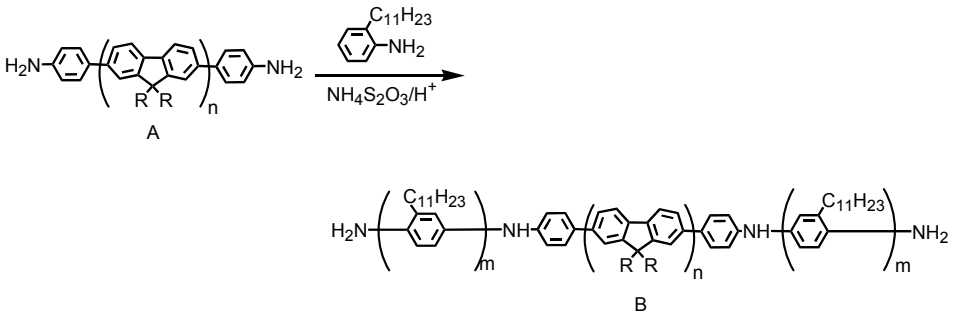

Scheme 1.13. Preparation of poly[9,9-dialkyl PF-*block*-(2-undecyl) PANI].

1.10.3. Rod-Coil Copolyfluorenes: Scope, Synthetic Approaches and Bulk Characteristics

A number of rod-coil copolymers incorporating fluorene segment lengths have also been prepared. Motivation for synthesizing these copolymers also stems from nanophase separation or separations they may adopt in the bulk. Phase separation on the micro or nanoscale can be advantageous, as evidenced by an early example of a PF-*b*-poly(ethylene oxide) (PEO) prepared by Marsitzky.[115] Marsitzky prepared PF-*b*-PEO by first synthesizing a low molecular weight (M_n = 3380, DP ~ 8) mono-end-functionalized PDOF (A, Scheme 1.14). End functionalization of the PF block with a benzyl alcohol group provided for subsequent deprotonation by treatment with potassium naphthalenide (B). Macroinitiator B was subjected to anionic polymerization with ethylene oxide in THF such that after purification of the copolymer (C) the PF:PEO block length ratio was found to be ~1.4 (8 : 5-6).

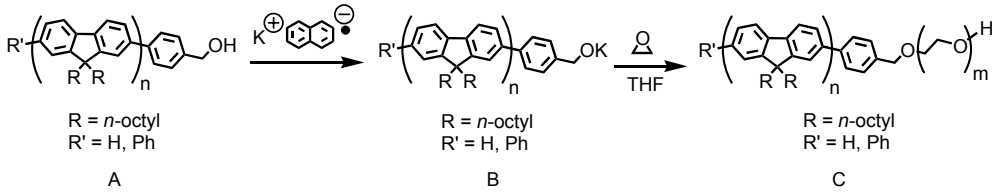

Scheme 1.14. PF-*b*-PEO as prepared by Marsitzky.

The absorption and emission measurements of PF-*b*-PEO showed that the coil blocks had a noticeable effect on the optoelectronic properties of the rod segments. Specifically, PF-b-PEO was found to have more order in the bulk. Absorbance measurements for the PF prepolymer (A in Scheme 1.14) showed λ_{max} = 369 nm, with a shoulder at 432 nm (Figure 1.16a). The absorption maximum of PF-b-PEO (C in Scheme 1.14) was found to be bathochromically shifted to λ_{max} = 377 nm with an additional peak at 428 nm (Figure 1.16b). Bulk ordering in PF-*b*-PEO

was further demonstrated by emission spectra of pristine, drop cast films. Whereas the PF prepolymer exhibited emission maxima at λ_{max} = 420, 437, and 460 nm with shoulders at 495 and 536 nm (Figure 1.16b), PF-*b*-PEO gave well-resolved maxima of λ_{max} = 437, 464 and 495 nm with shoulders at 420 and 536 nm. The pronounced features in the film emission spectrum of PF-*b*-PEO were attributed to enhanced order phenomena.

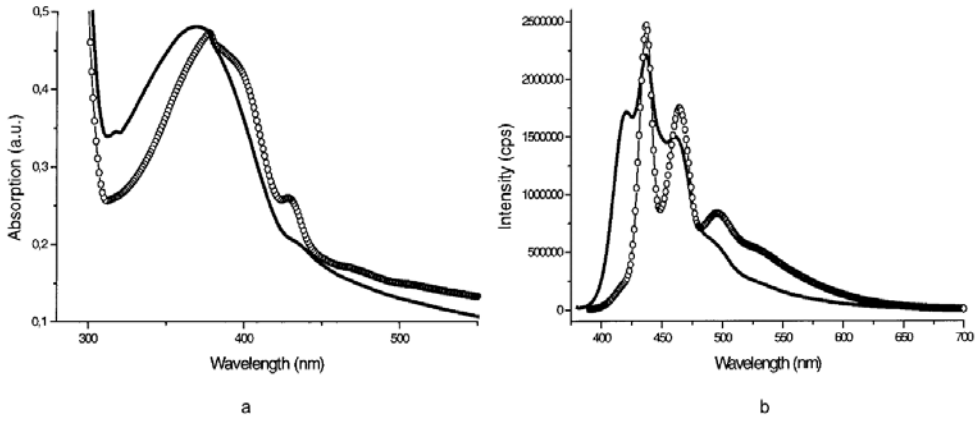

Figure 1.16. Absorbance (a) and PL emission (b) spectra for films of Marsitzky's benzyl alcohol-terminated PF (-) and PF-*b*-PEO (o). This figure is taken from Marsitzky, D.; Klapper, M.; and Müllen, K. *Macromolecules* **1999**, *32*, 8685-8688.

Another impressive example of a rod-coil copolyfluorene is the PDHF-poly(γ-benzyl-L-glutamate) [PBLG] polymer prepared by Kong.[116] This triblock copolymer, which ultimately is of interest for applications such as biosensors and stimuli-responsive biological components, was investigated for its ability to self assemble, which was promoted in this case by the nature of the polypeptide blocks, which are known to attain α-helix or β-sheet conformations depending on the PBLG block length. The copolymer was made starting with the preparation of block PDHF by the Yamamoto route. The PDHF block was then endcapped with *N*-(benzyl)phthalimide groups (A, Scheme 1.15). The end groups were converted to benzyl amines using hydrazine to yield

macroninitiator B, and ring opening polymerization of the γ-benzyl-L-glutamate derivatized *N*-carboxyanhydride to furnish triblock copolymer C.

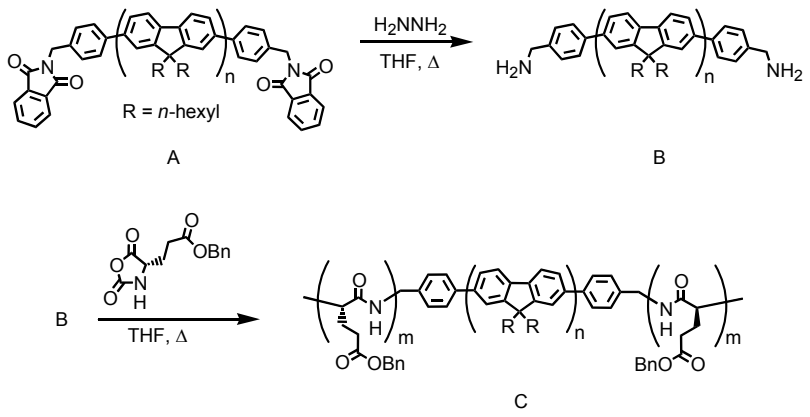

Scheme 1.15. Kong's synthesis of PBLG-PDHF-PBLG by ring opening polymerization.

Kong used stoichiometry to control the lengths of γ-benzyl-L-glutamate and 9,9-dihexylfluorene blocks in the product copolymers, preparing $PBLG_{23}PDHF_{15}PBLG_{23}$ and $PBLG_{16}PDHF_{28}PBLG_{16}$ (as determined by end group analysis of the ^1H NMR spectra). Studies performed using atomic force microscopy (AFM) revealed that the former copolymer had sufficiently long ($m > 20$) peptide segments to allow for α-helix formation to occur. In contrast, the latter copolymer sample possessed shorter ($m < 20$) peptide segments which destabilized α-helices, resulting in the appearance of the β-sheet conformation. Additionally, Kong was able to control self assembly processes in the copolymer samples depending on the solvent mixture from which films were cast. When a film of $PBLG_{23}PDHF_{15}PBLG_{23}$ was cast from 30% trifluoroacetic acid (TFA) in $CHCl_3$, the AFM image obtained showed a nanospherical orientation of the copolymer (Figure 1.17a). However, when $PBLG_{23}PDHF_{15}PBLG_{23}$ was cast from 3% TFA in $CHCl_3$ Kong observed parallel sheet-like orientation of the sample. (Figure

1.17b). Because helical polypeptides are known to possess large net dipoles, Kong proposed the side-by-side antiparallel conformation for $PBLG_{23}PDHF_{15}PBLG_{23}$ cast from 3% TFA.

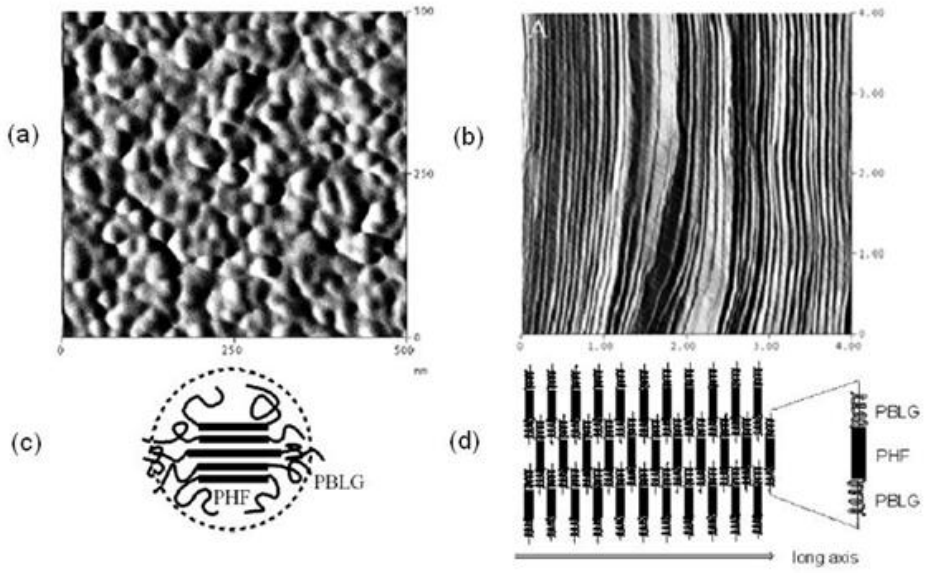

Figure 1.17. AFM amplitude images of $PBLG_{23}PDHF_{15}PBLG_{23}$ cast from (a) 30% TFA in $CHCl_3$ and (b) 3 % TFA in $CHCl_3$. (c): Representation of the triblock copolymer in (a). (d) Representation of the triblock copolymer in (b). The images in this figure were taken from Kong and Jenekhe, *Macromolecules* **2004**, *37*, 8180-8183.

Tsolakis used a rigid terfluorene macroinitiator for production of di- and triblock rod-coil copolymers by atom transfer radical polymerization (ATRP, Scheme 1.16).[117] This method of polymerization allowed for the attachment of polystyrene (PS, shown) and poly(^{t}butyl acrylate) blocks onto the light-emitting terfluorene moiety. The spectroscopic properties of the film cast polymers were found to be identical to the macroinitator. Perhaps more interestingly, when studied by differential scanning calorimetry the terfluorene-*b*-polystyrene copolymers were found to exhibit two T_g values. The first value (T_g ~ 30° C) stemmed from the glass transition for the terfluorene group, while the second observed transition (T_g ~ 100° C) was attributed to the PS block. The defined transitions indicated the separation of the terfluorene initiator and PS blocks

into microphase domains. This was found to be true for the terfluorene-*b*-PS copolymers even at modest molecular weights (M_n = 15,500), indicating that even short rod/coil block lengths exhibited phase separation in the bulk. ATRP as a route to interesting rod-coil block copolyfluorenes has been used to great success by Kallitsis.[118-120]

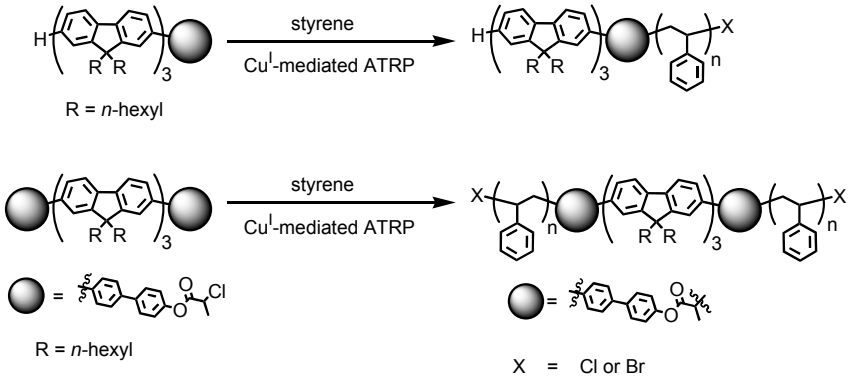

Scheme 1.16. ATRP-based synthesis of PS-PDHF-PS block copolymer.[117]

Kallitsis and Chochos have also reported the synthesis of poly(fluorene-*co*-polyether)s [PFcEs, Scheme 1.17].[35] Using a terfluorene substituted with *p*-phenol groups at the C2 and C2'' termini, α,ω-dibromoalkanes are used to produce the corresponding PFcEs by anionic polymerization. These can be considered repeating sequence copolymers in which the fluorene segment length is three and the ether segment length is one, though the ether segment can be engineered to possess nine through twelve methylene units depending on the dibromoalkane used. Kallitsis' PFcEs are discussed in more detail in Chapter 3.

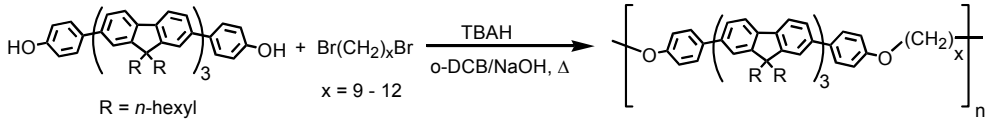

Scheme 1.17. Terfluorene macroinitiator synthesized by Kallitsis and Chochos for ATRP.

Other PF-containing rod-coil copolymers include Tirapattur's PF-*co*-polyester (Figure 1.18, A),[121] Zhang's diblock (B) and Surin's triblock (C) PF-*b*-poly(ethylene oxide), and Lu's PF-*b*-poly[2-(9-carbazolyl) ethyl methacrylate] (D).[122]

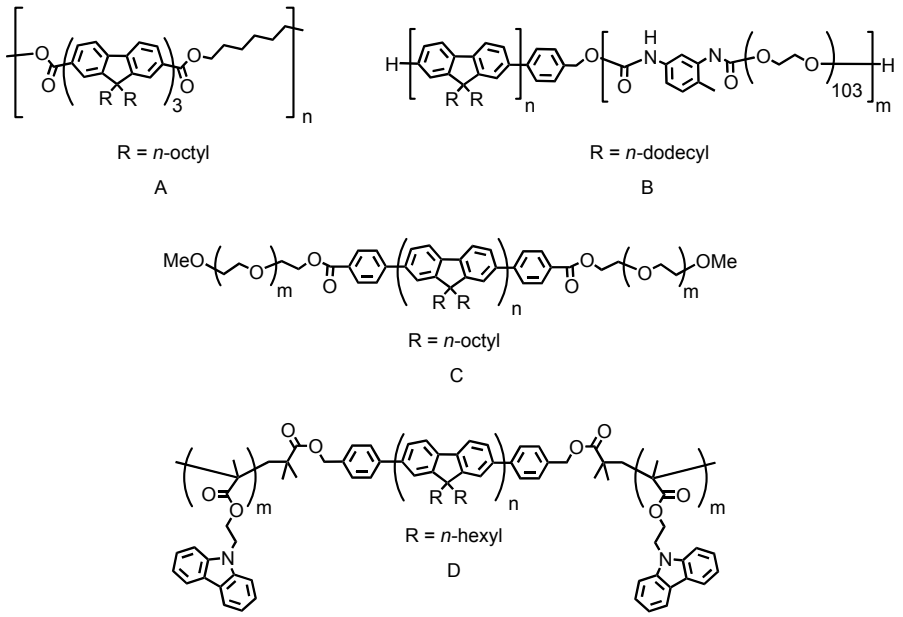

Figure 1.18. Rod-coil copolymers bearing fluorene segments.

1.11. Conjugated Polymers and Oligomers as Scaffolds for Sensory Applications

The fascinating properties conjugated materials present have led to significant interest in extending their use to sensor applications; McQuade, Pullen, and Swager issued a comprehensive review of this field in 2000.[123] The first CP modified for sensing purposes is believed to be the PT shown in Figure 1.19, synthesized by Roncali and coworkers in 1989.[124, 125] Roncali used cyclic voltammetry to study the response the pendant ether-substituted PT gave in the presence of complexing ions such as Bu_4N^+ and Li^+. Ion concentration in solution was found to impact the

conformation of the polymer backbone in the film, and modification of the glycol ether to a crown ether moiety allowed the polymer to display ion selectivity.

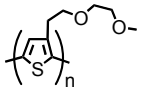

Figure 1.19. The glycol ether-substituted PT synthesized and studied by Roncali.[124, 125]

Conjugated macromolecules, oligomers and polymers present multiple avenues for sensing. First, they can display changing electronic character as detected by conductivity or potentiometry measurements. Sensing is then determined by an increase (generally dubbed "turn-on" sensing) or decrease ("turn-off" sensing) in the electrochemical signal as the analyte concentration is increased. The classical example of this method of sensing by a CP is that of *n*-doped polyacetylene, which was found by André to undergo a dramatic (~10^4) increase in conductivity upon dipping into THF followed by solvation of Na^+.[126]

A second method of sensing takes advantage of the colorimetric properties of conjugated materials. This pathway relies on the changing conformations CPs, for example, can display upon favorable interaction with an analyte, and as described in Section 1.3, the conformation of a CP affects its conjugation length, which determines its band gap properties. Kolushiva and Jelinek recently reported the use of poly(diacetylene) as the chromic component in a system designed for recognition of a peptide sequence by bovine serum albumin.[127] Regarding polyfluorene-based colorimetric sensing, Zhang and Ma used coordination-induced conformational changes in poly(bipyridine-*alt*-9,9-dihexylfluorene) and poly(phenanthroline-*alt*-9,9-dihexylfluorene) (Figure 1.20a) to show sensitivity to Ag^+, Zn^{2+}, Cr^{2+}, Mn^{2+}, and Sn^{2+}.[128] The

absorption spectrum of poly(phenanthroline-*alt*-9,9-dihexylfluorene) with increasing Sn^{2+} concentration is shown in Figure 1.20b.

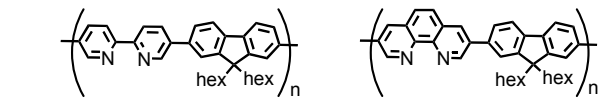

(a) (b)

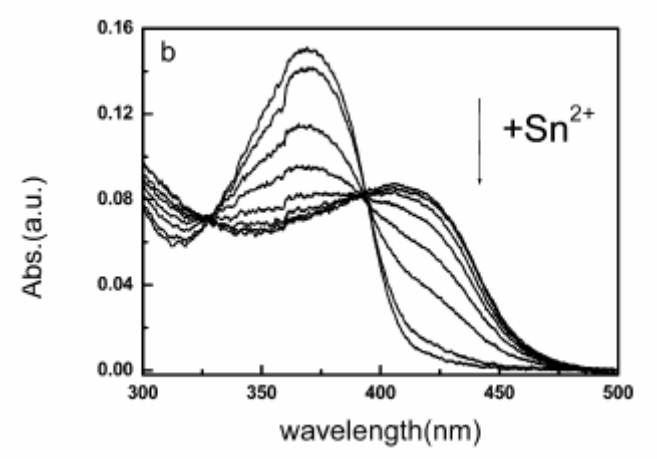

(c)

Figure 1.20. Zhang's poly(bipyridine-*alt*-9,9-dihexylfluorene) (a) and poly(phenanthroline-*alt*-9,9-dihexylfluorene) (b). (c) Absorption spectra of (b) at increasing concentration of Sn^{2+} (from top to bottom at 425 nm). Figure 20c is from Zhang, M.; Lu, P.; Ma, Y.; and Shen, J. *J. Phys. Chem. B* **2003**, *107*, 6535-6538.

Fluorescence response constitutes a third method of sensing by conjugated materials. Fluorescence spectrophotometry is inherently sensitive, and the potential for signal amplification by efficient energy transfer events makes this approach very attractive for turn-on sensor applications. Among the myriad conjugated materials developed for this purpose, polyfluorenes have been successfully implemented. This is evidenced by the imidazole-functionalized PF shown in Figure 1.21a, which Pei used for enhanced turn-off detection of Cu^{2+} in solution. This contrasted markedly with the polymer's response to treatment with solutions of Ag^{+}, Cd^{2+}, Co^{2+},

Cr^{3+}, Fe^{2+}, Mn^{2+}, Ni^{2+}, Pb^{2+}, and Zn^{2+}, which gave little or no quenching of the polymer's photoluminescence (Figure 1.21b).[129] Zhou, Wang and coworkers used a similar turn-off approach in their study of phosphonate-functionalized polyfluorenes, which selectively detected Fe^{3+} (Figure 1.21c).[130] And in a third example, Bazan and Liu used a water soluble statistical copolyfluorene to enable detection of single-stranded DNA (Figure 1.22a).[131] This implementation involved the turning off of photoluminescence emission associated with PF upon increasing the ss-DNA concentration in solution. However, the fluorescence response attributed to the 2,1,3-benzothiodiazole moiety exhibited a turn-on response to ss-DNA; this was observed as a more prominent green emission upon increasing the concentration of ss-DNA (Figure 1.22b).

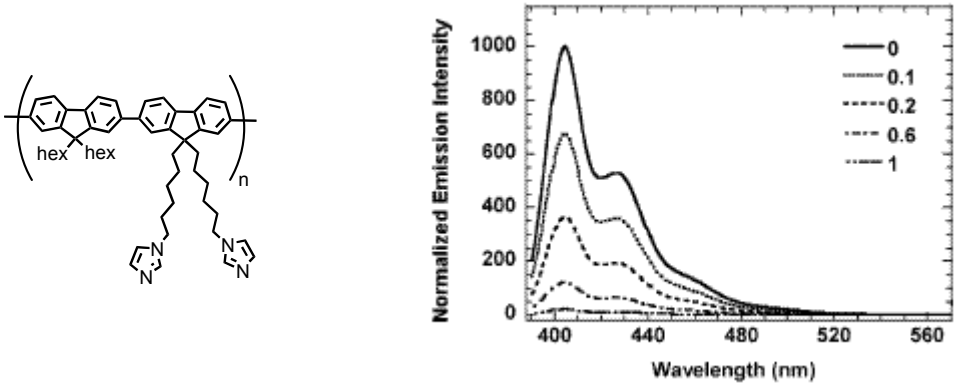

(a) (b)

Figure 1.21. (a) The imidazole-functionalized copolyfluorene synthesized by Zhou. (b) The fluorescence titration of the polymer in (a) upon addition of Cu^{2+}. Figure 21b is from Zhou, X.-H.; Yan, J.C.; and Pei, J. *Macromolecules* **2004**, *37*, 7078-7080.

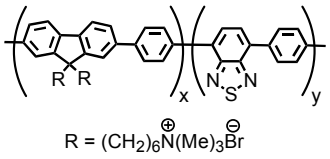

(a)

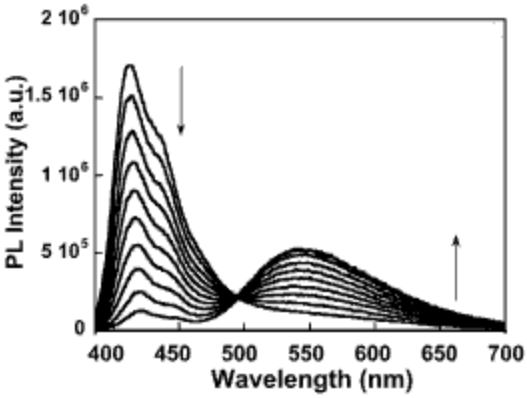

(b)

Figure 1.22. (a) The water soluble poly(fluorene-co-phenylene-co-benzothiadiazole) synthesized by Liu. (b) The fluorescence spectra of the polymer in (a) upon addition of ss-DNA. Figure 22b is from Liu, B.; and Bazan, G.C. *J. Am. Chem. Soc.* **2004**, *126*, 1942-1943.

2. Synthesis of PFMs

2.1. Overview

The synthesis of poly(9,9-dihexylfluorene-*multiblock*-polymethylene)s (PFMs) is presented. The product polymers are engineered to have completely-defined chemical compositions along their backbones, meaning that for each poly(*9,9*-dihexylfluorene-*mb*-polymethylene) synthesized, the fluorene and methylene segment lengths are predetermined, are entirely alternating, and are readily tailored using synthetic chemical strategies to give a copolymeric library. The library is comprised of PFMs having fluorene segments lengths of one, two, three, four, seven, or eight and having methylene segment lengths of ten or eighteen.

2.2. Introduction

Copolymer preparation has traditionally revolved around the making of alternating, block or random polymeric products (Figure 2.1). Examples of these are the poly(thiophene-*alt*-perfluoroarene)made by Wang and Watson[132] (Figure 2.2, top), the poly(ethylene glycol-*block*-*N*-vinylformamide) made by Shi, Chapman and Beckman (middle),[133] and the poly(*para*-*n*-butylstyrene-*co*-styrene) made by Thomann, Kressler, and coworkers (bottom).[134] A distinction can be made in comparing these copolymer architectures–the first case provides for exact structure-property relationships but lacks synthetic ease in varying chemical composition using the same alternating pattern. The opposite can be said to be true for the latter two cases, which

incorporate greater flexibility in terms of chemical composition but sacrifice a degree of certainty in relating structure to observed properties.

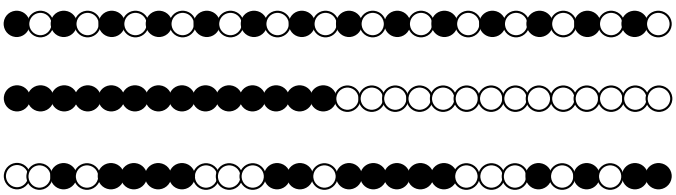

Figure 2.1. Conceptual representations of alternating (top) block (middle), and random (bottom) copolymer architectures.

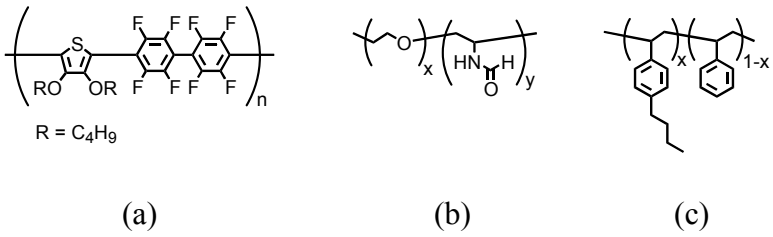

(a) (b) (c)

Figure 2.2. (a) Wang's poly(thiophene-*alt*-perfluoronaphthalene. (b) Shi's poly(ethylene glycol-*b*-N-vinylformamide. (c) Thomann's poly(*p*-*n*-butylstyrene-*co*-styrene).

The polymers herein were made for the purpose of combining compositional flexibility with exact structure-property relationships (Figure 2.3). As is discussed in Section 2.4, varying the segment lengths of each type of repeat unit allows for a library of copolymers to be produced. We designate the copolymers Repeating Sequence Copolymers (RSCs) to note the exactness of their repeating diblock composition. As already discussed in Sections 1.1.3-1.1.7, the fluorene repeat unit presents a number of interesting properties and as such lends itself to the preparation of this library. As a polycyclic aromatic compound, fluorene represents the classical rod-like repeat unit. In contrast, the methylene repeat unit ($-CH_2-$), which is a flexible chain, can be considered to be the prototypical coil repeat unit. The alkyl subunit also differs from the π-

conjugated and dopable polyfluorene in that it is insulating. Along these lines, Radano, Meijer and coworkers recently prepared PT-*b*-PE for the purpose of examining the morphology of a copolymer containing semiconducting and insulating blocks.[135]

Figure 2.3. RSC architecture.

2.3. Strategy Towards Polymer Synthesis

Our preparation of poly(fluorene-*mb*-polymethylenes (PFMs) proceeds according to the strategy depicted in Scheme 2.1. This approach involves the synthesis of a family of symmetrically substituted monodisperse oligofluorenes (A). Each oligofluorene is then converted to a polymerizable segmer compound (B) by the attachment of alkyl chains bearing polymerizable end-groups. Upon polymerization and another step to remove residual functionality left by coupling, a completely regular RSC of fluorene and methylene (C) is produced. Varying *x* and *y* in the chemical composition of B is necessary in order to arrive at a library of PFMs.

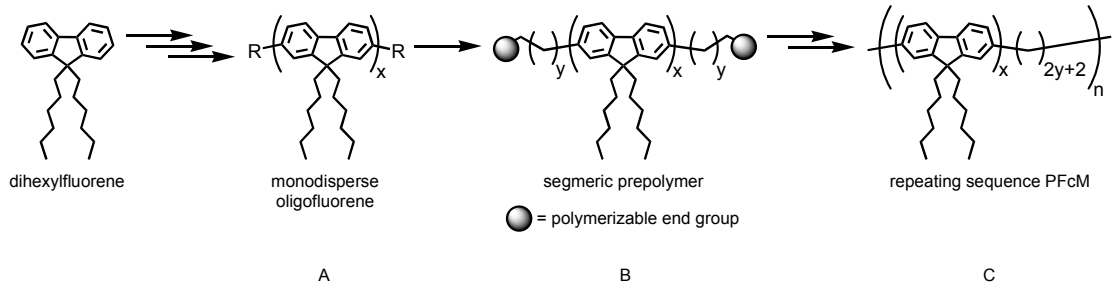

Scheme 2.1. General approach to PFMs.

Given that the modular route to monodisperse oligofluorenes had been previously developed by Geng, Chen, and coworkers,[85] new steps leading to the synthesis of each PFM that required development in our labs were (1) a Suzuki reaction used to couple olefin-terminated substituents to the oligomers, (2) an olefin metathesis reaction employed in the polymerization, and (3) a hydrogenation of residual olefin groups to yield the final RSC. These reactions are described as in Section 2.3.1 and Section 2.3.2.

2.3.1. The Suzuki Reaction

The Suzuki reaction is an extremely versatile method for catalytic C-C bond formation. As shown in Scheme 2.2, this reaction uses catalytic amounts of a Pd^0 species to mediate the coupling of an aryl, vinyl, or alkyl halide to an electrophilic boron partner. This component may be aryl, vinyl, or alkyl substituted. This reaction has found a myriad of uses in organic synthesis, and a review on this chemistry was recently written by Miyaura and Suzuki.[136]

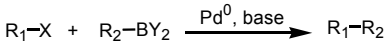

Scheme 2.2. Suzuki reaction.

The generally accepted mechanism (Figure 2.4) of this transformation begins by oxidative addition of Pd^0 into the carbon-halogen bond (A) of the organohalide. This addition initially yields the *cis*-palladium complex, though this rapidly converts to the *trans*-complex pictured. Reaction with base (typically an alkali metal alkoxide or carbonate) yields the oragnopalladium(II) alkoxide intermediate (B), which undergoes transmetallation with the

boron-ate complex to form the organopalladium intermediate (C). Reductive elimination of the desired product restores the catalyst to Pd^0, and the cycle begins anew (D).

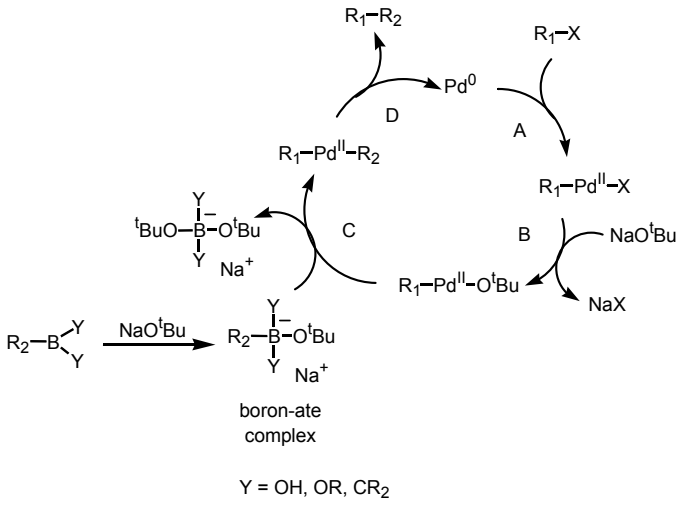

Figure 2.4. Mechanism of Pd^0-catalyzed Suzuki coupling.

We exploited the Suzuki coupling of halide-functionalized fluorenes with alkyl boranes to prepare the segmer prepolymer compounds as depicted in Scheme 2.3. A close precedent for the alkyl-fluorenyl coupling exists in the literature. In 1989, Peifer, Milius, and Alt reported the coupling of 2,7-diiodo-9*H*-fluorene with an ω-alkenyl derivatized 9-borabicyclo[2.2.1]nonane (9-BBN, Scheme 2.4).[137] Peifer did not, however, extend the reaction to oligofluorenes.

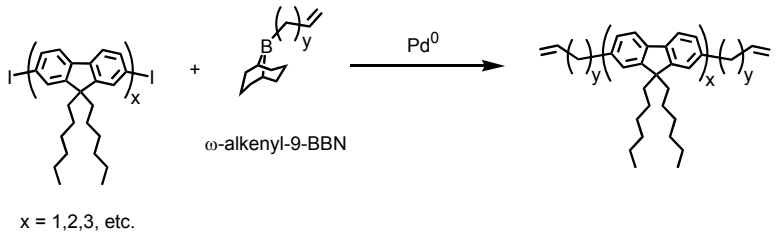

Scheme 2.3. Use of the Suzuki reaction to yield segmer compounds.

Scheme 2.4. Peifer's preparation of 2,7-dioct-7-enyl fluorene.

2.3.2. ADMET Polymerization and Subsequent Hydrogenation

The segmers bear terminal olefin functional groups which are polymerizable using the Acyclic Diene Metathesis (ADMET) reaction protocols established by Wagener.[138, 139] Metathesis is described in further detail in Chapter 4. The most commonly employed precatalysts for the ADMET reaction are the Grubbs-I and Grubbs-II Ru-carbenes shown in Figure 2.5. We elected to use the Grubbs-I catalyst over the Grubbs-II catalyst for these polymerizations in part because the former was shown by Lehman to be the more effective metathesis catalyst at moderate temperatures (30-45° C).[140] Performing ADMET polymerizations at moderate temperture is important to minimize competing olefin isomerization events, which are undesirable for the purpose of making a completely sequence-regular RSC. Were a segmer to undergo an isomerization event followed by ADMET, it would introduce a defect into the polymer backbone in the form of a shortened alkyl segment length. Furthermore, the Grubbs-II catalyst is known to promote a significant degree of olefin isomerization in ADMET polymerizations.[141]

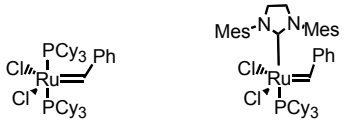

(a) (b)

Figure 2.5. Grubbs-I (a) and Grubbs-II (b) catalysts.

The Grubbs-I catalyst acts as a formal CHR (or in some cases (CR_2) transfer agent. In the absence of a driving force, metathesis is an equilibrium-controlled reaction. As shown in Figure 2.6, then, an incoming olefin, activated by coordination to the metal center, can undergo a [2+2] cycloaddition (A) to generate a metallocyclobutane intermediate. Cycloreversion can yield either the original substrate, $R_2HC{=}CHR_3$ or the metathesis product, $R_1HC{=}CHR_3$ (B), depending on which bonds are broken.

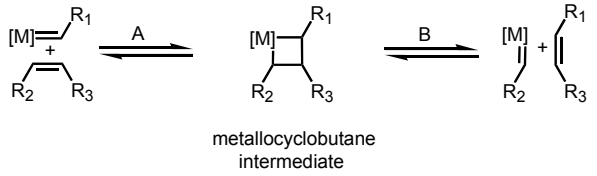

Figure 2.6. Principle of olefin metathesis.

The detailed pathway for ADMET is depicted in Figure 2.7. Following phosphine dissociation from the metal and coordination of olefin to the metal (A), conversion to the metallocyclobutane intermediate occurs (B). The productive cycloreversion (C) generates the active chain-growth polymerization agent. Reaction with a second olefin (D) produces a new metallocyclobutane which undergoes cycloreversion to yield the coupled product (E). The catalytic cycle proceeds (F) to give a transient ruthenium methylidene species, which can reassociate and dissociate phosphine (G), or coordinate an olefin and undergo another [2+2]

cycloaddition (H). This metathesis event generates ethylene byproduct (I) and generates the active catalytic species, ready for another coupling (J).

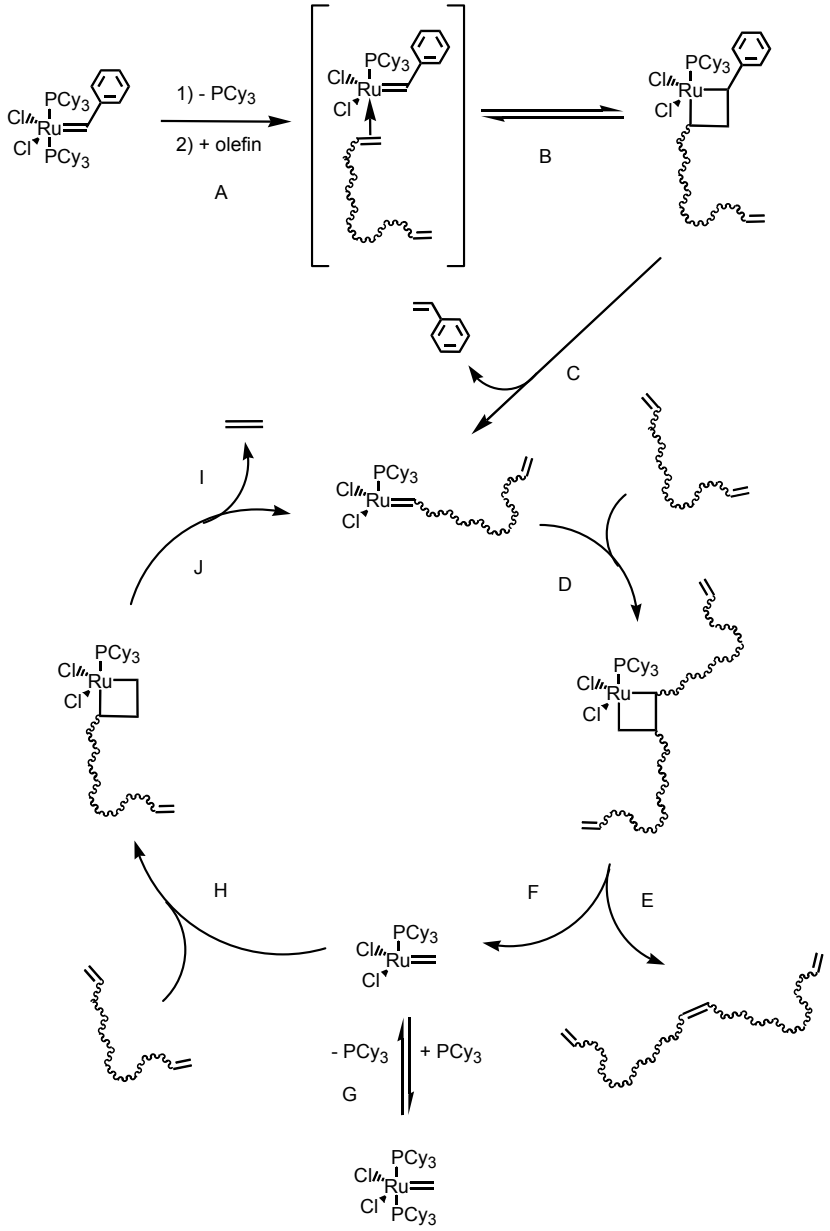

Figure 2.7. Mechanism of Grubbs-I catalyzed ADMET polymerization.

ADMET polymerization occurs under reduced pressure to drive the reaction through the entropically favorable condensation of ethylene. A wide variety of chemical motifs have been

incorporated into polymer backbones using the ADMET reaction. Some examples include hydrocarbons, ethers, amino acids, esters, carbonates, boronates, dichlorosilanes, phosphazenes, and phenylenevinylenes.[142]

As the products of ADMET polymerization possess unsaturation along the polymer backbone, it is necessary to submit the polymer to hydrogenation to obtain an RSC that bears no double bonds along the alkyl chain (Figure 2.8). Fortunately, a protocol has been developed by Watson and Wagener[143] that allows for a one-pot polymerization-hydrogenation reaction sequence. This reaction exploits the fact that the decomposition product of the Grubbs-I catalyst, a ruthenium hydride compound, is itself a hydrogenation catalyst.

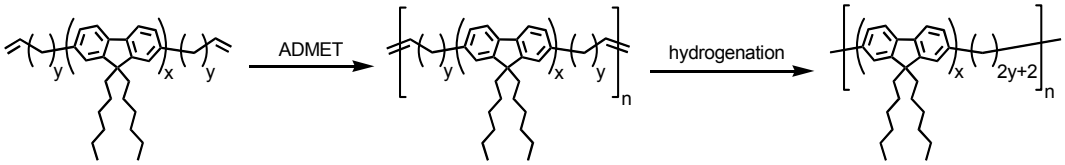

Scheme 2.5. ADMET polymerization/hydrogenaton route to RSCs.

2.4. Naming Conventions

As the full names are unwieldy and compound numbers are not descriptive, polymers and segmers have been given unique designations. Polymers are referred to in the text as **PFxMy**, where **P** indicates the material is a polymer, **x** indicates the fluorene (**F**) sequence length, and **y** indicates the methylene (**M**) sequence length. For example, **PF3M10** refers to the RSC having fluorene sequence lengths of three and methylene sequence lengths of ten. Segmer compounds are similarly identified as **SFxMy**, where **S** indicates the compound is a segmer, **x** denotes the

fluorene sequence length, and **y** denotes the methylene sequence sequence length *of the resultant RSC*. For example, the segmer compound polymerized to yield **PF3M10** is called **SF3M10**, even though it possesses 12 aliphatic carbons. Synthetic intermediates are assigned incremental numbers as per the normal convention.

2.5. Results

2.5.1. Synthesis of Poly(monofluorene-*mb*-methylene)s

To probe the practicality of the approach outlined in Section 2.3, monofluorenyl PFMs were initially synthesized. To generate segmer "arms" for M10 and M18 RSCs, terminal dienes 1,5-hexadiene and 1,9-decadiene were each subjected to hydroboration by 9-BBN to yield ω-alkenyl boranes **1** and **2**, respectively (Scheme 2.6).[144]

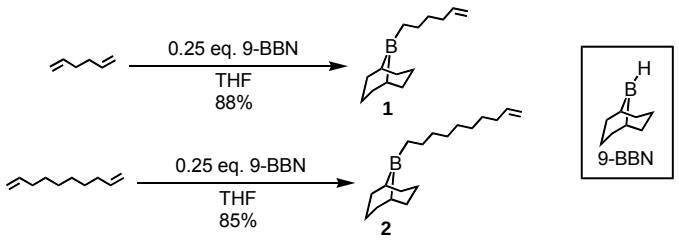

Scheme 2.6. Reaction of 9-BBN with 1,5-hexadiene and 1,9-decadiene.

To generate the fluorenyl partner, a two-fold hexylation of fluorene was first performed according to the protocol given by Ranger[58] to give 9,9-dihexylfluorene (**3**) in 88% yield after recrystallization (Scheme 2.7). Dihexylfluorene **3** was then electrophilically iodinated at carbons 2 and 7 to produce 2,7-diiodo-9,9-dihexylfluorene (**4**) in 91% yield after recrystallization. The

Suzuki reaction was used to couple borane **1** or **2** with diiododihexylfluorene **4**, producing monofluorenyl segmers **SF1M10** and **SF1M18** in yields of 46% and 49%, respectively. Substantial amounts of mono-coupled product were recovered from these reactions (typically ~20%). Attempts to increase the yield of this reaction by supplying excess borane reagent (~4 eq) and by running the reaction at temperatures greater than 23 °C were made, though neither approach increased the yield of desired product. Furthermore, performing the reaction at 45° C or greater led to significant isomerization of terminal olefin groups to more thermodynamicaly stable internal olefins. This isomerization was undesirable as the polymerization of these segmers would introduce errors in the backbone sequence. Despite the modest yields, suitable quantities of **SF1M10** and **SF1M18** were isolated, paving the way for ADMET polymerization.

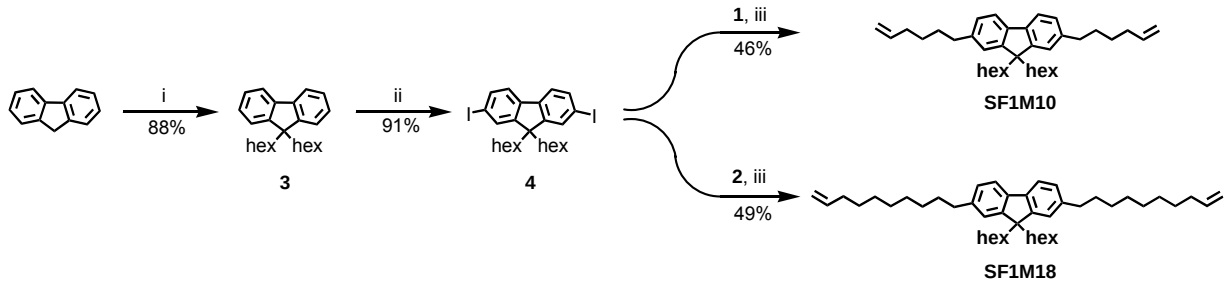

Scheme 2.7. Preparation of monofluorenyl segmers. (i) BuLi, bromohexane, THF, -78° C to RT, 4 h. (ii) I_2, H_5IO_6, H_2SO_4, AcOH, H_2O, 80° C, 3h. (iii) K_2CO_3, $Pd(Cl)_2(PPh_3)_2$, DMF, 8h.

The segmers **SF1M10** and **SF1M18** were polymerized using 2.5 mol% Grubbs-I catalyst in Ph_2O solvent (Scheme 2.8). The high boiling diphenyl ether solvent facilitates the polymerization by reducing the viscosity delaying gelation relative to the neat reaction.

The ADMET polymers **5** and **6** were generally not isolated. Instead the gelled reaction mixture was simply diluted with toluene and subjected to the hydrogenation conditions: 160-180

psi H_2, 80° C and 10-12 eq SiO_2. **PF1M10** and **PF1M18** were recovered as amorphous solids by precipitation into acetone in yields of 83% and 63%, respectively.

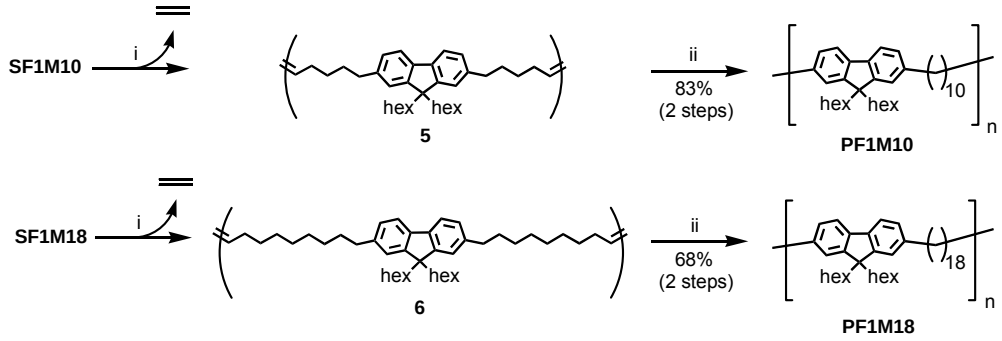

Scheme 2.8. Synthesis of **PF1M10** and **PF1M18**. (i) 2.5 mol% Grubbs-I catalyst, Ph_2O, RT to 45° C. (ii) SiO_2, H_2, PhMe, 80° C, 2 d.

2.5.2. Synthesis of Poly(bifluorene-*mb*-methylene)s

Having validated the synthetic approach for the preparation of monofluorenyl PFMs, the task of making PFMs incorporating longer oligofluorene segment lengths was undertaken.The route to segmeric bifluorenes **SF2M10** and **SF2M18** is shown in Scheme 2.9.

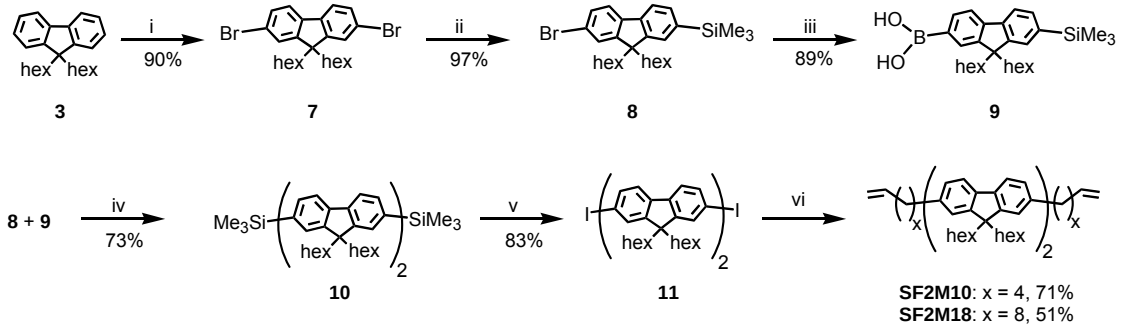

Scheme 2.9. Synthetic route to bifluorene segmers. (i) Br_2, $FeCl_3$, $CHCl_3$, 0° C to RT 3 h. (ii) BuLi, TMSCl, THF, -78° C to RT, 30 min. (iii) BuLi, $B(O^iPr)_3$,THF, -78° C to RT, 8 h. (iv) 3 mol% $Pd(PPh_3)_4$, 2 M $Na_2CO_{3(aq)}$, PhMe, 90° C, 2 d. (v) ICl, DCM, 0° C to RT, 15 min. (vi) **1** or **2**, $Pd(Cl)_2(Ph_3)_2$, K_2CO_3, DMF, PhMe, 40° C, 8 h.

Bromination of dihexylfluorene **3** yielded 2,7-dibromo-9,9-dihexylfluorene **7** in 90% yield after recrystallization. A synthetic sequence reported by Geng and coworkers was then used,[85] beginning with the desymmetrization of compound **7** by lithium-halogen exchange to give 2-bromo-7-trimethylsilyl **8** as a colorless oil in 97% yield after chromatography. A second lithium-halogen exchange followed by treatment with triisopropyl borate converted **8** to 2-trimethylsilylfluorenyl boronic acid **9**. Compound **9** was recovered as a white flaky solid in 89% yield after chromatography. An aryl-aryl Suzuki coupling protocol was employed to couple fluorenyl intermediates **8** and **9** using 3 mol% $Pd(PPh_3)_4$ to produce bis-trimethylsilylbifluorene **10** in 73% isolated yield. The trimethylsilyl groups in **10** serve as latent halogens, and as such bifluorene **10** underwent rapid electrophilic substitution upon treatment with ICl to yield 2,7'-diiodobifluorene **11** in 85% yield after column chromatography. Bifluorene **11** was thereafter treated with ω-alkenyl-9-BBN **1** or **2** using alkyl-aryl Suzuki coupling protocols modified slightly from those used in the preparation of **SF1M10** and **SF1M18**. Specifically, a 1:1 v/v mixture of DMF and PhMe was used; this permitted solvation of **11** at room temperature. Additionally, mild heat (40° C) was required as coupling did not occur at room temperature. Bifluorenyl segmer compounds **SF2M10** and **SF2M18** were recovered as viscous oils in 71% and 51% yield, respectively.

SF2M10 and **SF2M18** were then subjected to ADMET polymerization followed by hydrogenation (Scheme 2.10). Following precipitation of the polymers into acetone, **PF2M10** and **PF2M18** were recovered as colorless glassy solids in 60% and 61% yield, respectively.

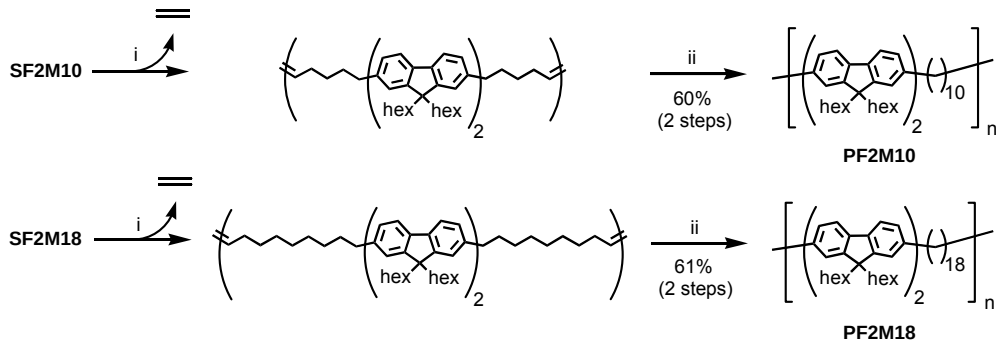

Scheme 2.10. Synthesis of **PF2M10** and **PF2M18**. (i) 2.5 mol% Grubbs-I catalyst, Ph_2O, RT to 45° C. (ii) SiO_2, H_2, PhMe, 80° C, 2 d.

2.5.3. Synthesis of Poly(terfluorene-*mb*-methylene)s

The pathway to the synthesis of PFMs possessing terfluorene moieties began with the preparation of terfluorenyl segmers. This route is given in Scheme 2.11. The synthesis began with the two-fold Suzuki coupling of diiodofluorene **4** with fluorenylboronic acid **9** to produce 2,7”-trimethylsilylterfluorene **12** in 55% yield. A small quantity (8 – 10%) of bifluorene **13** was also recovered. Worth noting is the use of tetra-*n*-butylammonium bromide ($^nBu_4NBr$, or TBABr) as a phase-transfer catalyst. The employment of $^nBu_4NCl$ for this same purpose was reported by Thiem, Stroreigl and coworkers[145] conceivably for two reasons. First, because the reaction is biphasic, the base necessary to turn the catalytic cycle over must do so after first crossing from H_2O into the organic solvent, PhMe. Base also aids in the converison of the boronic acid to the boron-ate complex. It follows that the likelihood of both of these events occurring increases dramatically with the use of a quaternary alkylammonium cation, which can act to shuttle the base into the organic phase of the reaction.

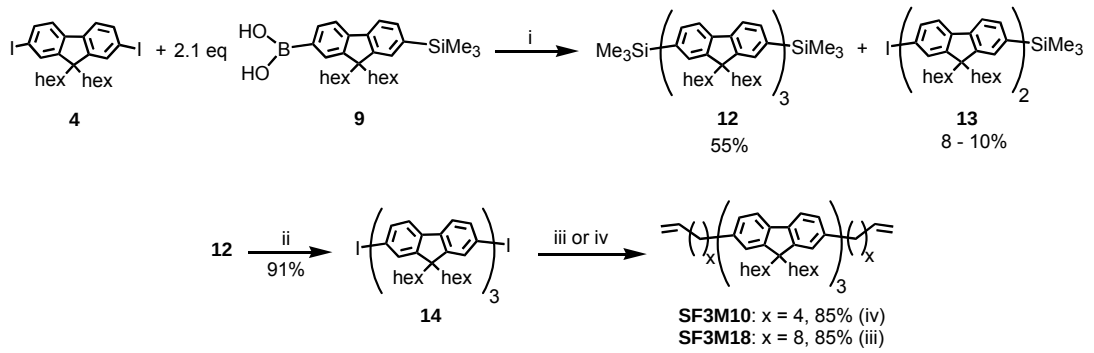

Scheme 2.11. Synthetic route to terfluorene segmers. (i) TBABr, 3 mol% $Pd(PPh_3)_4$, 2 M $K_2CO_{3(aq)}$, PhMe, 90° C, 12 h. (ii) ICl, DCM, 0° C to RT, 15 min. (iii) **2**, $Pd(Cl)_2(Ph_3)_2$, K_2CO_3, DMF, PhMe, 40° C, 8 h. (iv) **1**, $Pd(Cl)_2(Ph_3)_2$, 2M $K_2CO_{3(aq)}$, PhMe, 45° C, 8 h.

Upon isolation of bis-silated intermediate **12**, substitution of both trimethylsilyl groups for iodo groups proceeded rapidly (15 min) and in high yield (91%) to give 2,7"-diiodoterfluorene **14** as a white solid. This terfluorene intermediate was appropriately derivatized by Suzuki coupling with borane **1** or **2**.

Reactions to produce terfluorene segmers **SF3M10** and **SF3M18** were performed using two sets of reaction conditions which proved equally suited to generating the desired product. As in the synthesis of the bifluorene segmers, **SF3M18** was prepared using borane **2**, 4 mol% $Pd(Cl)_2(PPh_3)_2$ and K_2CO_3 in 1:1 DMF/PhMe at 40° C. Following column chromatography, **SF3M18** was recovered as a colorless, glassy solid in 85% yield.

SF3M10 was prepared using conditions adapted from aryl-aryl Suzuki couplings, and as such **SF3M10** was synthesized by reaction of diiodoterfluorene **12** with borane **1**, TBABr, 4 mol% $Pd(Cl)_2(PPh_3)_2$, aqueous K_2CO_3 and PhMe. Whereas aryl-aryl coupling to produce **12** was carried out at 90° C, this reaction proceeded at 45° C, which reflects the enhanced reactivity of trialkyl boranes relative to boronic acids and esters in Pd^0-catalyzed reactions. **SF3M10** is thereafter recovered as a colorless glassy solid in 85% yield. The isolated yields for **SF3M10** and **SF3M18** are an improvement over mono- and bifluorenyl segmer syntheses and suggest that the

coupling sites on oligofluorene substrates achieve electronic isolation at suitably long segment lengths.

SF3M10 and **SF3M18** were then subjected to ADMET polymerization-hydrogenation (Scheme 2.12). Following precipitation of the polymers into acetone, **PF3M10** and **PF3M18** were recovered as flaky white solids in 70% and 72% yield, respectively.

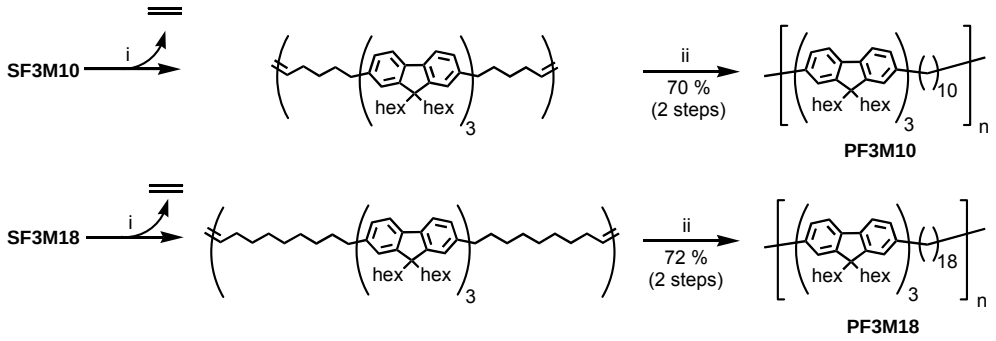

Scheme 2.12. Synthesis of **PF3M10** and **PF3M18**. (i) 2.5 mol% Grubbs-I catalyst, Ph_2O, RT to 45° C. (ii) SiO_2, H_2, PhMe, 80° C, 2 d.

2.5.4. Synthesis of Poly(quaterfluorene-*mb*-methylene)s

Preparation of quaterfluorene-containing PFMs began, as before, with assembly of the appropriate monodisperse oligofluorene. As shown in Scheme 2.13, Pd^0-catalyzed coupling using excess (2.1 eq) dibromofluorene **7** and boronic acid **9** generated bromobifluorene **15** as the major product in 59% isolated yield. Terfluorene **12**, the product of two-fold coupling, was recovered in 12% yield. It is worth noting that this reaction is essentially the same coupling reaction as that given in Scheme 2.11 in which **12** was isolated as the major product. In this case, however, the bifluorenyl product is desired, so reaction conditions given by Geng[85] were used in order to favor monocoupled intermediate **15**. Specifically, Geng's protocol used boronic acid **9**

as the limiting reagent to hinder two-fold coupling. Production of terfluorene **12** was further hindered by the absence of TBABr under these reaction conditions.

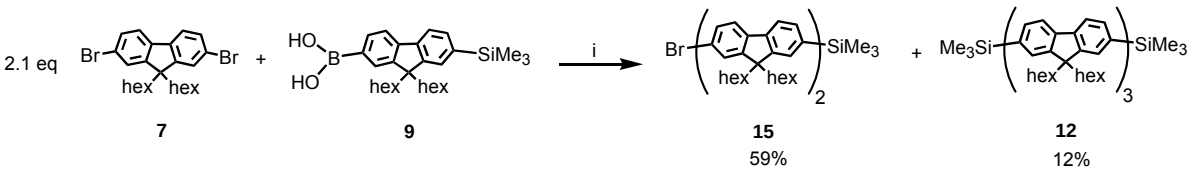

Scheme 2.13. Synthetic route to bromobifluorenyl intermediate **15**. (i) 3 mol% $Pd(PPh_3)_4$, 2 M $Na_2CO_{3(aq)}$, PhMe, 90° C, 2 d.

Subsequent elaboration on bifluorene **15** required the preparation of bis(1,5-cyclooctadiene)nickel(0) from $Ni(acac)_2$ according to the method used by Krysan and Mackenzie.[146] $Ni(COD)_2$ was isolated as a tan solid in 85% yield after recrystallization (Scheme 2.14).

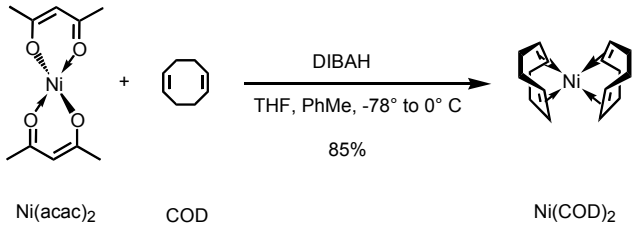

Scheme 2.14. Preparation of $Ni(COD)_2$.

Bromobifluorene **15** was then homocoupled using $Ni(COD)_2$ under Yamamoto coupling conditions to produce bistrimethylsilyl quaterfluorene **16** in 84% yield (Scheme 2.15). Iodination of compound **16** gave quaterfluorene **17** as a pale yellow solid in 87% yield following purification by column chromatography. Quaterfluorenyl segmers **SF4M10** and **SF4M18** were thereafter prepared using borane **1** or **2**, 4 mol% $Pd(Cl)_2(PPh_3)_2$ and K_2CO_3 in 1:1 DMF/PhMe at

40° C. **SF4M10** was recovered as a white solid in 90% yield, and **SF4M18** was recovered as a white solid in 82% yield.

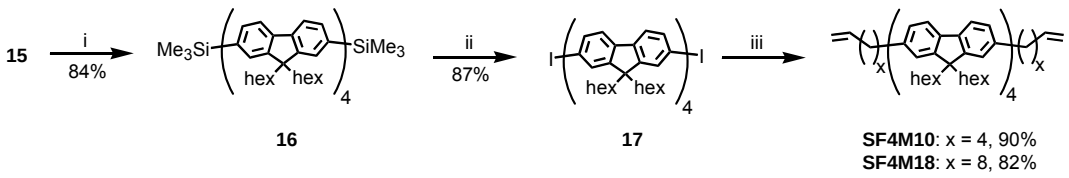

Scheme 2.15. Synthetic route to quaterfluorenyl segmers. (i) $Ni(COD)_2$, bipy, COD, PhMe, 80° C, 2 d. (ii) ICl, DCM, 0° C to RT, 15 min. (iii) **1** or **2**, $Pd(Cl)_2(Ph_3)_2$, K_2CO_3, DMF, PhMe, 40° C, 8 h.

Quaterfluorenyl segmers **SF4M10** and **SF4M18** were then subjected to ADMET polymerization-hydrogenation (Scheme 2.16). Following precipitation of the polymers into acetone, **PF4M10** and **PF4M18** were recovered as flaky white solids in 68% and 59% yield, respectively.

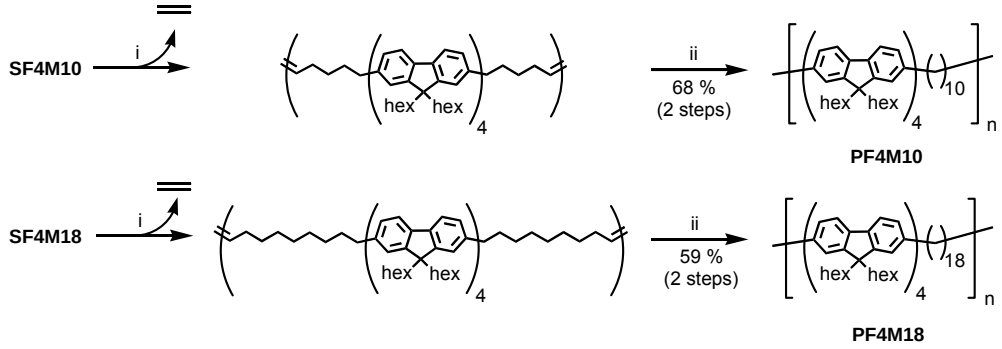

Scheme 2.16. Synthesis of **PF4M10** and **PF4M18**. (i) 2.5 mol% Grubbs-I catalyst, Ph_2O, RT to 45° C. (ii) SiO_2, H_2, PhMe, 80° C, 2 d.

2.5.5. Synthesis of a Poly(heptafluorene-*mb*-methylene)

The preparation of a PFM possessing 9,9-dihexylfluorene segment lengths of seven was accomplished following the synthetic pathway shown in Scheme 2.17. Bromobifluorene **15** first underwent lithium-halogen exchange upon treatment with BuLi, and addition of triisopropyl borate produced bifluorenyl boronic acid **18** in 79% yield following column chromatography. Bifluorene **18** was then treated with 0.45 eq terfluorene **14** using Pd^0 coupling conditions to produce bis(trimethylsilyl) heptafluorene **19**. This compound was recovered as a pale green solid in 59% yield after purification by column chromatography. As before, substitution of the trimethylsilyl groups for iodines proceeded rapidly to give bis(iodo) heptafluorene **20** in 95% yield following purification by silica gel filtration. Heptafluorenyl segmer **SF7M18** was prepared from **20** using borane **2**, 4 mol% $Pd(Cl)_2(PPh_3)_2$, TBABr, 2M $K_2CO_{3(aq)}$ and PhMe at 40° C. **SF7M18** was thereafter recovered as a pale green solid in 78% yield after column chromatography.

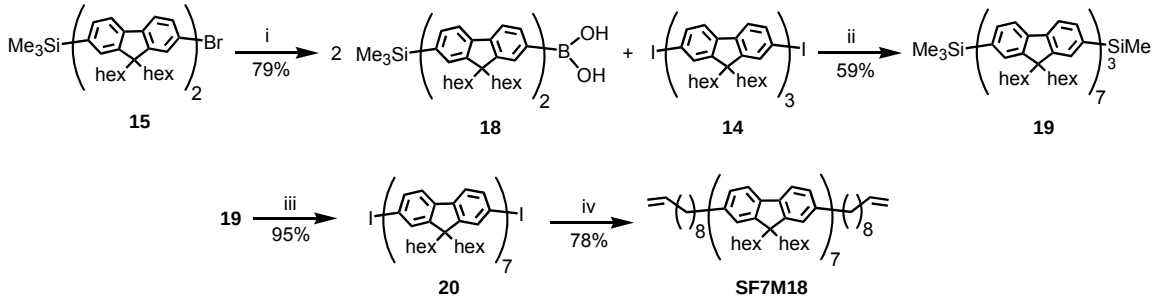

Scheme 2.17. Synthetic route to heptafluorene segmer **SF7M18.** (i) BuLi, $B(O^iPr)_3$, THF, -78° C to RT, 8 h. (ii) TBABr, 4 mol% $Pd(PPh_3)_4$, 2 M $K_2CO_{3(aq)}$, PhMe, 90° C, 12 h. (iii) ICl, DCM, 0° C to RT, 15 min. (iii) **2**, $Pd(Cl)_2(Ph_3)_2$, 2M $K_2CO_{3(aq)}$, PhMe, 45° C, 8 h.

SF7M18 was then subjected to ADMET polymerization-hydrogenation (Scheme 2.18). Following precipitation, **PF7M18** was recovered as a tan powder in 59% yield.

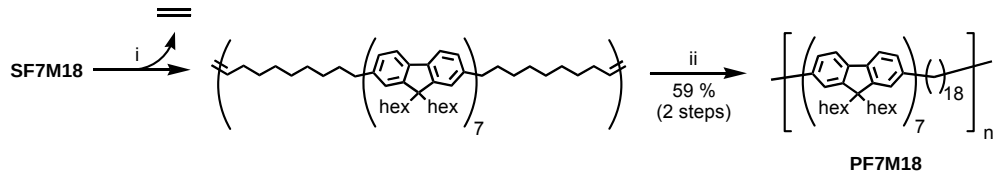

Scheme 2.18. Synthesis of PF7M18. (i) 2.5 mol% Grubbs-I catalyst, Ph_2O, RT to 45° C. (ii) SiO_2, H_2, PhMe, 80° C, 2 d.

2.5.6. Synthesis of a Poly(octafluorene-*mb*-methylene)

The preparation of a PFM possessing 9,9-dihexylfluorene segment lengths of eight was accomplished following the synthetic pathway shown in Scheme 2.19. Bifluorenyl boronic acid **18** was treated with 0.45 eq quaterfluorene **17** under Pd^0-catalyzed coupling conditions to produce bis(trimethylsilyl) octafluorene **21**. This compound was recovered as a pale green solid in 52% yield after purification by column chromatography. Substitution of the trimethylsilyl groups for iodines proceeded rapidly to give bis(iodo) octafluorene **22** in 92% yield following purification by column chromatography. Octafluorenyl segmer **SF8M18** was prepared from **22** using borane **2**, 4 mol% $Pd(Cl)_2(PPh_3)_2$, TBABr, 2M $K_2CO_{3(aq)}$ and PhMe at 40° C. **SF8M18** was thereafter recovered as a pale green solid in 71% yield after column chromatography.

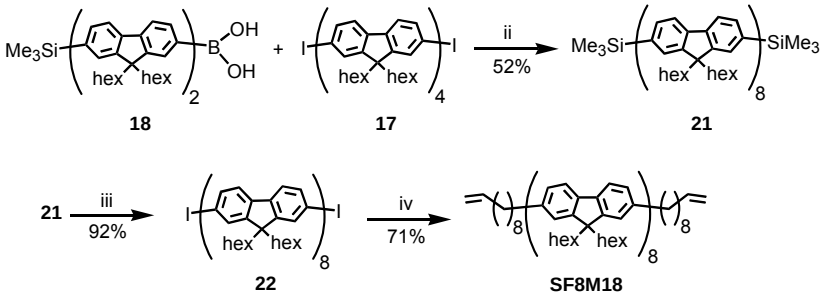

Scheme 2.19. Synthetic route to **SF8M18**. (i) BuLi, $B(O^iPr)_3$, THF, -78° C to RT, 8 h. (ii) TBABr, 4 mol% $Pd(PPh_3)_4$, 2 M $K_2CO_{3(aq)}$, PhMe, 90° C, 12 h. (iii) ICl, DCM, 0° C to RT, 15 min. (iii) **2**, $Pd(Cl)_2(Ph_3)_2$, 2M $K_2CO_{3(aq)}$, PhMe, 45° C, 8 h.

SF8M18 was then subjected to ADMET polymerization-hydrogenation (Scheme 2.20). Following precipitation of the polymer into acetone, **PF8M18** was recovered as a tan powder in 59% yield.

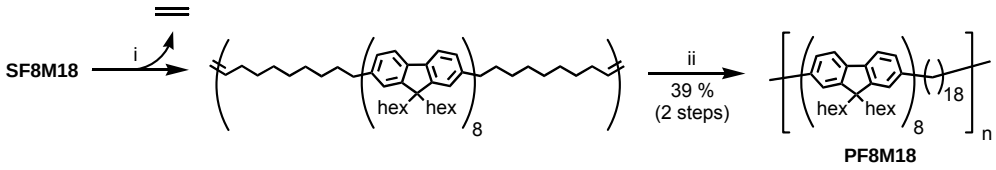

Scheme 2.20. Synthesis of **PF8M18.** (i) 2.5 mol% Grubbs-I catalyst, Ph_2O, RT to 45° C. (ii) SiO_2, H_2, PhMe, 80° C, 2 d.

2.5.7. Synthesis of Poly(9,9-dihexylfluorene)

The homopolymer, poly(9,9-dihexylfluorene) (**PDHF**), was synthesized using the Ni^0-promoted homocoupling of 2,7-dibromo-9,9-dihexylfluorene **7** reported by Kreyenschmidt, Miller and coworkers (Scheme 2.21).[89] End-capped and non-capped samples of PDHF were prepared. **PDHF-capped** was end-capped with phenyl groups by the addition of bromobenzene into the reaction after 2 d. Two samples of non-capped PDHF were prepared and studied these

are referred to as **PDHF-old** and **PDHF-new** for reasons described in Section 3.6. The polymers were each recovered by precipitation into a 1:1:1 mixture of con. HCl, acetone and MeOH followed by 2-3 reprecipitations into a 1:1 mixture of acetone and MeOH. **PDHF-capped** was recovered as a tan powder in 74% yield, while non-capped **PDHF-old** and **PDHF-new** were recovered as tan powders in 57% and 53% yield, respectively.

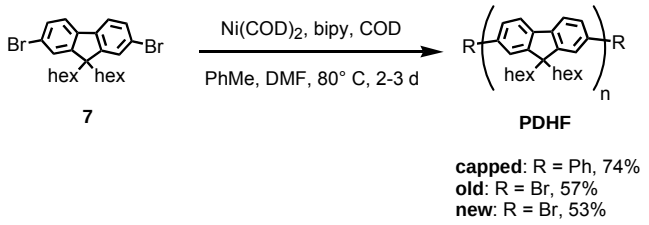

Scheme 2.21. Synthesis of PDHF samples.

2.5.8. Use of NMR Spectroscopy for Confirmation of Structural Regularity in PFMs

^{1}H NMR spectroscopy served as a diagnostic tool for gauging the progress of substrates through the Suzuki reaction-ADMET polymerization-hydrogenation synthetic sequence. Figures 2.8-2.11 serve to illustrate this by showing the ^{1}H NMR spectra for diiodofluorene **4**, **SF1M10**, the ADMET polymer **5**, and **PF1M10**, respectively. In Figure 2.8, the ^{1}H NMR spectrum of diiodofluorene **4** has, as defining features, the chemical shift pattern for *n*-hexyl chains at C9 and an arene pattern consistent with 2, 7-substitution.

The conversion of 2,7-diiodofluorene **4** to **SF1M10** is marked by numerous features in the ^{1}H NMR spectrum (Figure 2.9). First, the triplet at δ 2.67 is consistent with the presence of

benzylic protons in the product. The multiplets at δ 4.95 and δ 5.78 indicate the presence of a terminal alkene functionality.

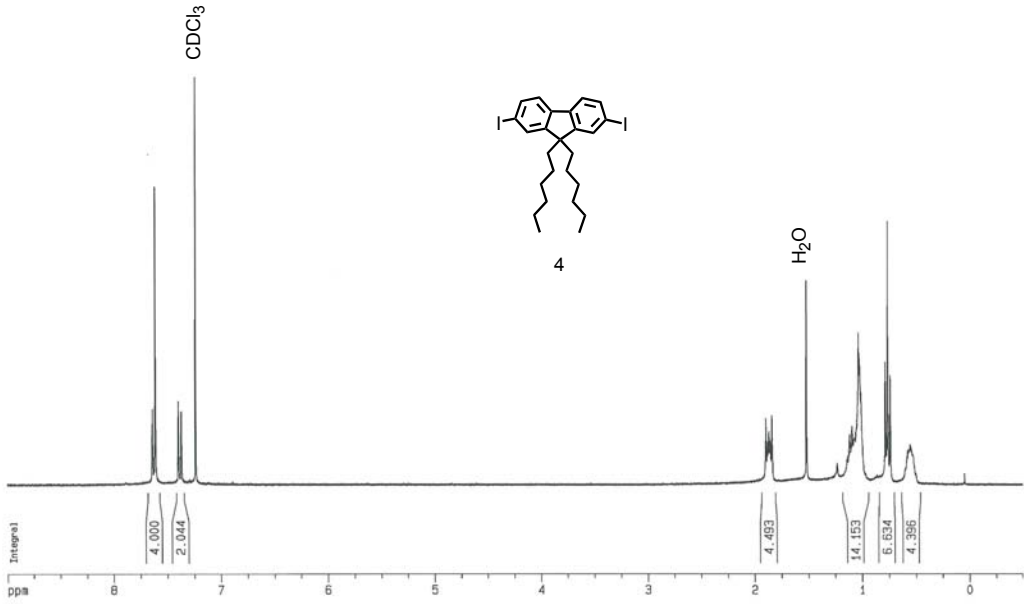

Figure 2.8. ^{1}H NMR spectrum of diiodofluorene **4** ($CDCl_3$).

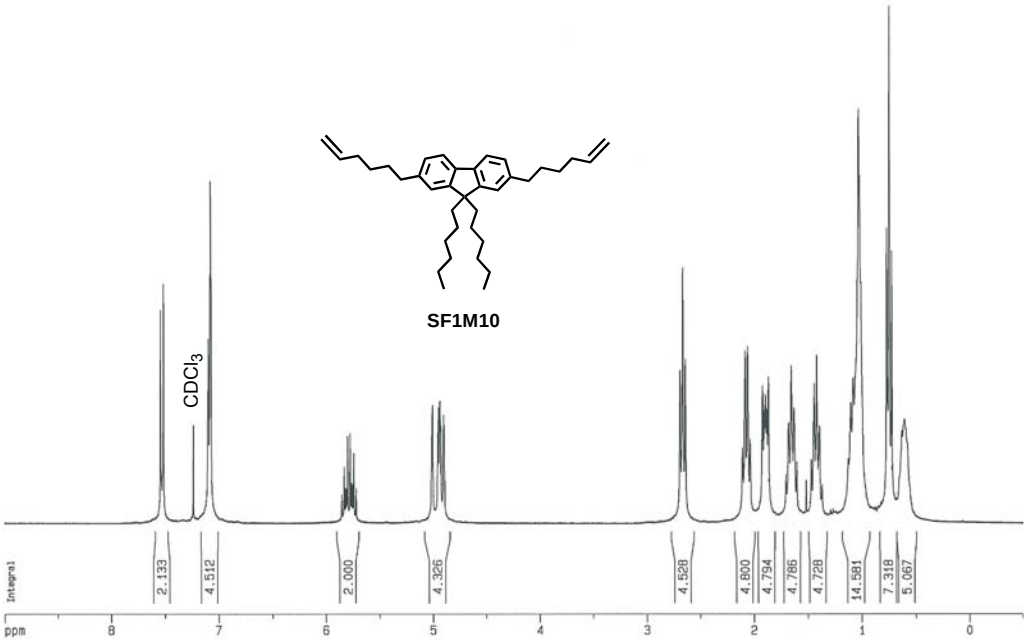

Figure 2.9. ^{1}H NMR spectrum of **SF1M10** ($CDCl_3$).

ADMET polymerization of **SF1M10** to **5** (Figure 2.10) is effectively monitored by ^{1}H NMR spectroscopy. The progress of this reaction is gauged by the disappearance of terminal olefin signals and the dominance of the internal olefin pattern. Monitoring the polymerization in this way ensures the production of polymer of suitably high DP. In this context, an aliquot of **5** showed DP = 42 by end-group analysis of its ^{1}H NMR spectrum. It should be noted that ADMET polymerizations were performed using diphenyl ether as solvent. This greatly complicates the aryl regions for the crude unsaturated polymers, as is evident upon inspection of the aryl region in Figure 2.10.

Hydrogenations of ADMET polymers can also be monitored by observing diagnostic changes in the ^{1}H NMR spectrum. In this instance the decrease of the olefinic signals indicates saturation of the alkyl segments in the polymer backbone (Figure 2.11). It is worth noting that the pattern in the aryl region in the product RSC is analogous to that of the parent segmer, as would be expected. Diphenyl ether is easily removed upon precipitation of the polymer.

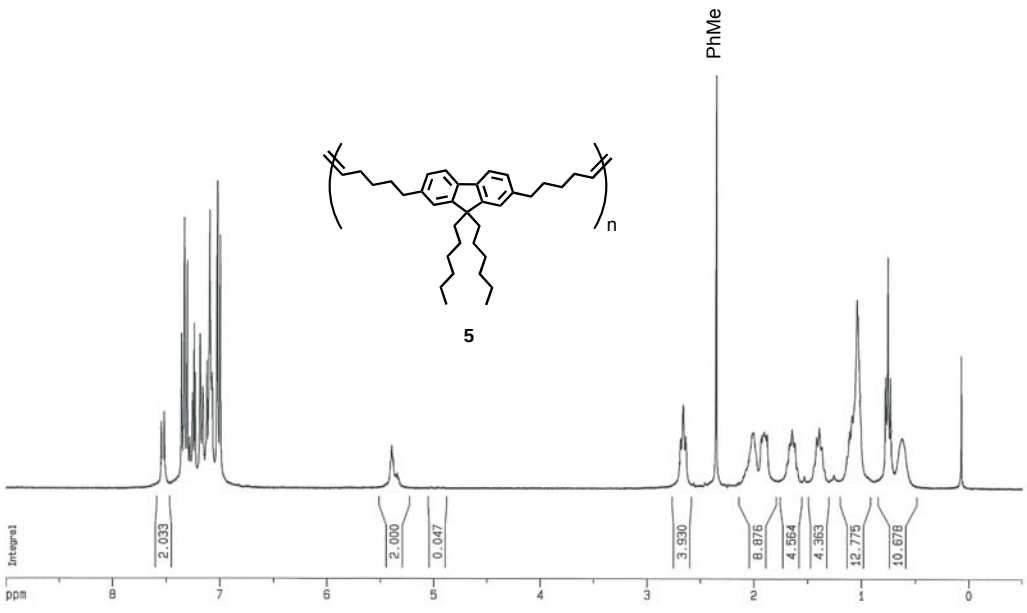

Figure 2.10. ^{1}H NMR spectrum of the crude ADMET polymer **5** generated from **SF1M10** ($CDCl_3$). The sample contains significant Ph_2O.

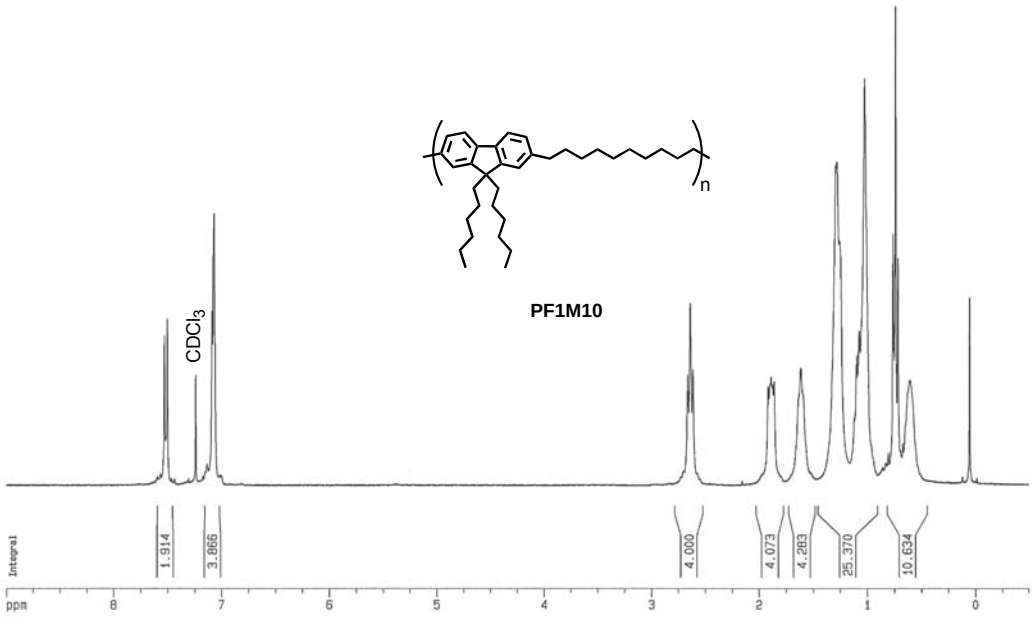

Figure 2.11. ^{1}H NMR spectrum of **PF1M10** ($CDCl_3$).

Characterization by ^{13}C NMR spectroscopy can also serve to confirm the structures of the intermediates and polymers. As an example, Figure 2.12 shows the ^{13}C NMR spectra of diiodoquaterfluorene **18** (top), **SF4M10** (middle), and **PF4M10** (bottom). The spectrum for diiodoquaterfluorene, like many oligofluorene intermediates, has a remarkably clear alkyl region (< δ 65). Though it possesses 56 aliphatic carbons, the eight *n*-hexyl chains are coincident and give the six chemical shifts furthest upfield. The quaternary carbons at C9 on the fluorene skeleton are found at δ 55.4 and δ 55.5, consistent with the slight difference in chemical environments between the internal and terminal fluorene units. The signal at δ 92.4 in the spectrum of **18** is assigned to the aryl carbon bearing the iodine substituent.

Upon coupling by the Suzuki reaction to give **SF4M10**, the chemical shift for C_{aryl}-I disappears and that for C_{aryl}-C_{benzyl} is observed at δ 138.5. Two more diagnostic chemical shifts worth noting are that for RHC=CH_2 (δ 114.4) and RHC=CH_2 (δ 138.9) on the terminal alkene.

ADMET polymerization followed by hydrogenation of **SF4M10** gives **PF4M10**, which is immediately characterizable by ^{13}C NMR spectroscopy for the disappearance of both olefinic carbon resonances. Additional ^{1}H and ^{13}C NMR spectra are included as Appendix A.

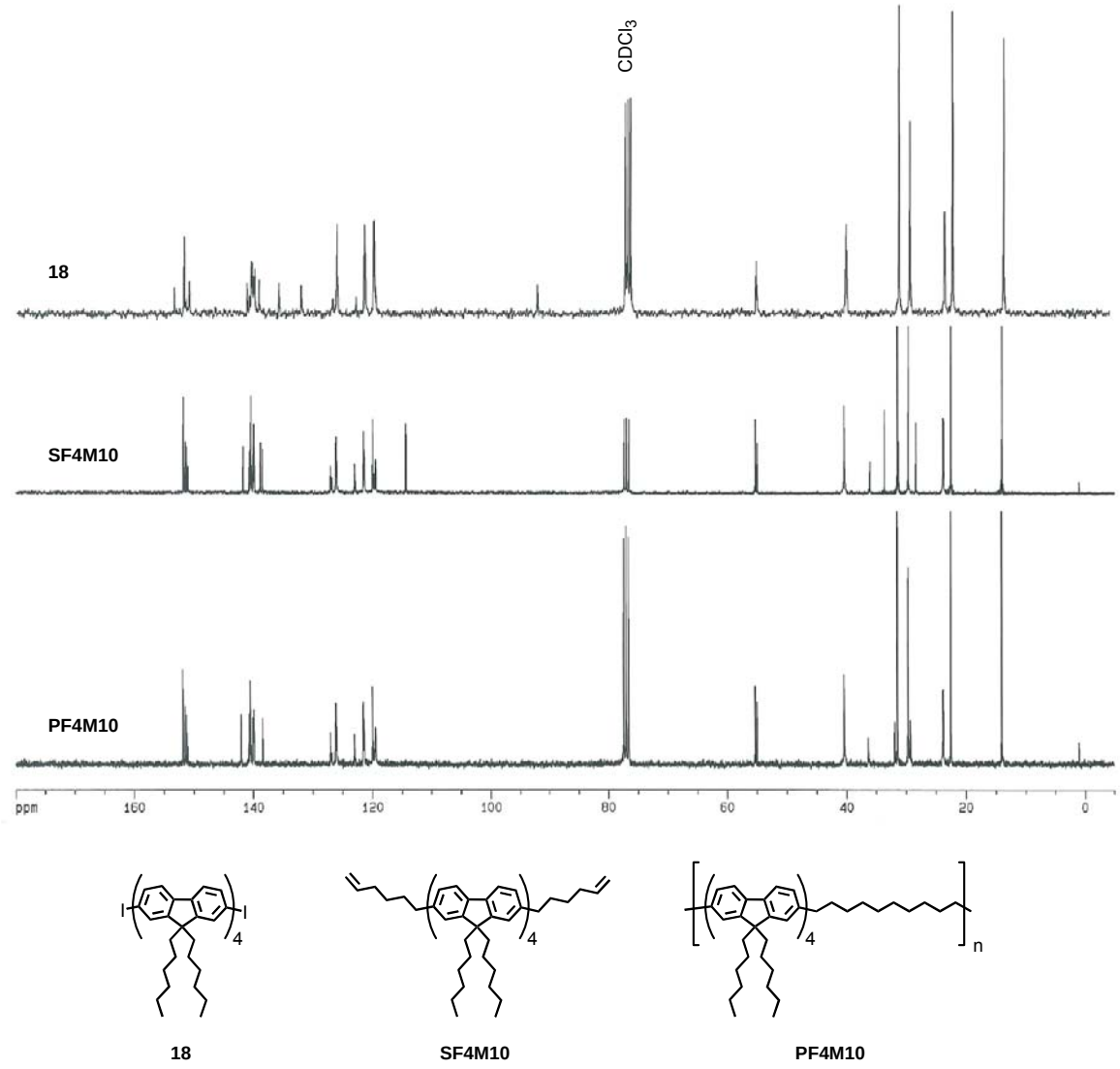

Figure 2.12. ^{13}C NMR spectra of quaterfluorene **18** (top spectrum), **SF4M10** (middle), and **PF4M10** (bottom, $CDCl_3$).

2.5.9. Crystal Structure of Bifluorene 10 by Determined X-Ray Diffractometry

An X-ray diffraction study of a single-crystal of bifluorene **10** provides some insight into the structures of the segmers comprising fluorene oligomers, despite the relatively poor quality of the data ($R_w = 0.23$). Particularly striking is the orthogonality of the alkyl chains relative to the plane of the fluorene rings. Although this geometry is necessitated by the fluorene structure, the conventional schematic representation of dialkylfluorenes as 2D objects can contribute to a mistaken impression that the alkyl groups extend away from the fluorene moiety in nearly the same plane rather than extending significantly above and below the plane. It should be noted that the poor quality of this structure is due mainly to disorder in these alkyl chains, a common problem in this type of molecule. The structure is pictured without thermal ellipsoids for the disordered carbons for reasons of clarity (Figure 2.13).

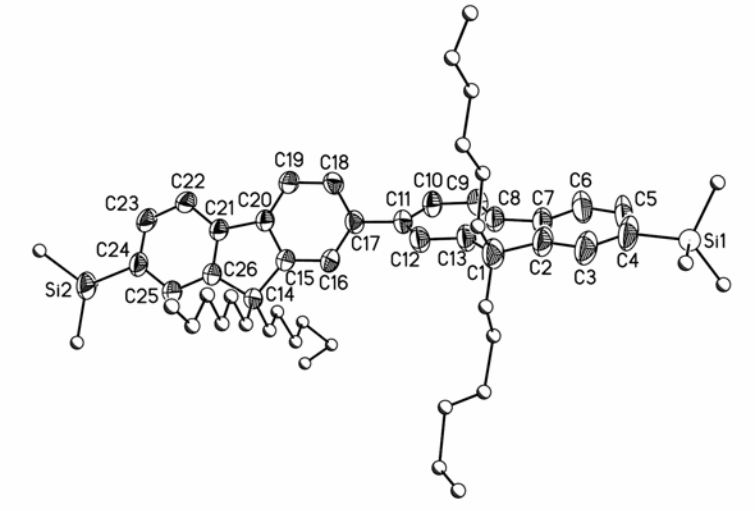

Figure 2.13. ORTEP rendering of bifluorene **10**.

The X-ray structure also gives some information about the conjugation within the fluorenes and between them. The presence of the C9 carbon serves to planarize the two phenyl rings relative to unbridged biphenyl groups. In particular, the dihedral angle between the phenyl groups within the fluorene is only 1.82°. The fluorene units, in contrast, are significantly twisted relative to each other (55.9°). While packing forces are dominant in the determination of this angle in the solid state crystal, it is well known that there are significant dihedral angles between arenes in polymeric materials. PF is known, for example, to exhibit a 15-24° angle between adjacent fluorene units.[50] Tables, including those specifying bond lengths and angles, can be found in Appendix B.

2.5.10. Gel Permeation Chromatography

PFMs were characterized by GPC in order to assess molecular weights M_n and M_w relative to PS standards. The data obtained are summarized in Table 2.1. Values of 7,000 – 36,000 were found for M_n, while values of 9,800 – 57,000 were found for M_w. PDIs ranged from 1.4–2.1 and DPs between 5 to 30 were determined. The majority of the polymers prepared exhibited monomodal distributions after isolation by precipitation. A typical GPC trace is shown for the case of **PF3M10** in Figure 2.14a. Polymers **PF4M10**, **PF4M18**, and **PF8M18** showed more complexity in their molecular weight distributions. The GPC trace for **PF4M10** is shown in Figure 2.14b. The polymodal character of these polymer samples are consistent with a lower DP and/or the formation of signifcant cyclic material. Molecular weights for **PF4M10** and **PF4M18** were in fact both low. Low MW in condensation polymerizations are usually due to the presence of small amounts of chain-terminating monofunctional monomer. Examples of likely chain

terminating species are shown in Figure 2.15. In preparing the segmer compounds, even trace amounts of impurities such as monocoupled segmer (Figure 2.15a) can act as chain-terminators. Also, additional deboronation/dehalogenation processes are known to occur in Suzuki reactions.[147] Dehalogenation in Pd-catalyzed reactions can be useful under certain circumstances.[148, 149] However, here this would "cap" the fluorene segment with hydrogen, resulting in another chain-terminator (Figure 2.15b).

	M_n[a]	M_w[a]	PDI	DP
PF1M10	14,000	30,000	2.1	28
PF2M10	9,200	17,000	1.9	11
PF3M10	26,000	44,000	1.7	22
PF4M10	7,000	9,800	1.4	5
PF1M18	16,000	33,000	2.1	30
PF2M18	13,000	21,500	1.7	15
PF3M18	13,000	20,000	1.5	11
PF4M18	7,600	10,600	1.4	5
PF7M18	36,000	57,000	1.6	14
PF8M18	14,000	22,000	1.6	5
PDHF-capped	22,000	56,000	2.6	66

[a] Molecular weights determined by comparison with polystyrene standards.

Table 2.1. GPC data for PFMs and **PDHF-capped**.

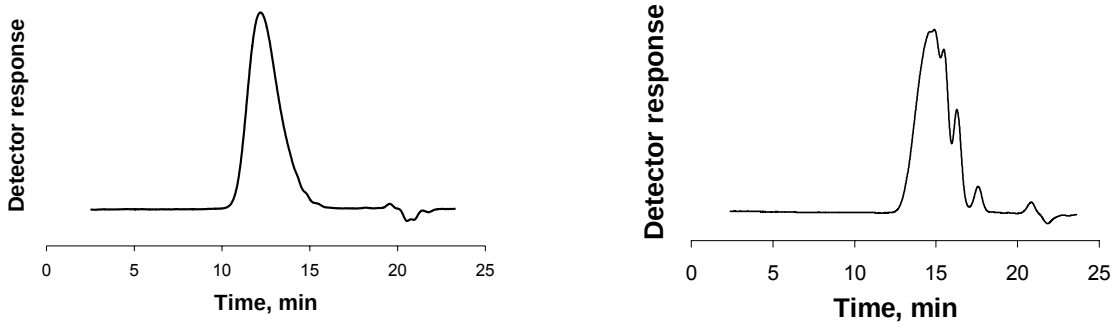

(a) (b)

Figure 2.14. GPC traces for **PF3M10** (a) and **PF4M10** (b).

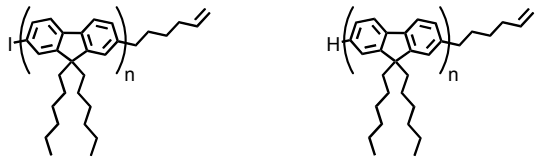

(a) (b)

Figure 2.15. ADMET polymerization chain terminators produced by incomplete coupling (a) and deboronation/dehalogenation (b) events.

2.5.11. Synthesis of a Terfluorene Substrate for Further Elaboration

A terfluorene substrate was synthesized for the application towards new chemical sensing materials as described in Section 1.1.11. Terfluorene **23** was prepared according to the reaction sequence shown Scheme 2.22. Fluorene was first iodinated at C2 and C7 to produce diiodofluorene **24** in 65% yield after recrystallization. Compound **24** was then alkylated using 1,6-dibromohexane to yield the 9,9-dibromohexyl-terminated intermediate **25** as a pale yellow solid in 52% yield after column chromatography. This compound was subjected to aryl-aryl Suzuki coupling conditions using fluorenyl boronic acid **9** to produce terfluorene **26**. The reaction to produce **26** involves the *in situ* formation of KI, which servef to transhalogenate a significant percentage of the terminal bromines. As such, intermediate **26** contained a mixture of bromo- and iodo-alkylated material. Regardless, it underwent electrophilic substitution to generate bis-iodo terfluorene **27**, which was treated with NaN_3 in DMF to yield diazide **28** as a pale yellow solid in 67% yield over three steps. Compound **28** was thereafter treated with $LiAlH_4$ under standard azide reduction conditions. In addition to reduction to the amine, treatment with

$LiAlH_4$ reductively dehalogenated **28**. Diamino terfluorene **23** was recovered as a flaky white solid in 87% yield.

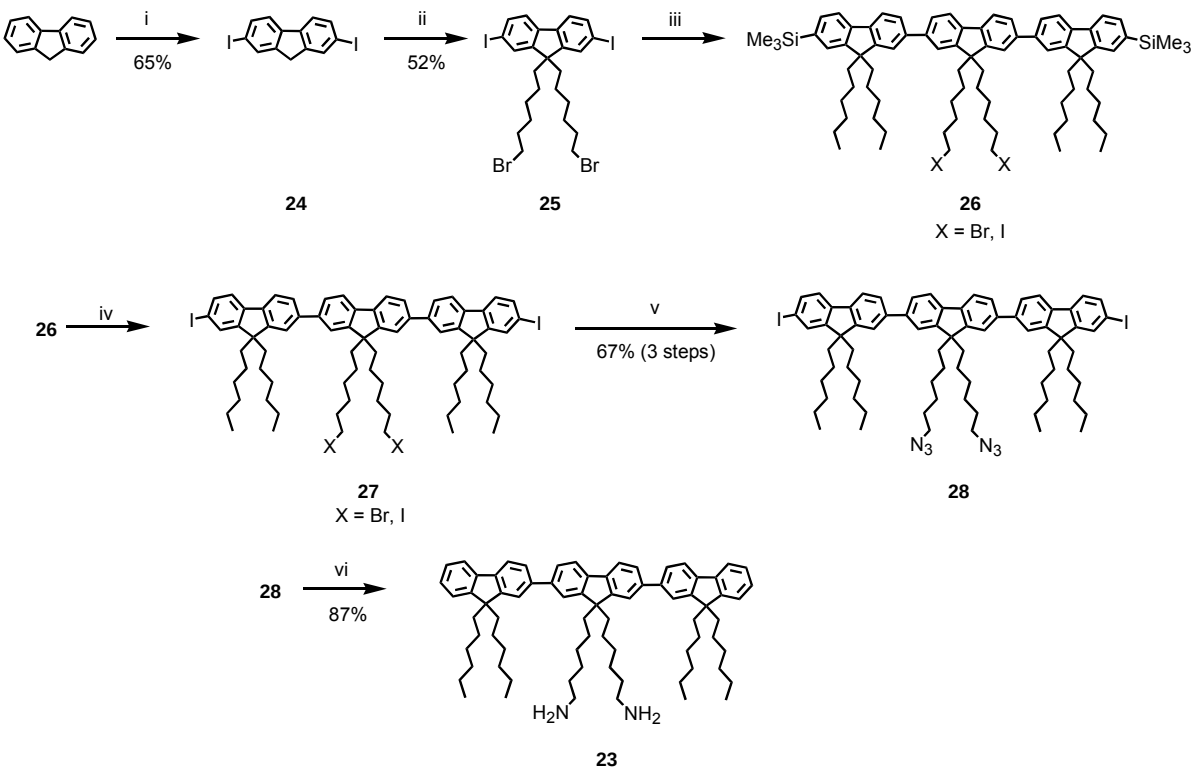

Scheme 2.22. The synthetic route to diamino terfluorene **23**. (i) I_2, H_5IO_6, H_2SO_4, AcOH, H_2O, 80° C, 3h. (ii) 1,6-dibromohexane, TBABr, KOH_{aq}. (iii) 2.1 eq **9**, 3 mol% $Pd(PPh_3)_4$, 2 M $K_2CO_{3(aq)}$, PhMe, 75° C, 12 h. (iv) ICl, DCM, 0° C to RT, 15 min. (v) NaN_3, DMF, 80° C, 12 h.

The amine functionalities on substrate **23** present opportunities for further modifications. Namely, **23** could be used to make amide linkages upon treatment with an anhydride. A potential implementation of **23** is shown in Scheme 2.23. Reaction of **26** with the bis-anhydride of diethylenetriaminepentaacetic acid (DTPA) under anhydride-opening conditions would generate the conjugated oligomer-macrocyclic hybrid **A**, which could facilitate efficient energy transfer to a coordinated metal ion (**B**) for sensing purposes as described in Section 1.1.11.

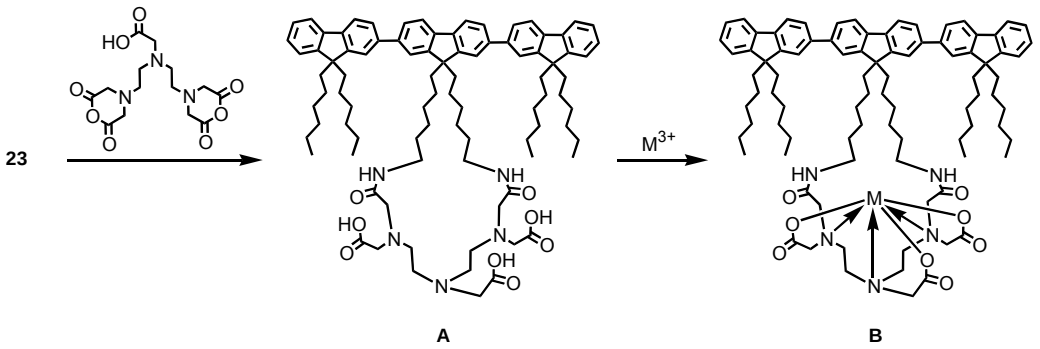

Scheme 2.23. A potential implentation of terfluorene **23**. In **B**, dative bonds from carbonyl oxygens to the coordinated M species have been omitted for the sake of clarity.

2.6. Experimental

2.6.1. General Methods

Ether and toluene were distilled under nitrogen from sodium. THF was passed through activated alumina using the SPS 400 (Innovative Technology, Inc.). CH_2Cl_2, 1,5-hexadiene and 1,9-decadiene were distilled under nitrogen from calcium hydride. $Pd(PPh_3)_4$ (Strem), $Pd(Cl)_2(PPh_3)_2$ (Strem), and bis(tricyclohexylphosphine)benzylideneruthenium(IV) dichloride (Aldrich) were commercially obtained and stored in a nitrogen-filled glove box. All other reagents were commercially obtained and used without further purification. ^{1}H- (300 MHz) and ^{13}C-NMR (75 MHz) spectra were recorded with Bruker spectrometers. Chemical shifts were referenced to residual ^{1}H or ^{13}C signals in deuterated solvents. Column chromatography was performed using Sorbent 60Å 40-63 μm standard grade silica. Gas chromatography-mass spectrometry (GC-MS) was performed on a Hewlitt Packard Series 5980 GC/5971 A MS with a Hewlitt Packard Series 1 column. Gas chromatography (GC) was performed on a Hewlitt Packard Series 6850 GC with a Hewlitt Packard Series 1 methyl siloxane column. High-

resolution mass spectra (HRMS) were obtained on a Fison VG Autospec in the Mass Spectral Facility of the University of Pittsburgh. Elemental analysis was performed independently by Atlantic Microlab, Inc., Norcross, Georgia.

2.6.2. X-ray Crystallography

Single-crystal X-ray crystallography was performed by Dr. Steven J. Geib at the University of Pittsburgh. Data was collected using a single crystal on a Bruker Smart Apex CCD diffractometer with graphite-monochromated MoKα (λ= 0.71073 A) radiation and MonoCap optics. The parameters used during the collection of diffraction data are summarized in Appendix X. Crystals were adhered to fine glass fibers with epoxy cement and placed in a cold N_2 stream (150 K) for data collection.

Unit-cell parameters, systematic absences, and photograph evidence indicated space group P 2_1/c. Unit-cell dimensions were derived from 90 data frames covering a wide range of reciprocal space. Data was collected with a crystal-detector distance of 5.0 cm using 0.3° ω scans and 20 s per frame. Data reduction was done with the SAINT program and data were corrected for absorption using the SADABS procedure. No significant crystal decay (<1%) was observed.

The structure was solved via direct methods, which located the positions of all non-hydrogen atoms which were refined anisotropically. Idealized atom positions were calculated for the hydrogen atoms (*d*-(C-H) = 0.96A, $U = 1.2U_{iso}$ of attached carbon).

Although final difference Fourier syntheses showed only chemically insignificant electron density, there was evidence of significant disorder in the alkyl chains. The final R_w of

0.23, which reflects this disorder, is sufficiently high that bond lengths and angles are likely to be inaccurate, particularly those near the γ-ends of the alkyl chains. An inspection of F_o vs. F_c values and trends based upon sin θ, Miller index, or parity group failed to reveal any systematic error in the data. All computer programs used in the data collection and refinements are contained in the Bruker program packages SMART, SAINT, and SHELXTL (version 6.10).

2.6.3. Preparation of Borane Reagents and Ni(COD)$_2$

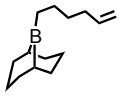

9-Hex-5-enyl-9-bora-bicyclo[3.3.1]nonane (1) *jecv3*: According to the method of Chung,[144] a flame-dried three-neck round-bottom flask was brought into a nitrogen-filled glove box 1, 5-hexadiene (65.0 mL, 0.548 mol, 4.0 eq) was added. 9-BBN (0.137 mol, added as a 0.5 M solution in THF) was added dropwise over 30 min, and the reaction mixture was allowed to stir for 8 h. Outside the glove box, the product was isolated by fractional distillation (60-62˚ C, 0.04 mmHg) under nitrogen as a colorless oil (28.7 mL, 88.4%). ^{1}H NMR (300 MHz, $CDCl_3$) δ 0.93 (q, 2 H), 1.33-1.84 (bs, 16 H), 2.07 (q, *J = 7.1 Hz*, 2 H), 4.95 (m, 2 H), 5.83 (m, *J = 7.0 Hz*, 1 H).^{13}C NMR (75 MHz, $CDCl_3$) δ 13.8, 19.0, 23.3, 24.0, 26.7, 28.0 (broad), 31.0 (broad), 32.2, 33.2, 33.8, 114.0, 139.2.

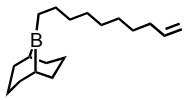

9-Dec-9-enyl-9-bora-bicyclo[3.3.1]nonane (2) *jecvi73/jecv8***:** According to the method of Chung,[144] a flame-dried three-neck round-bottom flask was brought into a nitrogen-filled glove box and 1, 9-decadiene (80.5 mL, 0.440 mol, 4.0 eq) was added. 9-BBN (0.110 mol, added as a 0.5 M solution in THF) was added dropwise over 45 min, and the reaction mixture was allowed to stir for 8 h. Outside the glove box, the product was isolated by fractional distillation (88-90˚ C, 0.015 mmHg) under nitrogen (28.3 mL, 85.2%). ^{1}H NMR (300 MHz, $CDCl_3$) δ 1.17-1.99 (b, 26 H), 2.02 (q, *J =6.8 Hz*, 2 H), 4.94 (m, 2 H), 5.78 (m, *J = 6.8 Hz*, 1 H). ^{13}C NMR (75 MHz, $CDCl_3$) δ 23.3, 24.5, 28.2 (broad), 29.0, 29.2, 29.6, 31.2 (broad), 33.0, 33.2, 33.9, 114.1, 139.2.

Bis(1,5-cyclooctadiene)nickel(0) *jecv1/jecv46***:** Using the method of Krysan and Mackenzie,[146] in a nitrogen-filled glove box a flame-dried Schlenk flask was charged with nickel(acetylacetonate) (35.00 g, 0.136 mol), 1,5-cyclooctadiene (97.8 mL, 0.546 mol, 4 eq), and 35 mL THF. The flask was brought out of the glove box and cooled to -78˚ C. DIBAH (0.341 mol, 2.5 eq, added as a solution in 1 M THF) was added dropwise over 3 h. The mixture was warmed to 0˚ C over 1 h and 250 mL diethyl ether was added. The contents were cooled to -78˚ C and the product was allowed to precipitate over 12 h. The majority of solvent was then removed by filter-tip cannula transfer. After further concentration under vacuum the reaction vessel was brought into the glove box. The product was isolated by filtration as a tan powder (32.098 g, 85.6 %). ^{1}H NMR (300 MHz, CD_2Cl_2) δ 2.34 (b, 8 H), 5.53 (b, 4 H). ^{13}C NMR (75 MHz, CD_2Cl_2) δ 27.9, 128.4.

2.6.4. Preparation of Fluorene Intermediates

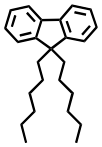

9,9-Dihexylfluorene (3) *jecv54***:** Using the method of Ranger *et. al.*,[58] fluorene (40.00 g, 0.241 mol) was dissolved in 450 mL anhydrous THF in a nitrogen atmosphere. After cooling to -78˚ C *n*-butyllithium in hexanes (318 mL x 1.6 M, 0.509 mol, 2.1 eq) was added over 4 h. After stirring for an additional 45 min, bromohexane (77.8 mL, 0.552 mol, 2.3 eq) was added dropwise over 30 min. After allowing the reaction mixture to warm to RT over 3h the contents were poured into water and extracted with diethyl ether (3 x 150 mL). The organic extracts were then combined, washed with brine, and then dried over $MgSO_4$. Solvent and excess bromohexane were removed by distillation under reduced pressure. The product was crystallized from hexanes at -30˚ C to yield the product as colorless crystals (70.37 g, 87.4%). ^{1}H NMR (300 MHz, $CDCl_3$) δ 0.57 (b, 4 H), 0.74 (t, 6 H), 1.93 (m, 4 H) 7.32 (m, 4 H), 7.69 (m, 2 H). ^{13}C NMR (75 MHz, $CDCl_3$) δ 13.9, 22.6, 23.8, 31.5, 40.4, 55.1, 119.6, 122.9, 126.7, 127.0, 141.2, 150.7. MS (EI), *m/z* 334 ($M^{\cdot+}$), 249, 179 (base), 165.

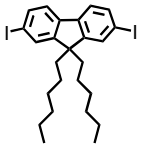

2,7-Diiodo-9,9-dihexylfluorene (4) *jecvi35***:** According to the method of Okumoto,[150] to a three-neck round-bottom flask equipped with a stir bar were added 210 mL AcOH, 40 mL H_2O, 7 mL concentrated H_2SO_4, H_5IO_6 (5.16 g, 0.023 mol, 0.5 eq), and I_2 (11.42 g, 1 eq). After stirring for 5

min 9,9-dihexylfluorene **3** (15.00 g, 0.449 mol) was added and the reaction mixture was heated to 80˚ C for 3 h. After cooling, solvent was removed under vacuum and hexanes were added to dissolve the crude product. The organic material was washed with aqueous K_2CO_3, aqueous $Na_2S_2O_3$, and brine before drying with $MgSO_4$. The organic phase was then concentrated and the product was purified by recrystallization to give a pale yellow powder (23.98 g, 91.1%). ^{1}H NMR (300 MHz, $CDCl_3$) δ 0.56 (b, 4 H), 0.76 (t, *J = 6.9 Hz*, 6 H), 1.07 (m, 14 H), 1.87 (m, J_1 = *8.4 Hz*, J_2 = *3.7 Hz*, 4 H), 7.37 (d, *J = 7.7 Hz*, 2 H), 7.61 (d, *J = 7.6 Hz*, 4 H). ^{13}C NMR (75 MHz, $CDCl_3$) δ 14.0, 22.5, 23.6, 29.5, 31.4, 40.1, 55.6, 93.1, 121.5, 132.1, 136.0, 139.8, 152.5. MS (EI), *m/z* 586 ($M^{\cdot+}$, base), 501, 417, 304, 189, 176.

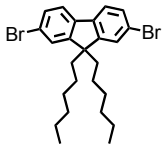

2,7-Dibromo-9,9-dihexylfluorene (7) *jecv57***:** Using the method of Price,[151] $FeCl_3$ (290 mg, 1.5 mol%) was added to a flame-dried flask in a nitrogen-filled glove box. The flask was brought out of the glove box and 9,9,-dihexylfluorene **3** (40.00 g, 0.120 mol) and 350 mL $CHCl_3$ were added under nitrogen. The contents were cooled to 0˚ C and the flask was wrapped in aluminum foil. Bromine (14.2 mL, 0.275 mol, 2.3 eq) was added dropwise over 20 min. After the flask was warmed to RT and stirred for 3 h, the contents were poured into aqueous $Na_2S_2O_3$. Upon discoloration of the organics, the aqueous phase was extracted with hexanes (3 x 150 mL). The organic extracts were combined, washed with brine,and dried over $MgSO_4$. After solvent removal under vacuum, the product was crystallized using hexanes at -30˚ C to yield the product as pale yellow crystals (52.86 g, 89.7%). ^{1}H NMR (300 MHz, $CDCl_3$) δ 0.56 (b, 4 H), 0.76 (t, 6 H), 1.11 (m, 14 H), 1.88 (m, 4 H), 7.42 (pd, 2 H), 7.48 (pd, 4 H). ^{13}C NMR (75 MHz, $CDCl_3$) δ

13.9, 22.5, 23.7, 29.6, 31.4, 40.2, 55.7, 121.1, 121.5, 126.2, 130.2, 139.1, 152.6. MS (EI), *m/z* 492 ($M^{\cdot+}$), 407, 323, 176 (base).

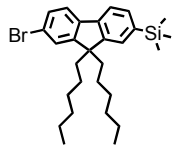

2-Bromo-7-trimethylsilyl-9,9-dihexylfluorene (8) *jecv61***:** According to the method of Geng,[85] 2,7-dibromofluorene **7** (32.09 g, 65.22 mmol) was added to a flame-dried Schlenk flask containing 470 mL anhydrous THF. After cooling to -78˚ C, *n*-butyllithium in hexanes (40.8 mL x 1.6 M, 65.3 mmol) was added over 2 h. After an additional 60 min, trimethylsilyl chloride (9.35 mL, 73.6 mmol, 1.13 eq) was added. The mixture was warmed to RT, stirred for approximately 45 min and poured into water prior to extraction with hexanes (3 x 100 mL). The organic extracts were combined and washed with brine, then dried over $MgSO_4$. After solvent removal under vacuum, the product was purified by column chromatography (silica, petroleum ether) to afford the desired product as a colorless oil (30.19 g, 95.5%). ^{1}H NMR (300 MHz, $CDCl_3$) δ 0.29 (s, 9 H), 0.61 (b, 4 H), 0.76 (t, 4 H), 0.87 (m, 4 H), 1.04 (m 14 H) 1.3 (b, 4 H), 1.9 (m, 4 H), 7.4 (m, 4 H), 7.5 (d, *J = 7.9 Hz*, 1 H), 7.6 (d, *J = 7.5 Hz*, 1 H). ^{13}C NMR (75 MHz, $CDCl_3$) δ -0.90, 13.9, 22.5, 23.7, 29.6, 31.4, 40.1, 55.5, 119.1, 121.1, 126.4, 127.7, 130.0, 130.3, 132.0, 139.8, 140.3, 140.8, 149.6, 153.3. MS (EI), *m/z* 486 ($M^{\cdot+}$, base), 471, 401, 315, 219, 73.

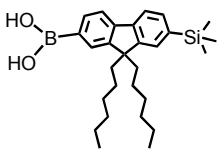

2-Trimethylsilyl-9,9-dihexylfluoren-7-yl boronic acid (9) *jecvi1***:** According to the method of Geng,[85] in a nitrogen-filled glove box, 2-bromo-7-trimethylsilylfluorene **8** (10.93 g, 22.53 mmol) and 75 mL THF were added to a flame-dried Schlenk flask. After the flask was brought out of the box and cooled to -78˚ C *n*-butyllithium in hexanes (15.4 mL x 1.6 M, 54.9 mmol), was added over 15 min. After stirring for 45 min triisopropyl borate (7.75 mL, 33.56 mmol, 1.5 eq) was added all at once and the flask was slowly warmed to RT under nitrogen for 8 h. The reaction mixture was then poured into water and extracted with diethyl ether (3 x 150 mL). The organic extracts were combined and washed with brine and dried with $MgSO_4$. After removal of solvent under vacuum, the organic material was chromatographed (silica, hexanes, then 10% EtOAc in hexanes, then 30% EtOAc in hexanes) to yield the desired product as a white powder (9.04 g, 89.2%). ^{1}H NMR (300 MHz, $CDCl_3$) δ 0.33 (s, 9 H), 0.72 (b, 10 H), 1.07 (m, 12 H, 2.07 (m, 4 H), 7.52 (m, 2 H), 7.79 (pdd, 2 H), 8.21 (s, 1 H), 8.28 (pd, 1 H)). ^{13}C NMR (75 MHz, $CDCl_3$) δ -0.87, 14.0, 22.5, 23.8, 29.6, 31.4, 40.2, 55.0, 119.4, 119.7, 127.8, 129.2, 129.8, 131.9, 134.6, 140.2, 141.4, 145.6, 150.4, 150.8. MS (EI), *m/z* 406, 321, 235, 73 (base).

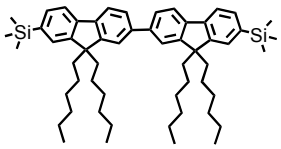

7,7'-Bis(trimethylsilyl)-9,9,9',9'-tetrakis(hexyl)-2,2'-bifluorene (10) *jecvi41/jecv65***:** According to the method of Geng,[85] in a nitrogen-filled glove box, 2-bromo-7-trimethylsilylfluorene **8** (2.38 g, 4.91 mmol) and 2-trimethylsilylfluoren-7-yl boronic acid **9** (2.21 g, 4.91 mmol) were added to a flame-dried Schlenk flask. $Pd(PPh_3)_4$ (0.060 g, 0.052 mmol, 1 mol%) was added and the mixture was dissolved in 12 mL toluene. The reaction flask was brought out of the glove box and aqueous Na_2CO_3 (7 mL x 2.0 M, 14 mmol) was added by

syringe. The reaction mixture was heated at 90˚ C for 48 h. Upon cooling, the organic phase was separated and solvent was removed. The material was then chromatographed (silica, petroleum ether, then hexanes, then 10% CH_2Cl_2 in hexanes) to yield the desired product as colorless crystals (2.90 g, 72.9%). ^{1}H NMR (300 MHz, $CDCl_3$) δ 0.31 (s, 18 H), 0.74 (m, 20 H), 1.06 (m, 24 H), 2.0 (t, 8 H), 7.48 (m, 4 H), 7.60 (m, 4 H), 7.75 (m, 4H). ^{13}C NMR (75 MHz, $CDCl_3$) δ -0.86, 13.9, 22.5, 23.8, 29.6, 31.4, 40.2, 55.1, 119.0, 120.0, 121.6, 126.0, 127.7, 131.8, 140.3, 140.8, 141.5, 150.2, 151.7.

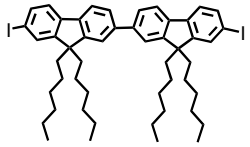

7,7'-Bis(iodo)-9,9,9',9'-tetrahexyl-2,2'-bifluorene (11) *jecvi72***:** According to the method of Geng,[85] bis(trimethylsilyl)bifluorene **10** (2.90 g, 3.58 mmol) was added to a round-bottom flask and dissolved in 17 mL CH_2Cl_2. The flask was cooled to 0˚ C and ICl in CH_2Cl_2 (7.70 mL x 1.0 M, 7.70 mmol) was added over 20 min. The reaction mixture was brought to RT and an aqueous solution of $Na_2S_2O_3$ was added with vigorous stirring to quench the reaction. Upon discoloration, the organic material was washed with brine and dried with $MgSO_4$. After solvent removal under vacuum, the crude product was chromatographed (silica, hexanes, then 10% CH_2Cl_2 in hexanes) to yield the product as a pale yellow powder (2.74 g, 83.3%). ^{1}H NMR (300 MHz, $CDCl_3$) δ 0.75 (m, 20 H), 1.15 (m, 24 H), 1.99 (oct, *J = 5.7 Hz*, 8 H), 7.34 – 7.73 (m, 12 H). ^{13}C NMR (75 MHz, $CDCl_3$) δ 14.0, 22.5, 23.7, 29.6, 31.4, 40.2, 55.5, 120.1, 121.4, 126.3, 132.2, 135.9, 139.4, 141.0, 151.0, 153.5.

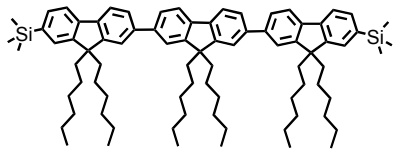

2,7’’-Bis(trimethylsilyl)-9,9,9’,9’,9’’,9’’-hexahexyl-7,2’;7’,2’’-terfluorene (12) *jecvii12***:** In a variation of the method of Thiem,[152] diiodofluorene **4** (1.17 g, 2.00 mmol) and boronic acid **9** (1.97 g, 4.38 mmol, 2.2 eq) were combined with TBABr (0.138 g, 0.778 mmol, 30 mol%), 19 mL toluene, and aqueous K_2CO_3 (10.0 mL x 2.0 M, 20.0 mmol) in a Schlenk flask. The mixture was thoroughly degassed and $Pd(PPh_3)_4$ (0.093 g, 4 mol%) was added under nitrogen. The reaction mixture was heated at 90˚ C for 12 h. Upon cooling, the organic phase was separated and the aqueous phase was extracted with CH_2Cl_2 (2 x 20 mL). The organic extracts were combined, washed with brine, and dried with $MgSO_4$. After solvent removal under vacuum, column chromatography (silica, petroleum ether, then hexanes, then 5% CH_2Cl_2 in hexanes, then 15% CH_2Cl_2 in hexanes) afforded the desired product as a white, glassy solid (1.25 g, 54.7%). ^{1}H NMR (300 MHz, $CDCl_3$) δ 0.33 (s, 18 H), 0.78 (b, 30 H), 1.10 (b, 36 H), 2.01-2.13 (m, 12 H), 7.50 (m, 4 H), 7.64-8.83 (m, 14 H). ^{13}C NMR (75 MHz, $CDCl_3$) δ -0.87, 13.9, 22.5, 23.8, 29.6, 31.4, 40.2, 40.4, 55.2, 55.4, 119.0, 120.0, 121.0, 121.7, 126.1, 126.2, 126.4, 127.7, 130.1, 131.9, 139.0, 140.1, 140.4, 140.7, 140.8, 141.6, 150.3, 151.8.

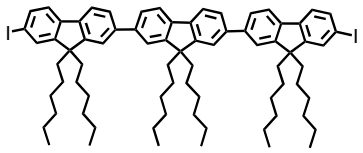

2,7’’-Diiodo-9,9,9’,9’,9’’,9’’-hexahexyl-7,2’;7’,2’’-terfluorene (14) *jecvi17/jecvi89***:** According to the method of Geng,[85] bis(trimethylsilyl)terfluorene **12** (1.39 g, 1.22 mmol) was added to a round-bottom flask and dissolved in 7.5 mL CH_2Cl_2. The flask was cooled to 0˚ C and ICl in

CH_2Cl_2 (2.44 mL x 1.0 M, 2.44 mmol) was added over 10 min. The reaction mixture was brought to RT and an aqueous solution of $Na_2S_2O_3$ was added with vigorous stirring to quench the reaction. Upon discoloration, the organic material was washed with brine and dried with $MgSO_4$. After solvent removal under vacuum, the crude product was chromatographed (silica, hexanes, then 10% CH_2Cl_2 in hexanes) to yield the product as a pale yellow powder (1.38 g, 90.6%). ^{1}H NMR (300 MHz, $CDCl_3$) δ 0.79 (m, 30 H), 1.07 (b, 36 H), 1.94-2.10 (m, 12 H), 7.45 (d, *J = 8.5 Hz*, 2 H), 7.52-7.81 (m 16 H). ^{13}C NMR (75 MHz, $CDCl_3$) δ 13.9, 22.5, 23.8, 29.6, 31.4, 40.2, 55.4, 92.4, 120.0, 121.4, 126.3, 132.2, 135.9, 139.3, 140.1, 140.4, 140.5, 141.3, 151.0, 151.9, 153.5.

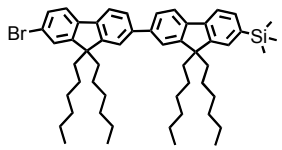

7-Bromo-7'-trimethylsilyl-9,9,9',9'-tetrakis(hexyl)-2,2'-bifluorene (15) *jecvi25***:** According to the method of Geng,[85] in a nitrogen-filled glove box, boronic acid **9** (5.40 g, 12.0 mmol, 2.5 eq) and dibromofluorene **7** (13.58 g, 27.6 mmol, 2.3 eq) were added to a flame-dried Schlenk flask. $Pd(PPh_3)_4$ (0.138 g, 0.120 mmol, 1 mol%) was added and the mixture was dissolved in 45 mL toluene. The reaction flask was brought out of the glove box and aqueous Na_2CO_3 (27 mL x 2.0.M, 54 mmol) was added by syringe. The reaction mixture was heated at 90˚ C for 48 h. Upon cooling, the organic phase was separated and the aqueous phase was extracted with CH_2Cl_2 (2 x 20 mL). The organic fractions were combined and washed with brine, then dried with $MgSO_4$ and solvent was removed under vacuum. The crude material was then chromatographed (silica, petroleum ether, then hexanes, then 5% CH_2Cl_2 in hexanes, then 15% CH_2Cl_2 in hexanes) to yield **15** as a colorless, glassy solid (5.78 g, 58.9%). ^{1}H NMR (300 MHz, $CDCl_3$) δ 0.31 (s, 9 H),

0.75 (b, 20 H), 1.07 (b, 24 H), 2.03 (m, 8 H), 7.44-7.50 (m, 4 H), 7.58-7.63 (m, 4 H), 7.71-7.77 (m, 4 H). ^{13}C NMR (75 MHz, $CDCl_3$) δ -0.87, 13.9, 22.5, 23.8, 29.6, 31.4, 40.1, 40.3, 55.1, 55.6, 119.0, 120.0, 121.0, 121.5, 126.1, 126.3, 127.7, 130.0, 131.9, 139.1, 139.2, 140.5, 141.2, 141.4, 150.2, 151.1, 151.8, 153.3.

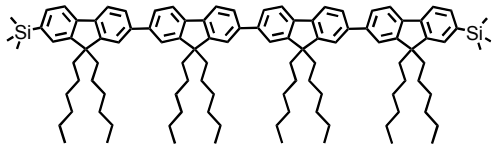

2,7’’’- Di(trimethylsilyl)-9,9,9’,9’,9’’,9’’,9’’’,9’’’-octahexyl-7,2’;7’,2’’;7’’,2’’’-tetrafluorene (16) *jecvi30***:** A flame-dried Schlenk flask was charged with 7-bromo-7’-trimethylsilylbifluorene **15** (5.78 g, 7.07 mmol). The flask was brought into a nitrogen-filled glove box and dissolved in 60 mL toluene. Ni(COD) (2.33 g, 8.46 mmol, 1.2 eq), bipyridine (1.32 g, 8.46 mmol, 1.2 eq), and 1, 5-cyclooctadiene (0.87 mL, 7.1 mmol) were then added. The reaction mixture was heated then at 80˚ C for 48 h. After cooling, the material was filtered through a celite pad with hexanes as eluant. After solvent removal under vacuum, the crude product was chromatographed (silica, hexanes, then 10% CH_2Cl_2 in hexanes) to yield the product as a white, flaky solid (4.38 g, 84.0%). ^{1}H NMR (300 MHz, $CDCl_3$) δ 0.31 (s, 18 H), 0.76 (b, 40 H), 1.10 (b, 48 H), 7.51-7.82 (m, 24 H). ^{13}C NMR (75 MHz, $CDCl_3$) δ -0.85, 14.0, 22.4, 22.5, 23.8, 23.9, 29.6, 29.7, 31.4, 31.5, 40.2, 40.4, 55.2, 55.4, 119.0, 120.0, 126.1, 126.2, 127.7, 131.9, 139.0, 140.0, 140.4, 140.6, 141.5, 150.2, 151.8.

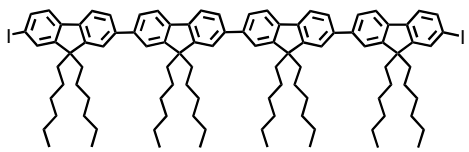

2,7’’’-Diiodo-9,9,9’,9’,9’’,9’’,9’’’-octahexyl-7,2’;7’,2’’;7’’,2’’’-quaterfluorene (17) *jecvi37***:** According to the method of Geng,[85] bis(trimethylsilyl)tetrafluorene **16** (3.88 g, 2.63 mmol) was added to a round-bottom flask and dissolved in 16 mL CH_2Cl_2. The flask was cooled to 0˚ C and ICl in CH_2Cl_2 (5.50 mL x 1.0 M, 5.50 mmol) was added over 20 min. The reaction mixture was brought to RT and an aqueous solution of $Na_2S_2O_3$ was added with vigorous stirring to quench the reaction. Upon discoloration, the organic material was washed with brine and dried with $MgSO_4$. After solvent removal under vacuum, the crude product was chromatographed (silica, hexanes, then 15% CH_2Cl_2 in hexanes) to yield the product as a light yellow solid (3.61 g, 86.8%). ^{1}H NMR (300 MHz, $CDCl_3$) δ 0.76 (b, 40 H), 1.10 (b, 48 H), 7.51-7.82 (m, 24 H). ^{13}C NMR (75 MHz, $CDCl_3$) δ 14.0, 22.5, 23.9, 29.7, 31.4, 40.4, 55.4, 55.5, 92.4, 119.7, 120.0, 121.6, 123.0, 126.2, 126.9, 132.2, 135.9, 139.3, 140.0, 140.2, 140.4, 140.5, 140.8, 141.3, 151.0, 151.5, 151.8, 153.5.

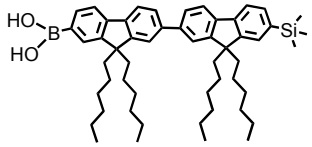

2-Trimethylsilyl-9,9,9’,9’-tetrakis(hexyl)-2,2’-bifluoren-7’-yl boronic acid (18) *jecvii15***:** According to the method of Geng,[85] in a nitrogen-filled glove box, 7-bromo-7’-trimethylsilylbifluorene **15** (1.13 g, 1.38 mmol) and 5 mL anhydrous THF were added to a flame-dried Schlenk flask. After the flask was brought out of the box and cooled to -78˚ C *n*-butyllithium in hexanes (0.94 mL x 1.6 M, 1.51 mmol) was added over 10 min. After stirring for

45 min, triisopropyl borate (0.47 mL, 2.07 mmol, 1.5 eq) was added all at once and the flask was slowly warmed to RT under nitrogen for 8 h. The reaction mixture was then poured into water and extracted with diethyl ether (3 x 25 mL). The organic extracts were combined and washed with brine and dried with $MgSO_4$. After removal of solvent under vacuum, the organic material was chromatographed (silica, 1% EtOAc in hexanes, then 10% EtOAc in hexanes, then 40% EtOAc in hexanes) to yield the desired product as a white powder (0.85 g, 78.9%). ^{1}H NMR (300 MHz, $CDCl_3$) δ 0.31 (s, 9 H), 0.76 (b, 20 H), 1.09 (m, 24 H), 2.00-2.06 (b, 8 H), 7.49 (d, 2 H), 7.63-7.94 (m, 8 H), 8.25 (s, 1H), 8.32 (m, 1H). ^{13}C NMR (75 MHz, $CDCl_3$) δ-0.85, 14.0, 22.5, 23.8, 23.9, 29.6, 29.7, 31.4, 31.5, 40.2, 40.4, 55.2, 55.3, 119.1, 119.3, 120.0, 120.6, 121.7, 126.2, 127.7, 129.0, 131.9, 134.8, 139.1, 139.9, 140.5, 140.6, 141.4, 141.6, 145.3, 150.3, 150.5, 151.8, 152.5.

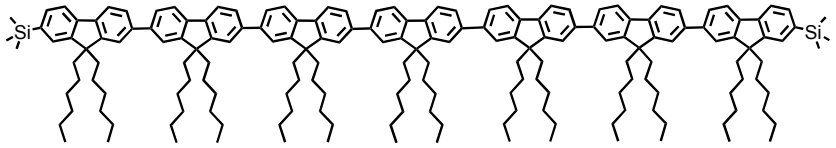

2,7’’’’’’’- Di(trimethylsilyl)-tetradecahexyl heptafluorene (19) *jecvii17***:** In a variation of the method of Thiem,[152] bis(iodo)terfluorene **14** (0.458 g, 0.367 mmol) and 2-trimethylsilylbifluoren-7’-yl boronic acid **18** (0.631 g, 0.807 mmol, 2.2 eq) were combined with TBABr (0.025 g, 0.140 mmol, 30 mol%), 3.5 mL toluene, and aqueous K_2CO_3 (2.0 mL x 2.0 M, 4.0 mmol) in a Schlenk flask. The mixture was thoroughly degassed and $Pd(PPh_3)_4$ (0.017 g, 0.014 mmol, 4 mol%) was added under nitrogen. The reaction mixture was heated at 90˚ C for 48 h. Upon cooling, the organic phase was separated and the aqueous phase was extracted with CH_2Cl_2 (2 x 20 mL). The organic extracts were combined, washed with brine, and dried with $MgSO_4$. After solvent removal under vacuum, column chromatography (silica, 2% CH_2Cl_2 in

hexanes, then 15% CH_2Cl_2 in hexanes) afforded the desired product as a pale green solid (0.522 g, 58.6%). ^{1}H NMR (300 MHz, $CDCl_3$) δ 0.32 (s, 18 H), 0.77 (b, 70 H), 1.11 (b, 84 H), 2.02-2.10 (b, 28 H), 7.49 (m, 4 H), 7.65-7.84 (m, 38 H). ^{13}C NMR (75 MHz, $CDCl_3$) δ -0.85, 14.0, 22.5, 23.9, 29.7, 31.4, 31.5, 40.2, 40.4, 55.2, 55.4, 119.0, 120.0, 121.6, 126.2, 127.7, 131.9, 140.1, 140.4, 140.6, 151.9.

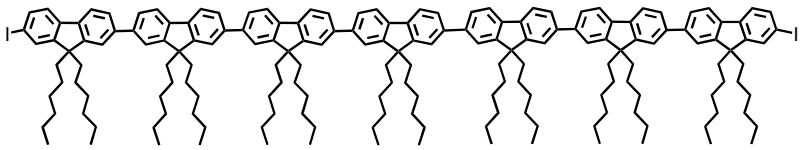

2,7’’’’’’’- Diiodo-tetradecahexyl heptafluorene (20) *jecvii24***:** According to the method of Geng,[85] bis(trimethylsilyl)heptafluorene **19** (0.493 g, 0.203 mmol) was added to a round-bottom flask and dissolved in 4 mL CH_2Cl_2. The flask was cooled to 0˚ C and ICl in CH_2Cl_2 (0.447 mL x 1.0 M, 0.447 mmol) was added over 10 min. The reaction mixture was brought to RT and an aqueous solution of $Na_2S_2O_3$ was added with vigorous stirring to quench the reaction. Upon discoloration, the organic material was washed with brine and dried with $MgSO_4$. After solvent removal under vacuum, the crude product was chromatographed (silica, 10% CH_2Cl_2 in hexanes, then 20% CH_2Cl_2 in hexanes) to yield the product as a pale green solid (0.490 g, 95.2%). ^{1}H NMR (300 MHz, $CDCl_3$) δ 0.77 (b, 70 H), 1.12 (b, 84 H), 1.98-2.10 (b, 28 H), 7.46 (pd, 4 H), 7.59-7.84 (m, 38 H). ^{13}C NMR (75 MHz, $CDCl_3$) δ 13.9, 22.5, 23.9, 29.6, 29.7, 31.5, 40.2, 40.4, 55.4, 55.5, 119.3, 121.7, 126.2, 132.3, 136.0, 139.3, 140.1, 140.7, 141.4, 151.0, 151.9.

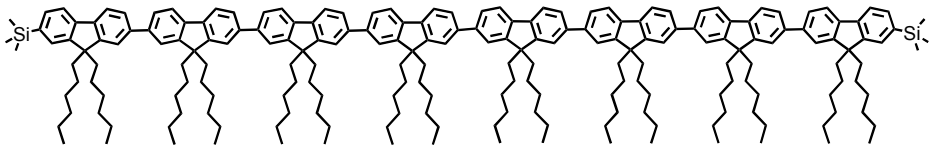

2,7’’’’’’’’- Di(trimethylsilyl)-hexadecahexyl octafluorene (21) *jecvii22***:** In a variation of the method of Thiem,[152] diiodoquaterfluorene **17** (0.650 g, 0.411 mmol) and boronic acid **18** (0.707 g, 0.904 mmol, 2.2 eq) were combined with TBABr (0.028 g, 0.157 mmol, 30 mol%), 4 mL toluene, and aqueous K_2CO_3 (2.3 mL x 2.0 M, 4.6 mmol) in a Schlenk flask. The mixture was thoroughly degassed and $Pd(PPh_3)_4$ (0.019 g, 0.016 mmol, 4 mol%) was added under nitrogen. The reaction mixture was heated at 90˚ C for 48 h. Upon cooling, the organic phase was separated and the aqueous phase was extracted with CH_2Cl_2 (2 x 20 mL). The organic extracts were combined, washed with brine, and dried with $MgSO_4$. After solvent removal under vacuum, column chromatography (silica, 2% CH_2Cl_2 in hexanes, then 15% CH_2Cl_2 in hexanes) afforded the desired product as a pale green solid (0.593 g, 51.6%). ^{1}H NMR (300 MHz, $CDCl_3$) δ 0.32 (s, 18 H), 0.77 (b, 82 H), 1.12 (b, 94 H), 2.11 (b, 32 H), 7.33 (m, 4 H), 7.49 (m, 4 H), 7.65-7.84 (m, 40 H). ^{13}C NMR (75 MHz, $CDCl_3$) δ -0.85, 14.0, 22.5, 23.9, 29.7, 31.5, 40.4, 55.4, 120.0, 121.6, 126.2, 140.1, 140.6, 151.9.

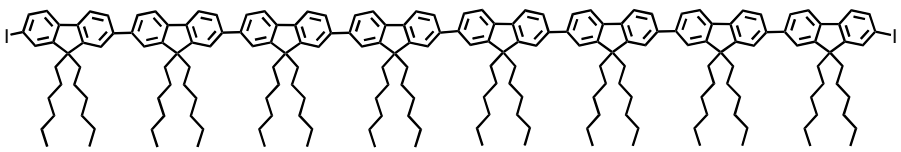

2,7’’’’’’’’- Diiodo-hexadecakis(hexyl) octafluorene (22) *jecvii30***:** According to the method of Geng,[85] bis(trimethylsilyl)octafluorene **21** (0.545 g, 0.195 mmol) was added to a round-bottom flask and dissolved in 4 mL CH_2Cl_2. The flask was cooled to 0˚ C and ICl in CH_2Cl_2 (0.428mL x 1.0 M, 0.428 mmol) was added over 10 min. The reaction mixture was brought to RT and an

aqueous solution of $Na_2S_2O_3$ was added with vigorous stirring to quench the reaction. Upon discoloration, the organic material was washed with brine and dried with $MgSO_4$. After solvent removal under vacuum, the crude product was chromatographed (silica, hexanes, then 15% CH_2Cl_2 in hexanes) to yield the product as a pale green solid (0.519 g, 91.5%). ^{1}H NMR (300 MHz, $CDCl_3$) δ 0.77 (b, 82 H), 1.11 (b 94 H), 2.10 (b, 32 H) 7.32 (m, 4 H), 7.46 (m, 2 H), 7.57-7.84 (m, 42 H). ^{13}C NMR (75 MHz, $CDCl_3$) δ 13.9, 22.5, 23.9, 29.7, 31.5, 40.2, 40.4, 55.4, 55.5, 120.0, 121.7, 126.2, 132.3, 136.0, 139.3, 140.1, 140.7, 141.4, 151.0, 151.9.

2.6.5. Preparation of a Terfluorene for Metal Chelation

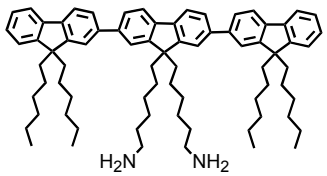

9',9'-Bis-(6-aminohexyl)-9,9,9'',9''-tetrahexyl-2,2';7',2''-terfluorene (23) *jecvii54*: Adapting the method of Wang,[153] terfluorene **28** (0.405 g) was added to a round-bottom flask and dissolved in 5 mL anhydrous THF. The flask was cooled to 0° C and $LiAlH_4$ (1.22 mmol, 1.22 mL 1M in diethyl ether) was added over 5 min. The flask was slowly warmed to RT and stirred 8 h. EtOH (0.5 mL) was added to destroy unreacted $LiAlH_4$, the mixture was poured into water, and the product was extracted into diethyl ether. The combined organic extracts were washed with brine and dried with $MgSO_4$. Solvent was removed under vacuum to give the product as a white, flaky solid (0.272 g, 67.1% yield over three steps). ^{1}H NMR (300 MHz, $CDCl_3$) δ 0.75 (b, 24 H), 1.07-1.25 (b, 36 H), 1.99-2.12 (b, 12 H), 2.53 (t, *J =6.9 Hz*, 4 H), 7.32 (q, *J = 5.8 Hz*, 6 H), 7.61-7.81 (m, 14 H). ^{13}C NMR (75 MHz, $CDCl_3$) δ 14.0, 22.5, 23.8, 26.5, 29.7, 29.9, 31.5,

33.7, 40.4, 42.1, 55.2, 119.7, 121.4, 122.9, 126.0, 126.2, 127.0, 140.0, 140.4, 140.6, 140.8, 151.0, 151.3, 151.7.

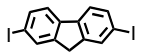

2,7-Diiodofluorene (24) *jeciv63***:** According to the method of Okumoto,[150] to a three-neck round- bottom flask equipped with a mechanical stirrer were added 1.0 L AcOH, 200 mL H_2O, 30 mL concentrated H_2SO_4, H_5IO_6 (24.05 g, 0.106 mol, 0.5 eq), and I_2 (53.58 g, 1 eq). After stirring for 10 min, fluorene (35.00 g, 0.211 g) was added and the reaction mixture was heated to 80˚ C for 3.5 h. After cooling, the volatile organics were removed under vacuum and toluene was added to dissolve the crude product. The toluene extract was washed with aqueous K_2CO_3, aqueous $Na_2S_2O_3$, and brine before drying with $MgSO_4$. The organic phase was then concentrated and the product crystallized as a light yellow powder (64.43 g, 73.1%). ^{1}H NMR (300 MHz, $CDCl_3$) δ 3.79 (s, 2 H), 7.46 (d, *J = 8.0 Hz*, 2 H), 7.68 (m, 2 H), 7.84 (s, 2 H). ^{13}C NMR (75 MHz, $CDCl_3$) δ 36.3, 92.4, 121.6, 134.2, 136.0, 140.4, 144.8. MS (EI), *m/z* 418 ($M^{\cdot+}$), 291, 163 (base).

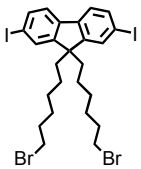

9,9-Di-(6-bromohexyl)-2,7-diiodofluorene (25) *jecvi83***:** Adapting the method of Liu,[76] 380 mL 50% KOH_{aq}, TBABr (1.27 g, 7.13 mmol, 0.36 eq), and 1,6-dibromohexane (30.67 mL, 198 mmol, 10 eq) were added to a round-bottom flask and brought to 75° C. Diiodofluorene **24** (8.25 g, 19.7 mmol) was added and the mixture was stirred for 15 min. After cooling to RT, the mixture was extracted with CH_2Cl_2. The organic extract was washed with water, 1 M HCl, water,

and brine. After drying with $MgSO_4$, excess 1,6-dibromohexane was removed by vacuum distillation. The crude product was purified by column chromatography (SiO_2, hexanes, then 10% CH_2Cl_2 in hexanes) to give **25** as a pale yellow solid (7.64 g, 52.1%). ^{1}H NMR (300 MHz, $CDCl_3$) δ 0.54 (m, 4 H), 1.03-1.21 (m, 8 H), 1.65 (quintet, *J = 6.9 Hz*, 4 H), 1.89 (m, 4 H), 3.28 (t, *J = 6.8 Hz*, 4H), 7.4 (d, *J = 7.9 Hz*, 2H), 7.63 (m, 4H). ^{13}C NMR (75 MHz, $CDCl_3$) δ 23.5, 27.7, 28.9, 32.6, 33.6, 39.9, 55.5, 93.1, 121.6, 132.1, 136.3, 139.8, 152.2.

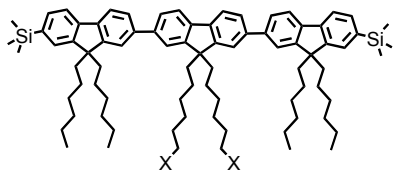

2,7''-Bis(trimethylsilyl)-9,9,9',9',9'',9''-hexahexyl-7,2';7',2''-terfluorene (26) *jecvii20***:** In a variation of the method of Thiem,[152] diiodofluorene **25** (1.30 g, 1.75 mmol) and 2-trimethylsilylfluoren-7-yl boronic acid **9** (1.73 g, 3.85 mmol, 2.2 eq) were combined with TBABr (0.260 g, 1.46 mmol, 30 mol%), 29 mL toluene, and aqueous K_2CO_3 (19.0 mL x 2.0 M, 38.0 mmol) in a Schlenk flask. The mixture was thoroughly degassed and $Pd(PPh_3)_4$ (0.090 g, 0.078 mmol, 4 mol%) was added under nitrogen. The reaction mixture was heated at 60˚ C for 48 h. Upon cooling, the organic phase was separated and the aqueous phase was extracted with CH_2Cl_2 (2 x 20 mL). The organic extracts were combined, washed with brine, and dried with $MgSO_4$. After solvent removal under vacuum, column chromatography (silica, petroleum ether, then hexanes, then 3% CH_2Cl_2 in hexanes, then 10% CH_2Cl_2 in hexanes) afforded the desired product as a pale yellow powder (1.80 g). ^{1}H NMR (300 MHz, $CDCl_3$) δ 0.32 (s, 18 H), 0.76 (b, 26 H), 1.12 (b, 34 H), 1.59 (m, 4 H), 1.99-2.05 (m, 12 H) 3.03 (t, 3 H), 3.25 (t, 1 H), 7.48 (d, *J = 8.5 Hz*, 4 H), 7.59-7.81 (m, 14 H). ^{13}C NMR (75 MHz, $CDCl_3$) δ -0.85, 6.6, 13.9, 22.5, 23.8,

27.8, 28.9, 29.6, 30.1, 31.4, 32.7, 33.4, 33.5, 40.2, 55.2, 55.3, 119.1, 120.1, 121.5, 121.6, 127.8, 131.9, 139.1, 140.1, 140.5, 140.7, 140.9, 141.5, 150.3, 151.5, 151.9.

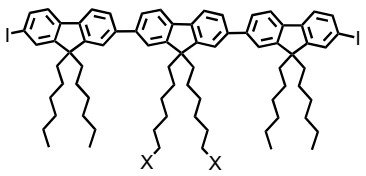

9,9,9'',9''-Tetrahexyl-7,7''-diiodo-9',9'-bis-(6-iodohexyl)-2,2';7',2''-terfluorene (27)

*jecvii26***:** According to the method of Geng,[85] bis(trimethylsilyl)terfluorene **26** (1.13 g, 0.8 mmol) was added to a round-bottom flask and dissolved in 11 mL CH_2Cl_2. The flask was cooled to 0˚ C and ICl in CH_2Cl_2 (1.88 mL x 1.0 M, 1.88 mmol) was added over 10 min. The reaction mixture was brought to RT and an aqueous solution of $Na_2S_2O_3$ was added with vigorous stirring to quench the reaction. Upon discoloration, the organic material was washed with brine and dried with $MgSO_4$. After solvent removal under vacuum, the crude product was chromatographed (silica, 3% CH_2Cl_2 in hexanes, then 20% CH_2Cl_2 in hexanes) to yield the product as a pale yellow powder (1.14 g,). ^{1}H NMR (300 MHz, $CDCl_3$) δ 0.76 (b, 26 H), 1.12 (b, 34 H), 1.59 (m, 4 H), 1.98-2.08 (m, 12 H) 3.03 (t, 3 H), 3.25 (t, 1 H), 7.48 (d, *J = 8.4 Hz*, 4 H), 7.59-7.82 (m, 14 H). ^{13}C NMR (75 MHz, $CDCl_3$) δ 6.8, 14.0, 22.5, 23.8, 27.7, 28.8, 29.6, 30.0, 31.4, 32.6, 33.3, 33.7, 40.2, 55.3, 55.5, 92.4, 120.1, 121.4, 126.3, 132.2, 135.9, 139.4, 140.1, 140.5, 141.1, 151.0, 151.5, 153.5.

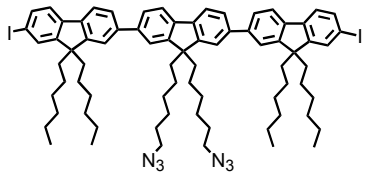

9,9,9’’,9’’-Tetrahexyl-7,7’’-diiodo-9’,9’-bis-(6-azidohexyl)-2,2’;7’,2’’-terfluorene (28)

*jecvii31***:** Diiodoterfluorene **27** (0.864 g) was added to a round-bottom flask and dissolved in 13 mL DMF. NaN_3 (89 mg, 1.37 mmol) was added and the contents were stirred at 80° C for 12 h. After cooling the flask to RT, the mixture was poured into water and extracted with hexanes. The combined organic extracts were washed with brine and dried with $MgSO_4$. Upon solvent removal under vacuum, the product was purified by column chromatography (SiO_2, 10% CH_2Cl_2 in hexanes, then 20% CH_2Cl_2 in hexanes) to give the product as an off-white solid (0.715 g) ^{1}H NMR (300 MHz, $CDCl_3$) δ 0.77 (b, 26 H), 1.13 (b, 34 H), 1.40 (m, 4 H), 1.95-2.08 (b, 12 H) 3.10 (t, *J =6.9 Hz*, 4 H), 7.46 (d, *J = 8.5 Hz*, 4 H), 7.58-7.82 (m, 14 H). ^{13}C NMR (75 MHz, $CDCl_3$) δ 14.0, 22.5, 23.78, 26.3, 28.7, 29.5, 29.6, 31.4. 40.2, 51.4, 55.3, 55.5, 92.5, 120.1, 121.4, 126.3, 132.2, 136.0, 139.4, 140.2, 140.5, 141.1, 151.0, 151.5, 153.5.

2.6.6. Fluorene-Methylene Segmer and Polymer Synthesis

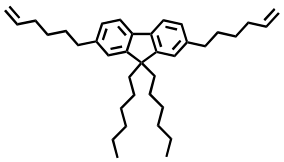

2,7-Bis-hex-5-enyl-9,9-dihexylfluorene (SF1M10) *jecv17/jecv22***:** According to the method of Peifer,[137] diiodofluorene **4** (3.00 g, 5.12 mmol) was combined with 180 mL DMF, $Pd(PPh_3)_2Cl_2$ (0.145 g, 2.5 mol%) and K_2CO_3 (2.97 g, 21.5 mmol, 4.2 eq) in a flame-dried Schlenk flask under nitrogen. 9-Hex-5-enyl-9BBN **1** (2.72 mL, 11.49 mmol, 2.25 eq) was then added under nitrogen

by syringe as a solution in 5 mL DMF. After the mixture was stirred for 8 h the contents were poured into water and the mixture was extracted with hexanes (3 x 100 mL). The organic extracts were combined, washed with brine, and dried with $MgSO_4$. After solvent removal under vacuum, column chromatography (silica, hexanes) afforded the desired product as a colorless oil (1.16 g, 45.5%). ^{1}H NMR (300 MHz, $CDCl_3$) δ 0.61 (b, 4 H), 0.75 (t, 6 H), 1.03 (m, 14 H), 1.39 (m, 4 H), 1.63 (quintet, 4 H), 1.88 (q, 4 H), 2.06 (q, 4 H), 2.66 (t, 4 H), 4.97 (m, 4 H), 5.77 (m, 2 H), 7.07 (m, 4 H), 7.51-7.54 (m, 2 H). ^{13}C NMR (75 MHz, $CDCl_3$) δ 14.1, 22.5, 23.6, 28.4, 29.7, 31.2, 31.4, 33.7, 36.0, 40.4, 54.6, 114.3, 119.0, 122.9, 126.8, 138.9, 141.1, 150.7. MS (EI), *m/z* 498 ($M^{\cdot+}$), 429, 343, 273 (base), 204, 55. HRMS calcd for $C_{37}H_{54}$: 498.4226. Found: 498.4229. Anal. calcd for $C_{37}H_{54}$: C, 89.09; H, 10.91. Found: C, 89.10, H, 11.02.

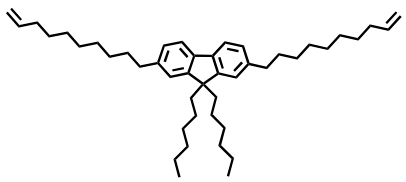

2,7-Bis-dec-9-enyl-9,9-dihexylfluorene (SF1M18) *jecv24***:** According to the method of Peifer,[137] diiodofluorene **4** (3.00 g, 5.12 mmol) was combined with 180 mL DMF, $Pd(PPh_3)_2Cl_2$ (0.145 g, 2.5 mol%) and K_2CO_3 (2.97 g, 21..5 mmol, 4.2 eq) in a flame-dried Schlenk flask under nitrogen. 9-Dec-9-enyl-9-BBN **2** (3.48 mL, 11.52 mmol, 2.25 eq) was then added under nitrogen by syringe as a solution in 5 mL DMF. The mixture was stirred for 8 h, at which point the contents were poured into water for extraction with hexanes (3 x 100 mL). The organic extracts were combined, washed with brine, and dried with $MgSO_4$. After solvent removal under vacuum, column chromatography (silica, hexanes) afforded the desired product as a colorless oil (1.53 g, 49.0%). ^{1}H NMR (300 MHz, $CDCl_3$) δ 0.66 (b, 4 H), 0.76 (t, 6 H), 1.10 (m, 16 H), 1.32 (b, 26 H), 1.64 (b, 6 H), 1.91 (m, 4 H), 2.02 (q, 4 H), 2.67 (t, 4 H), 4.95 (m, 4 H), 5.79 (m, 2 H),

7.09 (m, 4 H), 7.53 (m, 2 H). ^{13}C NMR (75 MHz, $CDCl_3$) δ 14.0, 22.6, 23.7, 29.0, 29.2, 29.5, 29.7, 31.5, 31.8, 33.8, 36.3, 40.5, 54.6, 114.1, 119.0, 122.8, 126.8, 138.9, 141.3, 150.7. HRMS calcd for $C_{45}H_{70}$: 610.5478. Found: 610.5487.

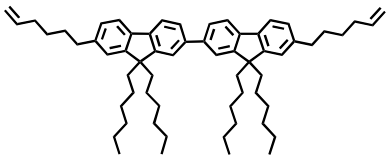

7,7'-Bis-hex-5-enyl-9,9,9'9'-tetrahexyl-2,2'-bifluorene (SF2M10) *jecvi81/jecv76***:** Adapting the method of Peifer,[137] diiodobifluorene **11** (1.18 g, 1.29 mmol) was combined with 28 mL DMF, 28 mL toluene, $Pd(PPh_3)_2Cl_2$ (0.045 g, 5 mol%) and K_2CO_3 (0.80 g, 5.80 mmol, 4.2 eq) in a flame-dried Schlenk flask under nitrogen. 9-Hex-5-enyl-9-BBN **1** (0.75 mL, 3.23 mmol, 2.25 eq) was then added under nitrogen by syringe as a solution in 5 mL DMF. The mixture was stirred for 8 h at 45˚ C, at which point the contents were poured into water for extraction with hexanes (3 x 50 mL). The organic extracts were combined, washed with brine, and dried with $MgSO_4$. After solvent removal under vacuum, column chromatography (silica, hexanes) afforded the desired product as a colorless oil (0.764 g, 71.4%). ^{1}H NMR (300 MHz, $CDCl_3$) δ 0.76 (b, 20 H), 1.07 (b, 26 H), 1.45 (quintet, 4 H), 1.69 (quintet, 4 H), 1.98-2.09 (m, 14 H), 2.70 (t, *J = 7.4 Hz*, 4 H), 4.95 (m, 4 H), 5.81 (m, 2 H), 7.13 (m, 4 H), 7.57-7.70 (m, 8 H). ^{13}C NMR (75 MHz, $CDCl_3$) δ 14.1, 22.7, 23.9, 28.6, 29.8, 31.4, 31.6, 33.8, 36.2, 40.5, 55.1, 114.5, 119.6, 121.4, 123.2, 126.0, 127.2, 138.6, 139.0, 140.2, 140.5, 141.8, 151.2, 151.5. Anal. calcd for $C_{62}H_{86}$: C, 89.57; H, 10.43. Found: C, 89.61, H, 10.51. HRMS calcd for $C_{70}H_{102}$: 830.6730. Found: 830.6846.

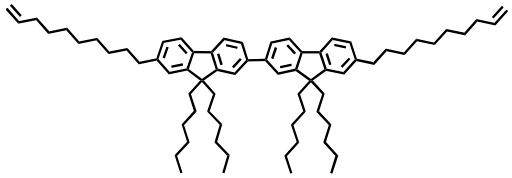

7,7'-Bis-dec-9-enyl-9,9,9'9'-tetrahexyl-2,2'-bifluorene (SF2M18) *jecvi85/jecv78***:** Adapting the method of Peifer,[137] diiodobifluorene **11** (1.18 g, 1.29 mmol) was combined with 28 mL DMF, 28 mL toluene, $Pd(PPh_3)_2Cl_2$ (0.045 g, 5 mol%) and K_2CO_3 (0.80 g, 5.80 mmol, 4.2 eq) in a flame-dried Schlenk flask under nitrogen. 9-Dec-9-enyl-9-BBN **2** (0.97 mL, 3.23 mmol, 2.25 eq) was then added under nitrogen by syringe as a solution in 5 mL DMF. The mixture was stirred for 8 h at 45˚ C, at which point the contents were poured into water for extraction with hexanes (3 x 50 mL). The organic extracts were combined, washed with brine, and dried with $MgSO_4$. After solvent removal under vacuum, column chromatography (silica, hexanes) afforded the desired product as a colorless oil (0.624 g, 51.4%). ^{1}H NMR (300 MHz, $CDCl_3$) δ ^{1}H NMR (300 MHz, $CDCl_3$) δ 0.70 (b, 24 H), 1.11 (b, 28 H), 1.32 (b, 20 H), 2.05 (m, 12 H), 2.69 (t, 4 H), 4.96 (m, 4 H), 5.76 (m, 2 H), 7.14 (m, 4 H), 7.58-7.73 (m, 8 H). ^{13}C NMR (75 MHz, $CDCl_3$) δ 14.0, 22.5, 23.7, 28.9, 29.1, 29.2, 29.5, 29.7, 31.4, 31.8, 33.8, 36.3, 40.4, 54.9, 114.1, 119.4, 121.3, 123.0, 125.9, 127.0, 138.4, 139.2, 140.0, 140.3, 141.9, 151.1, 151.4. HRMS calcd for $C_{70}H_{102}$: 942.7982. Found: 942.8060.

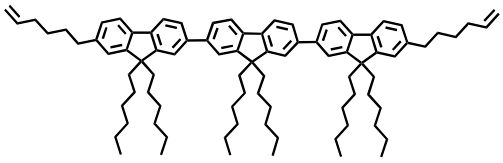

2,7''-Bis-hex-5-enyl-9,9,9',9',9'',9''-hexahexyl-7,2';7',2''-terfluorene (SF3M10) *jecvi26/jecvii38***:** Terfluorene **SF3M10** was prepared using the following methods:

Method 1: Adapting the method of Peifer,[137] diiodoterfluorene **14** (0.56 g, 0.45 mmol) was combined with 10 mL DMF, 10 mL toluene, $Pd(PPh_3)_2Cl_2$ (0.012 g, 2 mol%) and K_2CO_3 (0.27 g, 1.96 mmol, 4.2 eq) in a flame-dried Schlenk flask under nitrogen. 9-Hex-5-enyl-9-BBN **1** (0.43 mL, 1.80 mmol, 4 eq) was then added under nitrogen by syringe as a solution in 2 mL DMF. The mixture was stirred for 8 h at 45˚ C, at which point the contents were poured into water for extraction with hexanes (3 x 30 mL). The organic extracts were combined, washed with brine, and dried with $MgSO_4$. After solvent removal under vacuum, column chromatography (silica, hexanes, then 10% CH_2Cl_2 in hexanes) afforded the desired product as a white powder (0.443 g, 84.9%).

Method 2: In a variation of the method of Thiem,[152] diiodoterfluorene **14** (0.63 g, 0.51 mmol) was combined with TBABr (0.025 g, 0.15 mmol, 30 mol%), 17 mL toluene, and aqueous K_2CO_3 (6.8 mL x 2.0 M, 13.6 mmol) in a Schlenk flask. The mixture was thoroughly degassed and $Pd(PPh_3)_2Cl_2$ (0.017 g, 3 mol%) and 9-hex-5-enyl-9BBN **1** (0.43 mL, 1.80 mmol, 4 eq) were added under nitrogen. The reaction mixture was heated at 45˚ C for 8 h. Upon cooling, the organic phase was separated and the aqueous phase was extracted with hexanes (3 x 30 mL). The organic extracts were combined, washed with brine, and dried with $MgSO_4$. After solvent removal under vacuum, column chromatography (silica, hexanes, then 10% CH_2Cl_2 in hexanes) afforded the desired product as a white powder (0.497 g, 84.5%). ^{1}H NMR (300 MHz, $CDCl_3$) δ 0.77 (b, 30 H), 1.10 (b, 44 H), 1.42 (quintet, 4 H), 1.67 (quintet, 4 H) 2.02-2.11 (m, 16 H), 2.71 (t, 4 H), 4.97 (m, 4H), 5.82 (m, 2 H), 7.14 (m, 4 H), 7.60-7.81 (m, 14 H). ^{13}C NMR (75 MHz, $CDCl_3$) δ 13.9, 22.5, 23.9, 28.5, 29.7, 31.2, 31.5, 33.6, 36.2, 40.4, 55.1, 55.4, 114.3, 119.5, 119.7, 121.6, 123.1, 126.1, 126.7, 127.1, 138.7, 138.9, 140.1, 140.3, 140.6, 140.8, 141.8, 151.4, 151.6, 151.9. Anal. calcd for $C_{87}H_{118}$: C, 89.78; H, 10.22. Found: C, 89.54, H, 10.21.

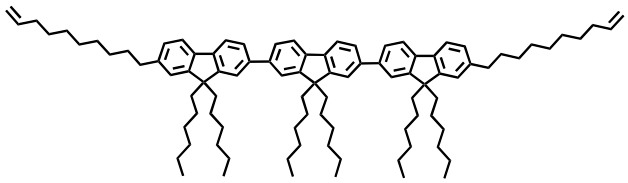

2,7’’-Bis-dec-9-enyl-9,9,9’,9’,9’’,9’’-hexahexyl-7,2’;7’,2’’-terfluorene (SF3M18)

*jecvi90***:** Adapting the method of Peifer,[137] diiodoterfluorene **14** (0.58 g, 0.46 mmol), was combined with 10 mL DMF, 10 mL toluene, $Pd(PPh_3)_2Cl_2$ (0.013 g, 2 mol%) and K_2CO_3 (0.27 g, 1.96 mmol, 4.2 eq) in a flame-dried Schlenk flask under nitrogen. 9-Dec-9-enyl-9-BBN **2** (0.56 mL, 1.85 mmol, 4 eq) was then added under nitrogen by syringe as a solution in 2 mL DMF. The mixture was stirred for 8 h at 45˚ C, at which point the contents were poured into water for extraction with hexanes (3 x 30 mL). The organic extracts were combined, washed with brine, and dried with $MgSO_4$. After solvent removal under vacuum, column chromatography (silica, hexanes, then 10% CH_2Cl_2 in hexanes) afforded the desired product as a white powder (0.417 g, 71.0%). ^{1}H NMR (300 MHz, $CDCl_3$) δ 0.77 (b, 30 H), 1.14-1.40 (b, 60 H), 1.67 (b, 4 H) 2.01-2.07 (b, 12 H), 2.70 (t, *J = 7.2 Hz*, 4 H), 4.95 (m, 4H), 5.83 (m, 2 H), 7.16 (m, 4 H), 7.61-7.81 (m, 14 H). ^{13}C NMR (75 MHz, $CDCl_3$) δ 13.9, 22.5, 23.9, 29.0, 29.2, 29.5, 31.5, 31.7, 33.8, 36.3, 40.4, 55.1, 55.4, 114.1, 119.5, 119.9, 121.6, 123.1, 125.7, 127.1, 138.6, 139.1, 140.1, 140.2, 140.6, 140.8, 142.0, 151.3, 151.5, 151.9.

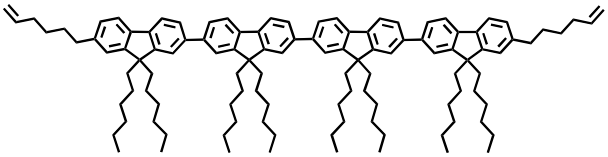

2,7’’’-Bis-hex-5-enyl-octahexyl-7,2’;7’,2’’;7’’,2’’’-quaterfluorene (SF4M10) *jecvi59***:** Adapting the method of Peifer,[137] diiodoquaterfluorene **17** (0.86 g, 0.54 mmol), was combined

with 10 mL DMF, 10 mL toluene, $Pd(PPh_3)_2Cl_2$ (0.015 g, 2 mol%) and K_2CO_3 (0.33 g, 5.80 mmol, 4.5 eq) in a flame-dried Schlenk flask under nitrogen. 9-Hex-5-enyl-9-BBN **1** (0.52 mL, 2.17 mmol, 4.0 eq) was then added under nitrogen by syringe as a solution in 2 mL DMF. The mixture was stirred for 8 h at 45˚ C, at which point the contents were poured into water for extraction with hexanes (3 x 40 mL). The organic extracts were combined, washed with brine, and dried with $MgSO_4$. After solvent removal under vacuum, column chromatography (silica, hexanes, then 10% CH_2Cl_2 in hexanes) afforded the desired product as a white powder (0.731 g, 89.8%). ^{1}H NMR (300 MHz, $CDCl_3$) δ 0.77 (b, 70 H), 1.12 (b, 86 H), 1.42 (quintet, *J = 7.7 Hz*, 4 H), 1.67 (quintet, *J = 7.6 Hz*, 4 H) 2.02-2.13 (m, 30 H), 2.71 (t, *J = 7.1 Hz*, 4 H), 4.97 (m, 4H), 5.83 (m, 2 H), 7.16 (bs, 4 H), 7.36 (q, 4 H), 7.62-7.83 (m, 32 H). ^{13}C NMR (75 MHz, $CDCl_3$) δ. 14.0, 22.5, 23.8, 28.4, 29.7, 31.4, 33.7, 36.1, 40.4, 55.0, 55.3, 114.4, 119.5, 119.9, 121.4, 121.5, 123.0, 126.0, 127.1, 138.5, 138.9, 139.9, 140.3, 140.6, 141.7, 151.2, 151.4, 151.5, 151.8. Anal. calcd for $C_{112}H_{150}$: C, 89.90; H, 10.10. Found: C, 89.26, H, 10.03.

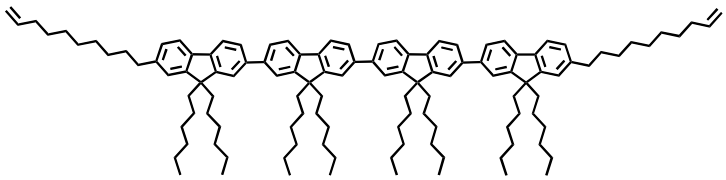

2,7’’’-Bis-dec-9-enyl-octahexyl-7,2’;7’,2’’;7’’,2’’’-quaterfluorene (SF4M18) *jecvi92***:** Adapting the method of Peifer,[137] diiodoquaterfluorene **17** (0.85 g, 0.54 mmol), was combined with 12 mL DMF, 12 mL toluene, $Pd(PPh_3)_2Cl_2$ (0.015 g, 2 mol%) and K_2CO_3 (0.80 g, 5.80 mmol, 4.5 eq) in a flame-dried Schlenk flask under nitrogen. 9-Dec-9-enyl-9-BBN **2** (0.65 mL, 2.15 mmol, 4.0 eq) was then added under nitrogen by syringe as a solution in 2 mL DMF. After stirring for for 8 h at 45˚ C, the contents were poured into water for extraction with hexanes (3 x 40 mL). The organic extracts were combined, washed with brine, and dried with $MgSO_4$. After

solvent removal under vacuum, column chromatography (silica, hexanes, then 10% CH_2Cl_2 in hexanes) afforded the desired product as a white powder (0.705 g, 81.7%). ^{1}H NMR (300 MHz, $CDCl_3$) δ 0.77 (b, 48 H), 1.13 (b, 52 H), 1.33 (b, 20 H), 1.67 (b, 4 H) 2.01-2.09 (b, 20 H), 2.71 (t, *J = 7.3 Hz*, 4 H), 4.97 (m, 4H), 5.83 (m, 2 H), 7.17 (bs, 4 H), 7.36 (q, 4 H), 7.62-7.81 (m, 16 H). ^{13}C NMR (75 MHz, $CDCl_3$) δ 13.9, 22.3, 23.9, 29.0, 29.2, 29.5, 29.7, 29.9, 31.5, 31.7, 33.8, 36.4, 40.4, 55.1, 55.3, 114.1, 119.6, 120.0, 121.7, 123.0, 126.2, 126.3, 126.9, 127.2, 138.6, 139.7, 140.0, 140.2, 140.7, 140.9, 142.0, 151.3, 151.6, 151.9.

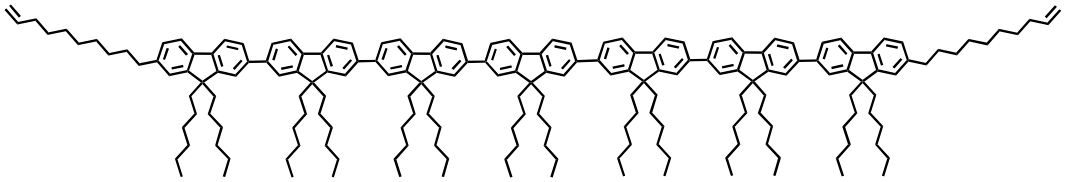

2,7’’’’’’’-Bis-dec-9-enyl-tetradecahexyl heptafluorene (SF7M18) *jecvii35***:** In a variation of the method of Thiem,[152] diiodoheptafluorene **20** (0.46 g, 0.18 mmol) was combined with TBABr (9 mg, 0.05 mmol, 30 mol%), 6 mL toluene, and aqueous K_2CO_3 (2.4 mL x 2.0 M, 4.8 mmol) in a Schlenk flask. The mixture was thoroughly degassed and $Pd(PPh_3)_2Cl_2$ (6 mg, 3 mol%) and 9-dec-9-enyl-9-BBN **2** (0.22 mL, 0.72 mmol, 4 eq) were added under nitrogen. The reaction mixture was heated at 45˚ C for 8 h. Upon cooling, the organic phase was separated and the aqueous phase was extracted with hexanes (3 x 20 mL). The organic extracts were combined, washed with brine, and dried with $MgSO_4$. After solvent removal under vacuum, column chromatography (silica, hexanes, then 15% CH_2Cl_2 in hexanes) afforded the desired product as a white powder (0.356 g, 77.5%). ^{1}H NMR (300 MHz, $CDCl_3$) δ 0.77 (b, 70 H), 1.11-1.47 (b, 114), 1.63 (b, 4 H), 1.86-2.11 (b, 30 H.) 2.69 (t, 4 H), 4.95 (m, 4 H), 5.79 (m, 2 H), 7.16 (b, 4 H), 7.59-7.84 (m, 38 H). ^{13}C NMR (75 MHz, $CDCl_3$) δ 13.9, 22.5, 23.9, 29.0, 29.2, 29.5, 29.7, 31.5, 31.8, 33.8, 36.3, 40.4, 55.1, 55.4, 114.1, 119.4, 119.5, 120.0, 121.7, 123.1, 126.0, 126.2, 127.1, 138.6, 140.0, 140.1, 140.6, 140.7, 140.9, 142.0, 151.3, 151.5, 151.9.

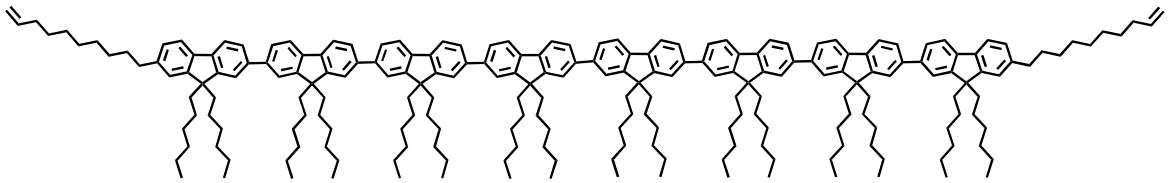

2,7’’’’’’’’-Bis-dec-9-enyl-hexadecahexyl octafluorene (SF8M18) *jecvii40***:** In a variation of the method of Thiem,[152] diiodooctafluorene **22** (0.42 g, 0.15 mmol) was combined with TBABr (7 mg, 0.05 mmol, 30 mol%), 5 mL toluene, and aqueous K_2CO_3 (2.0 mL x 2.0 M, 4.0 mmol) in a Schlenk flask. The mixture was thoroughly degassed and $Pd(PPh_3)_2Cl_2$ (5 mg, 3 mol%) and 9-dec-9-enyl-9-BBN **2** (0.18 mL, 0.58 mmol, 4 eq) were added under nitrogen. The reaction mixture was heated at 45˚ C for 8 h. Upon cooling, the organic phase was separated and the aqueous phase was extracted with hexanes (3 x 20 mL). The organic extracts were combined, washed with brine, and dried with $MgSO_4$. After solvent removal under vacuum, column chromatography (silica, hexanes, then 15% CH_2Cl_2 in hexanes) afforded the desired product as a white powder (0.306 g, 71.4%). ^{1}H NMR (300 MHz, $CDCl_3$) δ 0.77 (b, 82 H), 1.12-1.41 (b, 118 H), 1.66 (b, 4 H), 1.90-2.25 (b, 32 H), 2.69 (t, 4 H), 4.96 (m, 4 H), 5.83 (m, 2 H), 7.15 (bs, 4 H), 7.34 (m, 4 H), 7.64-7.84 (m, 40 H). ^{13}C NMR (75 MHz, $CDCl_3$) δ 13.9, 22.5, 23.9, 24.0, 29.0, 29.2, 29.5, 29.7, 31.5, 31.8, 33.8, 40.4, 55.1, 55.4, 114.1, 119.5, 120.0, 121.7, 123.0, 123.1, 126.0, 126.2, 126.8, 127.1, 138.6, 140.0, 140.1, 140.7, 140.9, 142.0, 151.3, 151.6, 151.9.

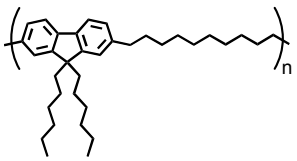

Poly(9,9-dihexylfluorene-*co*-decane) (PF1M10) *jecvi47***:** Adapting the method of Watson,[143] a pear-shaped flask was charged with **SF1M10** (0.607 g, 1.22 mmol). A gas adapter was fitted to

the top and the flask was evacuated thoroughly. The flask was brought into a nitrogen-filled glove box and diphenyl ether (0.5 g) and bis(tricyclohexylphosphine)benzylideneruthenium(IV) dichloride (25 mg, 2 mol%, added as a solution in 2 mL toluene) were added. The flask was brought out of the glove box and vacuum was applied to the mixture until the stir bar was immobilized. Stirring was reestablished by heating the flask at 45˚ C, and vacuum was applied overnight. The flask was then cooled to RT and brought into the glove box. The reaction mixture was taken up in 10 mL toluene and transferred to a stainless steel reaction vessel. To this vessel was added 1.9 g silica. The vessel was brought out of the glove box, charged with 180 psi H_2, and heated at 80˚ C for 48 h. After cooling the vessel, the contents were subjected to centrifugation and the mother liquor was removed and concentrated. The polymer was isolated by precipitation into acetone with vigorous stirring to yield the desired product as a white solid (0.391 g, 67.9%). M_w = 30,000; M_n = 14,000; PDI = 2.1. ^{1}H NMR (300 MHz, $CDCl_3$) δ 0.60 (b, 6 H), 0.74 (t, 6 H), 1.02 (m, 16 H), 1.22-1.29 (b, 32 H), 1.61 (b, 4 H), 1.88 (m, 4 H), 2.64 (t, 4 H), 7.07 (m, 4 H), 7.50 (d, *J = 8.1 Hz*, 2 H). ^{13}C NMR (75 MHz, $CDCl_3$) δ 14.0, 22.5, 23.7, 29.3, 29.7, 31.4, 31.8, 36.3, 40.4, 54.6, 118.9, 122.9, 126.8, 138.9, 141.4, 150.8.

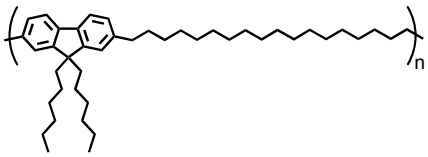

Poly(9,9-dihexylfluorene-*co*-octadecane) (PF1M18) *jecvi78***:** Adapting the method of Watson,[143] a pear-shaped flask was charged with **SF1M18** (0.573 g, 0.94 mmol). A gas adapter was fitted to the top and the flask was evacuated thoroughly. The flask was brought into a nitrogen-filled glove box and diphenyl ether (0.56 g) and bis(tricyclohexylphosphine)benzylideneruthenium(IV) dichloride (17 mg, 2 mol%, added as a

solution in 2 mL toluene) were added. The flask was brought out of the glove box and toluene was removed under high vacuum with stirring. High vacuum was then applied to the mixture until the stir bar was immobilized. Stirring was reestablished by heating the flask at 45˚ C, and vacuum was applied overnight. The flask was then cooled to RT and brought into the glove box. The reaction mixture was taken up in 8.5 mL toluene and transferred to a stainless steel reaction vessel. To this vessel was added 1.6 g silica. The vessel was brought out of the glove box, charged with 180 psi H_2, and heated at 80˚ C for 48 h. After cooling the vessel, the contents were subjected to centrifugation and the mother liquor was removed and concentrated. The polymer was isolated by precipitation into acetone with vigorous stirring to yield the desired product as a white solid (0.454 g, 82.8%). M_w = 33,000; M_n = 16,000; PDI = 2.1. ^{1}H NMR (300 MHz, $CDCl_3$) δ 0.60 (b, 4 H), 0.76 (t, 6 H), 1.02 (m, 12 H), 1.22-1.29 (b, 28 H), 1.61 (t, 4 H), 1.89 (m, 4 H), 2.64 (t, 4 H), 7.07 (m, 4 H), 7.50 (d, 2 H). ^{13}C NMR (75 MHz, $CDCl_3$) δ 14.0, 22.5, 23.6, 29.3, 29.6, 29.7, 31.4, 31.8, 36.2, 40.4, 54.6, 118.9, 122.9, 126.8, 138.8, 141.3, 150.7.

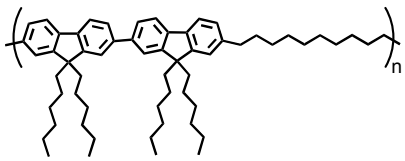

Poly(9,9,9',9'-tetrahexyl-2,2'-bifluorene-*co*-decane) (PF2M10) *jecvi84*: Adapting the method of Watson,[143] a pear-shaped flask was charged with **SF2M10** (0.473 g, 0.57 mmol). A gas adapter was fitted to the top and the flask was evacuated thoroughly. The flask was brought into a nitrogen-filled glove box and diphenyl ether (0.3 g) and bis(tricyclohexylphosphine)benzylideneruthenium(IV) dichloride (10 mg, 2 mol%, added as a solution in 2 mL toluene) were added. The flask was brought out of the glove box and toluene was removed under high vacuum with stirring. High vacuum was then applied to the mixture

until the stir bar was immobilized. Stirring was reestablished by heating the flask at 45˚ C, and vacuum was applied overnight. The flask was then cooled to RT and brought into the glove box. The reaction mixture was taken up in 5.5 mL toluene and transferred to a stainless steel reaction vessel. To this vessel was added 0.97 g silica. The vessel was brought out of the glove box, charged with 180 psi H_2, and heated at 80˚ C for 48 h. After cooling the vessel, the contents were subjected to centrifugation and the mother liquor was removed and concentrated. The polymer was isolated by precipitation into acetone with vigorous stirring to yield the desired product as a white solid (0.275 g, 60.0%). M_w = 17,000; M_n = 9,200; PDI = 1.9. ^{1}H NMR (300 MHz, $CDCl_3$) δ 0.75 (b, 16 H), 1.06 (b, 24 H), 1.31 (b, 16 H), 1.65 (b, 4 H), 1.97 (b, 8 H), 2.67 (t, 4 H), 7.14 (bs, 4 H), 7.56-7.69 (m, 8 H). ^{13}C NMR (75 MHz, $CDCl_3$) δ 14.0, 22.5, 23.7, 29.3, 29.6, 31.4, 31.9, 36.3, 40.4, 54.9.119.4, 119.5, 121.3, 123.0, 125.9, 127.0, 138.4, 140.0, 140.3, 141.9, 151.1, 151.4. Anal. calcd for $C_{60}H_{84}$: C, 89.49; H, 10.51. Found: C, 89.24, H, 10.46.

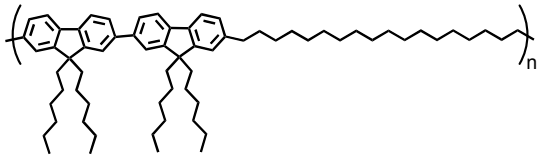

Poly(9,9,9',9'-tetrahexyl-2,2'bifluorene-*co*-octadecane) (PF2M18) *jecvi88***:** Adapting the method of Watson,[143] a pear-shaped flask was charged with **SF2M18** (0.488 g, 0.53 mmol). A gas adapter was fitted to the top and the flask was evacuated thoroughly. The flask was brought into a nitrogen-filled glove box and diphenyl ether (0.5 g) and bis(tricyclohexylphosphine)benzylideneruthenium(IV) dichloride (12 mg, 2 mol%, added as a solution in 2 mL toluene) were added. The flask was brought out of the glove box and toluene was removed under high vacuum with stirring. High vacuum was then applied to the mixture until the stir bar was immobilized. Stirring was reestablished by heating the flask at 45˚ C, and

vacuum was applied overnight. The flask was then cooled to RT and brought into the glove box. The reaction mixture was taken up in 5.5 mL toluene and transferred to a stainless steel reaction vessel. To this vessel was added 0.96 g silica. The vessel was brought out of the glove box, charged with 180 psi H_2, and heated at 80˚ C for 48 h. After cooling the vessel, the contents were subjected to centrifugation and the mother liquor was removed and concentrated. The polymer was isolated by precipitation into acetone with vigorous stirring to yield the desired product as a white solid (0.298 g, 61.2%). M_w = 21,500; M_n = 13,000; PDI = 1.7. ^{1}H NMR (300 MHz, $CDCl_3$) δ 0.77 (b, 16 H), 1.08 (b, 24 H), 1.26-1.40 (b, 32 H), 1.66 (b, 4 H), 2.02 (b, 8 H), 2.70 (t, 4 H), 7.15 (bs, 4 H), 7.59-7.70 (m, 8 H). ^{13}C NMR (75 MHz, $CDCl_3$) δ 14.0, 22.5, 23.7, 29.3, 29.7, 31.4, 31.8, 36.3, 40.4, 54.9, 119.4, 119.5, 121.3, 123.0, 125.9, 127.0, 138.4, 140.0, 140.4, 141.9, 151.1, 151.4.

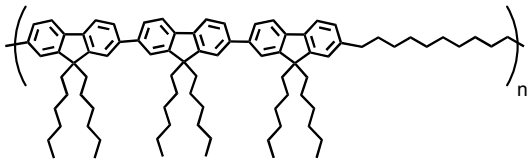

Poly(9,9,9',9'', 9'',9''-hexahexyl-2,2';2',2''-terfluorene-*co*-decane) (PF3M10) *jecvii47*: Adapting the method of Watson,[143] a pear-shaped flask was charged with **SF3M10** (0.989 g, 0.851 mmol). A gas adapter was fitted to the top and the flask was evacuated thoroughly. The flask was brought into a nitrogen-filled glove box and diphenyl ether (0.9 g) and bis(tricyclohexylphosphine)benzylideneruthenium(IV) dichloride (14 mg, 2 mol%, added as a solution in 2 mL toluene) were added. The flask was brought out of the glove box and toluene was removed under high vacuum with stirring. High vacuum was then applied to the mixture until the stir bar was immobilized. Stirring was reestablished by heating the flask at 45˚ C, and vacuum was applied overnight. The flask was then cooled to RT and brought into the glove box. The reaction mixture was taken up in 11 mL toluene and transferred to a stainless steel reaction

vessel. To this vessel was added 1.5 g silica. The vessel was brought out of the glove box, charged with 180 psi H_2, and heated at 80˚ C for 48 h. After cooling the vessel, the contents were subjected to centrifugation and the mother liquor was removed and concentrated. The polymer was isolated by precipitation into acetone with vigorous stirring to yield the desired product as a white solid (0.673 g, 69.6%). M_w = 44,000; M_n = 26,000; PDI = 1.7. ^{1}H NMR (300 MHz, $CDCl_3$) δ 0.75 (b, 24 H), 1.08 (b, 34 H), 1.29 (b, 20 H), 1.52 (b, 4 H) 2.01 (b, 12 H), 2.68 (t, 4 H), 7.15 (bs, 4 H), 7.59-7.80 (m, 14 H). ^{13}C NMR (75 MHz, $CDCl_3$) δ 14.1, 22.7, 24.1, 29.5, 29.9, 31.7, 32.0, 36.6, 40.6, 55.3, 55.6, 119.7, 119.9, 121.8, 123.3, 126.3, 126.4, 127.3, 138.8, 140.3, 140.4, 140.8, 141.0, 142.3, 151.5, 151.7, 152.1.

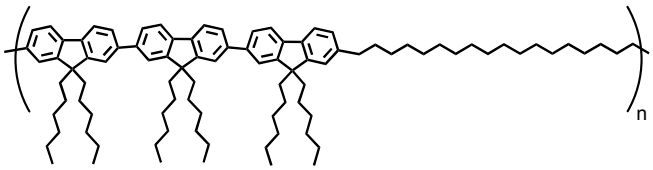

Poly(9,9,9',9', 9'',9''-hexahexyl-2,2';2',2''-terfluorene-*co*-octadecane) (PF3M18) *jecvi91*: Adapting the method of Watson,[143] a pear-shaped flask was charged with **SF3M18** (0.310 g, 0.243 mmol). A gas adapter was fitted to the top and the flask was evacuated thoroughly. The flask was brought into a nitrogen-filled glove box and diphenyl ether (0.3 g) and bis(tricyclohexylphosphine)benzylideneruthenium(IV) dichloride (5 mg, 2 mol%, added as a solution in 2 mL toluene) were added. The flask was brought out of the glove box and toluene was removed under high vacuum with stirring. High vacuum was then applied to the mixture until the stir bar was immobilized. Stirring was reestablished by heating the flask at 45˚ C, and vacuum was applied overnight. The flask was then cooled to RT and brought into the glove box. The reaction mixture was taken up in 3 mL toluene and transferred to a stainless steel reaction vessel. To this vessel was added 0.45 g silica. The vessel was brought out of the glove box,

charged with 180 psi H_2, and heated at 80˚ C for 48 h. After cooling the vessel, the contents were subjected to centrifugation and the mother liquor was removed and concentrated. The polymer was isolated by precipitation into acetone with vigorous stirring to yield the desired product as a white solid (0.227 g, 74.9%). M_w = 20,000; M_n = 13,000; PDI = 1.5. ^{1}H NMR (300 MHz, $CDCl_3$) δ 0.77 (b, 76 H), 1.09 (b, 38 H), 1.66 (b, 4 H), 2.00-2.06 (b, 12 H), 2.69 (t, *J = 7.2 Hz*, 4 H), 7.15 (b, 4 H), 7.60-7.81 (m, 12 H). ^{13}C NMR (75 MHz, $CDCl_3$) δ 14.2, 22.7, 23.9, 29.4, 29.8, 31.6, 32.0, 36.4, 40.5, 55.1, 55.4, 119.5, 119.6, 120.0, 121.5, 123.2, 126.0, 126.2, 127.2, 138.5, 140.0, 140.6, 140.7, 142.2, 151.2, 151.5, 151.8.

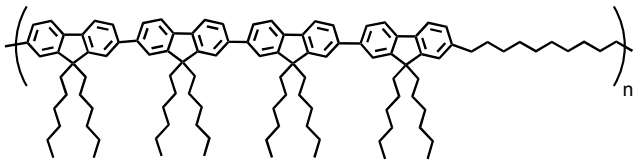

Poly(9,9,9',9', 9'',9'',9''',9'''-octahexyl-2,2';2',2''-quaterfluorene-*co*-decane) (PF4M10) *jecvi71***:** Adapting the method of Watson,[143] a pear-shaped flask was charged with **SF4M10** (0.400 g, 0.268 mmol). A gas adapter was fitted to the top and the flask was evacuated thoroughly. The flask was brought into a nitrogen-filled glove box and diphenyl ether (0.3 g) and bis(tricyclohexylphosphine)benzylideneruthenium(IV) dichloride (5 mg, 2 mol%, added as a solution in 2 mL toluene) were added. The flask was brought out of the glove box and toluene was removed under high vacuum with stirring. High vacuum was then applied to the mixture until the stir bar was immobilized. Stirring was reestablished by heating the flask at 45˚ C, and vacuum was applied overnight. The flask was then cooled to RT and brought into the glove box. The reaction mixture was taken up in 3.5 mL toluene and transferred to a stainless steel reaction vessel. To this vessel was added 0.47 g silica. The vessel was brought out of the glove box, charged with 180 psi H_2, and heated at 80˚ C for 48 h. After cooling the vessel, the contents were

subjected to centrifugation and the mother liquor was removed and concentrated. The polymer was isolated by precipitation into acetone with vigorous stirring. After reprecipitating into acetone, **PF4M10** was recovered as a white solid (0.272 g, 69.1%). M_w = 9,800; M_n = 7,000; PDI = 1.4. ^{1}H NMR (300 MHz, $CDCl_3$) δ 0.78 (b, 60 H), 1.12-1.40 (b, 86 H), 1.67 (b, 4 H), 2.03-2.10 (b, 22 H), 2.70 (t, 4 H), 7.15 (b, 4 H), 7.35 (q, 2 H), 7.61-7.81 (m, 28 H). ^{13}C NMR (75 MHz, $CDCl_3$) δ 14.0, 22.6, 23.8, 29.3, 29.7, 31.4, 31.9, 36.3, 40.4, 55.1, 55.3, 119.4, 119.9, 121.4, 123.0, 125.9, 126.1, 127.0, 138.3, 139.8, 139.9, 140.3, 140.4, 140.6, 142.0, 151.1, 151.4, 151.8.

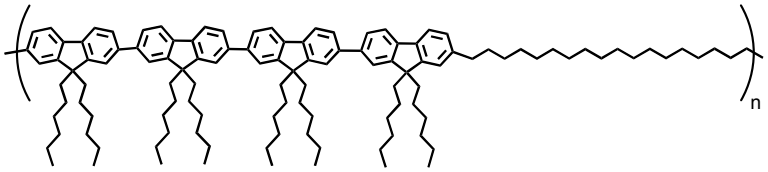

Poly(9,9,9',9', 9'',9'',9''',9'''-octahexyl-2,2';2',2''-quaterfluorene-*co*-octadecane) (PF4M18) *jecvi94***:** Adapting the method of Watson,[143] a pear-shaped flask was charged with **SF4M18** (0.468 g, 0.291 mmol). A gas adapter was fitted to the top and the flask was evacuated thoroughly. The flask was brought into a nitrogen-filled glove box and diphenyl ether (0.4 g) and bis(tricyclohexylphosphine)benzylideneruthenium(IV) dichloride (5 mg, 2 mol%, added as a solution in 2 mL toluene) were added. The flask was brought out of the glove box and toluene was removed under high vacuum with stirring. High vacuum was then applied to the mixture until the stir bar was immobilized. Stirring was reestablished by heating the flask at 45˚ C, and vacuum was applied overnight. The flask was then cooled to RT and brought into the glove box. The reaction mixture was taken up in 4 mL toluene and transferred to a stainless steel reaction vessel. To this vessel was added 0.53 g silica. The vessel was brought out of the glove box, charged with 180 psi H_2, and heated at 80˚ C for 48 h. After cooling the vessel, the contents were

subjected to centrifugation and the mother liquor was removed and concentrated. The polymer was isolated by precipitation into acetone with vigorous stirring. After reprecipitating into acetone, **PF4M18** was recovered as a white solid (0.312 g, 67.9%). M_w = 10,600; M_n = 7,600; PDI = 1.4. ^{1}H NMR (300 MHz, $CDCl_3$) δ 0.77 (b, 60 H), 1.09-1.33 (b, 104 H), 1.66 (b, 4 H), 2.03-2.10 (b, 22 H), 2.70 (t, 4 H), 7.15 (b, 4 H), 7.61-7.81 (m, 28 H). ^{13}C NMR (75 MHz, $CDCl_3$) δ 14.0, 22.5, 23.8, 29.3, 29.6, 31.4, 31.8, 36.3, 40.4, 55.0, 55.3, 119.4, 119.5, 119.9, 121.4, 121.5, 123.0, 125.9, 126.1, 127.0, 138.4, 139.8, 140.0, 140.3, 140.6, 140.8, 142.0, 151.0, 151.1, 151.4, 151.5, 151.8.

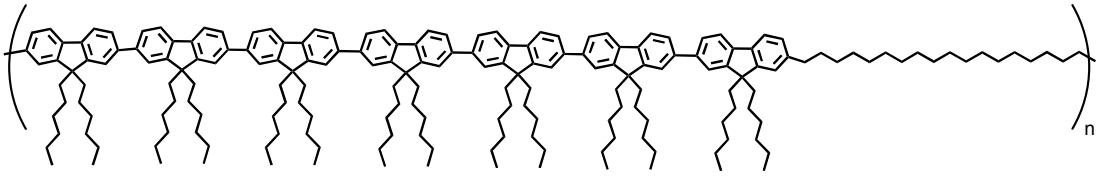

Poly(tetradecahexyl heptafluorene-*co*-octadecane) (PF7M18) *jecvii48***:** Adapting the method of Watson,[143] a pear-shaped flask was charged with **SF7M18** (0.324 g, 0.125 mmol). A gas adapter was fitted to the top and the flask was evacuated thoroughly. The flask was brought into a nitrogen-filled glove box and diphenyl ether (0.15 g) and bis(tricyclohexylphosphine)benzylideneruthenium(IV) dichloride (3 mg, 2 mol%, added as a solution in 2 mL toluene) were added. The flask was brought out of the glove box and toluene was removed under high vacuum with stirring. High vacuum was then applied to the mixture until the stir bar was immobilized. Stirring was reestablished by heating the flask at 45˚ C, and vacuum was applied overnight. The flask was then cooled to RT and brought into the glove box. The reaction mixture was taken up in 3 mL toluene and transferred to a stainless steel reaction vessel. To this vessel was added 0.22 g silica. The vessel was brought out of the glove box, charged with 180 psi H_2, and heated at 80˚ C for 48 h. After cooling the vessel, the contents were

subjected to centrifugation and the mother liquor was removed and concentrated. The polymer was isolated by precipitation into acetone with vigorous stirring. After reprecipitation into hexanes, **PF7M18** was recovered as a tan powder (0.190 g, 59.0%). M_w = 57,000; M_n = 36,000; PDI = 1.6. ^{1}H NMR (300 MHz, $CDCl_3$) δ 0.76 (b, 70 H), 1.10-1.32 (b, 104 H), 1.52-1.65 (b, 12 H), 2.09 (b, 28 H), 2.68 (b, 4 H), 7.14 (b, 4 H), 7.59-7.83 (b, 38 H). ^{13}C NMR (75 MHz, $CDCl_3$) 14.0, 22.5, 23.9, 29.3, 29.7, 31.5, 36.3, 40.4, 55.0, 55.4, 119.5, 120.0, 121.6, 123.0, 126.2, 127.1, 138.5, 140.1, 140.6, 142.1, 151.2, 151.5, 151.9

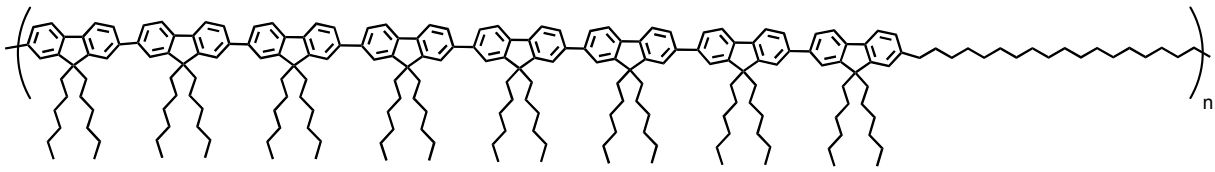

Poly(hexadecahexyl octafluorene-*co*-octadecane) (PF8M18) *jecvii49***:** Adapting the method of Watson,[143] a pear-shaped flask was charged with **SF8M18** (0.277 g, 0.094 mmol). A gas adapter was fitted to the top and the flask was evacuated thoroughly. The flask was brought into a nitrogen-filled glove box and diphenyl ether (0.15 g) and bis(tricyclohexylphosphine)benzylideneruthenium(IV) dichloride (3 mg, 2 mol%, added as a solution in 2 mL toluene) were added. The flask was brought out of the glove box and toluene was removed under high vacuum with stirring. High vacuum was then applied to the mixture until the stir bar was immobilized. Stirring was reestablished by heating the flask at 45˚ C, and vacuum was applied overnight. The flask was then cooled to RT and brought into the glove box. The reaction mixture was taken up in 5 mL toluene and transferred to a stainless steel reaction vessel. To this vessel was added 0.17 g silica. The vessel was brought out of the glove box, charged with 180 psi H_2, and heated at 80˚ C for 48 h. After cooling the vessel, the contents were subjected to centrifugation and the mother liquor was removed and concentrated. The polymer

was isolated by precipitation into acetone with vigorous stirring. After reprecipitation into hexanes, **PF8M18** was recovered as a tan powder (0.107 g, 39.1%). M_w = 22,000; M_n = 14,000; PDI = 1.6. ^{1}H NMR (300 MHz, $CDCl_3$) δ 0.77 (b, 84 H), 1.12-1.32 (b, 112 H), 1.52-1.66 (b, 12 H), 2.10 (b, 32 H), 2.69 (t, 4 H), 7.15 (s, 4 H), 7.66-7.84 (m, 44 H). ^{13}C NMR (75 MHz, $CDCl_3$) δ 13.9, 22.5, 23.9, 29.7, 31.5, 40.4, 55.0, 55.4, 118.8, 120.0, 121.6, 123.1, 126.2, 140.1, 140.6, 151.2, 151.5, 151.9.

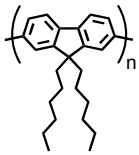

Poly(9,9-dihexylfluorene) (PDHF) *jecv96/jecvii7/jecvii55***:** Three samples of PDHF were prepared based on the method of Kreyenschmidt.[89]

PDHF-old: A flame-dried Schlenk flask was brought into a nitrogen-filled glove box and charged with $Ni(COD)_2$ (2.58 g, 9.38 mmol, 1.5 eq) and bipyridine (1.47 g, 9.38 mmol, 1.5 eq). The mixture was dissolved in 15 mL DMF and COD (1.02 g, 9.38 mmol, 1.5 eq) was added. After the flask was brought out of the glove box and heated to 80˚ C for 30 min, 2,7-dibromofluorene **7** (3.00 g, 6.10 mmol, as a solution in 10 mL anhydrous toluene) was added under nitrogen. The flask was wrapped in aluminum foil and the reaction was stirred at 80˚ C for 48 h. The hot solution was then added dropwise to an equivolume mixture of rapidly stirring concentrated HCl, acetone, and methanol. After filtering through a sintered glass frit, the polymer was redissolved in CH_2Cl_2 and precipitated twice into an equivolume mixture of acetone and methanol. The recovered polymer was dried under vacuum for 12 h to yield the desired product as a tan powder (1.160 g, 57.0%).

PDHF-new: A flame-dried Schlenk flask was brought into a nitrogen-filled glove box and charged with $Ni(COD)_2$ (1.29 g, 4.69 mmol, 1.5 eq) and bipyridine (0.75 g, 4.69 mmol, 1.5 eq). The mixture was dissolved in 8 mL DMF and COD (0.51 g, 4.69 mmol, 1.5 eq) was added. After the flask was brought out of the glove box and heated to 80˚ C for 30 min, 2,7-dibromofluorene **7** (1.50 g, 3.05 mmol, as a solution in 5 mL anhydrous toluene) was added under nitrogen. The flask was wrapped in aluminum foil and the reaction was stirred at 80˚ C for 48 h. The hot solution was then added dropwise to an equivolume mixture of rapidly stirring concentrated HCl, acetone, and methanol. After filtering through a sintered glass frit, the polymer was redissolved in CH_2Cl_2 and precipitated twice into an equivolume mixture of acetone and methanol. The recovered polymer was dried under vacuum for 12 h to yield the desired product as a tan powder (0.543 g, 53.4%).

PDHF-capped: A flame-dried Schlenk flask was brought into a nitrogen-filled glove box and charged with $Ni(COD)_2$ (1.29 g, 4.69 mmol, 1.5 eq) and bipyridine (0.75 g, 4.69 mmol, 1.5 eq). The mixture was dissolved in 8 mL DMF and COD (0.51 g, 4.69 mmol, 1.5 eq) was added. After the flask was brought out of the glove box and heated to 80˚ C for 30 min, 2,7-dibromofluorene **7** (1.50 g, 3.05 mmol, as a solution in 5 mL anhydrous toluene) was added under nitrogen. The flask was wrapped in aluminum foil and the reaction was stirred at 80˚ C for 48 h. Bromobenzene (20 μL, 5 mol%) was added as a solution in .4 mL dry toluene, and the mixture was stirred an additional 24 h. The hot solution was then added dropwise to an equivolume mixture of rapidly stirring concentrated HCl, acetone, and methanol. After filtering through a sintered glass frit, the polymer was redissolved in CH_2Cl_2 and precipitated twice into an equivolume mixture of acetone and methanol. The recovered polymer was dried under vacuum for 12 h to yield the desired product as a tan powder (0.745 g, 73.6%). M_w = 56,000; M_n

= 22,000; PDI = 2.6. ^{1}H NMR (300 MHz, $CDCl_3$) δ 0.78 (b, 10 H), 1.12 (b, 12 H), 2.11 (b, 4 H), 7.66-7.84 (b, 6 H). ^{13}C NMR (75 MHz, $CDCl_3$) δ 14.0, 22.6, 23.8, 29.7, 31.5, 40.4, 55.3, 120.0, 121.5, 126.1, 140.0, 140.5, 151.8.

3. Degradation Characteristics of PFMs

3.1. Overview

With the synthesis of a PFM library achieved, this chapter is devoted to their characterization. Since future applications of these polymers are likely to involve the blue-light emission properties that have made the parent PF materials attractive for device fabrication, a particular focus is given to their photophysical properties and to their stability. Studies comparing these new PFMs to PDHF in terms of their thermal and photo stabilities are then described.

3.2. Introduction: Degradation of PF

As mentioned in Sections 1.5-1.7, PFs exhibit a number of desirable properties. As homopolymers they emit in the blue (440-500 nm) in dilute solution and when cast as thin (<100 nm) films. As copolymers they can be chemically tuned to emit across the visible spectrum. The high quantum yields generally reported for PFs make them attractive materials for photoluminescent devices.

A primary barrier to the incorporation of PF in light-emitting applications has been the instability of these materials under device-operating conditions. For a material to warrant incorporation in an OLED, for example, intense light emission at static color purity over long periods of time is desired. PF presents highly desirable emission intensity, but is deficient in both

color purity and lifetime characteristics under device-operating conditions. Specifically, 9,9-dialkyl PF suffers from degradation of the purity of its light emission which manifests itself as a change from an intense sky blue color to a green-yellow color. This is observed in dilute solutions, and more problematically, in solid films of PF. As shown in Figure 3.1, the green-yellow color arises in photoluminescent (PL) spectra of PF in the form of a broad, featureless emission centered at ca. 525 nm. Concurrent with the increasing intensity of this emission is the diminishing intensity of the original transitions in PF. These changes occur when PF is exposed to current or to UV light. Figure 3.1 shows this degradation as the result of exposure to light of λ = 351 nm (intensity ~ 80 mW/cm^2). Reported by Sims, Grell, Bradley, and coworkers,[154] Figure 3.1 clearly shows the declining of desired emission in a thin film of PDOF. After only six minutes of exposure (sixth spectrum from bottom), the intensity of PDOF film emission at 450 nm has already diminished by more than 50%. The broad green band around 525 nm has simultaneously increased in intensity–after 8.5 min (fifth from bottom) this emission is essentially as intense as that at 450 nm.

The degradation of 9,9-dialkyl PF is also observed upon thermal treatment. As reported by Gong, Moses, Heeger and coworkers (Figure 3.2, right),[155] treatment of PDOF films in open atmosphere results in bleaching of the 0-0 (450 nm) and 0-1 (478 nm) emissions, though this result is obscured by normalization of the data. These spectra also show that after annealing 12 h in an open air environment, PDOF films suffer degradation that increases with increasing temperature. This behavior contrasts greatly with similar treatment of PDOF films in a N_2 environment (Figure 3.2, left). Examination of the spectrum produced after annealing PDOF at 140° C for 8 h shows that the broad band centered at 525 nm is noticeably less intense for PDOF annealed in N_2 compared to open air. The durations of annealing differ (8 h in N_2 vs. 12 h in air)

and as such the spectra are not directly comparable, but this observation serves to illustrate the fact that the thermal stability of 9,9-dialkyl PF differs by environment. Gong showed thereafter that PF electroluminescence (EL) was affected to an even greater extent by this degradation.

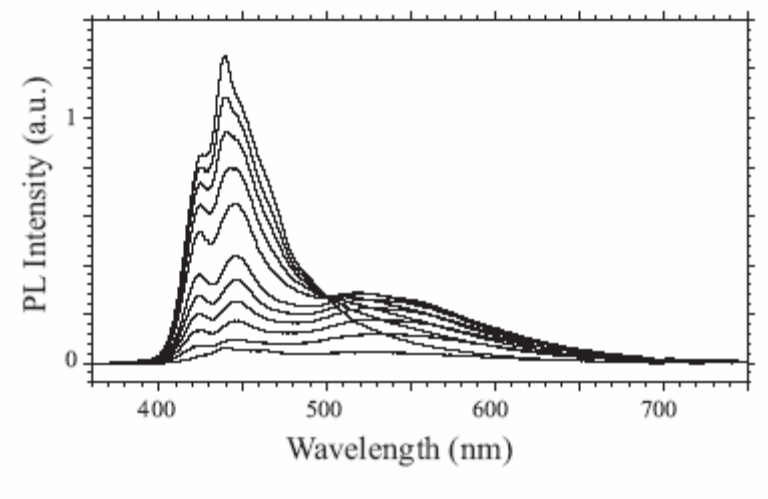

Figure 3.1. The photoluminescence spectra of a thin film of PDOF (film thickness < 100 nm, relative intensities, λ_{ex} = 351 nm, from top to bottom at 450 nm) at 0, 0.5, 1, 1.5, 3, 6, 8.5, 12, 18, 36, and 95 min UV exposure. This figure is from Sims, M.; Bradley, D.D.C.; Ariu, M. ; Koeberg, M., Asimakis, A., Grell, M.; and Lidzey, D.G. *Adv. Func. Mat.* **2004**, *14*, 765-781.

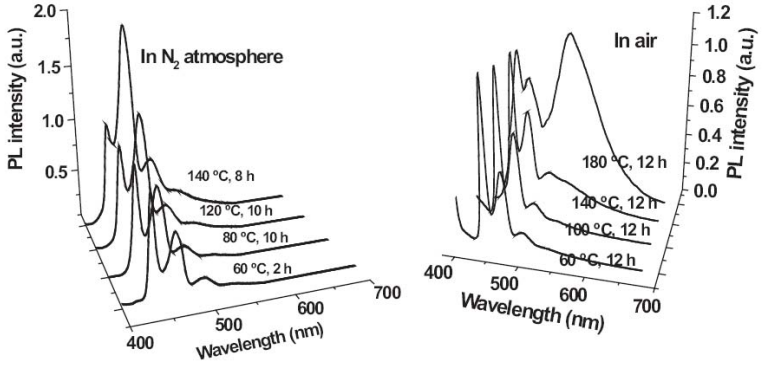

Figure 3.2. The photoluminescence spectra (normalized intensities, λ_{ex} = 380 nm) of thin films of PDOF annealed at varying temperatures in N_2 (left) and open air (right) atmospheres. The duration of annealing is indicated for each sample. This figure is from Gong, X.; Iyer, P.K.; Moses, D.; Bazan, G.C.; Heeger, A.J.; and Xiao, S.S. *Adv. Func. Mat.* **2003**, *13*, 325-330.

3.3. Reported Causes of PF Degradation

3.3.1. Degradation Processes in Related Conjugated Polymers

The root cause of degradation processes in CPs has been studied. Tada examined the circumstances by which an alkoxy-derivatized PPV degraded upon incorporation in a polymeric light emitting device (PLED) and noted that main chain scission and photooxidation were both occurring.[156] Bond scission occurring at vinylene sites along the polymer chain resulted in reduction of the polymer's molecular weight, and photooxidation was found to quench electroluminescence in the device, resulting in decreased average conjugation length. Tada noted that the decrease in emission intensity during the first minute of EL device operation was significantly slower than that subsequently observed, an observation which may suggest autocatalytic behavior within the film cast polymer. Included in Tada's findings was the idea that photooxidized defect groups present in the form of carbonyls quenched light emission from the active species, the active species in the case of alkoxy-PPVs being singlet excitons. The idea that minute amounts of carbonyl-bearing impurities could degrade polymer emission in LEDs was originally put forth by Galvin and coworkers at AT&T Bell Laboratories, who reported the detection of carbonyl species introduced during the pyrolytic synthesis of PPV in 1994.[157] The presence of carbonyl defects was established on the basis of IR spectroscopic data, which showed carbonyl stretching modes of weak intensity in the 1720 cm^{-1} region.

3.3.2. Excimer Emission and Interchain Aggregation Effects

The degradation of PF films marked by the growth of a broad green band at 525 nm has been widely reported. In fact, Pei's initial report on the regioselective preparation of 2,7-polyfluorene (Section 1.8) includes this finding.[64] The PL spectrum of Pei's BDOH-PF shows significant green emission for the pristine film–the band at 525 nm is already half as intense as the maximum intensity observed at 420 nm (Figure 3.3). Pei found BDOH-PF to be suitably stable to photochemical treatment, but upon heating the polymer film (1 h at 110° C under N_2) it was reported that fluorescence emission occurred across the visible spectrum, producing a white light of low relative intensity. As the band's intensity was greatly diminished in dilute solutions of THF, Pei concluded its enhancement in the film was the result of excimer formation. Excimers form in species with delocalized ground states, and PFs are, ideally, totally delocalized in the ground state. They are excited state dimer complexes formed by the interaction of an excited chromophore with an unexcited neighbor. Also, the reporting of interchain excimer formation had precedent in similar spectral features observed in the closely related ladder PPP-type materials.[158] Excimer formation had been postulated to result in red-shifted emission in ground state aggregates,[81] and so interchain excimer formation was initially proposed to explain the degradation pathway of PF systems.

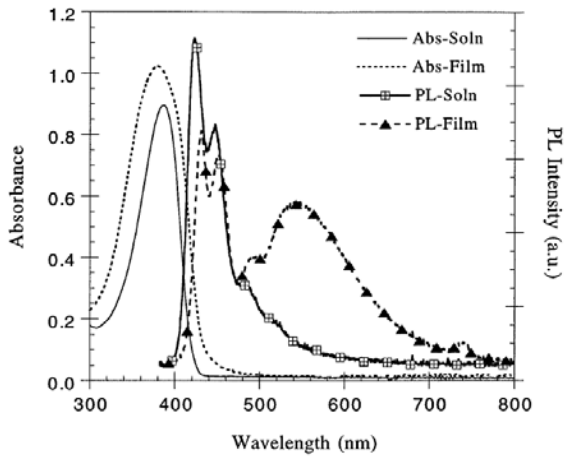

Figure 3.3. The absorbance and PL spectra for BDOH-PF in solution (THF) and as a thin film spun-cast from THF. This figure is from Pei, Q.; and Yang, Y. *J. Am. Chem. Soc.* **1996**, *118*, 7416-7417.

Bradley thereafter published studies showing that, when dissolved in poor solvents, PFs formed clusters which resulted in aggregation behavior in those solvents as well as in thin films cast from those solvents.[82] Solution-based aggregation effects of CPs can be identified as a function of solvent composition–a common two-component system used is $CHCl_3$-MeOH, or as a function of temperature, where aggregation is promoted upon cooling. Teetsov and Fox examined aggregation-based behavior of PFs bearing *n*-hexyl (PDHF), *n*-octyl (PDOF), and *n*-dodecyl substituents at C9. The polymers were found to undergo reversible absorbance features at high concentration (10 μg/mL) in good solvents (toluene and THF) as well as poor solvents (n-heptane, cyclohexane) and aggregation behavior was postulated. Fluorescence measurements of these polymers in *n*-heptane revealed that, in addition to the emissive S_1,S_0 singlet exciton responsible for the light produced by PFs, long-lived species of 2 ns and 8 ns were observed at 550 nm which were not observed in THF at similar concentration.

On the observation that, after annealing, a film of PDHF saw its fluorescence quantum yield decrease (albeit only slightly) Teetsov postulated that packing of shorter-length alkyl

chains brought fluorene moieties in closer proximity. This, in turn, could promote interchain aggregation over excimer emission. Vastly decreased quantum yields for these three polymers (reported ~3%) were found and attributed to aggregation-imposed packing forces.

3.3.3. Keto Formation and/or Exciton Migration

List, Scherf and coworkers found evidence that led to another credible hypothesis for the origin of the broad green emission in PFs. They invoked the presence of fluorenone defects in the polymer chain.[74, 159] Furthermore, they described a possible mechanism for the formation of these defects based on the presence of trace amounts of monoalkylated or non-alkylated impurities in monomers used to prepare PFs. Specifically, List and Scherf found that 9,9-monoalkylated and 9,9-dihydrofluorenes (i.e. non-alkylated) could conceivably undergo photo- and electrooxidative processes to generate keto defects along the polymer backbone. This mechanism was identified as a possible pathway to PF degradation by IR studies which revealed the C=O stretching mode (1721 cm^{-1}) at weak intensity upon photooxidation. Their IR spectra for monoalkylated PF and the assumed-dialkylated PF are reproduced in Figure 3.4. The top diagram shows mono-alkyl PF as the dashed line spectrum superimposed on that of dialkyl PF. It is evident that the mono-alkylated PF already shows evidence of some C=O stretching. The dialkyl PF material, on the other hand, shows an absence of this stretching mode. Upon irradiation by the halogen lamp for periods of two, four, and six minutes, the dialkyl PF is observed to undergo a changing IR spectrum in the carbonyl region. The bottom spectra in Figure 3.4 show the evolution of the C=O stretch over this time span. List and Scherf tied this finding in with PL spectra that showed that a film of dialkyl PF, when irradiated *for the same*

periods of time, underwent the familiar change showing the dramatic and dominant appearance of the broad band at 525 nm. EL evidence also pointed to a connection between the weak C=O stretch and the broad band.

Due to the fact that their PFs had been prepared using Yamamoto couplings, List and Scherf initially proposed a Ni^0-mediated pathway that yielded intermediate fluorenyl anion (Scheme 3.1). The mechanism for this initial step is not well understood, but nonetheless upon deprotonation the anion can conceivably react with molecular oxygen to form highly reactive hydroperoxide anions. Rearrangement to yield a keto defect thus forms the fluorenone moiety.

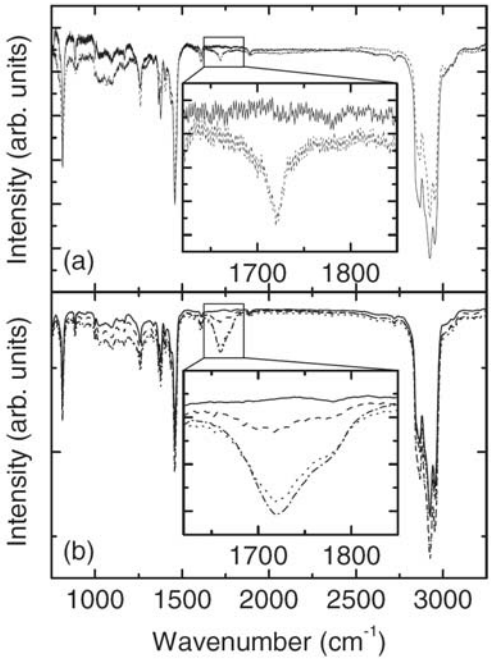

Figure 3.4. The IR spectra reported by List and Scherf for monoalkylated and dialkylated PF. (a) Inset: The carbonyl region for pristine dialkyl PF (solid line) and monoalkyl (dashed line) PF films. (b) Inset: The evolution of the carbonyl stretching mode upon photooxidation for (from top to bottom at 1721 cm^{-1}) 0, 2, 4, and 6 min. This figure is taken from List, E.J.W.; Guentner, R.; Freitas, S.-d. P.; and Scherf, U. *Adv. Mater.* **2002**, *14*, 374-378.

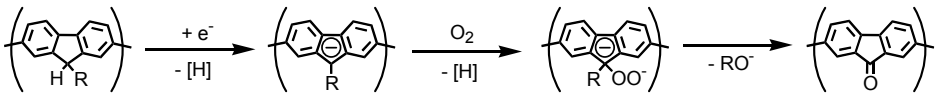

Scheme 3.1. The Ni^0-mediated pathway proposed by List and Scherf to explain the appearance of keto defects in PF. This figure is reproduced from Scherf, U., and List, E.J.W. *Adv. Mat.* **2002** , 477-487.

Ma and coworkers have recently proposed the radical pathway shown in Scheme 3.2.[160] Although the initiation requires the presence of monoalkylated defects, the proposed propagation steps show oxidation of dialkylated fluorene units. Consistent with this proposal is the observation by Meijer and coworkers that established that rigorous purification of monomers to remove mono-alkylated contaminants prior to polymerization increased the stability of the resulting PF.[161] Also relevant was the discovery by List and coworkers that mono-alkylated fluorenes could be converted into fluorenones under the common polymerization conditions.[159] Samples of PF that have been exposed to heat, light or current under an oxygen atmosphere show new bands in the IR at 1717 and 1707 cm^{-1} that are comparable to those exhibited by small molecule fluorenone.[162] Moreover, several groups have deliberated synthesized fluorene-*co*-fluorenone oligomers whose absorption and emission spectra are consistent with that of the degraded PF samples.[100, 163-168]

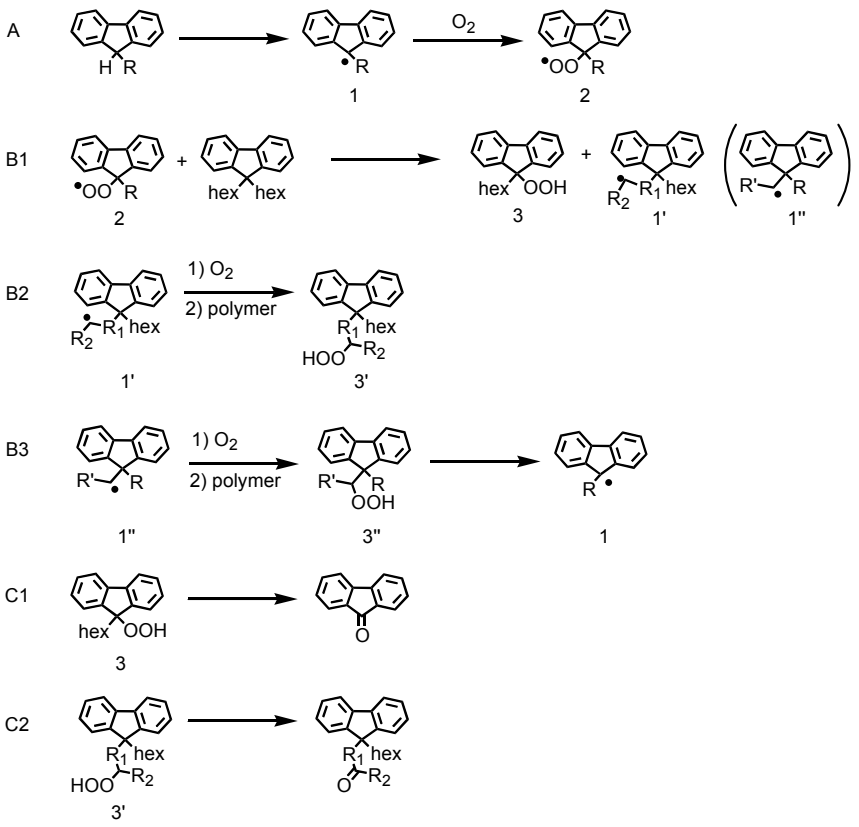

Scheme 3.2. The mechanism for keto formation by (A) radical initiation, (B1–B3) radical propagation, and (C1 and C2) peroxide rearrangement to keto defects. This figure is reproduced from Liu, L;, Tang, S.; Liu, M.; Xie, Z.; Zhang, W.; Lu, P;, Hanif, M.; and Ma, Y. *J. Phys. Chem. B* **2006**, *110*, 13734-13740.

3.3.4. Evidence In Favor of Keto Formation

Recent studies by several groups have convincingly established that the green emission is due to on-chain keto defects and that excimer formation is both unlikely and unnecessary to the formation of the 525 nm band in PF and in ladder poly(para-phenylenes).[169-173] The presence of fluorenones are now acknowledged in most circles as being crucial to the appearance of the 525 nm band, though some continue to invoke excimers because they claim that the defects are "necessary but not sufficient" to produce the observed spectra.[119, 154] Other groups have also

presented arguments in favor of excimer formation as well although it is not clear if these researchers continue to support the hypothesis given recent reports.[69, 174]

Lupton and coworkers carried out experiments on *single* polymer chains of fluorene-*co*-fluorenone.[168] They found a high correlation between the % fluorenone, the intensity of the green emission, and the intensity of the blue emission for a sampling of 1152 isolated individual chains. Moreover, they found no evidence for excimer emission from a control molecule which placed two fluorenone units in a cofacial arrangement to simulate a situation where two fluorenone units in a single polymer chain could interact (Figure 3.5).

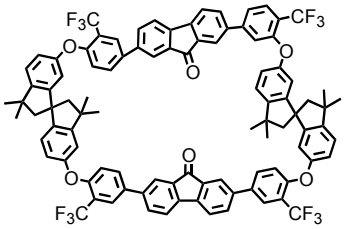

Figure 3.5. Macrocycle studied by Lupton for proximity-enhanced excimer formation.

The work of Chi and coworkers also substantiates the primary role of keto defects. They prepared a series of 9,9-dialkyl oligofluorenes (Figure 3.6a) with central fluorenone defects.[167] The characteristic green emission was found to be concentration independent, which ruled out bimolecular excimers as the source of the emission. When these oligomers were blended with pristine PF, the lifetime of the blue emission from PF decreased dramatically (from 273 to 33 ps) and became multiexponential as the weight percent of the oligomer in the blend was increased from 0-10%. This finding is represented in the steady-state fluorescence spectra shown in Figure 3.6b. Moreover, the obvious quenching of the PF emission by the added fluorenone-containing oligomers is strong evidence for Förster-type energy transfer from non fluorenone-containing

polymer to the oligomers. It should be noted that overlap between the emission of PF and the absorption of fluorenone that is a prerequisite for efficient energy transfer is observed.[165]

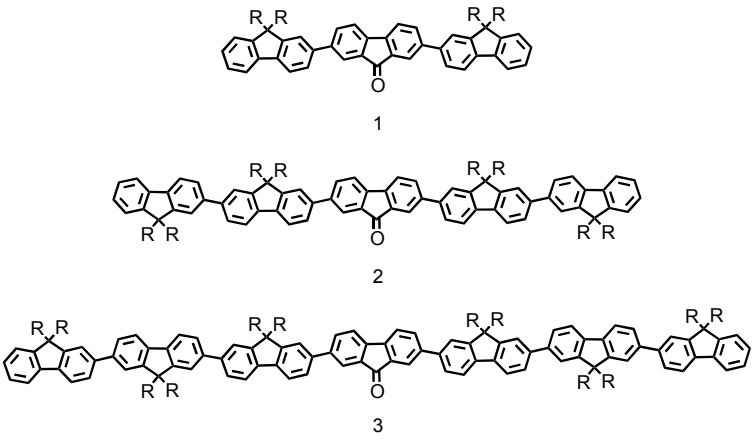

(a)

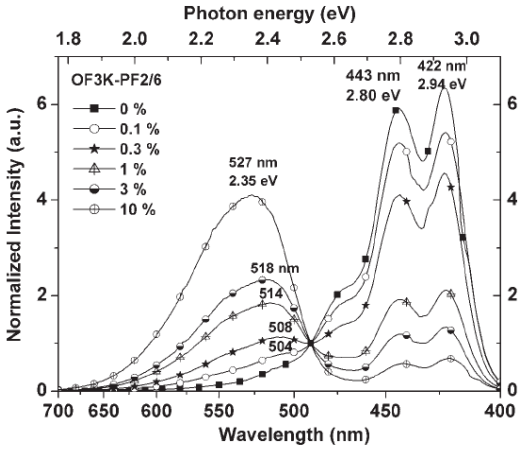

(b)

Figure 3.6. (a) The oligofluorenes prepared by Chi. (b) Steady-state fluorescence spectra of PF doped with amounts of Chi's oligofluorenes at increasing concentration (0 – 10%). This figure is taken from Chi, C.; Im, C.; Enkelmann, V.; Ziegler, A.; Lieser, G.; and Wegner, G. Chem. Euro. J. **2005**, *11*, 6833-6845.

In summary, experimental evidence from several groups suggests that fluorenones that are present either from the original reaction conditions or that are formed when the sample is

exposed to thermal, photo or electrical energy act as exiton traps. Intrachain and Förster energy transfer events result in the quenching of the original blue fluorene emission in favor of the fluorenone-based green emission. The inhbition or prevention of this occurrence in PFs is of great importance.

3.4. Approaches to Green Band Inhibition in PFs

Soon after Pei's original observation of undesired green emission in PFs, approaches to homo- and copolyfluorenes with inhibited green emission were reported. A number of these approaches were recently reviewed by Neher.[81] As this chapter is concerned with the inhibition by chemical means of keto formation and green emission, only chemical approaches to this problem are described, though physical approaches (i.e. blending, MW control, see for ref. Neher) have been used. Chemical strategies have used the following rationale:

That substitution of dendritic groups at C9 (see for ref.: M and N in Figure 1.7, Section 1.4) limits access at this position to radical/oxidative species. This has been shown to slow the rate of keto defect formation, though the complete prevention by this method has not been reported. End-capping PF with charge-trapping groups. An example cited for this purpose is the anthracene moiety.

End capping with hole-trapping groups. Triarylamines have been used for this purpose to yield PF with an observed green emission component which decreases with increasing end capper concentration. Related to this is the copolymerization with hole trapping monomer units. Owing to the synthetic

flexibility of the Yamamoto route to PFs a variety of triarylamines have been incorporated as stastical comonomers on main chain of PFs.[93]

End capping with crosslinking groups. This approach uses postpolymerization modification to create a rigid, liquid crystalline network. Thermal crosslinking of fluorene-styrene copolymers has been performed to create a fixed matrix for encapsulation of fluorene segments. Photochemical crosslinking of acrylate groups terminating an oligofluorene macromonomer was communicated (but not performed) recently.[152]

Interruption of conjugation by m-phenyl linkage incorporation. Ritchie, Crayston and coworkers used this approach to produce rigid rod PFs with shortened effective conjugation lengths as a method for decreasing the likelihood of excimer contamination.[175] This is represented conceptually in Figure 3.7. Ritchie found that although excimer formation was inhibited, the copolymers produced were of lower molecular weight with increasing amount of *meta*-phenylene monomer unit used. Presumably this was a result of decreased solubility conferred to the material by the *meta* linkage. A hypothesis offered for the trend towards decreased excimer formation with increasing meta-phenylene was that conjugation breaks in the copolymers prevented excitons from easily migrating to ketone groups present on PF segments. In preventing exciton migration, then, keto defect emission was effectively suppressed.

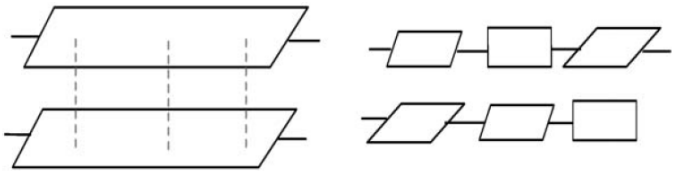

Figure 3.7. Depiction of approach used by Crayston to describe employment of conjugation interrupters in PF. This figure is taken from Ritchie, J.; Crayston, J. A.; Markham, J.P.J.; and Samuel, I.D.W. *J. Mat. Chem.* 2006 **16**, 1651-1656.

Interruption of conjugation by aliphatic linkage incorporation. Whereas *m*-phenyl linkages preserve the rigid rod motif while decreasing the effective conjugation lengths of segments within the polymer, the copolymerization of PF with aliphatics yields rod-coil copolymers with broken conjugation. An example from the literature is the recent report of poly(terfluorene-*co*-ether)s produced by Chochos and Kallitsis.[35] This copolymer was described in Section 1.1.10.3 and is considered in comparison to PFcMs in Section 3.6.3.

3.5. Experimental

3.5.1. Differential Scanning Calorimetry

Differential scanning calorimetry (DSC) was performed on 2–5 mg samples in a Thermal Analyst 2000 (TA Instruments) DSC 2910 differential scanning calorimeter. A typical method involved a first heating scan at 20° C/min over a temperature range of -40 to 270° C. After a hold time of 2 min, a cooling scan was performed at -20° C/min over a temperature range of 270° C to

-40° C. Following another holding time of 2 min, a second heating scan was performed at 20° C/min to 290° C.

3.5.2. UV-Vis Spectroscopy

Absorption spectra for all PFMs were obtained in dilute chloroform (~10^{-6} M by fluorene content) on a Perkin-Elmer UV/VIS/NIR Spectrometer Lambda 9. Spectra were analyzed using UV Winlab software supplied by Perkin-Elmer.

3.5.3. Photoluminescence Spectroscopy

PL spectra for all PFMs were obtained in dilute chloroform (~10^{-6} M by fluorene content) on a Varian Cary Eclipse Fluorescence Spectrophotometer. Spectra were analyzed using software supplied by Varian. Thin film PFM samples were prepared by drop casting from 20-25 mg/mL solutions in toluene onto quartz slides (Chemglass, 75x25 mm) and, after allowing for slow evaporation, removing remaining solvent at RT under high vacuum. Films of PDHF were prepared in the same manner from 50 mg/mL solutions in $CHCl_3$.

3.5.3.1. Photoinduced Film Degradation

Pristine films were irradiated using a UVP Blak-Ray lamp, Model UVL-21 (λ = 366 nm, 115 V, 60 Hz, 0.16 A). PL spectra were recorded at total irradiation times of 0, 5, 15, and 30 min.

3.5.3.2. Thermally Induced Film Degradation

Films were annealed in a nitrogen filled glove box for 30 min at 200-230° C, then heated in open air at 160° or 200° C. Spectra were recorded at total heating times of 0, 0.5, 1, 2, and 4 h (160° C) or 0, 0.5 and 1 h (200° C). Films were cooled to RT prior to collection of spectra.

3.5.4. Infrared Spectroscopy

Thin film PFM samples were prepared by drop casting from 20-25 mg/mL solutions in toluene onto single-crystal NaCl disks and, after allowing for slow evaporation, removing remaining solvent at RT under high vacuum. Films of PDHF were prepared in the same manner from a 50 mg/mL solution in $CHCl_3$. IR spectra were collected on a Nicolet Avatar 360 Fourier transform infrared spectrometer (FT-IR) using the Transmission ESP Program. All spectra were averaged over 16 scans.

3.5.4.1. Photoinduced Film Degradation

Samples were irradiated using a UVP Blak-Ray lamp, Model UVL-21 (λ = 366 nm, 115 V, 60 Hz, 0.16 A). IR spectra were recorded at total irradiation times of 0, 20, 40, 60 and 120 min.

3.5.4.2. Thermally Induced Film Degradation

Samples were heated in open air at 200° C. Spectra were recorded at total heating times

of 0, 30, and 60 min. Films were cooled to RT prior to collection of spectra.

3.5.5. Exposure of PF3M10 to Ni^0-mediated PDHF Preparation Conditions

Following the method of Kreyenschmidt, a flame-dried Schlenk flask was brought into a nitrogen-filled glove box and charged with $Ni(COD)_2$ (59 mg, 0.214 mmol, 1.5 eq) and bipyridine (33 mg, 0.214 mmol, 1.5 eq). The mixture was dissolved in 2 mL DMF and COD (26 μL, 0.214 mmol, 1.5 eq) was added. After the flask was brought out of the glove box and heated to 80˚ C for 30 min, **PF3M10** (158 mg, 0.139 mmol by fluorene content, as a solution in 2 mL anhydrous toluene) was added under nitrogen. The flask was wrapped in aluminum foil and the reaction was stirred at 80˚ C for 48 h. The hot solution was then added dropwise to an equivolume mixture of rapidly stirring concentrated HCl, acetone, and methanol. After filtering through a sintered glass frit, the polymer was redissolved in CH_2Cl_2 and precipitated twice into an equivolume mixture of acetone and methanol. The recovered polymer, **PF3M10-2** was dried under vacuum for 12 h to yield the product as a white solid (102 mg, 64.6%).

3.6. Results and Discussion

One of the fundamental goals that motivated our synthesis of PFM RSCs is the correlation of properties with sequence. In this chapter we present our initial characterization studies: DSC, UV-Vis, PL, and IR. In addition, we present detailed studies on the thermal- and photo-stability of PFMs.

As we also compare the properties of our segmented PFMs to those of the parent homopolymer. It is important to reiterate that the samples of PDHF comprise three separate preparations and are distinguished as follows: **PDHF-old**, **PDHF-new**, and **PDHF-capped**. **PDHF-old** was prepared in August 2005 using the preparation described in Section 2.5.7. **PDHF-new** was prepared by the same procedure in August 2006. **PDHF-capped** is described in Section 2.5.7 as phenyl-capped polymer and was prepared in June, 2006. As these samples did not behave equivalently, particularly under degradation conditions, the collection dates for affected spectra are noted in the text.

3.6.1. Solution and Bulk Phase Optical Properties of PFMs

Absorption data were collected for dilute solutions of each PFM in chloroform. Emission spectra for each RSC were collected in the solution phase and in the solid phase as thin films (Figure 3.8 and Figure 3.9). Solution and bulk phase spectra for **PDHF-new** are included for reference. The data are summarized in Table 3.1.

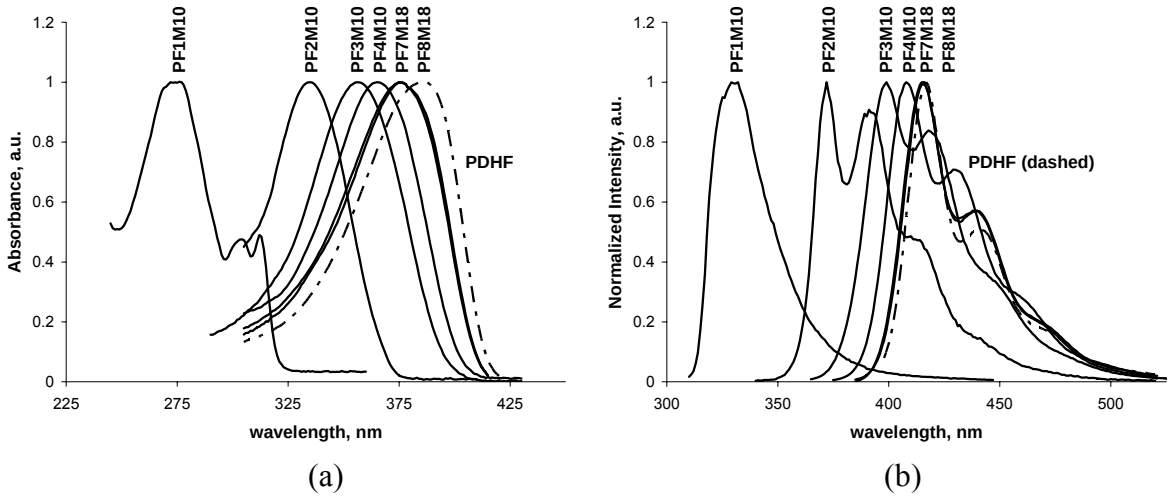

Figure 3.8. The absorbance (a) and emission (b) spectra of PFMs as dilute (~10^{-6} M) solutions in $CHCl_3$. Spectra for **PDHF-new** are included for reference.

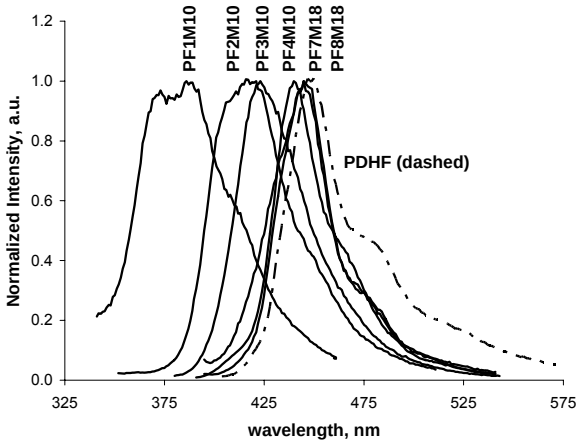

Figure 3.9. The emission spectra of indicated PFMs as thin films. The spectrum for **PDHF-new** is included for reference.

	PFM	λ_{abs}, in $CHCl_3$ (nm)	λ_{em}, nm, in $CHCl_3$ (λ_{ex}, nm)[a]	λ_{em}, film (nm)
1	**PF1M10**	279	330 (300)	386
2	**PF2M10**	335	371 (335)	416
3	**PF3M10**	356	401 (355)	423
4	**PF4M10**	365	409 (365)	438
5	**PF1M18**	278	332 (300)	390
6	**PF2M18**	335	372 (335)	414
7	**PF3M18**	354	399 (355)	429
8	**PF4M18**	366	408 (365)	438
9	**PF7M18**	376	416 (375)	445
10	**PF8M18**	375	415 (375)	445
11	**PDHF-new**	385	417 (388)	450

[a] Values in parentheses are the excitation wavelengths used to collect emission spectra for dilute solutions and thin films of the PFcM.

Table 3.1. Summary of PFM absorbance and emission maxima.

For reasons already discussed (Section 1.6 and Section 1.10.1), light absorbance and emission are qualities of primary interest in fluorene-bearing polymer systems. To provide a context for our data it is important to consider the results of Geng's and Chen's extensive studies on monodisperse oligofluorenes,[85] and Klaerner's and Miller's prior to that.[48] Both groups have shown that exact control of chromophore segment length allows for the tuning of the substrate's light absorbance and emission maxima. Specifically, they found that the absorption and emission maxima shifted to the red with increasing oligomer length. At short segment lengths ($n < 6$) the magnitude of red shifting was observed to be fairly large at 5 to 20 nm from segment length n to $n+1$, consistent with the notion that, percentage-wise, the oligomer's conjugation length was increasing most rapidly at this stage. For example, Geng's terfluorene exhibited a first absorbance maximum at λ = 350 nm in $CHCl_3$; this figure shifted 11 nm to 361 nm for the quaterfluorene. Shifts in maxima of nearly equal magnitudes were observed in absorbance and emission spectra for thin films of short length oligofluorenes. As oligofluorenes of longer segment lengths were prepared, their optical properties were found to plateau. For example, hexafluorene (n = 6) was found by Geng to give $\lambda_{max,\ abs}$ = 370 nm; dodecafluorene (n = 12)

exhibited $\lambda_{max,\ abs}$ = 379 nm, a comparatively small movement of 9 nm over a lengthening of six oligomeric units. That the optical maxima were leveling off was confirmation of Miller's assessment of the effective conjugation length of polyfluorene being approximately twelve repeat units, or 24 aromatic rings.

As the PFMs we produced incorporated oligofluorenes of exact segment lengths, our expectation was that their solvent-based and bulk phase optical properties would track with the trends reported in literature for the isolated oligomers. PFMs in dilute solution ($CHCl_3$, ~10^{-6} M based on fluorene content) are indeed found to give maximum light absorption at progressively longer wavelengths. Monofluorenyl PFMs (entries 1 and 5, Table 3.1) absorb at the shortest wavelengths. Increasing the fluorene segment length to two units shifts the wavelength of maximum absorption bathochromically by approximately 55 nm (entries 2 and 6). A similar shift of 10 nm is observed in going from quaterfluorenyl PFMs (entries 4 and 8) to the heptafluorenyl **PF7M18** (entry 9, λ_{abs} = 376 nm). A barely discernible decrease in λ_{abs} is observed for **PF8M18** (entry 10, λ_{abs} = 375 nm). This finding is interpreted as an indication that the absorption properties of PFMs are reaching a plateau, i.e. that they are beginning to approach the effective conjugation present in PDHF. Comparison of the absorption maximum of **PF8M18** with an as-prepared sample of **PDHF-new** (entry 11, λ_{abs} = 385 nm) supports this notion. Furthermore, Geng observed movement to the red of only 1 nm in going from the oligomeric heptafluorene to octafluorene.[85] Given that the precision associated with the UV-Vis instrument used to perform these studies is +/- 2 nm, the trend, as outlined above, holds.

Emission spectra of PFMs also show that they are chemically tuned according to oligofluorene segment length. As summarized in Table 3.1, a range of 85 nm within the violet-blue region of the visible spectrum is covered by the copolymers studied. Light at the low end of

this range is emitted by monofluorenyl PFMs at λ_{max} = 330 and 332 nm (entries 1 and 5). As with absorption, emission moves significantly to the red (40-41 nm) for bifluorenyl PFMs (entries 2 and 6). Excellent agreement of light emission is observed within each pair of PFMs having identical fluorene segment lengths. As was observed in the absorption spectra, a movement to the red, this time of 8 nm, is found in comparing the emission of **PF4M18** (entry 8, λ_{max} = 408 nm) with **PF7M18** (entry 9, λ_{max} = 416 nm). The emission maximum for **PF8M18** comes 1 nm less than for **PF7M18**. The trend toward longer wavelength emission has clearly leveled at this point, however. **PDHF-new** is found to emit just 1 nm greater than that found for **PF7M18**, at λ_{max} = 417 nm. The emission maxima for terfluorene–through octafluorene-containing PFMs fall squarely in the sky blue portion of the visible spectrum.

As observed for the copolymers in dilute solution, thin films of the PFMs exhibit emission maxima at successively longer wavelengths and as the fluorene block length lengthens the series rapidly converges to the thin film emission of PDHF (dashed series). Film emission studies of these copolymers are discussed in detail in Section 3.6.3.

3.6.2. Differential Scanning Calorimetry

A selection of the PFMs have been characterized by DSC: **PF2M10**, **PF3M18**, **PF4M10**, **PF4M18**, **PF7M18**, and **PF8M18**. Figure 3.10 shows the calorimetric data obtained for the first heating scans of each PFM studied. DSC data sets for **PF2M10**, **PF3M18**, **PF4M18**, and **PF7M18** can be found in Appendix H. The data are summarized in Table 3.2. It should be noted that many of the assignments are tentative. Data for some members of the complete PFM series

have yet to be collected and it may be necessary to examine samples with multiple thermal histories before all features will be well understood.

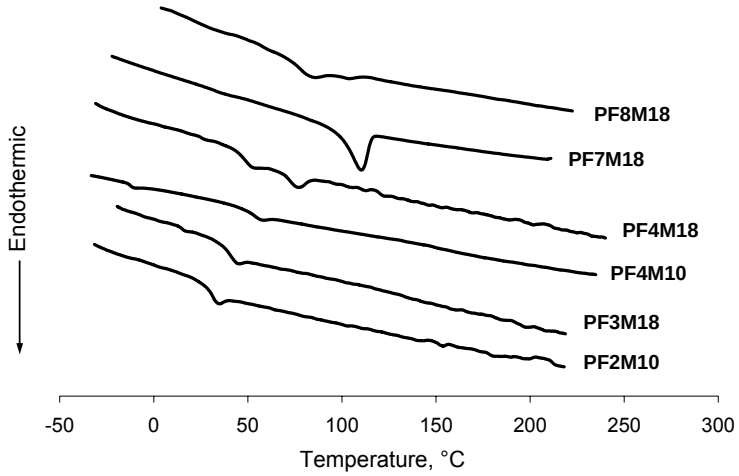

Figure 3.10. DSC scans for first heating cycles of indicated PFMs. Data was recorded at 20° C/min heating rate.

	T_g (° C)	T_{endo} (° C)
PF2M10	-9[a]	29
PF3M18	18	40
PF4M10	-9	55
PF4M18	47	78
PF7M18	64[b]	111
PF8M18	77[a]	105
PDHF		168

[a] Tentative assignment. Transitions are weakly defined.

[b] This transition is not visible in the cycle, but has been estimated based on the cooling data.

Table 3.2. Phase transitions for PFMs as found by DSC.

In general, the PFMs show two transitions, a very weak transition at low temperatures that, by the shape, is clearly a T_g and a stronger endothermic transition that is likely a T_m. Focusing particularly on the M18 series, this pattern is very clear–except for **PF7M18** polymer, the spectrum of which displays only a very strong endothermic transition in the first heating. An

assignment of a T_g for this polymer can be made from the cooling scan (not shown), but without further verification this assignment must be regarded as tentative at best. Even with the tenuous T_g assignment **PF7M18** does not fit well into the series, however. It is not known at this point whether the data itself is anomalous or if the DSC data is revealing thermal behavior that is particular to the F7M18 sequence. If the data for **PF7M18** is excluded, the behavior of the remaining M18 polymers can be generalized: the initial T_g and the second endothermic transition are observed to shift to higher temperatures as a function of fluorene segment length.

It is also of interest to compare the M10 and M18 polymers. Both of the M10 polymers exhibit a very weak T_g at < -9 °C. Given the differences in sequence it is tempting to assign this transition to the shorter methylene segment. Although the higher temperature endotherm shifts to higher temperature between **PF2M10** and **PF3M10**, the temperatures observed for **PF3M10** and **PF3M18**, the only comparable samples, are not the same. Based only on these limited data, however, we could hypothesize that the transition corresponds to a T_m for the whole F_xM_y segmer rather than for an individual block. Clearly, further data must be collected before this hypothesis can be evaluated.

As a reference for the interpretation of the thermal data, it is useful to examine the DSC traces for the oligofluorenes prepared by Yoon, Wegner and coworkers (Figure 3.11).[176] Their oligomeric substrates, which bear branched side chains, exhibit T_gs ranging from -21 to 42 °C that increase with the number of repeating units. A second, endothermic transition is also observed for oligomers with four or more fluorene units. This transition, which also increases with increasing oligomer length (64-246 °C) is identified as the liquid-crystalline to isotropic transition by polarized optical microscopy (POM) study. The Schlieren texture that is characteristic of a nematic phase was observed for each of these oligomers below T_{iso}.

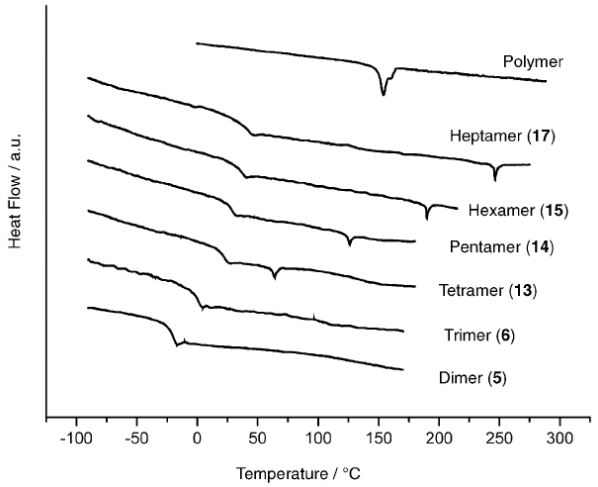

Figure 3.11. The first heating runs of monodisperse oligofluorenes. This figure is from Jo, J.; Chi, C.; Hoeger, G.; Wegner, G.; Yoon, D.Y. *Chem Euro. J.* **2004**, *10*, 2681-2688.

These data suggest that the second endothermic transition for the PFM RSCs could be a crystalline-to-liquid crystalline transition, rather than a simple T_m. An analysis of **PF3M18**, **PF4M18**, and **PF7M18** by POM, however, did not give any evidence to support this supposition. Neither did segmers **SF3M10**, **SF3M18** or **SF4M18** show any birefringence when heated. **PF8M18** is still being studied.

The lower bulk-phase order of our RSC polymers relative to the isolated oligomers of Yoon and Wegner is not surprising. The linking of the oligomers would be expected to kinetically hinder the close packing of the fluorene segments and possibly interfere physically with the alignment. Moreover, as described in Section 1.7, branched side chains stabilize liquid crystalline phases relative to their straight-chain analogs.

3.6.3. Degradation Studies

As discussed in Section 3.3, the instability of PF when processed into thin films is a barrier to its application in, among other things, LEDs. The degradation of PF is believed to result primarily from the oxidative formation of fluorenone units. Degradation studies were performed to gauge the ability of PFMs to withstand this type of keto defect formation. As degradation may be photoinduced and thermally induced, both pathways were explored with regard to PFM stability. Studies were performed using PL and IR spectroscopy.

3.6.3.1. PFM Photostability Monitored by PL Spectroscopy

Photooxidation as a cause of PL degradation in PFs has been described (Section 3.3). With this in mind, the stability of a selection of PFMs towards radiation from a UV light source was investigated. Films of **PF3M10**, **PF3M18**, **PF4M10**, **PF4M18**, **PF7M18**, and **PDHF-capped** were prepared for this purpose. PL spectra of relative and normalized intensities for **PDHF-capped** and a typical PFM, **PF4M18**, are presented in Figures 3.12 and 3.13, respectively. PL spectra for **PF3M10**, **PF3M18**, **PF4M10** and **PF7M18** investigated in this study are included as Appendix D.

As shown in Figure 3.12a, the PL spectrum of pristine **PDHF-capped** changes rapidly–there is visible evidence of color degradation in the form of the green band *after only five min UV irradiation*. At the 15 min mark (dashed line, Figure 3.12a), the desired blue emission at 450 nm has photobleached to roughly 40% its original intensity. More importantly, the green emission is now at comparable intensity. At 30 min UV irradiation, the green emission

dominates the PL spectrum of PDHF-capped. The normalized spectra in Figure 3.12b bear this out.

By contrast, PL spectra obtained for **PF4M18** after the same periods of UV radiation show a noticeably slower rate of photobleaching (Figure 3.13). Further, after 30 min UV exposure **PF4M18** shows *total absence* of green emission about 525 nm. PL profiles for the five PFMs and PDHF-capped examined in this study have been summarized in chart form in Figures 3.14 and 3.15.

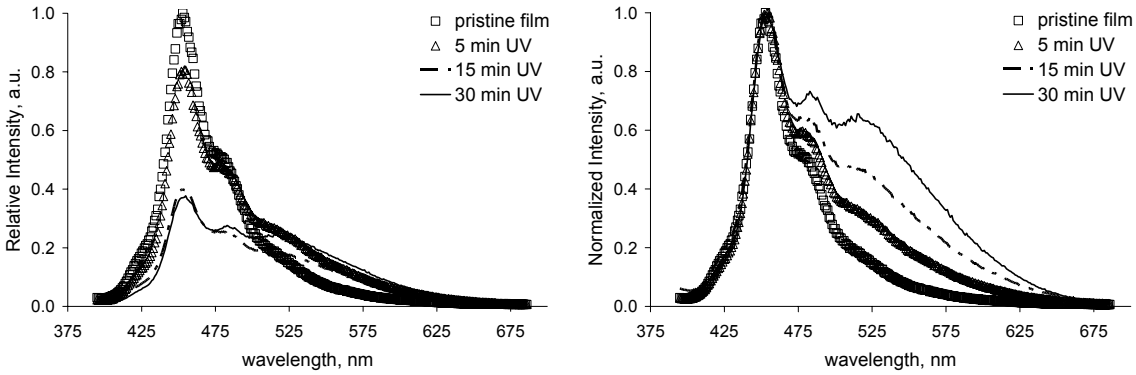

(a) (b)

Figure 3.12. PL spectra of relative (a, λ_{max} for pristine film = 1) and normalized (b, λ_{max} for all spectra = 1) intensities for a film of **PDHF-capped** irradiated by UV (λ = 366 nm) light.

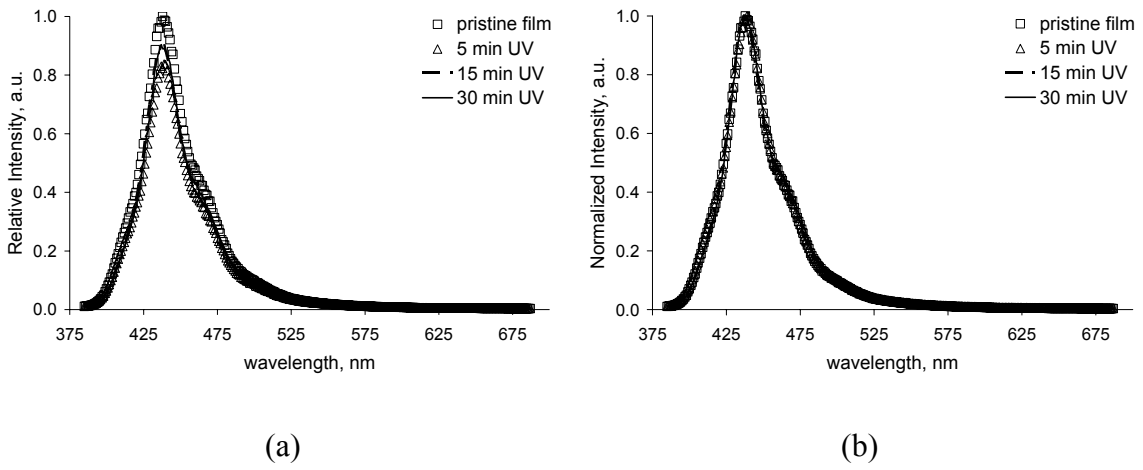

(a) (b)

Figure 3.13. PL spectra of relative (a, λ_{max} for pristine film = 1) and normalized (b, λ_{max} for all spectra = 1) intensities for a film of **PF4M18** irradiated by UV (λ = 366 nm) light.

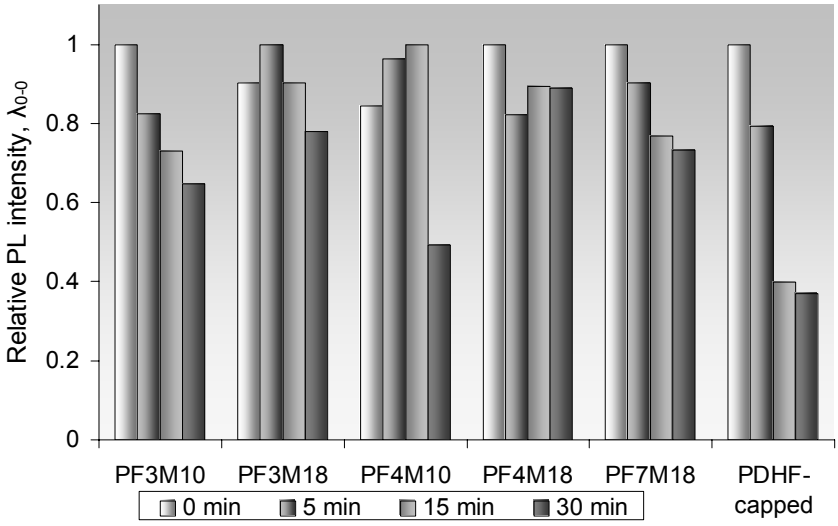

Figure 3.14. Relative intensities of blue emission maxima for **PF3M10**, **PF3M18**, **PF4M10**, **PF4M18**, **PF7M18**, and **PDHF-capped** after UV irradiation (λ_{ex} = 366 nm) for periods of 0, 5, 15, and 30 min total.

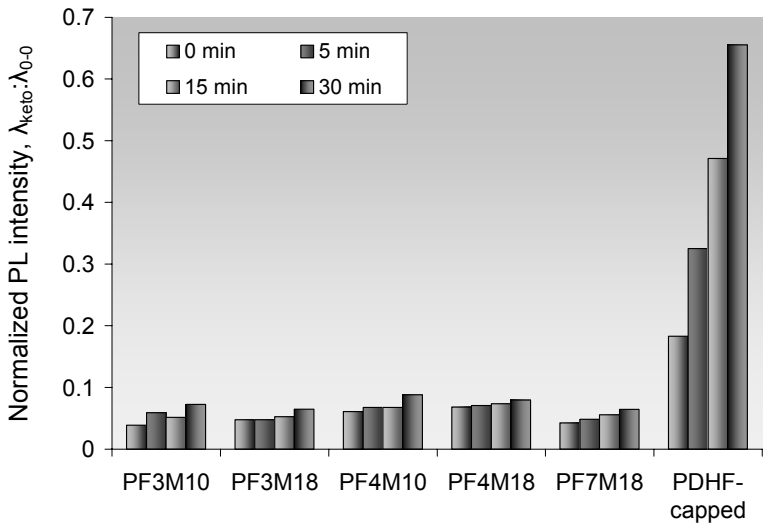

Figure 3.15. Ratio of green band emission maximum normalized relative to blue emission maximum for **PF3M10**, **PF3M18**, **PF4M10**, **PF4M18**, **PF7M18**, and **PDHF-capped** after UV irradiation (λ_{ex} = 366 nm) for periods of 0, 5, 15, and 30 min.

Figure 3.14 charts the relative intensities of the blue emission maxima for each PFM as well as **PDHF-capped**. With the possible exception of **PF4M10**, each PFM shows enhanced blue light emission over the duration of testing with respect to **PDHF-capped**. These observations suggest that bleaching processes occur less readily for PFM films. It was noted that **PDHF-capped** had aged approximately two months at the time this study was performed, which explains in part the pronounced decrease in relative intensity for this film. However, the ages of each PFM were similar, if not older at the time of their characterization in this study.

In addition to longer lived blue emission properties, the PFMs studied show a marked decrease in the growth of the green emission at λ = 525 nm as illustrated in Figure 3.15. This behavior was typical of every PFM studied–there is essentially zero increase in emission in the green band for films of these copolymers, whereas **PDHF-capped** underwent an increase in emission intensity at λ = 525 nm by a factor of 3.5. Photostabilities for the PFMs selected for this study do not appear to vary based on fluorene or alkyl segment length. Under the conditions used

herein they exhibit superior photostabilities relative to **PDHF-capped** when subjected to UV irradiation.

PFMs can also be compared to related rod-coil copolyfluorenes. One pertinent example is the PFcE copolymer series prepared by Chochos and Kallitsis.[177] As mentioned in Section 1.10.3, these copolyfluorenes feature terfluorene segments with α,ω-bisalkoxy spacer groups. The general PFcE chemical structure is shown in Figure 3.16. Chochos prepared PFcEs having methylene segments nine to twelve units in length.

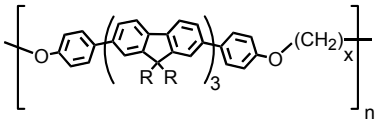

Figure 3.16. An example of a PFcE prepared by Chochos and Kallitsis.[177]

An investigation into the photostabilities of PFcEs was performed using PL spectroscopy. The relative and normalized PL spectra from a typical experiment on a PFcE (for $x = 10$ in Figure 3.16) are shown in Figure 3.17. As shown in Figure 3.17a, extensive bleaching of the blue emission occurred within 5 min UV exposure; this progressed over 30 min to the point that blue emission was severely quenched. Furthermore, as revealed in the normalized spectra in Figure 3.17b, keto formation was not inhibited as green emission at $\lambda = 525$ nm became approximately 20% as intense as the desired blue emission after 30 min. Due to differences in irradiation sources, the photostabilities of PFMs and PFcEs can not be directly compared. That detail notwithstanding, **PF3M10** and **PF3M18** compare very favorably to Chochos' PFcEs, of which the values used in Figure 3.18 have been reasonably estimated using the spectra in Figure 3.17. For the PFcE possessing methylene segment lengths of 10 units, **PF3M10** and **PF3M18** are seen

to maintain their blue emission at greater relative intensity over identical time periods (Figure 3.18a). Furthermore, green emission at λ = 525 nm looks to be dramatically reduced in PFMs (Figure 3.18b). After 30 min UV irradiation Chochos' PFcE displays green emission at approximately five times the intensity relative to **PF3M10** and **PF3M18**.

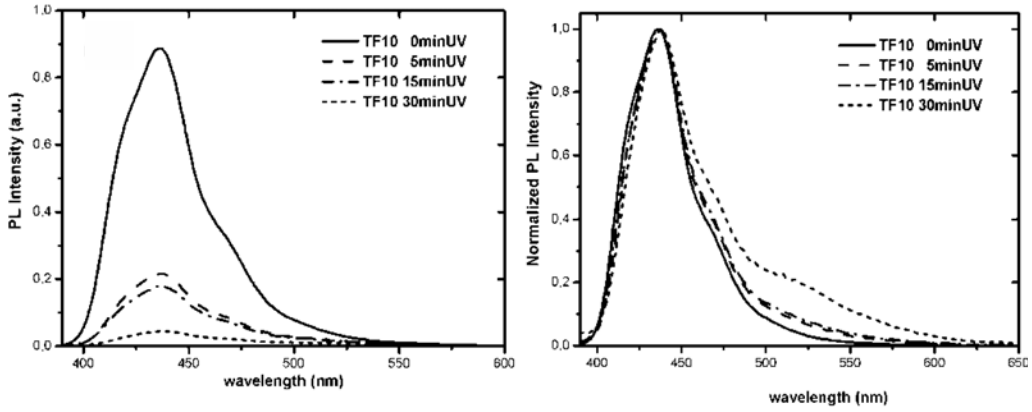

(a) (b)

Figure 3.17. The relative (a) and normalized (b) PL spectra of a PFcE. This figure is from Chochos, C.L.; Papakonstandopoulou, D.; Economopolous, S.P.; Gregoriou, V.G.; and Kallitsis, J. *J. Macromol. Sci. A: Pure & Appl. Chem.* **2006** *43*, 419-431.

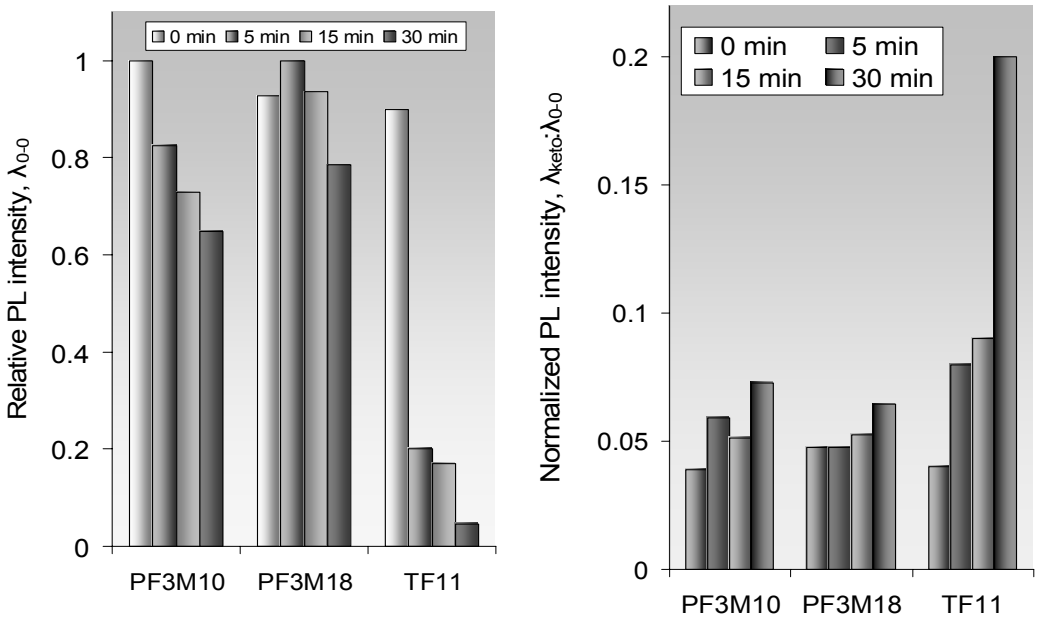

(a) (b)

Figure 3.18. (a) Relative intensities of blue emission maxima for **PF3M10**, **PF3M18**, and estimated values for the PFcE shown in Figure 3.16 after UV irradiation for periods of 0, 5, 15, and 30 min total. (b) Ratio of normalized green band emission maximum to blue emission maximum for **PF3M10**, **PF3M18**, and estimated values for the PFcE shown in Figure 3.16 after UV irradiation (λ_{ex} = 366 nm) for periods of 0, 5, 15, and 30 min.

3.6.3.2. PFM Photostability Monitored by IR Spectroscopy

The presence of trace amounts of monoalkyl fluorene (as well as 9,9-*H*-fluorene) in PF was first put forth as a reason for its degradation by List and Scherf.[159] List and Scherf reported the deliberate preparation and subsequent degradation of monoalkylated PF as supporting evidence. The results of that degradation were compared side-by-side with the deliberate degradation of an authentic sample of 9,9-dialkyl PF. A primary finding upon irradiating each sample under a halogen lamp was the change apparent in the IR spectra of each polymer. Specifically, the appearance of a band centered at 1721 cm^{-1} was noted. List and Scherf assigned

this as a C=O stretching mode of weak intensity, indicating that only a small population of the material contained the C=O functionality.

Inspired by Scherf's studies on PDHF, the photostabilities of a selection of PFMs were also investigated using IR spectroscopy. The RSCs investigated were **PF3M10**, **PF3M18**, **PF4M10**, and **PF4M18**. IR spectra of normalized absorptions for **PF4M18** and **PDHF-capped** are presented in Figures 3.19 and 3.20, with expansions of the C=O stretching mode regions (1550 – 2000 cm^{-1}) for each. IR spectra for **PF3M10**, **PF3M18**, and **PF4M10** investigated in this study are included as Appendix E.

IR spectra of PFMs are characterized by sp^3 C-H stretches from 2800 to 3000 cm^{-1} of great intensity and sp^2 C-H stretching from 3000 to 3100 cm^{-1} of moderate to weak intensity. This is the case for **PF4M18** in Figure 3.19a. A second characteristic stretch is the C=C stretch, which is observed in Figure 3.19b as a sharp peak of weak intensity at 1610 cm^{-1}. These features are also present in **PDHF-capped**, for which the IR spectra is given in Figure 3.20.

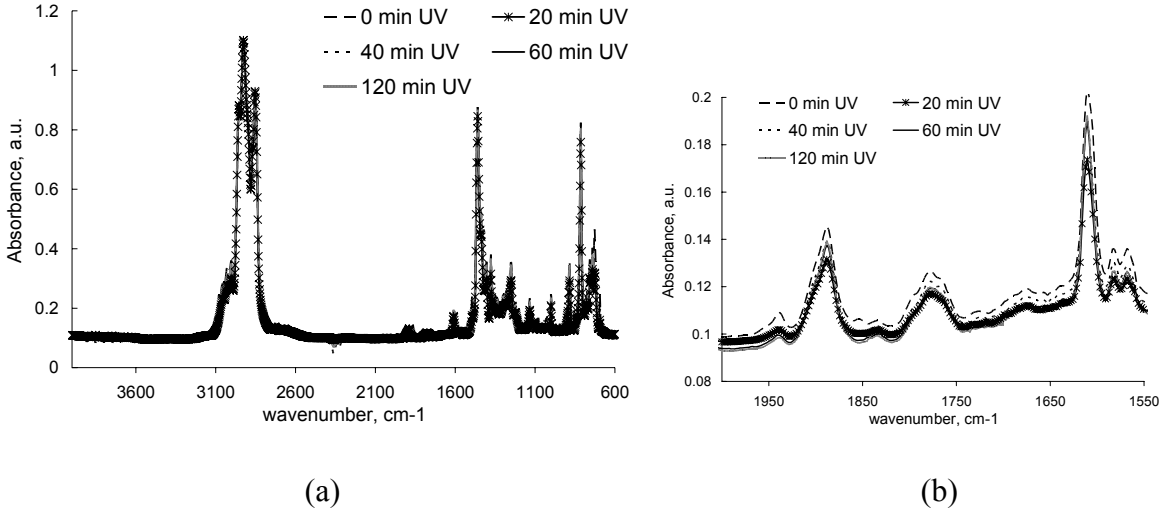

Figure 3.19. (a) IR spectra of **PF4M18** recorded after UV irradiation (λ = 366 nm) for 0, 20, 40, 60, and 120 min. (b) Expansion of the C=O region of the IR spectrum.

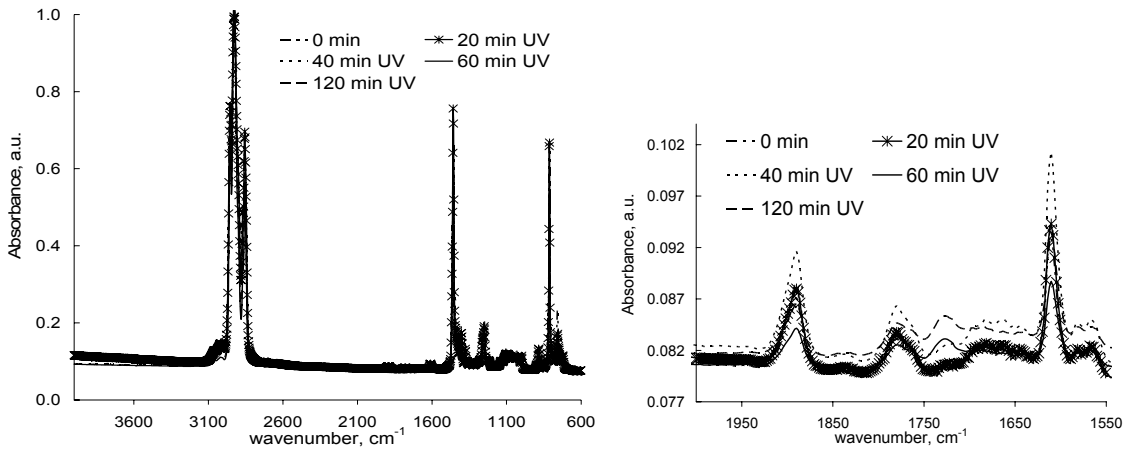

Figure 3.20. (a) IR spectra of **PDHF-capped** recorded after UV irradiation (λ = 366 nm) for 0, 20, 40, 60, and 120 min. (b) Expansion of the C=O region of the IR spectrum.

A notable difference in the IR spectra of **PF4M18** and **PDHF-capped** arises after irradiating both films. Upon exposure to UV light (λ = 366 nm) for 1 h, a very weak absorption at 1731 cm^{-1} indicative of C=O stretching is observed in the IR spectrum of **PDHF-capped** (Figure 3.20b, solid line). This peak is also observed after 2 h irradiation (dashed line). The fact that this stretch is weak should not be reason to discount it as the proportion of fluorenone units is expected to be quite small, despite the strong effects on the UV-Vis spectra. In contrast, **PF4M18** does not show any absorption changes at all in the carbonyl region IR spectrum. This lack of evidence for significant CO formation upon UV irradiation is typical of all the PFMs included in this study. Lack of carbonyl stretching in the IR spectrum for PFMs is a further indication of their improved photostability with respect to PDHF.

Comparison can also be made with the PFcEs prepared by Chochos and Kallitsis.[177] In examining the photostabilities of PFcEs by IR spectroscopy, Chochos detected carbonyl stretching at 1726 cm^{-1} after 5 min UV exposure (Figure 3.21). The inset shown in Figure 3.21

highlights the carbonyl region, which undergoes a dramatic change over the course of the experiment, indicating significant keto formation has occurred. Based on the appearance of the shoulder at 1775 cm^{-1}, Chochos also suggested the formation of a second species generated by UV irradiation. Though the source of their light generator is not the same used in our investigation this difference in photostability is worth noting.

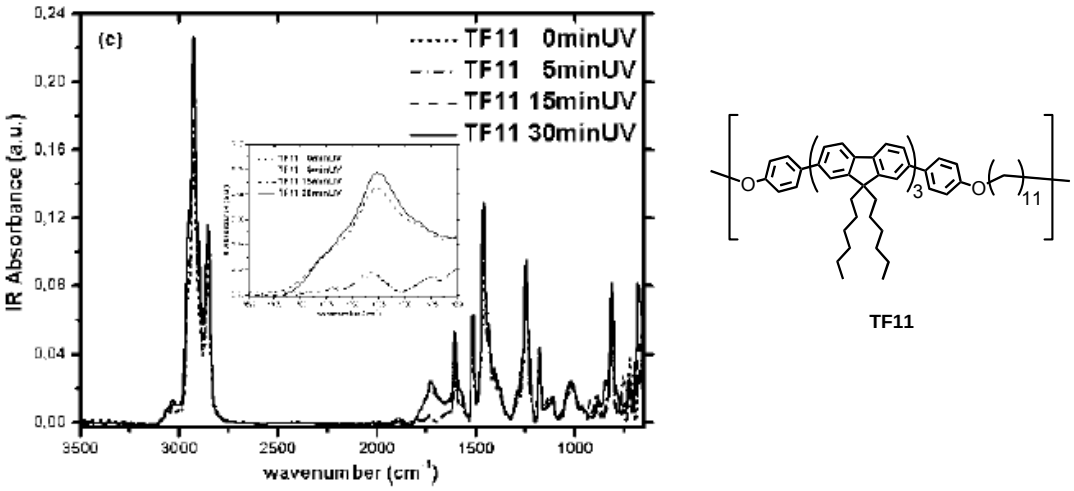

Figure 3.21. IR spectra of **TF11** after UV radiation (λ = 365 nm for 0, 5, 15, and 30 min). The carbonyl region is highlighted as the inset. This figure is from Chochos, C.L.; Papakonstandopoulou, D.; Economopolous, S.P.; Gregoriou, V.G.; and Kallitsis, J. *J. Macromol. Sci. A: Pure & Appl. Chem.* **2006** *43*, 419-431.

3.6.3.3. PFM Thermal Stability at 160° C Monitored by PL Spectroscopy

Film-cast PF undergoes degradation/oxidation processes upon heating in an open air environment. (Section 3.3). For this reason a selection of PFMs were investigated for their light emission characteristics when heated at 160° C for designated time intervals. As the basis for comparison is PDHF, relative and normalized PL spectra of **PDHF-new** are presented in Figure 3.22. The relative intensity of the blue emission at λ_{max} = 450 nm is the greatest for the annealed film (0 h, top spectrum at λ = 450 nm in Figure 3.22a). Heating the film causes this emission

peak to decrease in intensity such that after 4 h it is 33% as intense as the initial measurement. The green emission concomitantly increases in intensity–from the normalized spectra in Figure 3.22b it is observed that after 4 h at 160° C this emission is 39% as intense as the desired blue emission (top spectrum at λ = 525 nm).

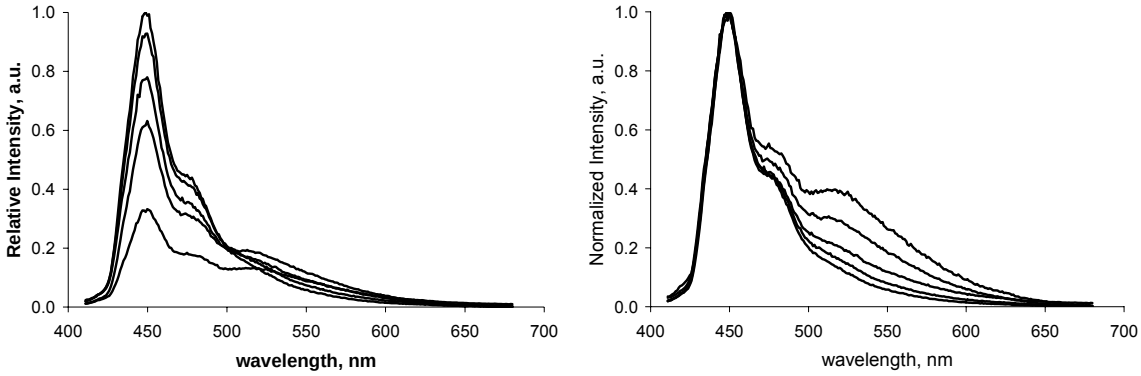

Figure 3.22. Relative (a) and normalized (b) PL spectra of **PDHF-new**, prepared August, 2006. Spectra were recorded August, 2006 at λ_{ex} = 388 nm after heating at 160° C for (from top to bottom at 450 nm in left figure, bottom to top at 525 nm in right figure) 0, 0.5, 1, 2, and 4 h. (b) is normalized with respect to the 0-0 transition.

Corresponding spectra for PFMs show similar features. Spectra of relative and normalized intensities for a representative PFM, **PF7M18**, are presented in Figure 3.23. The relative intensity at λ_{max} = 445 nm is greatest for the annealed film, i.e. the PL intensity at λ_{max} = 1.0 by definition. Heating this film at 160° C results in a steady decrease in the intensity of this emission, defined as arising from the 0-0 singlet transition. After 4 h, the emission at λ_{max} = 445 nm has decreased to roughly 35% its original intensity, while the band produced by emission of the fluorenone products of oxidation keto formation has grown to roughly 10% relative intensity. The normalized spectrum of **PF7M18** shows the steady increase of the keto emission upon heating–it begins in the annealed film as an ill-defined shoulder (bottom spectrum at λ = 525 nm,

Figure 3.23b) but after 4 h has grown to be 22% as intense as the desired blue emission (top spectrum at λ = 525 nm, Figure 3.23b).

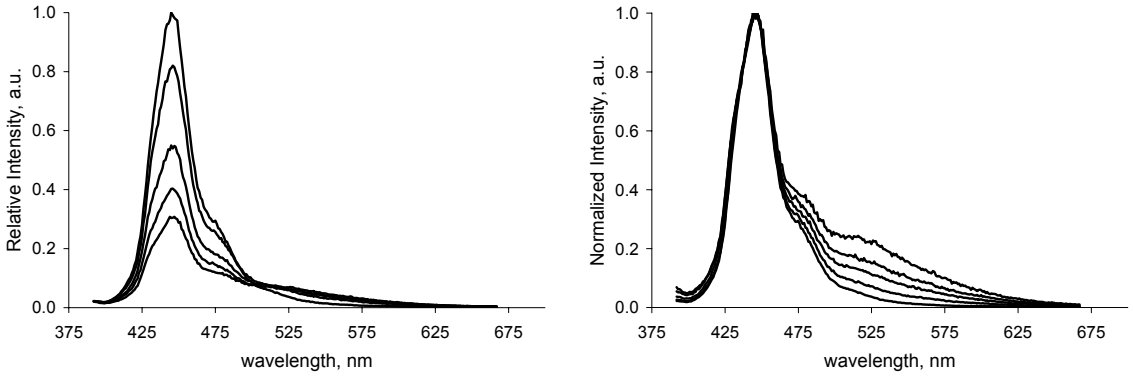

(a) (b)

Figure 3.23. Relative (a) and normalized (b) PL spectra of **PF7M18**. Spectra were recorded at λ_{ex} = 375 nm after heating at 160° C for (from top to bottom at 440 nm in left figure, bottom to top at 525 nm in right figure) 0, 0.5, 1, 2, and 4 h.

PFMs incorporating shorter (1-2) fluorene segment lengths undergo rapid bleaching at 160° C. A representative example is **PF2M10**, the relative and normalized spectra for which are shown in Figure 3.24. The emission at λ_{max} = 416 nm is reduced to 21% relative intensity after only 30 min heating.

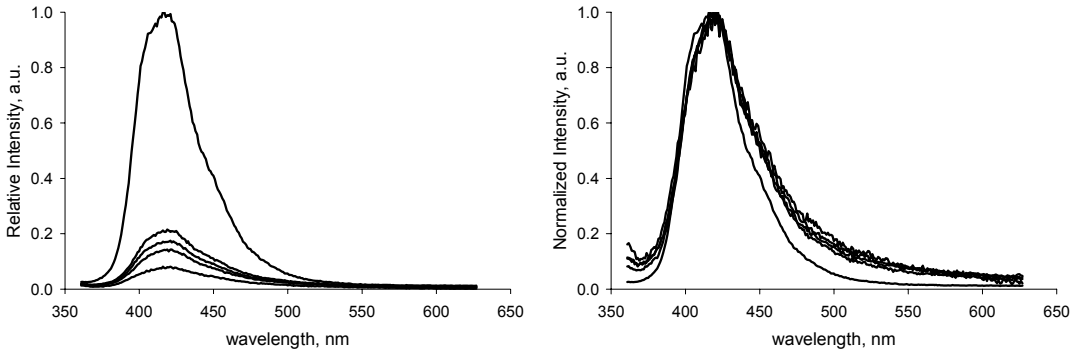

Figure 3.24. Relative (a) and normalized (b) PL spectra of **PF2M10**. Spectra were recorded at λ_{ex} = 335 nm after heating at 160° C for (from top to bottom at 425 nm in left figure, bottom to top at 525 nm in right figure) 0, 0.5, 1, 2, and 4 h.

The stabilities of all PFMs were investigated at this temperature; the remaining spectra are included in Appendix F. The data for these thermal stability studies is summarized in Figures 3.25 and 3.26. Figure 3.25 charts the progression of relative intensities for each PFM over the course of each PL measurement from 0 to 4 h. For the PFMs with short (1-2) fluorene segment lengths, the effect of heating on the intensity at λ_{max} is readily observed–bleaching reduces the intensities of blue emission in **PF1M10** and **PF1M18** to 18% and 11% after only 30 min. In contrast to this observation, it was found that PFMs generally benefit from longer fluorene segments. This was the case for films of **PF3M10**, **PF4M10**, **PF7M18**, and **PF8M18**. The blue emission maxima for each of these copolymers maintained an intensity that tracked well with that for **PDHF-new**, which after 4 h emitted at λ_{max} = 449 nm at 32% its original intensity. It should be noted that the films of **PF3M18** and **PF4M18** do not fit this trend, however; they rapidly bleached under these thermal conditions.

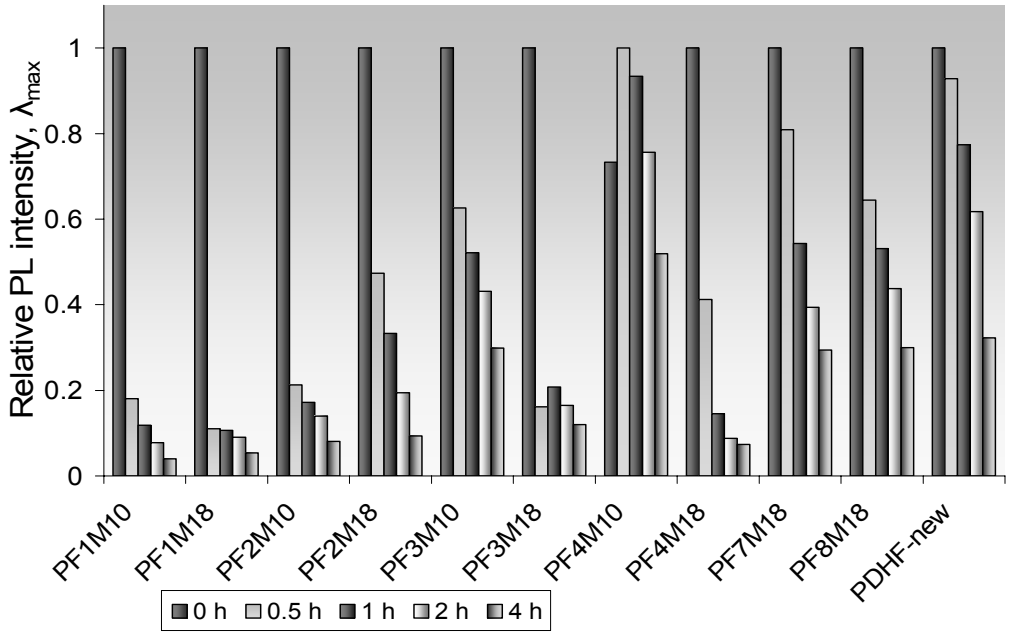

Figure 3.25. Bar graph representation of relative intensities of λ_{max} for PFMs after heating 160° C for periods of 0, 0.5, 1, 2, and 4 h total ($\lambda_{max,0\ h} = 1$). The λ_{max} progression for **PDHF-new** is shown for comparison.

Interestingly, the growth of the green emission band in PFMs was generally found to be slower with respect to that observed in PDHF. This point is illustrated in Figure 3.26, which charts the intensity of emission in the green band against the normalized maximum intensity for PFMs with segment lengths of three and greater. The series for **PDHF-new** is presented for ease of comparison. In the cases of **PF3M10**, **PF4M10**, **PF7M18** and **PF8M18**, the extent of emission in the green band of the PL spectrum is markedly less than that observed in **PDHF-new**. As shown in Figure 3.26, samples of **PF3M18** and **PF4M18** give apparently anomalous results. It is important to note again that we are plotting the ratio of intensities of the two emissions; the green band appears to be growing in faster for these samples, not because it was actually very intense relative to the other PFMs, but because the loss of intensity of the blue emission was more pronounced. If these two samples are treated as atypical it can be concluded that PFMs generally exhibit a slower growth of green band emission than PDHF at 160 °C.

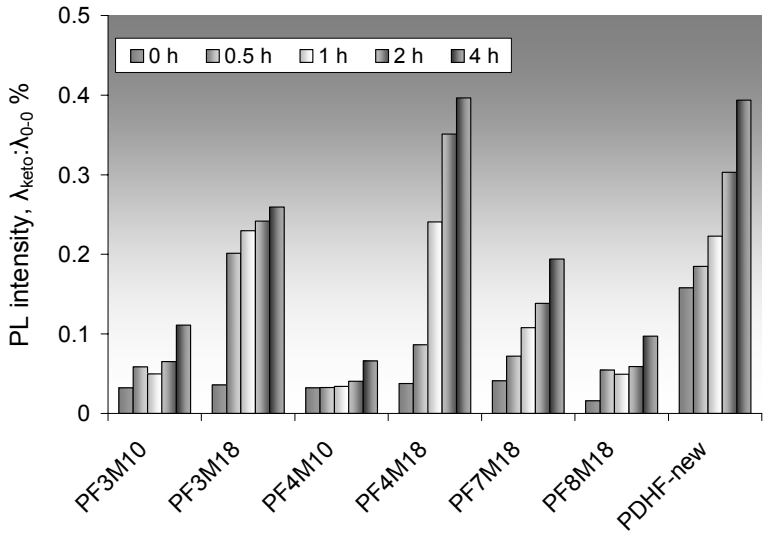

Figure 3.26. Ratio of green band emission maximum normalized relative to ble emission maximum for **PF3M10**, **PF3M18**, **PF4M10**, **PF4M18**, **PF7M18**, **PF8M18**, and **PDHF-new**.

3.6.3.4. PDHF Thermal Stability at 160° C Monitored by PL Spectroscopy

Over the course of these investigations into the stabilities of PFMs, multiple samples of PDHF were prepared and characterized for comparison. It soon became apparent that these separate samples of PDHF possessed varying stabilities, an observation which was borne out in PL spectra for each sample after heating at 160° C. The PL spectra of relative and normalized intensities for **PDHF-old** are shown in Figure 3.27. Note that **PDHF-old** was prepared in August, 2005 and the PL spectra shown in Figure 3.27 were obtained in August, 2006. The PL spectra of **PDHF-old** contrasts greatly with that of **PDHF-new**, which was prepared in August, 2006. The spectra of **PDHF-new** shown in Figure 3.28 were obtained in August, 2006. A third sample, **PDHF-capped**, was prepared in June, 2006. The spectra of relative and normalized intensities for **PDHF-capped** after heating at 160° C were obtained in July, 2006 and are presented in Figure 3.29.

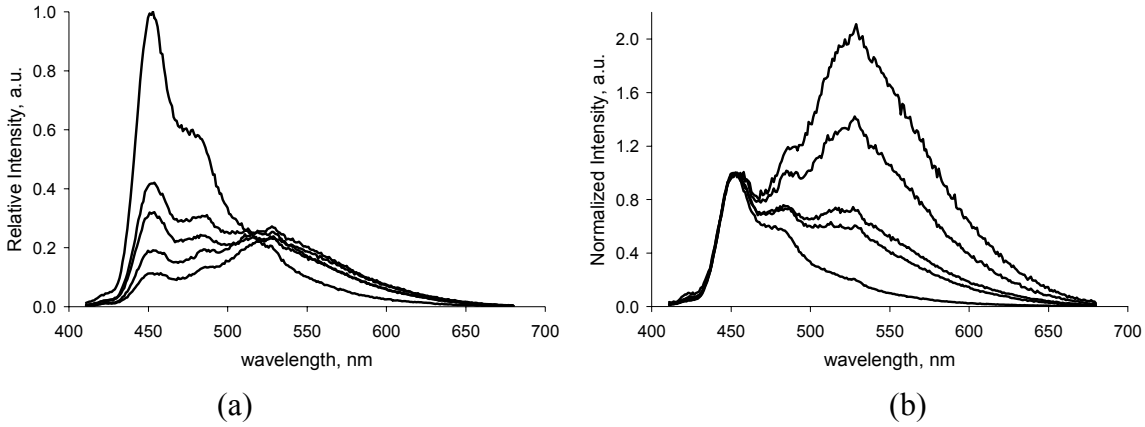

Figure 3.27. Relative (a) and normalized (b) PL spectra of **PDHF-old**, prepared August, 2005. Spectra were recorded August, 2006 at λ_{ex} = 388 nm after heating at 160° C for (from top to bottom at 450 nm in left figure, bottom to top at 525 nm in right figure) 0, 0.5, 1, 2, and 4 h. (b) is normalized with respect to the 0-0 transition.

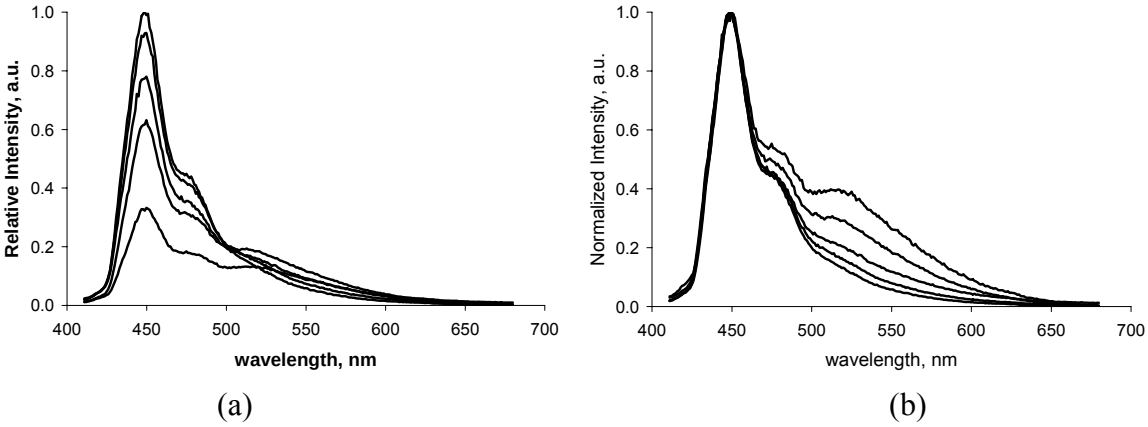

Figure 3.28. Relative (a) and normalized (b) PL spectra of **PDHF-new**, prepared August, 2006. Spectra were recorded August, 2006 at λ_{ex} = 388 nm after heating at 160° C for (from top to bottom at 450 nm in left figure, bottom to top at 525 nm in right figure) 0, 0.5, 1, 2, and 4 h. (b) is normalized with respect to the 0-0 transition.

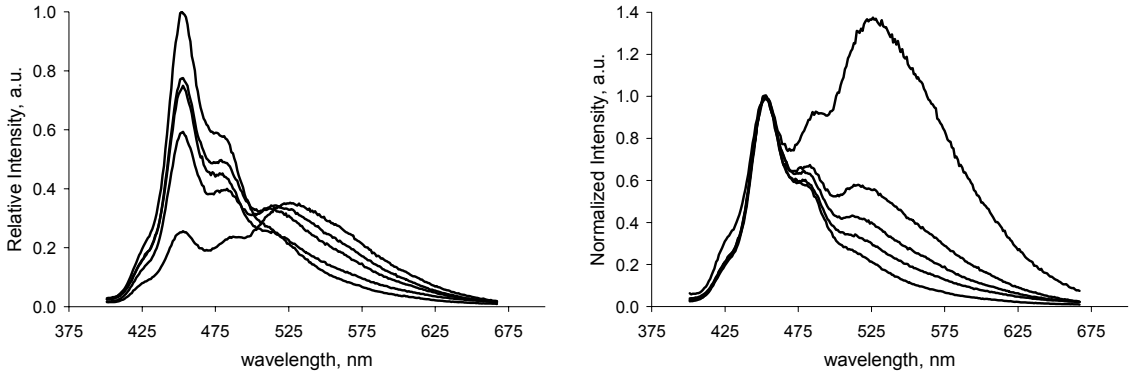

(a) (b)

Figure 3.29. Relative (a) and normalized (b) PL spectra of **PDHF-capped**, prepared June, 2006. Spectra were recorded June, 2006 at λ_{ex} = 388 nm after heating at 160° C for (from top to bottom at 450 nm in left figure, bottom to top at 525 nm in right figure) 0, 0.5, 1, 2, and 4 h. (b) is normalized with respect to the 0-0 transition.

The thermal stabilities these samples display after heating at 160° C are anything but static. On the contrary, **PDHF-new** exhibits the greatest degree of stability at 160° C, which stands to reason given that it was characterized for its thermal stability almost immediately following its preparation. **PDHF-capped**, which was characterized for its thermal degradation behavior one month following its preparation, exhibits a very different stability profile, as shown in Figure 3.29. The green emission in **PDHF-capped** after 4 h is 1.4 times as intense as the desired emission at λ = 448 nm. **PDHF-old**, which was a year old when characterization as shown in Figure 3.27 was performed, is even less stable upon heating. After 4 h at 160° C the emission at λ = 448 nm is only 11% as intense as the annealed film's emission. Further, green emission around λ = 525 nm is 2.1 times as intense as the blue emission. Pertinent data in Figures 3.27-3.29 are redisplayed in Figure 3.30.

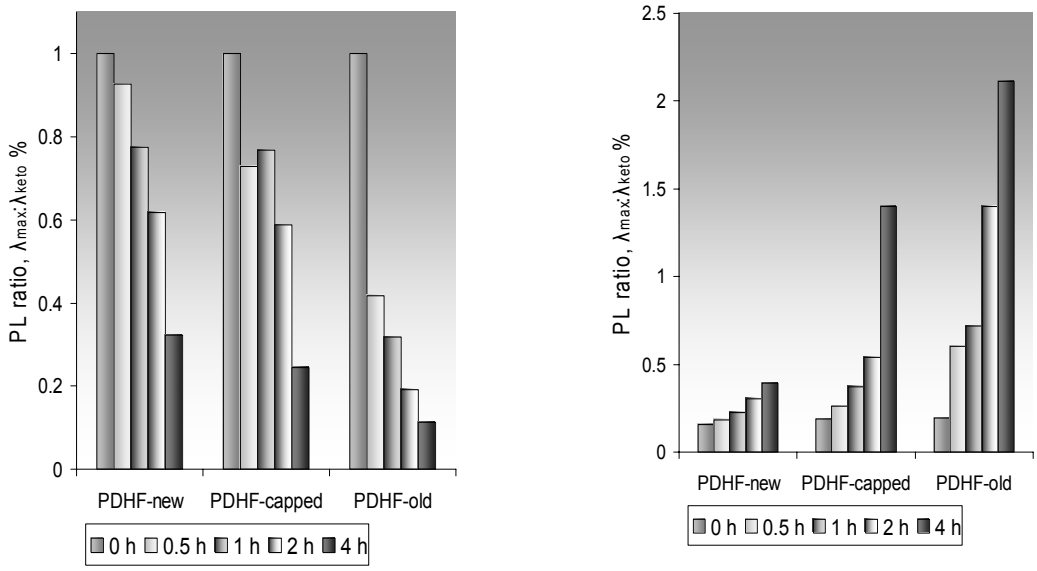

(a) (b)

Figure 3.30. (a) Bar graph of relative intensities of λ_{max} for **PDHF-old**, **PDHF-new**, and **PDHF-capped** after heating 160° C for periods of 0, 0.5, 1, 2, and 4 h total ($\lambda_{max,0\ h} = 1$). (b) The ratio of emission maxima resulting from keto defects and 0-0 excitation taken from the normalized plots of **PDHF-old**, **PDHF-new**, and **PDHF-capped**.

In each sample of PDHF the blue emission does weaken in intensity as the film is heated. However, **PDHF-new** and **PDHF-capped** undergo a much more gradual decrease throughout the investigation. This is not the case with **PDHF-old**, which undergoes a significant (58%) reduction in the intensity of the blue emission maximum at λ = 448 nm after 30 min at 160° C. The extent to which the green band dominates the PL spectrum also looks to be based on sample age. **PDHF-old** shows a PL profile at the green band which points to its severe thermal instability after having aged one year.

3.6.3.5. Investigation into Ni^0-mediated PDHF Preparation Conditions as a Source of Fluorenone Defects

A portion of **PF3M10** was subjected to the reaction conditions used to prepare samples of PDHF. This was performed to investigate the method of preparation of PDHF as a potential

cause of its optical instability. As such, **PF3M10** was treated under conditions identical to the preparation of PDHF to yield **PF3M10-2** (Section 3.5.5). To examine the extent to which PDHF preparation conditions actually *accelerate* keto defect formation, **PF3M10** and **PF3M10-2** were cast as thin films and their relative thermal stabilities at 160° C were investigated in parallel. Figures 3.31 and 3.32 show the relative and normalized PL spectra for **PF3M10** and re-treated **PF3M10-2**, respectively. Figure 3.33 charts the relative intensity of the blue emission maxima (a, λ_{max} = 423 nm) and the normalized intensity of the keto band emission (b, λ_{max} = 525 nm).

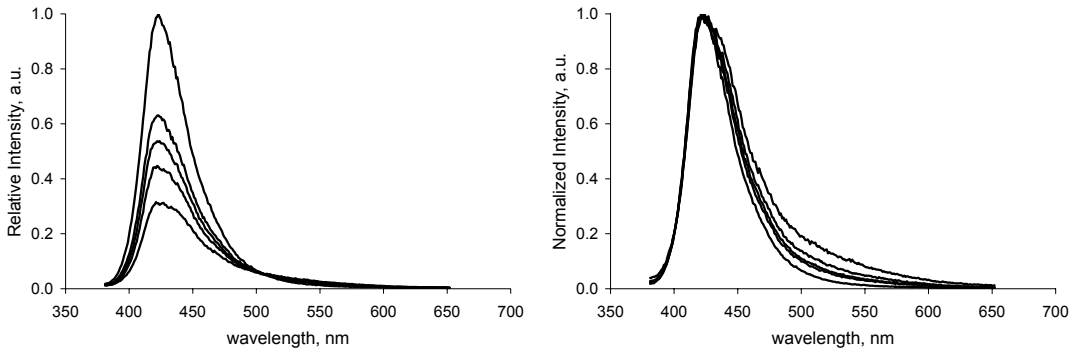

(a) (b)

Figure 3.31. Relative (a) and normalized (b) PL spectra of **PF3M10**. Spectra were recorded at λ_{ex} = 355 nm after heating at 160° C for (from top to bottom at 440 nm in left figure, bottom to top at 525 nm in right figure) 0, 0.5, 1, 2, and 4 h.

Comparison of the PL profiles of **PF3M10** and **PF3M10-2** shows that the blue emission in re-treated **PF3M10-2** lost intensity much more rapidly than did **PF3M10**–after 4 h the relative intensity of the emission at λ_{max} for **PF3M10** (31% of initial intensity) is still greater than that for re-treated **PF3M10-2** after 0.5 h (23%). The greater thermal stability of the blue emission in **PF3M10** over re-treated **PF3M10-2** is evident.

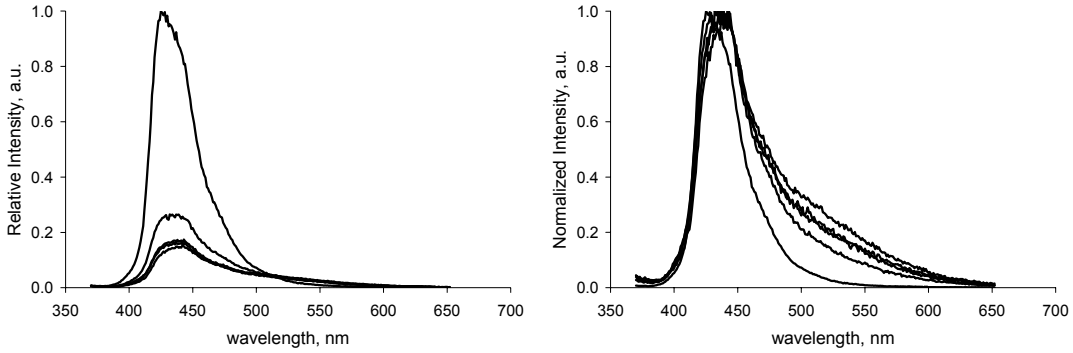

Figure 3.32. Relative (a) and normalized (b) PL spectra of re-treated **PF3M10-2**. Spectra were recorded at λ_{ex} = 355 nm after heating at 160° C for (from top to bottom at 440 nm in left figure, bottom to top at 525 nm in right figure) 0, 0.5, 1, 2, and 4 h.

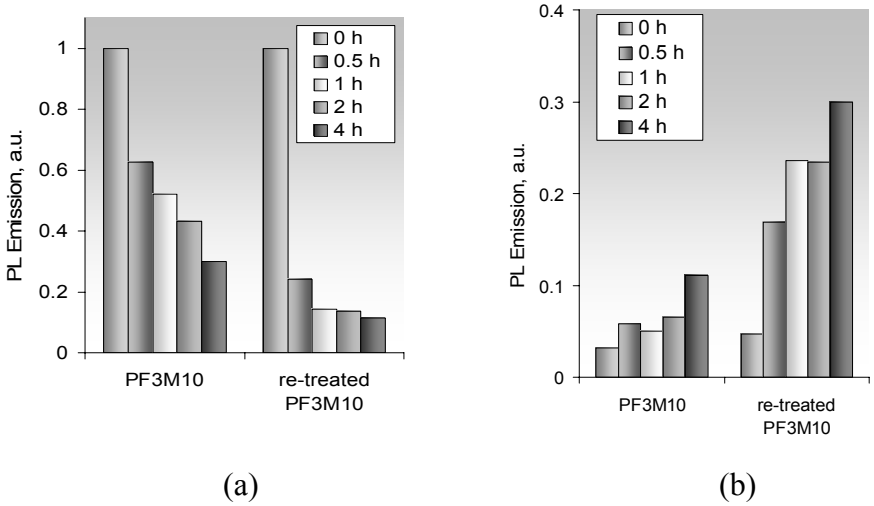

Figure 3.33. (a) Relative intensities of blue emission maxima (λ_{max} = 423 nm) for **PF3M10** and **PF3M10-2** after heating 160° C for periods of 0, 0.5, 1, 2, and 4 h total ($\lambda_{max,0\ h}$ = 1). (b) Keto defect:blue emission maxima taken from the normalized plots of **PF3M10** and re-treated **PF3M10**.

The notion that keto formation is accelerated by synthetic conditions used in making PDHF is also strengthened by the data given in Figures 3.31-3.33. The normalized PL spectra in Figures 3.31b and 3.32b make clear the observation that green emission at λ = 525 nm is enhanced in **PF3M10-2**. The graph in Figure 3.33b facilitates further comparison of the extent to

which green emission is present in each sample of **PF3M10**. It is seen that re-treating **PF3M10** with reaction conditions used in preparing PDHF results in a more prevalent green emission.

3.6.3.6. PFM Thermal Stability at 200° C Monitored by PL Spectroscopy

A selection of PFMs were investigated at 200° C. The RSCs investigated were **PF2M10**, **PF3M18**, and **PF4M10**. Spectra of relative and normalized intensities for **PF2M10**, **PF3M18**, **PF4M10**, and **PDHF-capped** are presented in Figures 3.34-3.37.

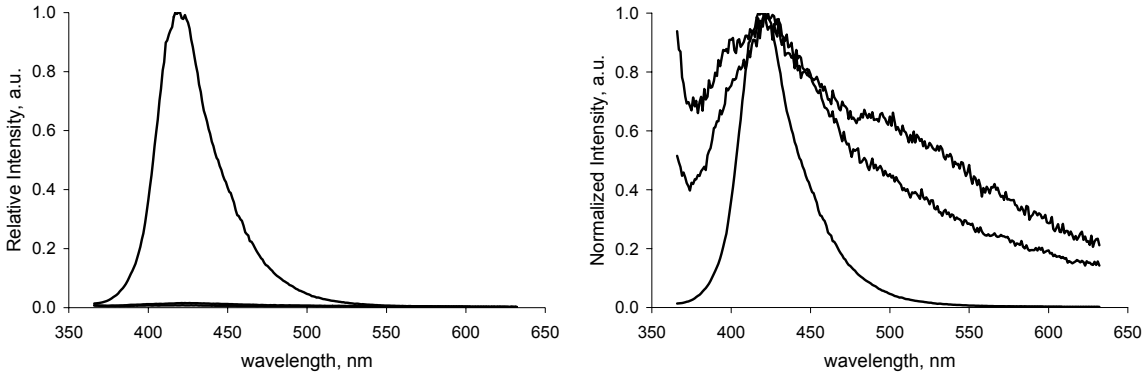

Figure 3.34. Relative (a) and normalized (b) PL spectra of **PF2M10**. Spectra were recorded at λ_{ex} = 335 nm after heating at 200° C for (from top to bottom at 440 nm in left figure, bottom to top at 525 nm in right figure) 0, 0.5, and 1 h.

The PL spectra taken of a film of **PF2M10** clearly show that at 200° C it undergoes rapid thermal bleaching (Figure 3.35). After 30 min the relative intensity of the emission at λ_{max} = 420 nm is only 1.5% the intensity of the pristine drop cast film. As such, **PF2M10** did not lend itself well to assessing blue emission characteristics at this temperature. Films of PFMs with longer fluorene segments were more durable under these conditions, however. The PL spectra of **PF3M18** (Figure 3.36) show that after heating 30 min the relative intensity of blue emission at

λ_{max} = 423 nm is severely diminished (to 8%). After 60 min this intensity has decreased to 4% and is accompanied by a green emission band of significant intensity, which indicates significant loss of thermal stability in **PF3M18** in comparing experiments performed at 160° C (see Section 3.6.3.3) to 200° C.

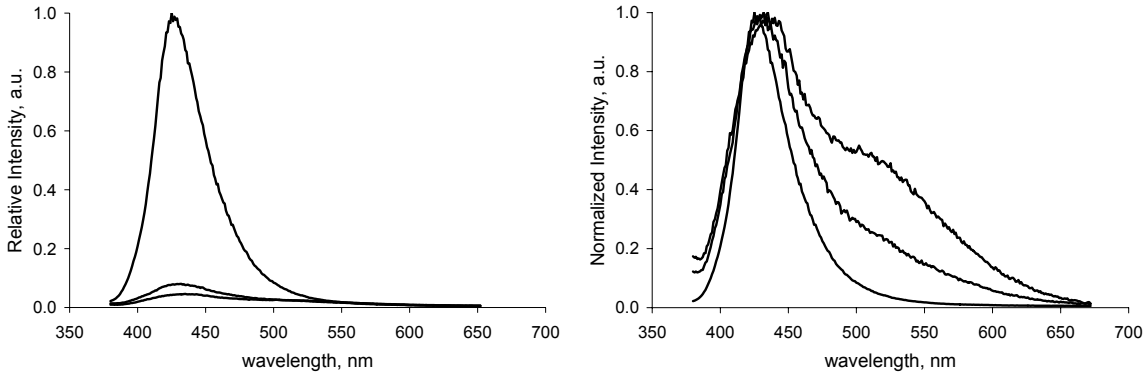

(a) (b)

Figure 3.35. Relative (a) and normalized (b) PL spectra of **PF3M18**. Spectra were recorded at λ_{ex} = 355 nm after heating at 200° C for (from top to bottom at 440 nm in left figure, bottom to top at 525 nm in right figure) 0, 0.5, and 1 h.

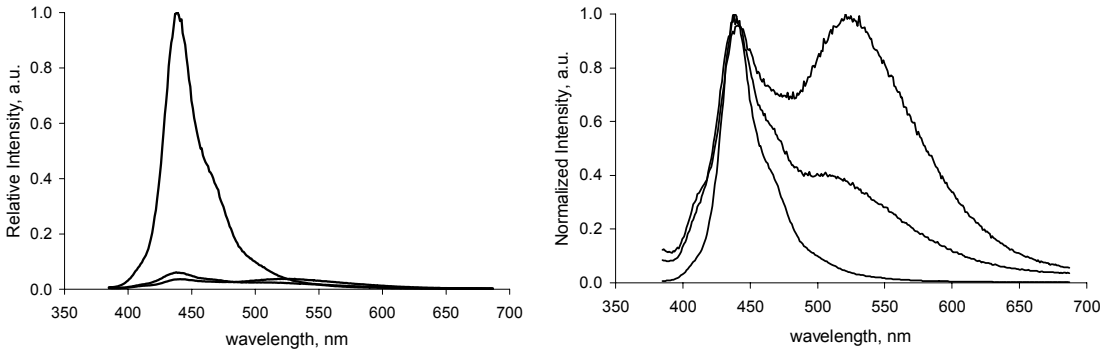

(a) (b)

Figure 3.36. Relative (a) and normalized (b) PL spectra of **PF4M10**. Spectra were recorded at λ_{ex} = 365 nm after heating at 200° C for (from top to bottom at 440 nm in left figure, bottom to top at 525 nm in right figure) 0, 0.5, and 1 h.

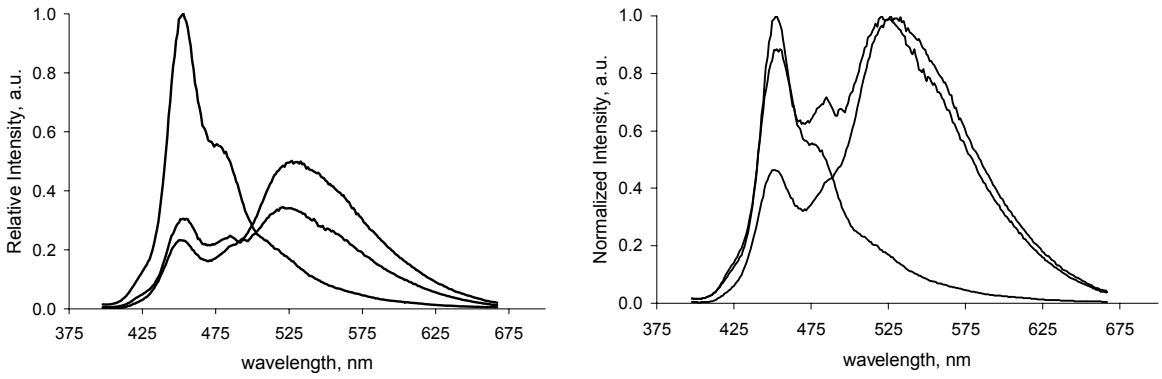

(a) (b)

Figure 3.37. Relative (a) and normalized (b) PL spectra of **PDHF-capped**. Spectra were recorded at λ_{ex} = 388 nm after heating at 200° C for (from top to bottom at 440 nm in left figure, bottom to top at 525 nm in right figure) 0, 0.5, and 1 h.

The loss in thermal stability observed in **PF3M18** is also seen in **PF4M10** (Figure 3.36). Heating a thin film of **PF4M10** results in a rapid decrease in the blue emission at λ_{max} = 438 nm. Inspection of the normalized spectra of **PF4M10** (Figure 3.36b) reveal that keto formation is rapid to the degree that after 60 min green emission is as intense as blue emission.

Comparison of the PFMs included in this study can be made to PDHF. **PDHF-capped** (Figure 3.37) was found to be more stable at 200° C than any PFM studied. This was demonstrated by the fact that after heating for 60 min the relative intensity of blue emission at λ_{max} = 450 nm was still 23% that of the pristine film. However, keto formation in **PDHF-capped** was extensive. After heating for 60 min the green emission band dominated the PL spectrum and exceeded the emission intensity at λ_{max} = 450 nm by a factor of greater than 2.

Key spectral features for this study are represented in Figure 3.38. As already noted, the relative intensities of PFMs (Figure 3.38a) at their blue emission maxima rapidly diminish due to thermal bleaching and fluorescence quenching upon formation of keto defects. This latter finding is shown for the PFMs with respect to **PDHF-capped** in Figure 3.38b. The rate of keto formation

is found to be greatly accelerated at 200° C in relation to investigations of PFMs performed at 160° C. Likewise, blue emission diminishes at a greater rate at 200° C relative to investigations performed at 160° C. Comparison of PFMs to **PDHF-capped** in this study shows that the rate of keto formation is similar. Additionally, PFMs show similar thermal stabilities in relation to the PFcEs studied by Chochos and Kallitsis. The normalized keto emission of a film of **TF11** (Figure 3.16) after 30 min at 200° C is estimated to be aproximately 0.25 a.u. This value is charted in Figure 3.38b for ease of comparison and the PL spectrum reported by Chochos is reproduced in Figure 3.39.[177]

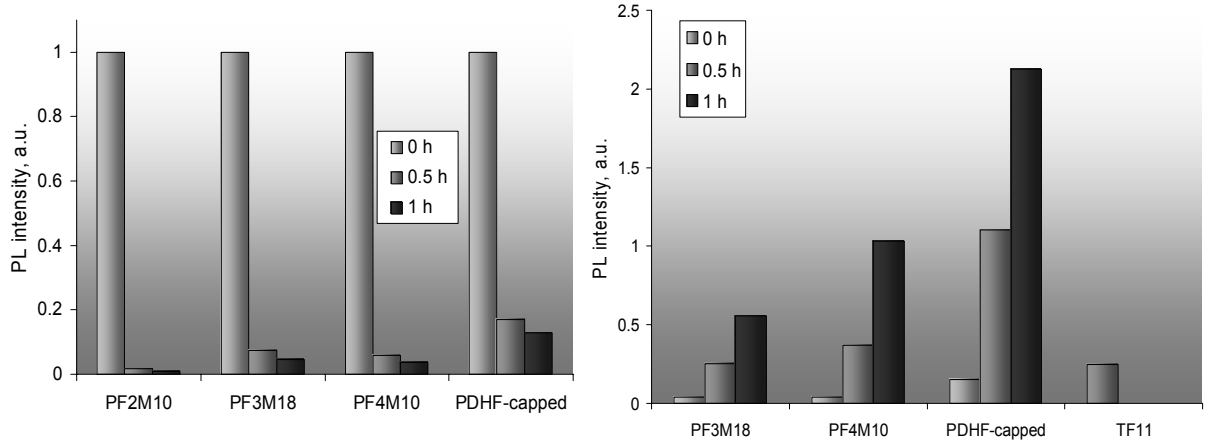

(a) (b)

Figure 3.38. (a) Bar graph representation of relative intensities of λ_{max} for **PF2M10**, **PF3M18**, **PF4M10**, and **PDHF-capped** after heating 200° C for periods of 0, 0.5, and 1 h total ($\lambda_{max,0\,h} = 1$). (b) The ratio of normalized emission maxima resulting from keto defects and 0-0 excitation taken from the normalized plots of **PF3M18**, **PF4M10**, and **PDHF-capped**. The estimated normalized emission of the PFcE **TF11** at λ = 535 nm after heating 30 min at 200° C.

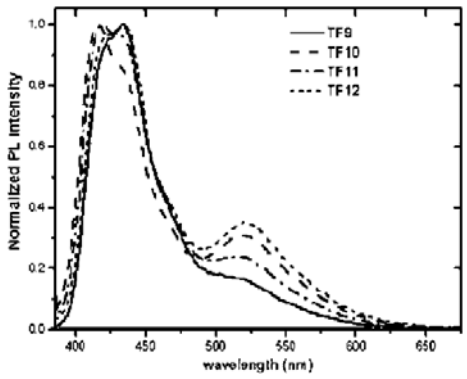

Figure 3.39. The solid state normalized PL spectra of PFcEs studied by Chochos after heating pristine films 200° C for 30 min. This figure is taken from Chochos, C.L.; Papakonstandopoulou, D.; Economopolous, S.P.; Gregoriou, V.G.; and Kallitsis, J. *J. Macromol. Sci. A: Pure & Appl. Chem.* **2006** *43*, 419-431.

3.6.3.7. PFM Thermal Stability Monitored by IR Spectroscopy

The stabilities of a selection of PFMs heated to 200° C were investigated using IR spectroscopy. The RSCs investigated were **PF3M10**, **PF3M18**, **PF4M10**, and **PF4M18**. Spectra of normalized absorptions for **PF3M10** are presented in Figure 3.40. Figure 3.40b is an expansion of the C=O sretching mode region (1540 – 1840 cm^{-1}). IR spectra for all remaining PFMs studied are included as Appendix G.

The observation by PL spectroscopy that PFMs undergo rapid and extensive degradation at 200° C is reinforced by examination of their IR spectra after being subjected to the same conditions. After 30 min at 200° C, then, the C=O stretching mode absent from the IR spectrum of the pristine film becomes plainly visible in the form of the band centered at 1715 cm^{-1} in Figure 33b. This finding is consistent throughout the four PFMs studied by IR spectroscopy at this temperature; **PDHF-capped** gives the same band in this region.

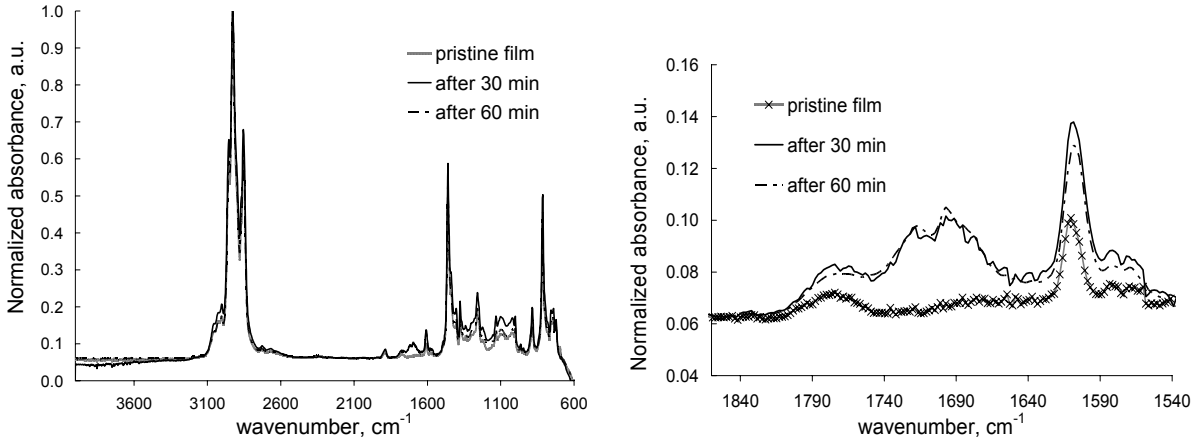

Figure 3.40. Left: Infrared spectra for a film of **PF3M10** heated at 200° C for 0, 30, and 60 min. Right: Expansion of the C=O region of the IR spectrum.

3.6.4. Conclusions

The synthesis of a PFM library enabled the characterization studies described in this Chapter. Studies based on DSC, UV-Vis, IR, and PL spectroscopy were performed, and the reasons for doing so were two-fold.

First, systematic changes in chemical composition allowed for investigations into correlation with functional properties. DSC studies were performed in order to better understand this relationship. The PFMs studied showed weak T_gs at low temperature which followed no clear trend with chemical composition. T_ms were more readily observed and increased with increasing fluorene segment length, consistent with results obtained by Yoon for oligofluorene T_ms.[176] **PF7M18** exhibits phase behavior which does not readily fit with other PFMs investigated in that a T_g is not observed in the first heating scan, though crystallization is identified by

inspection of the first cooling scan. PFMs show transitions which vary by chemical composition and further studies by DSC are planned.

A second motivation for characterizing PFMs is to compare their optical behavior with that of PDHF. It is found that PFMs appear to be more stable to UV decomposition than PDHF. For example, comparison of the PL spectra of **PF4M18** (Figure 3.13) with **PDHF-capped** (Figure 3.12) show the dramatically improved emission characteristics of PFMs. PFMs bleach less readily under the photoexcitation conditions used, and they generate no observable keto emission band at 525 nm. This result bodes well for the incorporation of PFMs in LEDs, for example. Another finding with implications for the applicability of PFMs is that, by interrupting conjugated fluorene segments with methylene segments, the drive to form observable keto defects upon thermal treatment of films is effectively suppressed. We also speculate that keto emission is inhibited by the regularly situated methylene segments. These segments serve to "turn off" keto emission by interrupting intrachain charge migration and by isolating interchain fluorenone sites. Because Förster energy transfer is an interchain event, isolating fluorenone moeities diminishes the likelihood of generating the keto emission at λ_{em} = 525 nm.

Lastly, over the course of these studies it became evident that histories of the PFM and PDHF samples are extremely important in determining their stabilities. It is likely the case that film degradation is auto-catalytic. We hypothesize that the perceived time course of degradation can be dramatically affected by small differences in the number of fluorenone groups present initially, something that is very difficult to control.

4. Imine Metathesis: Design of a System to Produce Cyclic Oligomers

4.1. Introduction

4.1.1. General Aspects

We were interested in applying tandem olefin and imine metathesis for the production of controlled length cyclic oligomers. Transition metal-catalyzed heteroalkene metathesis has remained fairly undeveloped in terms of its application in organic synthesis. There are, however, examples of this which attest to the practicality of the overall transformation. The most familiar example is carbonyl olefination using the Tebbe reagent, which is a titanium carbene complex. The reagent is used stoichiometrically to produce terminal olefins (Figure 4.1).

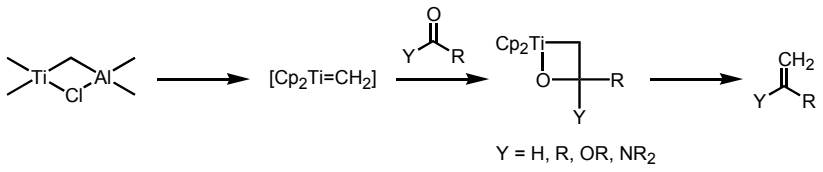

Figure 4.1. Use of the Tebbe reagent to produce a terminal olefin from a carbonyl-containing substrate.

Carbonyls have also been ring-closed using stoichiometric amounts of Schrock's alkylidene to give the cyclic alkene.[178] The molybdenum-oxo compound produced excludes any possibility of catalytic activity, as it is a thermodynamic sink (Figure 4.2).

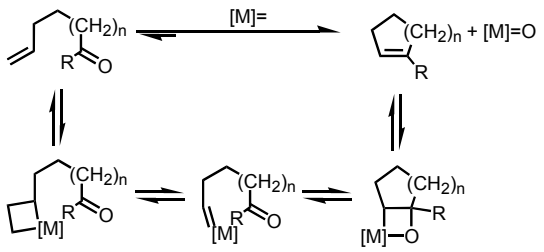

Figure 4.2. The stoichiometric reaction of an α,ω-carbonyl olefin produces a cyclic alkene and the metal-oxo compound.[178]

Another recent development in heteroalkene metathesis is the metathesis of imines. Following an analogous pathway to olefin metathesis, imine metathesis can proceed by the reaction of an imine with an imide (Scheme 4.1). Reaction of two imines in the presence of such an imide catalyst gives =NR exchange between sp^2 carbons.

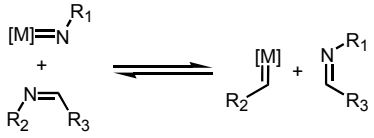

Scheme 4.1. General principle of imine metathesis.

As was achieved with olefin metathesis, catalytic imine metathesis cycles were reported for numerous transition metal based systems. To date, imine metathesis has been achieved using tungsten,[179] tantalum,[180] niobium,[181] rhenium,[182, 183] zirconium,[184, 185] titanium[186-188] and molybdenum-based catalysts. The (=NR) exchange reaction for the molybdenum bis-imide cycle was reported by Cantrell and Meyer to proceed by the mechanism shown in Scheme 4.2.[189, 190] In the absence of significant driving force to the product side, this cycle yields a statistical mixture of all possible imines.

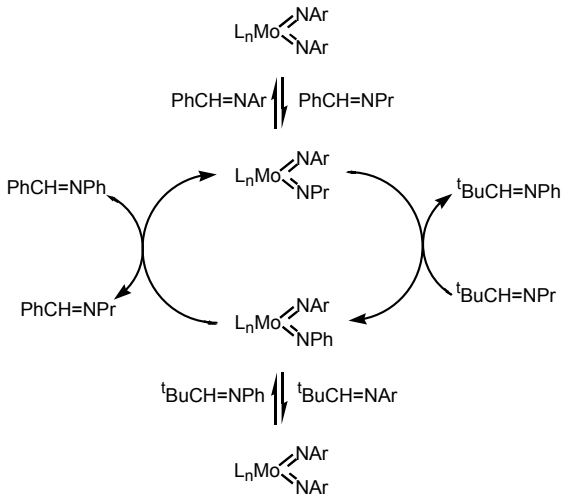

Scheme 4.2. The Chauvin-like mechanism for catalytic imine metathesis by a Schrock-type alkylidene.[189]

Transition metal catalyzed cyclic oligomer production is relatively rare, though recent reports serve to show just how useful a method of controlled cyclic oligomer production can be. Sen used a tantalum halide system to trimerize ethylene exclusively to 1-hexene.[191] This development has immediate implications for the improved production of linear low density polyethylene. Bielawski and Grubbs reported the use of a variation of Grubbs-II catalyst to produce cyclic polyoctene macrocycles, which were then hydrogenated to give cyclic polyethylenes.[192]

Apart from these examples, our interest in this area has its origin in work by Badawood and Meyer, who reported Ring Closing Metathesis (RCM) of α,ω-iminoolefins to produce cyclic alkenes (Figure 4.3).[193] This result was in accordance with findings reported by Cantrell and Meyer which suggested that alkylidene/imine metathesis was slower than alkylidene/olefin metathesis but feasible with Schrock-type alkylidenes.[194] It was also shown that, when the ancillary ligands were alkoxides rather than chlorides, the resulting molybdenum (bis)imide

species was stable towards further metathesis, being brought to a thermodynamic energy minimum.

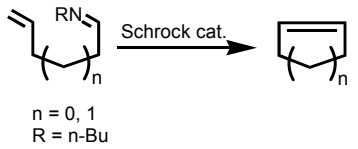

Figure 4.3. RCM of α,ω-iminoolefins.

Our approach to probe the feasibility of controlled ROMP-RCM sequencing using tandem olefin and imine metathesis is given in Scheme 4.3. An imine-olefin substrate is used to produce a novel alkylidene (**A**). Alkylidene **A** benefits by possessing both the olefin metathesis-active Mo=C bond and the thermodynamically attractive C=N bond. It is the presence of both interactions on the same substrate which constitutes the initial basis of this approach. Once generated, the alkylidene containing the remote imine functionality is treated under ROMP-type conditions with a compatible monomer such as norbornene to produce the initial kinetic product, a linear oligomeric chain (**B**). This species, after *n* insertions of norbornene, could orient itself such that the proximity of the imine functionality with respect to the Mo=C bond provides for ring-closing, giving the metal-imido species **C** and the cyclic oligomer **D**.

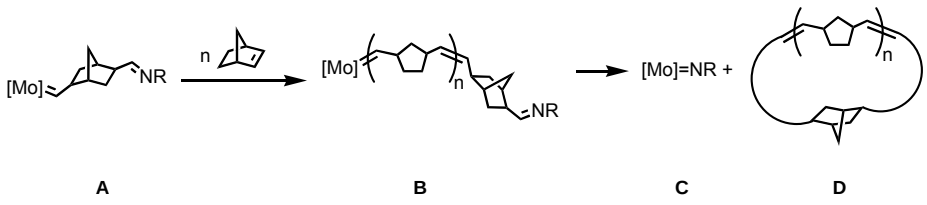

Scheme 4.3. Proposed reaction for oligomer growth and ring-closing.

Preliminary molecular mechanics calculations (MM/2) run with the Gaussian 98 package reinforced the plausibility of this approach. The total molecular mechanical energy of certain *n*-mer compounds was calculated as a function of norbornene units. A representative example is given in Figures 4.4-4.6, with tin substituted for molybdenum because the version of MM/2 used was not parameterized for transition metals. Since we were primarily interested in examining the conformations of the oligomeric chain, the substitution was not expected to preclude any findings. The simplified models show the oligomeric chain growing away from the metal center in a more-or-less linear fashion, as pictured in Figure 4.4.

As more and more monomer units insert into the growing chain, the oligomer gradually acquires more possible conformational arrangements, to the extent that a conformer similar to that shown in Figure 4.5 becomes energetically accessible. Finally, once the alkylidene and imine functionalities come into close proximity, it is conceivable that the alkylidene will ring-close the growing oligomer, as is represented in Figure 4.6. As stated before, alkylidene-imine metathesis is possible, though it is slow to occur. It represents the thermodynamic minimum. Initially, we are looking to test the validity of these hypotheses. Should ring closing take place, however, we would then turn our attention to the regularity of ring closing. Determining the range of monomer units inserted prior to ring closing will be significant and could prove to be of great synthetic value.

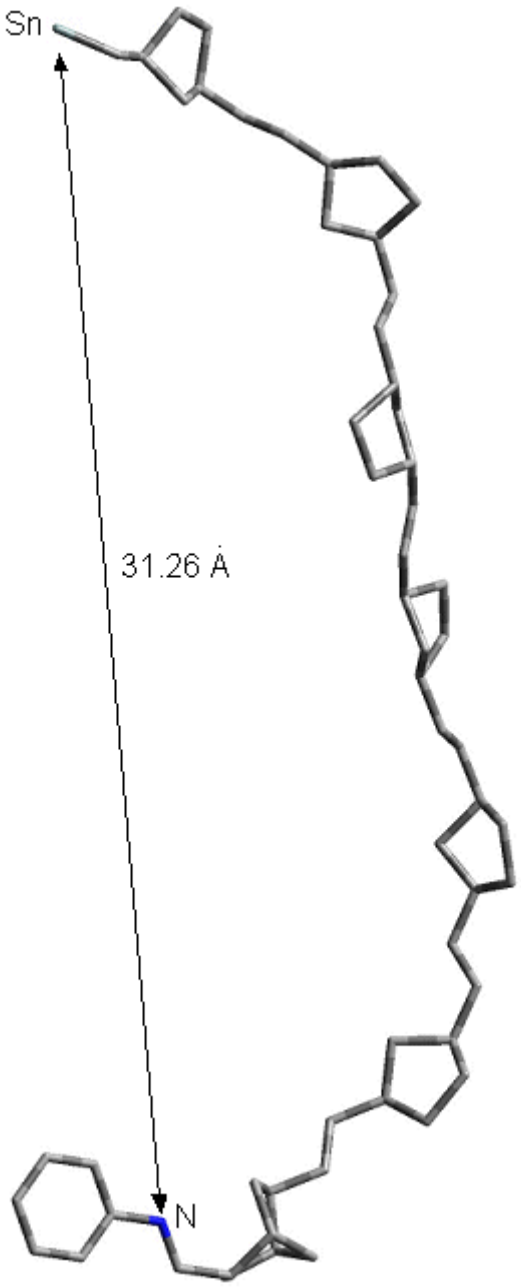

Figure 4.4. A possible minimum energy conformation of the compound after six monomer insertions.

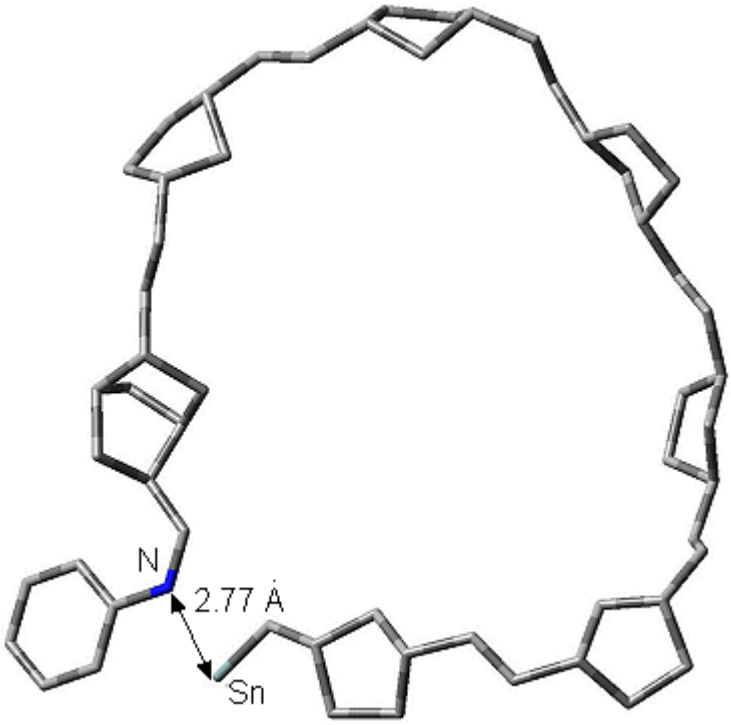

Figure 4.5. A second conformer of the same species.

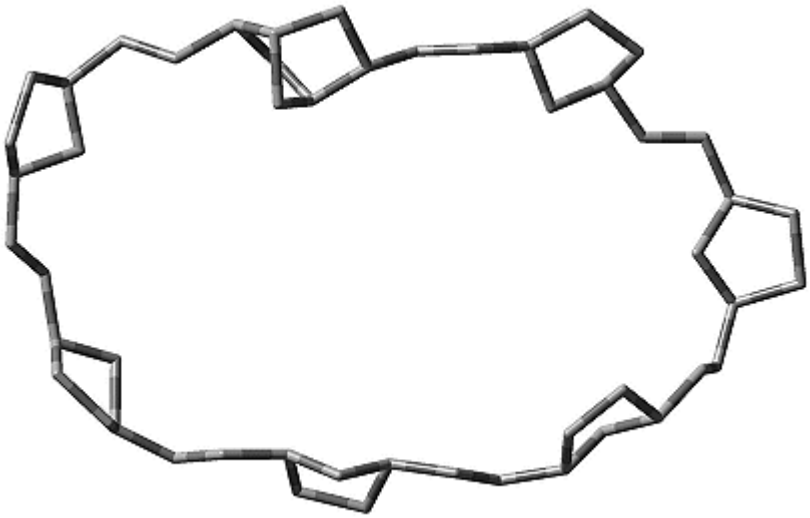

Figure 4.6. The product formed after ring closing of the six-mer.

4.1.2. Substrate Design

Accordingly, alkylidene **Mo-1** (Figure 4.7) was chosen as the target substrate for very specific reasons. The first, most evident, reason involved the basic placement of the terminal olefin and imine functionalities. That they are remote and fixed assures that ring-closing will not immediately occur.

Mo-1

Figure 4.7. Target alkylidene **Mo-1.**

A second feature of this system is the isomeric family of **Mo-1** generated using the selected transformations shown in Scheme 4.4. Two diastereomers are introduced initially with the use of aldehyde **1**, which is shipped as the mixture of *endo*- and *exo*-aldehydes. A second stereocenter is introduced upon the net addition of ethylene across the internal C=C bond. Because the norbornene skeleton lacks any regiospecific directors, *endo*- and *exo*-species for both **2a** and **2b** are generated. This gives eight isomers, which are subjected to an imine-forming step to produce **3a** and **3b** and then treated with Schrock's catalyst to yield **Mo-1a** and **Mo-1b**. Geometrical isomerization of the new molybdenum system would then produce sixteen isomers, as the Schrock catalyst is known to exist in the *syn* and *anti* form. In essence, then, what is synthesized is a library of isomeric alkylidenes. Ostensibly, then the as-formed small library of substrates will provide for the running of sixteen experiments simultaneously. This organometallic approach would conceivably allow for direct identification of the alkylidene species which most lends itself to the production of cyclic *n*-mers.

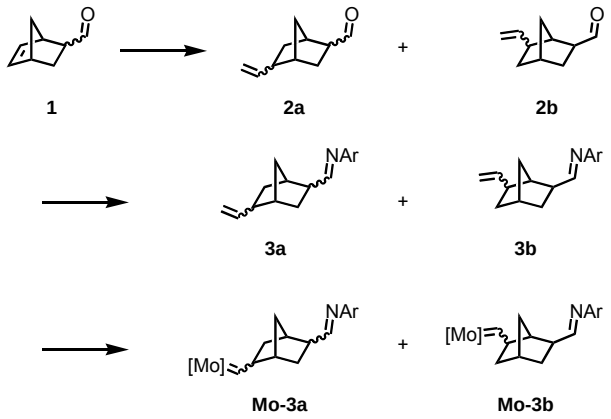

Scheme 4.4. Synthetic approach to alkylidenes **Mo-3a** and **Mo-3b**.

A third consideration given to the selection of **Mo-1** as the substrate of choice has to do with the fragment it leaves behind after ring closing. Alkylidene **Mo-1** transfers to the cyclic oligomer its norbornyl center. This ensures that the ring product is entirely composed of a series of cyclic hydrocarbons separated by unsaturated linkers when norbornene is used as a monomer. Norbornene is an attractive monomer for this application because it is known to be well-behaved to ROMP and because the 2,5-substitution of the cyclopentane rings biases the oligomers for macrocycle formation.

Polynorbornene (PNB, Figure 4.8) generated by ROMP is known to be atactic with respect to carbons 2 and 5 because the five-membered rings are randomly *R*,*S* and *S*,*R* disubstituted. It is the bond across carbons 6 and 7, however, which gives insight into the conformational preference of PNB. Reports have shown that this bond is up to 73% cis in PNB, and it is this preference which gives PNB its blockiness, which is the ratio of cis-cis to trans-trans strings.[195] PNB which achieves a blockiness ratio of 4.5 is known to be soluble in organic solvents.

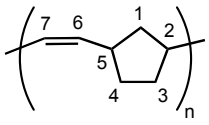

Figure 4.8. Polynorbornene.

4.2. Results

4.2.1. Overview

Though the ultimate goal of using a bifunctional organometallic compound to mediate the formation of cyclic oligomers has yet to be achieved, the synthesis of an initial substrate for ligand substitution onto the metal center has been performed. This section describes synthetic trials *en route* to the substrate and notes early-stage progress in this project.

4.2.2. Preparation of a Rigid Mo^{VI}-Alkylidene for Cyclic Oligomerization

The key to the production of cyclic oligomers is the preparation of a rigid bifunctional imine olefin substrate (**3**) that can be attached to a Schrock-type metathesis catalyst. The resulting catalyst **Mo-3** will have both an active alkylidene site for olefin metathesis and an imine terminating group. Previous studies on analogous systems have shown that the metathesis polymerization should take place at the alkylidene site but that the kinetically slower but thermodynamically more favorable reaction with the imine will terminate the reaction and kill the catalyst. Based on this reasoning, compound **3** was prepared as the catalyst for the cyclic oligomer study (Scheme 4.5).

A number of approaches to the synthesis of alkylidene **Mo-1** were examined. The most successful and efficient route began with the conversion of aldehyde **1** to the dimethyl acetal **4**. Acetal **4** was obtained in 89% yield by the addition of the addition of *meso*-2,3-butanediol to 5-norbornene-2-carboxaldehyde and its structure was confirmed by ^{1}H NMR spectroscopy and GC-MS analysis. Acetal formation was evident by the disappearance of the *exo*- (δ 9.40) and *endo*- (δ 9.18) aldehyde C*H*O signals and the presence of four doublets indicating the C*H*(dimethyl-1,3-dioxolane) proton from δ 4.46 – 5.49. The GC-MS exhibited an $[M]^{+\cdot}$ peak at m/z 194 and a base peak at m/z 101, which corresponded to the mass of the dimethyl-(1,3-dioxolane) ion. As expected, acetal **4** was produced as a mixture of exo- and endo- products.

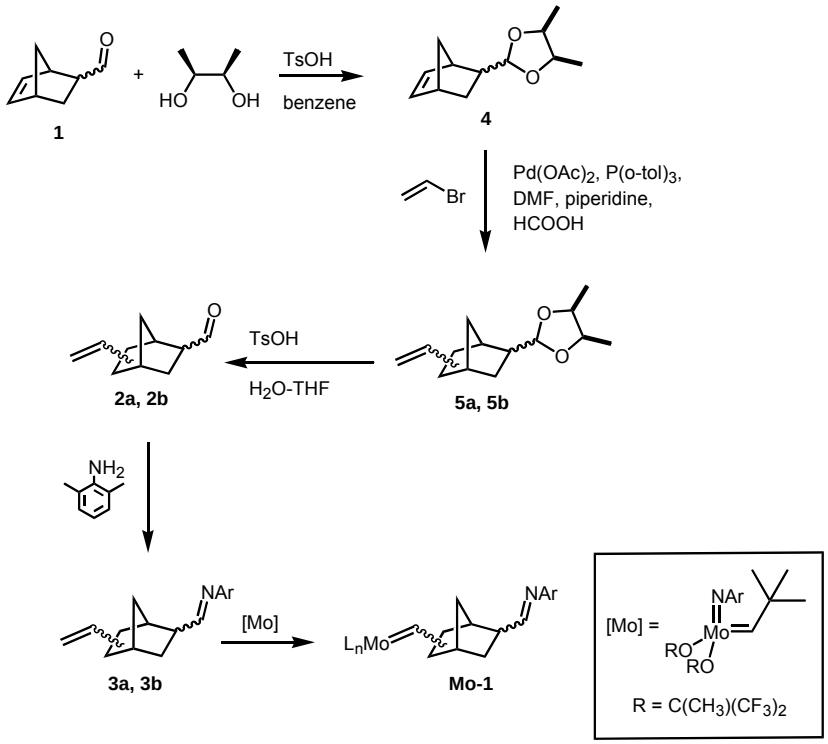

Scheme 4.5. Synthesis of **Mo-1** for imine-olefin competition study.

Hydrovinylation of **4** to give the 5-vinyl compound **5** was then achieved using a Heck reaction. 5-Vinyl **5** was produced as the diastereomeric mixtures of both **5a** and **5b** as indicated in Scheme 4.5. The vinyl product family **5** was recovered as a yellow liquid in yields ranging from 49 to 65% and its structure was verified by ^{1}H NMR spectroscopy and GC-MS analysis. ^{1}H NMR confirmed the presence of the vinyl group by the appearance of two multiplets in the region δ 4.5 – δ 5.8. Integration showed the more downfield signal to be roughly half that of the more upfield signal, which held with the presence of a vinyl group. A more conclusive determination could not be made owing to the number of isomeric vinyl groups present and the overlapping C*H*(dimethyl-1,3-dioxolane) signals. GC-MS showed the production of a family of isomeric compounds all with a peak at m/z 222. This corresponded to the $[M]^{+\cdot}$ peak for 5-vinyl **5**. The product mixture was purified by column chromatography to remove phosphine and trace unreacted substrate.

Aldehyde **2** was obtained using standard deprotection protocol using catalytic TsOH in a mixture of THF and H_2O. Because this step offered the last chance of rigorous purification, the product was painstakingly refined by column chromatography to remove persisting phosphine and unreacted starting material. Characterization by ^{1}H and ^{13}C NMR spectroscopy confirmed the successful formation of aldehyde **2**. The ^{1}H NMR spectrum showed the presence of aldehyde signals for various isomers from δ 9.24 to δ 9.45 as well as the absence of all signals associated with the dioxolane, suggesting that cleavage of the protecting group had proceeded cleanly. The ^{13}C NMR spectrum exhibited distinct signals characteristic corresponding to the parent aldehyde at δ 200.9, δ 201.1, and δ 202.5. GC-MS indicated the production of a family of isomeric compounds all exhibiting an $[M]^{+\cdot}$ peak at m/z 150, and an $[M-29]^{+}$ peak at m/z 121, indicating

loss of the aldehyde functionality. Aldehyde **2** was finally isolated as a yellow liquid at 65% yield.

Imine **3** was readily made from the condensation reaction of aldehyde **2** and 2,6-dimethylaniline. Removal of excess aniline by purification with ROMPGEL[196] was then attempted. ROMPGEL is convenient for amine sequestration because any amine encountered leads to opening of anhydride functionality on the polymer (Scheme 4.6), and as a polymer reagent ROMPGEL is then removed by simple filtration. Unfortunately, however, ROMPGEL proved to be ineffective owing to steric bulkiness surrounding the amine functionality. The remaining amine was found to be present by GC as a 5% impurity, and so it was deemed a tolerable impurity. Solvent was removed *in vacuo* to give imine **3** at 111% yield. The product was determined to be 91% pure by integration of GC, with the bulk of the impurity being excess amine. GC-MS showed the production of a family of isomeric imines giving identical fragmentation patterns. The mass spectrum of each isomer resolved through chromatography gave the expected parent $[M]^{+\cdot}$ peak at m/z 253. ^{1}H NMR showed signals corresponding to RC*H*=NR' at δ 7.19 and δ 7.21. Additional imine signals may have been obscured by benzene. The amine impurity was identified by the RNH_2 signal at δ 2.75. The signal for H_2C=C*H* was present as a multiplet centered at δ 5.65 and integrated to 1.00. The signal for H_2C=CH was present as a series from δ 4.91 to δ 4.97 and integrated to 2.01. The ^{13}C NMR spectrum showed signals for R*C*H=NR' at δ 169.2, δ 169.3, and δ 169.4.

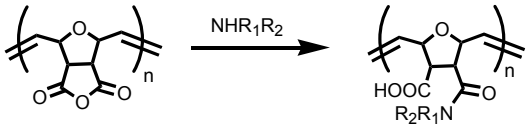

Scheme 4.6. Reaction showing the mode by which amine is sequestered by ROMPGEL.

4.2.3. Investigation of Norbornene Hydrovinylation Catalyzed by [Ru]-H 6

4.2.3.1. Hydrovinylation Performed on Norbornene Substrates Bearing Remote Acetal Functionalities

A second method of hydrovinylation was explored and met with mixed results (Figure 4.7). Using $(PCy_3)_2Ru(H)(Cl)CO$ **6**, aldehyde **2** was produced directly from aldehyde **1** and its identity confirmed by comparison of GC-MS data with the previous route to this compound. Though there was convincing agreement among the data, this route to 5- vinyl-2-carboxaldehyde **2** was complicated greatly by the presence of byproduct aldehyde **7** (Figure 4.7). The aldehyde families **2** and **7** were determined by GC to exist in a 2:3 ratio, which meant the desired aldehyde was the minor product. Additionally, repeated attempts at separating **2** from **7** by column chromatography were unsatisfactory, with only a trace amount of pure aldehyde **2** recovered.

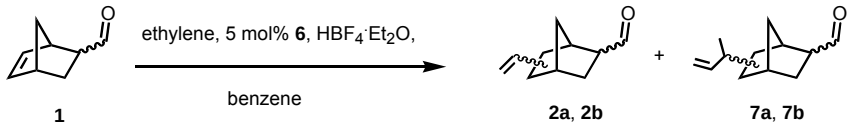

Scheme 4.7. Reaction giving singly- and doubly-hydrovinylated aldehydes **2** and **7**.

Before we discovered that Pd fixed the double vinylation problem we explored the use of alternate protecting schemes in an attempt to facilitate better separation of the singly- from the doubly hydrovinylated product. For that reason aldehyde **1** was converted to a series of three acetals: dioxolane **8**, dimethyldioxolane **5**, and tetramethyldioxolane **9** (Scheme 4.8). Ru-mediated hydrovinylation was then attempted on each dioxolane (Scheme 4.9).

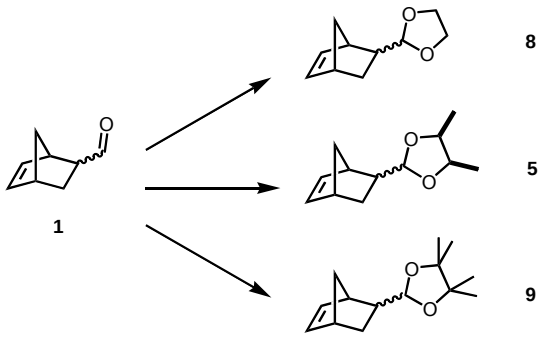

Scheme 4.8. Series of protected substrates tested for hydrovinylation by [Ru]-H **6**.

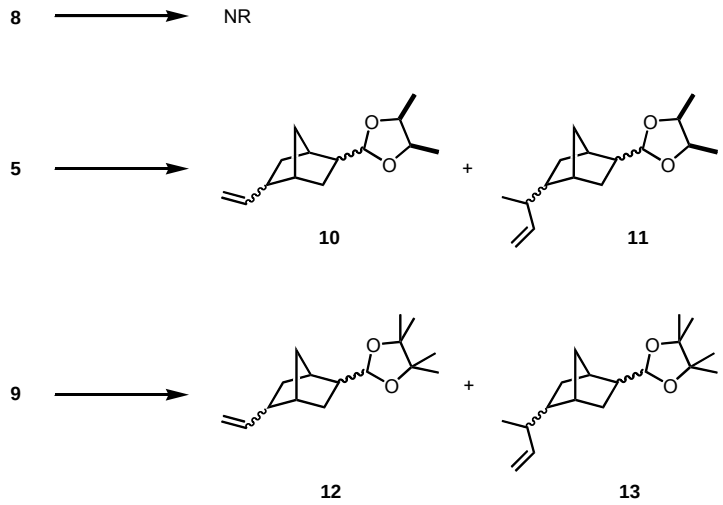

Scheme 4.9. Summary of hydrovinylation tests.

Acetal **8** was obtained in 81% yield by the nucleophilic addition of ethylene glycol to 5-norbornene-2-carboxaldehyde **1** and its structure confirmed by ^{1}H NMR spectroscopy. In particular, the aldehydic doublets at δ 9.48 (*exo*-C*H*O) and δ 9.26 (*endo*-C*H*O) were absent, and signals were present in the form of doublets from δ 4.30-4.70. These signals indicated diastereomeric acetal formation. The acetal was used without further purification. Attempts at hydrovinylating **8** using ruthenium hydride **6** were unsuccessful, however. It was thought that this might be due to the steric accessibility of the acetal oxygens, which could presumably have

made either or both of them available for coordination to ruthenium. With this in mind, more sterically hindered diols were explored.

Dimethyl acetal **5** was obtained by the addition of the addition of *meso*-2,3-butanediol to 5-norbornene-2-carboxaldehyde and its structure was confirmed by ^{1}H NMR spectroscopy. The acetal was refined by column chromatography to 96% purity (52% yield) as determined by NMR inspection. Hydrovinylating **5** gave a mixture of **10** and **11**. The production of **10** and **11** was verified by GC-MS analysis, though purification by column chromatography was still far from ideal.

Tetramethyl acetal **9** was obtained in 83% yield by the addition of pinacol to 5-norbornene-2-carboxaldehyde and its structure confirmed by ^{1}H NMR spectroscopy. The acetal was used without further purification. Hydrovinylating **9** gave a mixture of **12** and **13**. This product mixture was separated from other impurities by distillation The structures of **12** and **13** were verified by ^{1}H NMR spectroscopy and GC-MS analysis. Subsequent attempts at regenerating the respective aldehydes using 5-25% HCl in aqueous THF were unsuccessful owing to the familiar rearrangement tendencies of the pinacolato moiety.

In the cases where the dioxolane substrate did hydrovinylate using [Ru]-H **6**, the catalyst inevitably cycled through two net ethylene additions and the resulting product mixture was no easier to separate.

4.2.3.2. Hydrovinylation Performed on a Norbornene Substrate Bearing a Remote Imine Functionality

One final set of experiments was conducted using catalyst **6** on a preformed imine. This served to test the affinities of norbornenes with remotely placed aldehydes in comparison with

remotely placed imines and if successful, hydrovinylating an imine-substituted norbornene would have eliminated a synthetic step *en route* to the alkylidene **3**.

Several attempts to synthesize the imine prior to hydrovinylation were made. The reaction of aldehyde **1** with 2,6-diisopropylaniline went to 88-91% conversion to the imine as determined by GC (Scheme 4.10). Because separation by column chromatography was not an option, attempts were made to consume unreacted aldehyde with excess amine. Amine left unreacted was then to be scavenged by ROMPGEL. Repeated attempts of this approach proved unsuccessful. Incomplete conversion to the imine was attributed to the large steric demand of the *ortho* isopropyl groups.

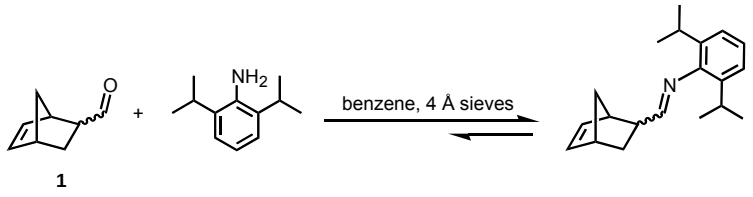

Scheme 4.10. Reaction of aldehyde **1** and 2,6-diisopropylaniline does not got to completion.

Accordingly, an attempt to synthesize the less hindered imine **14** was undertaken (Scheme 4.11). Imine **14** was successfully prepared in 52% yield by the condensation of 2,6-dimethylaniline with 5-norbornene-2-carboxaldehyde, and its structure confirmed by ^{1}H NMR spectroscopy and GC-MS analysis. Hydrovinylation of imine **14** proved unsuccessful, however.

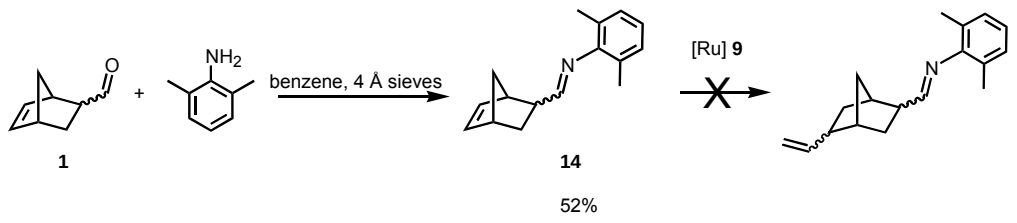

Scheme 4.11. Hydrovinylation check on imine-substituted **14** gave no reaction.

4.3. Summary of Further Studies

Imine **3**, after being prepared as described in Section 4.2.2, was reacted with Schrock's catalyst to produce **Mo-1**. It quickly became clear, however, that the ω-imino alkylidene species underwent decomposition in the reaction mixture which precluded any polymerization. This instability was likely due to the presence to amine, which can react in an uproductive fashion with the metal if not consumed.

In an attempt to circumvent this problem we decided to investigate the preparation of a ruthenium based-linker molecule. Aldehyde **2** was treated with a phosphorus ylide to yield enol ether **15** in 50% yield following column chromatography (Scheme 4.12). Compound **15** was then investigated as a substrate for ligand substitution onto the Grubbs-I catalyst to produce **Ru-A** as shown in Scheme 4.13. Use of **15** as a bifunctional substrate followed the same rationale described for the employment of imine **3**–ROMP reactions mediated by Grubbs carbenes are typically quenched by the addition of ethyl vinyl ether.[197] The resulting ethoxy methylidene species is a thermodynamic sink and, as such, is inactive to further metathesis (Scheme 4.14).

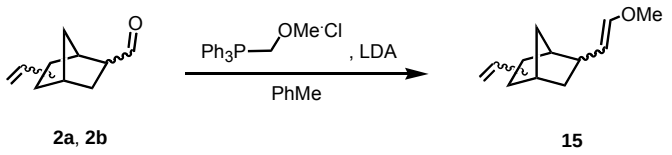

Scheme 4.12. Preparation of enol ether **8** using the Wittig reaction.

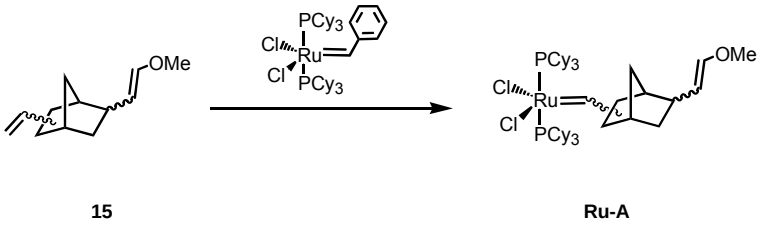

Scheme 4.13. Reaction of enol ether **8** with Grubbs-I catalyst.

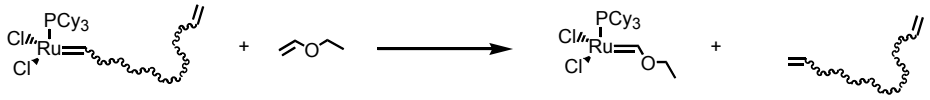

Scheme 4.14. The immediate quenching event of a Grubbs-type metathesis catalyst upon treatment with ethyl vinyl ether.

The competition of the vinyl and enol ether functionalities for productive metathesis onto the metal center was then examined. This experiment is described by Scheme 4.15 and was performed to better understand the interplay between formation of the kinetic (**Ru-A**) and thermodynamic (**Ru-B**) products. ^{1}H NMR experiments were conducted at various temperatures for the reaction of Grubbs-I and 4.5 eq enol ether **15**. The Ru product distributions for these experiments after 12 h are shown in Figure 4.9. The spectra collected after 12 h at -78° and -25° C clearly indicate preferential reactivity at the vinyl end of substrate **15**–the [Ru]=C*H*R integrations are approximately 10:1 **Ru-A**:**Ru-B** at -78° C and 3:1 Ru-A: Ru-B at -25° C. However, spectra collected after 12 h at 0° and 23° C show that the rate of reaction has increased

such that undesired metathesis to give Ru-B dominates. The alkylidene product distribution for the reaction after 12 h at 23° C is approximately 1:10 **Ru-A**:**Ru-B** by integration.

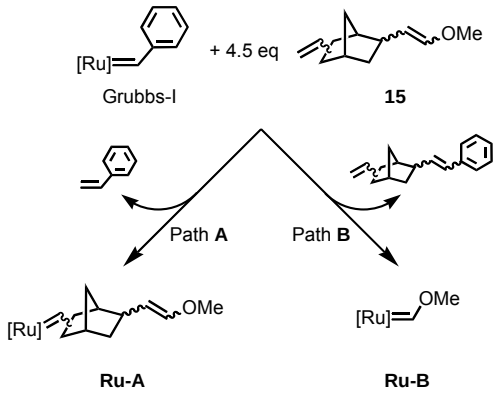

Scheme 4.15. The competition experiment of Grubbs-I and substrate **15**.

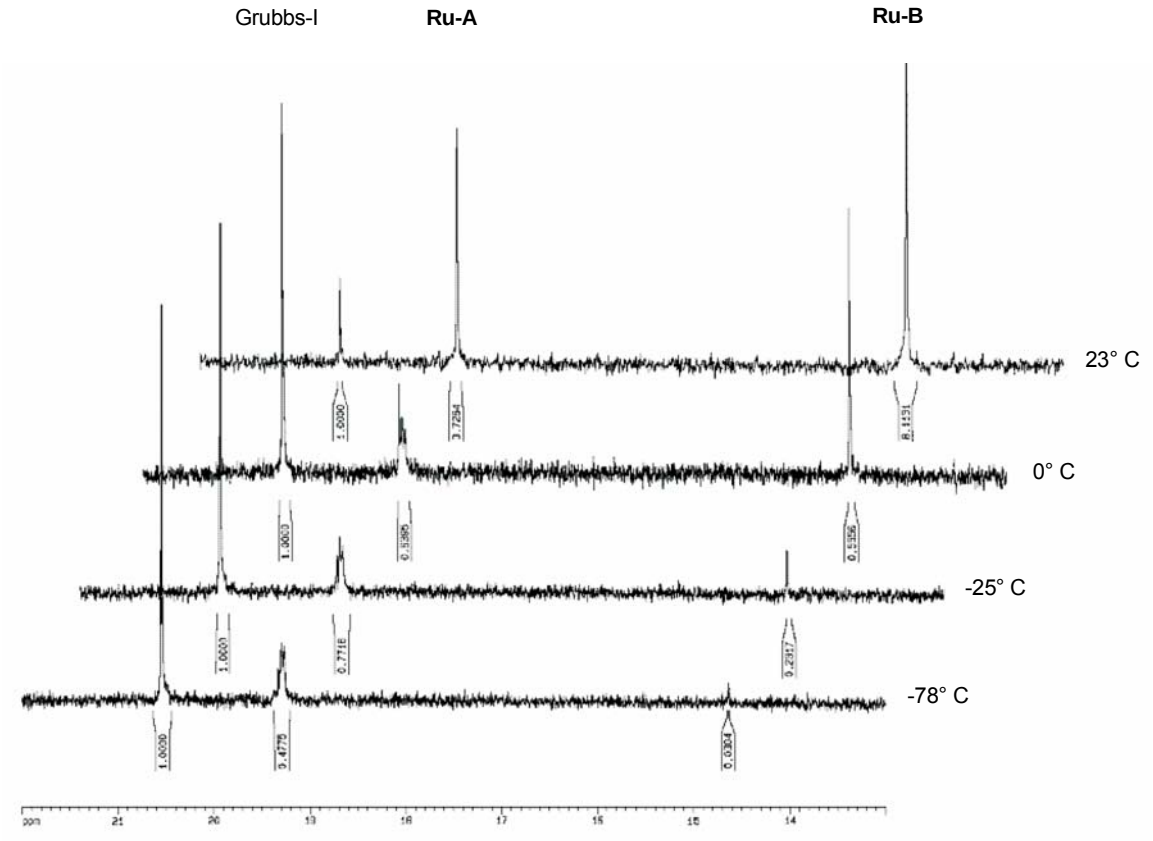

Figure 4.9. ^{1}H NMR spectra taken after 12 h for competitive metathesis experiments using Grubbs-I and enol ether **15** at -78°, -25°, 0°, and 23° C (d_8-PhMe).

4.4. Experimental

General Considerations. All manipulations of air- and/or water-sensitive compounds were performed in a nitrogen filled glove box or by standard Schlenk techniques. Solid organometallic compounds were transferred in a nitrogen filled glove box and stored at -33 ˚C, unless otherwise stated.

^{1}H and ^{13}C NMR spectra were recorded with Bruker spectrometers at 300 MHz. Chemical shifts were referenced to residual ^{1}H signals in deuterated solvents. Significant ^{1}H data

are tabulated in the order: multiplicity, number of protons, coupling constant(s) in hertz. Gas chromatography-mass spectrometry (GC-MS) was performed on a Hewlett Packard Series 5980 GC-5971 A MS with a Hewlett Packard Series 1 capillary column. Column chromatography was performed using Sorbent 60 32-60 standard grade silica gel.

Materials. Unless otherwise indicated, materials were obtained from commercial suppliers and used without further purification. Aniline, 2,6-dimethylaniline, and 2,6-diisopropylaniline were distilled from calcium hydride. 5-norbornene-2-carboxaldehyde (**1)** was purified by column chromatography using benzene as eluant. Benzene and diethyl ether were distilled under nitrogen from sodium and benzophenone. Benzene-d_6 was dried over sodium and benzophenone, degassed by repeated freeze-pump-thaw cycles, vacuum transferred, and stored in a nitrogen glove box.

5-Vinyl-norbornane-2-carbaldehyde (2a), 6-Vinyl-norbornane-2-carbaldehyde (2b), 5-(1-Methyl-allyl)-norbornane-2-carbaldehyde (7a), and **6-(1-Methyl-allyl)-norbornane-2-carbaldehyde (7b)**:

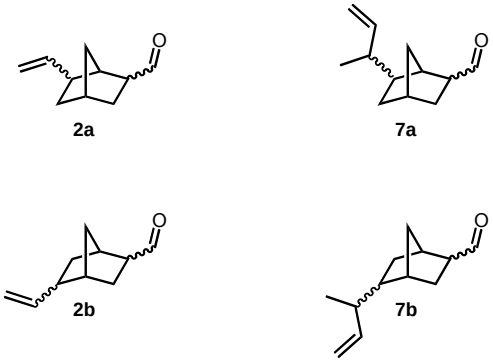

In a nitrogen-filled glove box, a solution of complex **6** (5 mol%) in 25 mL benzene was added to a 200 mL Schlenk tube equipped with a Teflon stopcock. The reaction tube was brought

out of the box and 84 μL 54 wt % $HBF_4{\cdot}Et_2O$ (1.5 equiv) was added via syringe under inert atmosphere. The mixture was stirred for 30 min and was cooled in a liquid nitrogen bath. The reaction mixture was treated with a solution of aldehyde **1** (1.00 mL, 8.17 mmol) in 1 mL benzene was added. Excess ethylene was condensed into the reaction tube, and the reaction mixture was stirred for 12 h at room temperature. The tube was opened to air, the mixture was filtered through a pipet packed with 20 cm of silica gel, and the solvent was removed *in vacuo* to give the isomeric families **2** and **7** (0.43 mL). GC-MS **2a**, **2b**: $[M]^{+\cdot}$ m/z 150, $[M\text{-}CHO]^+$ m/z 121, $[C_6H_5O]^+$ m/z 93, base peak, $[C_7H_7]^+$ m/z 91. GC-MS **7a**, **7b**: $[M]^{+\cdot}$ m/z 178, $[M\text{-}CHO]^+$ m/z 149, $[M\text{-}C_4H_9]^+$ m/z 121, $[C_6H_5O]^+$ m/z 93, base peak, $[C_7H_7]^+$ m/z 91.

A second method was utilized which yielded only **2a** and **2b**. Dimethyl acetal products **5a** and **5b** (3.12 mL, 14.76 mmol) and TsOH (255 mg) were dissolved in THF (100 mL). H_2O (25 mL) was added and the contents were refluxed 6 h. Upon coling, the organic product was extracted with ether (15 mL), washed, dried with Na_2SO_4, and the solvent removed *in vacuo*. The product was purified by column chromatography (SiO_2, 10% hexanes in EtOAc) to give the isomeric products **2a** and **2b** (.904 g, 35%). ^{1}H NMR (C_6D_6) δ 9.24 – 9.44 (ss, 1, C*H*O), δ 5.50-5.56 (m, 1, C*H*=CH_2), δ 4.83-4.88 (m, 2, CH=C*H*$_2$). Numerous unresolved chemical shifts were present from δ 0.72-2.20 and indicated presence of protons on the norbornane skeleton. ^{13}C NMR (C_6D_6) δ 200.8, 201.1, 202.4, 202.5 (*C*HO), δ 143.0, 143.3, 143.4 (CH_2=*C*H), δ 112.3, 112.6, 112.7 (*C*H_2=CH). Numerous chemical shifts were present from δ 28.5-54.6 and indicated presence of carbons on the norbornane skeleton. GC-MS $[M]^{+\cdot}$ m/z 150, $[M\text{-}CHO]^+$ m/z 121, $[C_6H_5O]^+$ m/z 93, base peak, $[C_7H_7]^+$ m/z 91.

(2,6-Dimethyl-phenyl)-(5-vinyl-norborn-2-ylmethylene)-amine (3a) and (2,6-Dimethyl-phenyl)-(6-vinyl-norborn-2-ylmethylene)-amine (3b):

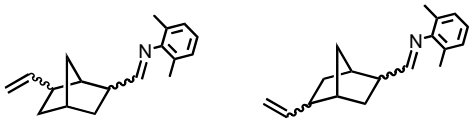

3a **3b**

2,6-Dimethylaniline (50 μL, 0.40 mmol) and the aldehyde mixture of **2a** and **2b** (66 mg, 0.44 mmol) were added to a Schlenk flask containing 20 mL benzene and molecular sieves (4 Å, 8 g). Filtration and solvent removal gave **3a** and **3b** (136 mg, 111%). ^{1}H NMR (C_6D_6) δ 7.19-7.21 (m, 1, C*H*=NR), δ 6.93-7.02 (m, 3, H_m, H_p), δ 5.67 (quint, 1, CH_2=C*H*), δ 4.92 (m, 2, CH_2=CH), δ 2.07 (s, 6, *Me*$_2$Ph). The remaining chemical shifts were noted as indicative of protons on the norbornane skeleton. ^{13}C NMR (C_6D_6) δ 169.2, 169.3, 169.4 (*C*H=N), δ 152.0, 126.6, 123.4 (Me$_2$*Ph*), 143.3, 143.6 (CH_2*C*H), 112.1, 112.3 (*C*H_2CH), δ 18.4 (*Me*$_2$Ph). Numerous chemical shifts were present from δ 32.4-48.2 and indicated presence of carbons on the norbornane skeleton. GC-MS $[M]^{+\cdot}$ m/z 253, $[M\text{-}C_4H_7]^+$ m/z 198, $[M\text{-}C_6H_7N]^+$ m/z 160, base peak.

Norborn-5-en-2-yl-4,5-dimethyl-[1,3]dioxolane (5):

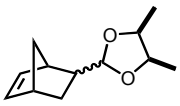

To a Schlenk flask was added 100 mL benzene, followed by toluenesulfonic acid (35.0 mg, .202 mmol), aldehyde **1** (0.65 mL, 5.4 mmol), and *meso*-2,3-butanediol (0.50 mL, 5.5 mmol). The contents were refluxed and water was removed as a benzene azeotrope using a

Dean-Stark apparatus. After cooling, the reaction mixture was quenched with a saturated solution of $NaHCO_3$. The benzene layer was collected and dried over $MgSO_4$, and the solvent was removed *in vacuo*. The product was purified by flash chromatography (SiO2, benzene) to give **5** as a colorless oil (0.52 mL, 52%). ^{1}H NMR (C_6D_6) δ 6.04 (m, 2, *H*C=), δ 4.40-4.78 (d series, 1, *J* 8.5, 2-*endo*/2-*exo*), δ 4.00 (m, 1, OC*H*$_s$Me or OC*H*$_a$Me), δ 3.77 (m, 1, OC*H*$_a$Me or OC*H*$_s$Me), δ 3.03-3.18 (m, 1, bridgehead 4 C*H*), δ 2.60-2.70 (m, 1, bridgehead 1 C*H*), δ 2.35 (sept, 1, C*H*CHOCH$_2$), δ 1.87 (m A of AB, 1, bridging 7 CH$_a$ or CH$_s$), δ 1.39 (m B of AB, 1, bridging 7 CH$_s$ or CH$_a$), δ 1.08 (m, 1, 3-*endo*/3-*exo*), δ 0.93 (m, 6, CH*Me*). GC-MS: $[M]^{+\cdot}$ m/z 194, $[M-C_5H_7]^+$ m/z 127, $[M-C_7H_9]^{+\cdot}$ m/z 101, base peak.

$(PCy_3)_2$Ru(H)(Cl)(CO) (6):

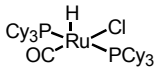

Using the method of Esteruelas,[198] a solution of $RuCl_3 \cdot 3H_2O$ (0.383 g, 1.46 mmol) in 45 mL anhydrous methanol was treated with tricyclohexylphosphine (1.94 g, 6.92 mmol) and the mixture was heated for 24 hours under reflux. The resulting yellow precipitate was filtered off, washed with methanol and diethyl ether, and dried *in vacuo* to give **6** (0.593 g, 58%). ^{1}H NMR (C_6D_6) δ 1.07-1.31, 1.60-1.72, 2.01-2.21, 2.40-2.57 (m, P*Cy*$_3$), δ -24.2 (t, 1, J_{PH} = 18.0, Ru-*H*). Characterization matched known literature.

Norborn-5-en-2-yl-[1,3]dioxolane (8):

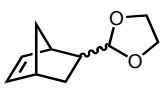

To a Schlenk flask was added 100 mL benzene, followed by toluenesulfonic acid (113 mg, 0.653 mmol), aldehyde **1** (2.0 mL, 17 mmol), and ethylene glycol (1.4 mL, 25 mmol).The

contents were refluxed and water was removed as a benzene azeotrope using a Dean-Stark apparatus. After cooling, the reaction mixture was quenched with a saturated solution of $NaHCO_3$. The benzene layer was collected and dried over $MgSO_4$, and the solvent was removed *in vacuo* to give pure **8** (2.26 g, 81%). ^{1}H NMR (C_6D_6) δ 6.02 (m, 2, *H*C=), δ 4.30-4.70 (d series, 1, *J* 8.5, 2-*endo*/2-*exo*), δ 3.54 (m, 2, OCH_sHCH_sHO or OCH_aHCH_aHO), δ 3.35 (m, 2, OCH_aHCH_aHO or OCH_sHCH_sHO), δ 3.01-3.14 (m, 1, bridgehead 4 C*H*), δ 2.59-2.68 (m, 1, bridgehead 1 C*H*), δ 2.33 (sept, 1, C*H*CHOCH_2), δ 1.81 (m B of AB, 1, bridging 7 CH_a or CH_s), δ 1.60 (m, 1, 3-*exo*), δ 1.36 (m A of AB, 1, bridging 7 CH_s or CH_a), δ 1.07 (m, 1, 3-*endo*). GC-MS: $[M]^{+\cdot}$ m/z 166, $[M\text{-}C_5H_7]^+$ m/z 99, $[M\text{-}C_5H_8O_2]^{+\cdot}$ m/z 66, base peak.

Norborn-5-en-2-yl-4,4,5,5-tetramethyl-[1,3]dioxolane (9):

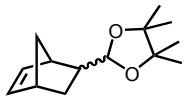

Using the procedure that was employed for **5**, toluenesulfonic acid (53.6 mg, .310 mmol), aldehyde **1** (1.7 mL, 14.28 mmol), and pinacol (1.85g, 15.7 mmol) were reacted to give **9** (2.64g, 83%). ^{1}H NMR (C_6D_6) δ 6.06 (m, 2, *H*C=), δ 4.66-5.00 (d series, 1, *J* 8.7, 2-*endo*/2-*exo*), δ 3.10-3.18 (m, 1, bridgehead 4 C*H*), δ 2.61-2.67 (m, 1, bridgehead 1 C*H*), δ 2.30 (sept, 1, C*H*CHOCH_2), δ 1.87 (m B of AB, 1, bridging 7 CH_a or CH_s), δ 1.40 (m A of AB, 1, bridging 7 CH_s or CH_a), δ 1.11 (m, 12, CMe_2). The chemical shift for 3-*endo*/3-*exo* was obscured by CMe_2. GC-MS: $[M]^{+\cdot}$ m/z 222, $[M\text{-}C_5H_6]^{+\cdot}$ m/z 156, $[M\text{-}C_7H_9]^+$ m/z 129.

4,5-Dimethyl-2-(5-vinyl-norborn-2-yl)-[1,3]dioxolane (10a), 4,5-Dimethyl-2-(6-vinyl-norborn-2-yl)-[1,3]dioxolane (10b), 4,5-Dimethyl-2-(5-(1-methyl-allyl)-norborn-2-yl)-

[1,3]dioxolane (11a), and **4,5-Dimethyl-2-(6-(1-methyl-allyl)-norborn-2-yl)-[1,3]dioxolane (11b)**:

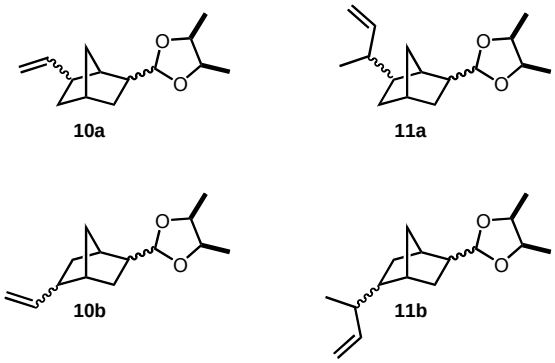

Method 1:

Using the method of Yi,[199] in a nitrogen-filled glove box, a solution of catalyst **6** (5 mol%) in 2 mL benzene was added to a 20 mL Schlenk tube equipped with a Teflon stopcock. $HBF_4{\cdot}Et_2O$ (15 μL, 54 wt %, 1.5 equiv,) was added via syringe under inert atmosphere. After stirring and cooling, the reaction mixture was treated with a solution of alkene **5** (90.7 μL, 0.50 mmol) in 1 mL benzene. Ethylene (6 mmol) was condensed into the reaction tube, and the reaction mixture was stirred for 12 h at room temperature. The tube was opened to air and work up gave the isomeric families **10** and **11** (115 μL). GC-MS **10a**, **10b**: $[M]^{+\cdot}$ m/z 222, $[C_5H_9O_2]^+$ m/z 129, $[M\text{-}C_7H_9]^{+\cdot}$ m/z 101, base peak. GC-MS **11a**, **11b**: $[M\text{-}1]^+$ m/z 249, $[C_5H_9O_2]^+$ m/z 129, $[M\text{-}C_7H_9]^{+\cdot}$ m/z 101, base peak.

Method 2:

A second approach produced **10a** and **10b** in the absence of **11a** or **11b**. Based on the method of Arcadi,[200] $Pd(OAc)_2$ (90 mg, 0.41 mmol), $P(o\text{-tolyl})_3$ (482 mg, 1.59 mmol), and piperidine (2.11 g, 24.8 mmol) were massed and added in a nitrogen-filled glove box to a 20 mL Schlenk tube equipped with a Teflon stopcock. The tube was brought out of the glove box and

the contents were frozen. Dimethyl acetal **5** (1.45 mL, 8.00 mmol), DMF (3.3 mL) and 88% formic acid (0.894 g) were added. The tube was evacuated, and vinyl bromide (8.00 mmol) was condensed into the reaction flask. The contents were allowed to come to room temperature and were stirred for 8 h. The contents were then heated in a 60˚ C for 4 h. The tube was cooled, and the mixture was diluted with ethyl acetate. The organic product was extracted with ethyl acetate, washed, dried with Na_2SO_4, and the solvent removed *in vacuo*. The product was purified by column chromatography using benzene as eluant to give the isomeric products **10a** and **10b** (1.04 mL, 65%). ^{1}H NMR (C_6D_6) δ 5.77 (m, 1, CH_2=C*H*), δ 5.02-5.45 (d series, 1, *J* 8.5, 2-*endo*/2-*exo*) δ 4.92 (m, 2, CH_2=CH), δ 3.98 (m, 1, OCH_sMe or OCH_aMe), δ 3.82 (m, 1, OCH_aMe or OCH_sMe), δ 2.69-2.74 (m, 1, bridgehead 4 C*H*), δ 2.39-2.43 (m, 1, bridgehead 1 C*H*), δ 2.08 (m, 2, 6-*endo*/6-*exo*), δ 1.77 (m, 1, 2-*endo*/2-*exo*). Numerous chemical shifts present from δ 0.93-2.73 were poorly resolved but were taken to indicate presence of protons on the norbornane skeleton.

4,4,5,5-Tetramethyl-2-(5-vinyl-norborn-2-yl)-[1,3]dioxolane (12a), 4,4,5,5-Tetramethyl-2-(6-vinyl-norborn-2-yl)-[1,3]dioxolane (12b), 4,4,5,5-Tetramethyl-2-[5-(1-methyl-allyl)-norborn-2-yl]-[1,3]dioxolane (13a), and **4,4,5,5-Tetramethyl-2-[6-(1-methyl-allyl)-norborn-2-yl]-[1,3]dioxolane (13b)**:

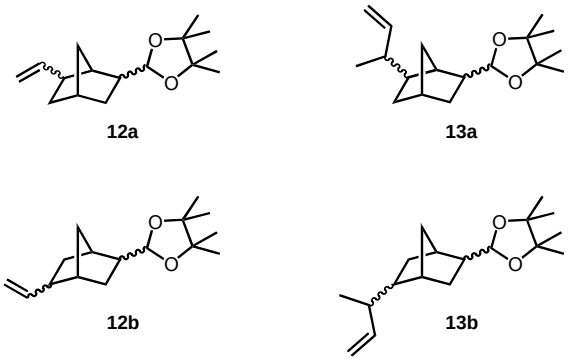

Using the procedure that was employed for **10** and **11**, a solution of complex **6** (5 mol%) in 20 mL benzene was added to a 200 mL Schlenk tube equipped with a Teflon stopcock. The reaction tube was brought out of the box and 122 μL 54 wt % $HBF_4{\cdot}Et_2O$ (1.5 equiv) was added via syringe under inert atmosphere. After stirring and cooling the mixture a solution the reaction mixture was treated with a solution of alkene **9** (1.44 g, 6.50 mmol) in 8 mL benzene. Excess ethylene (40 mmol) was then condensed into the reaction tube, and the reaction mixture was stirred for 13 h at room temperature. The tube was opened to air, the mixture was filtered through a column packed with 20 cm of silica gel, and the solvent was removed in vacuo to give the isomeric families **12** and **13**. GC-MS **12a**, **12b**: $[M]^{+\cdot}$ m/z 250, $[M\text{-}C_9H_{13}]^+$ m/z 129, $[M\text{-}C_7H_9]^{+\cdot}$ m/z 101, base peak. GC-MS **13a**, **13b**: $[M\text{-}1]^+$ m/z 277, $[M\text{-}C_9H_{15}]^+$ m/z 155, $[M\text{-}C_{11}H_{17}]^+$ m/z 129, base peak, $[M\text{-}C_7H_9]^{+\cdot}$ m/z 101.

Schrock norbornyl-alkylidene (Mo-1):

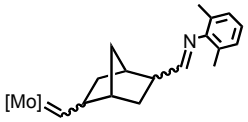

Mo-1

In a nitrogen-filled glove box, imine olefin **3** was dissolved in .200 mL C_6D_6 and transferred to a screw-valve NMR tube. To this was added enough of a 1.7 M standard solution of Schrock's catalyst, $Mo(=CHCMe_2Ph)(=NAr)[OCMe(CF_3)_2]_2$ (Ar = 2,6-diisopropylphenyl) to convert the catalyst to the new alkylidene. The contents of the tube were allowed to mix for 30 min. A ^1H NMR spectrum was then collected to determine the extent of the reaction. 1H NMR (C_6D_6) δ 12.37 (s, 1, Mo=C*H*), δ 7.00 (m, 3, $Mo{=}NC_6\mathit{H}_3(CHMe_2)_2$), δ 6.95 (m, 3, $CH{=}N\mathit{Me}_2Ph$),

δ 3.56 (s, 4, Mo=$NC_6H_3(CHMe_2)_2$) δ 2.08 (s, 6, CH=NMe_2Ph), δ 1.53 (s, 6, OC$Me(CF_3)_2$), δ 1.19 (s, 12, Mo=$NC_6H_3(CHMe_2)_2$). Diagnostic peak shifts indicating presence of free neophylidene were also observed: δ 5.97 (m, 1, CH_2=C*H*Me_2Ph), δ 4.98 (m, 2, CH_2=CHMe_2Ph), δ 1.27 (s, 6, CH_2=CHMe_2Ph).

APPENDIX A

Selected ^{1}H and ^{13}C NMR Spectra

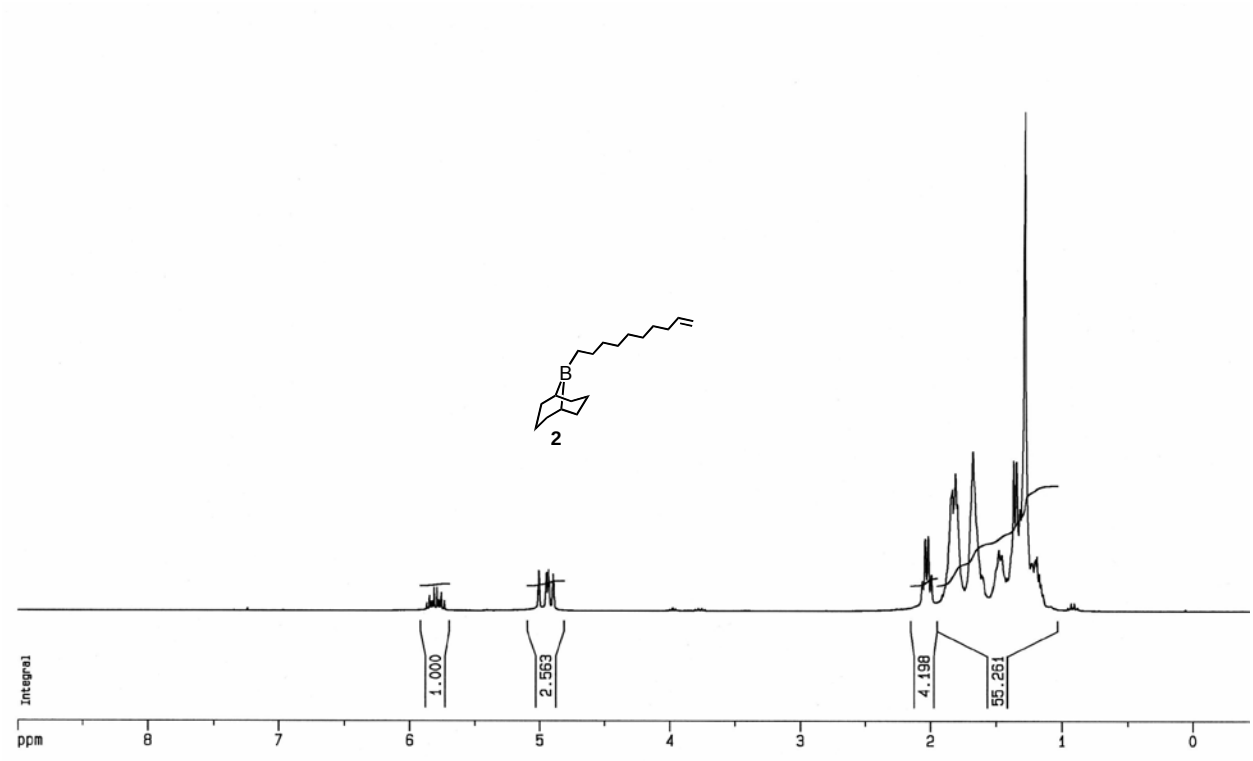

Figure A.1. The ^{1}H NMR spectrum of decenyl-9-BBN **2**.

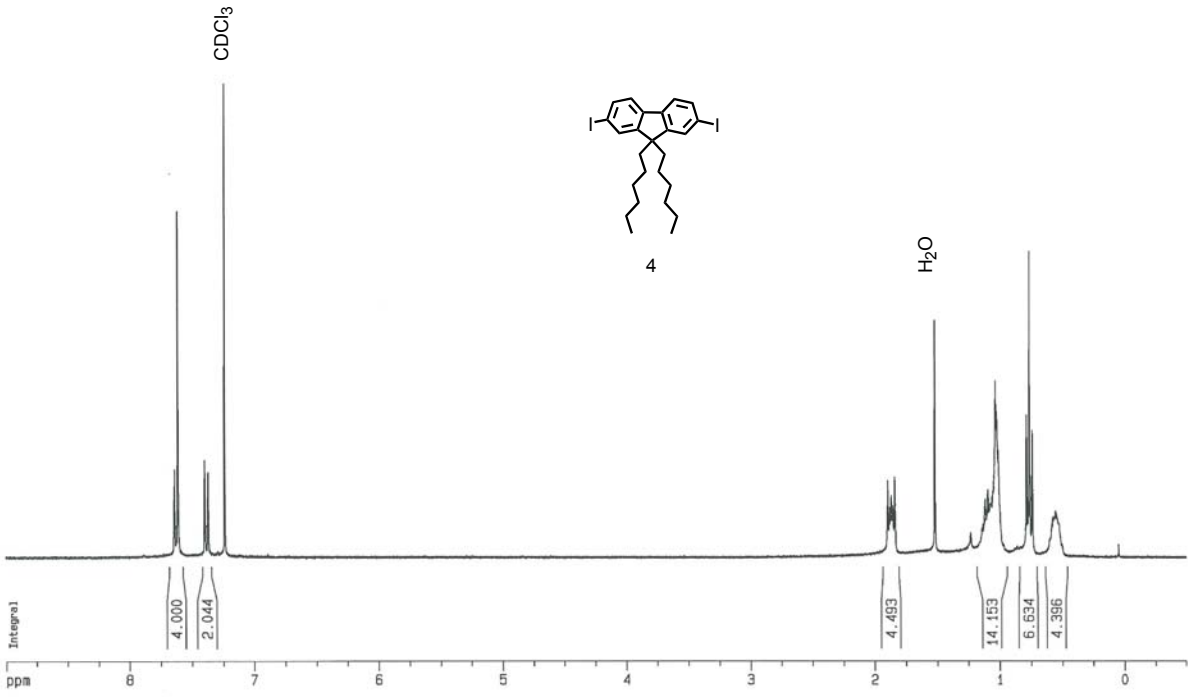

Figure A.2. The ^{1}H NMR spectrum of diiodofluorene **4**.

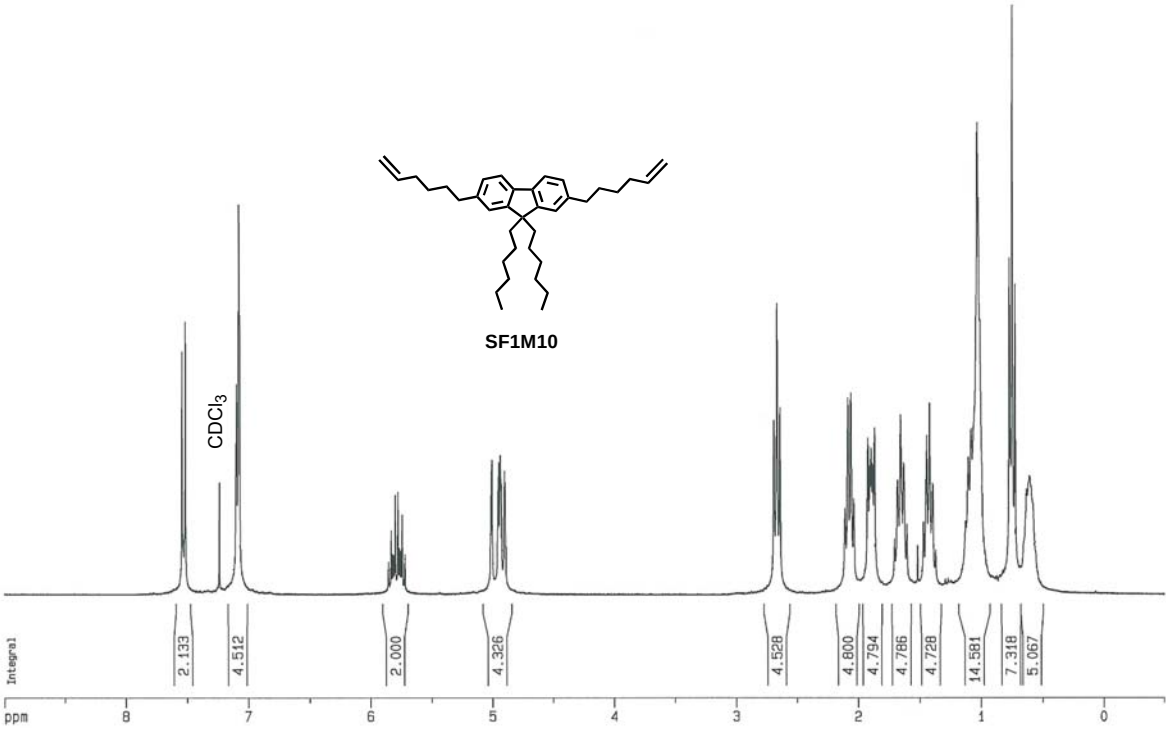

Figure A.3. The ^{1}H NMR spectrum of **SF1M10**.

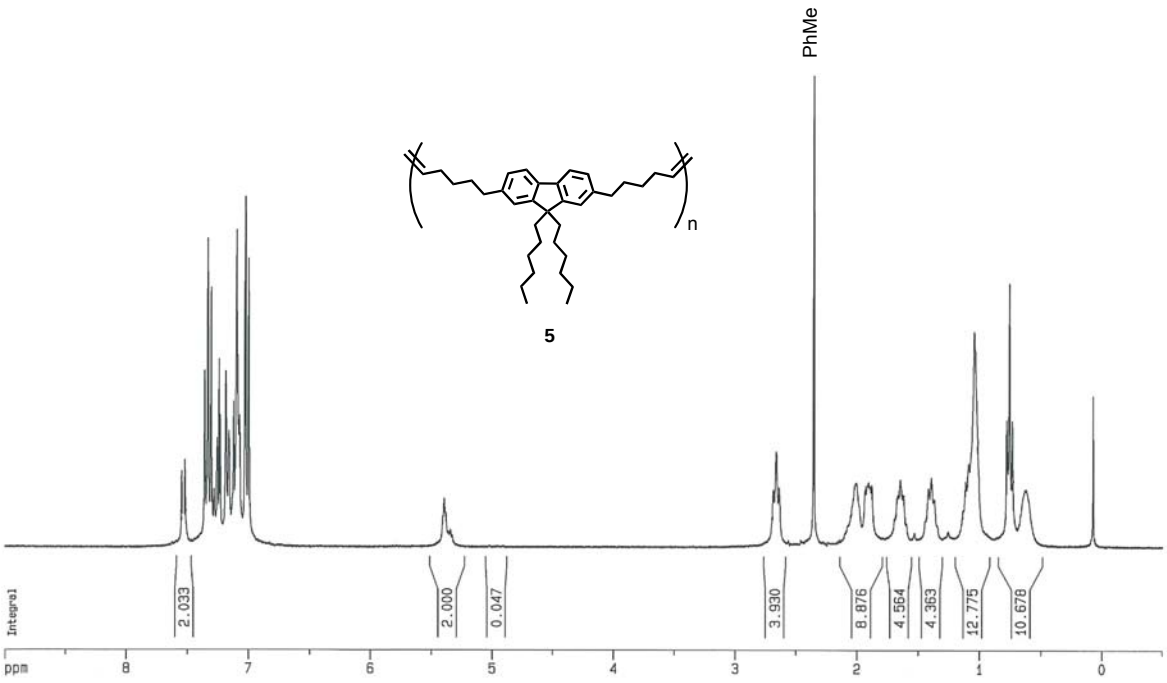

Figure A.4. The ^{1}H NMR spectrum of ADMET polymer **5**.

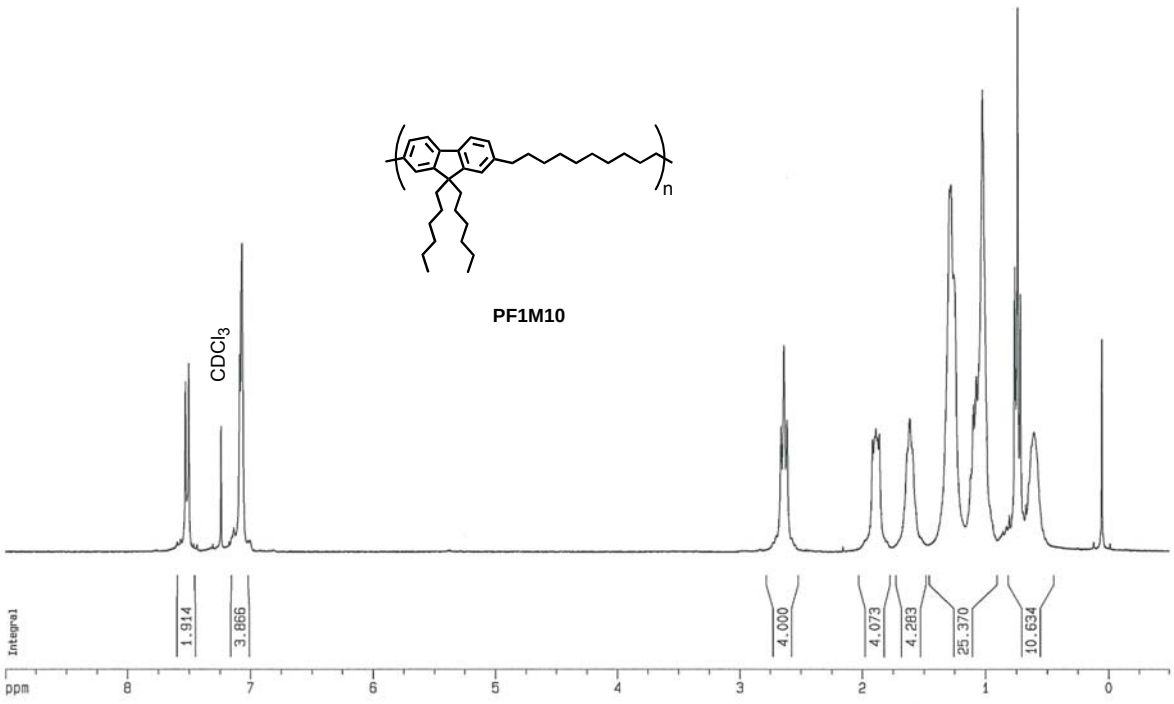

Figure A.5. The ^{1}H NMR spectrum of **PF1M10**.

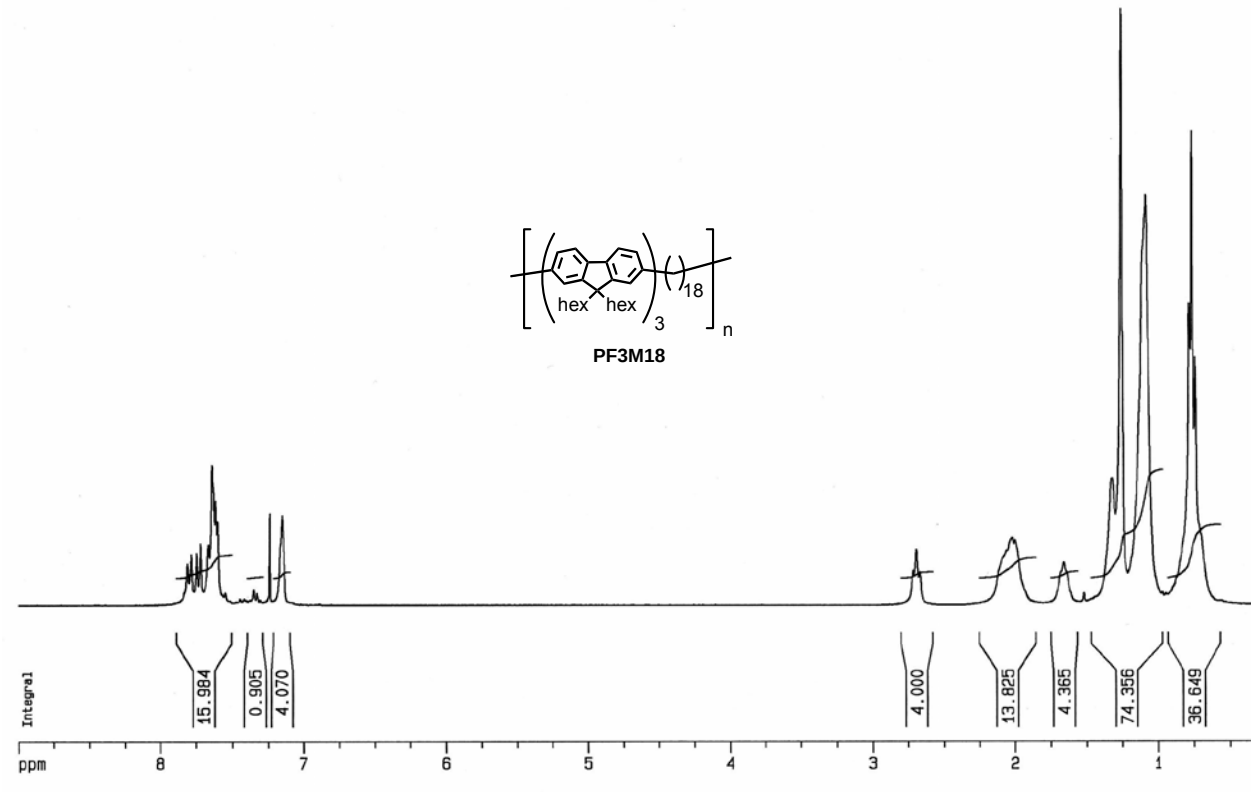

Figure A.6. The ^{1}H NMR spectrum of **PF3M18**

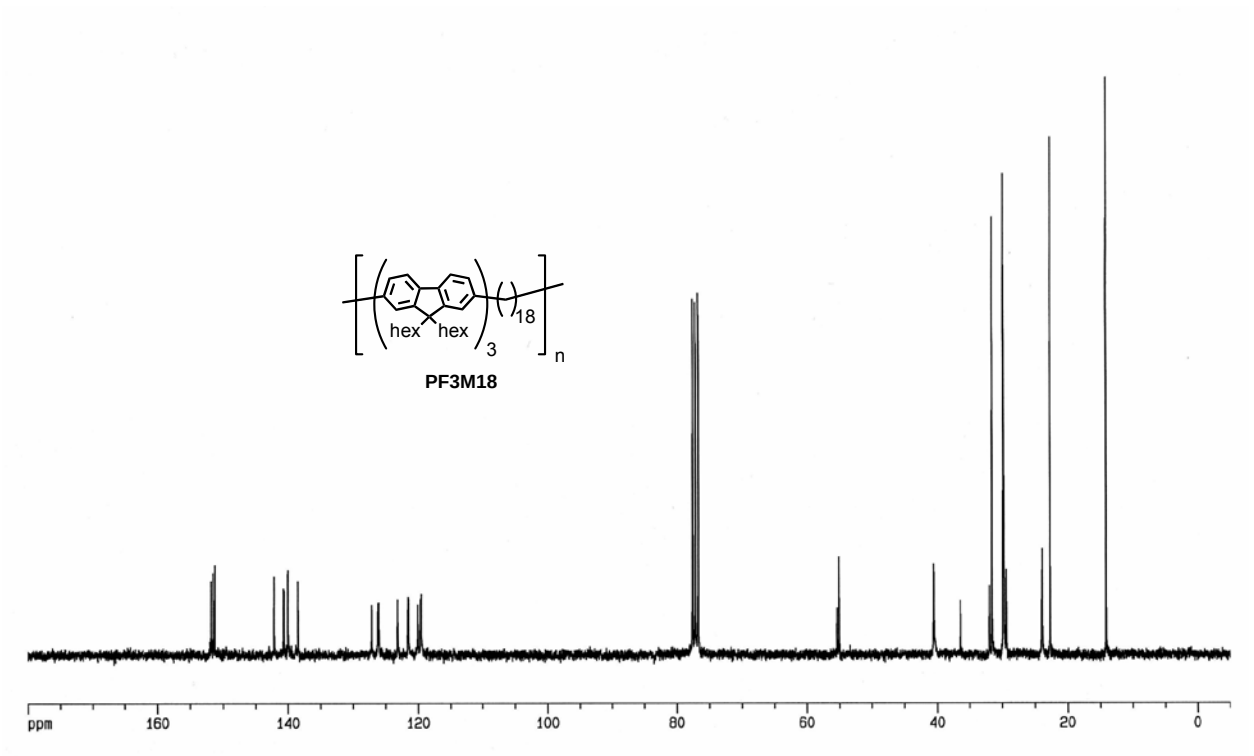

Figure A.7. The ^{13}C NMR spectrum of **PF3M18**

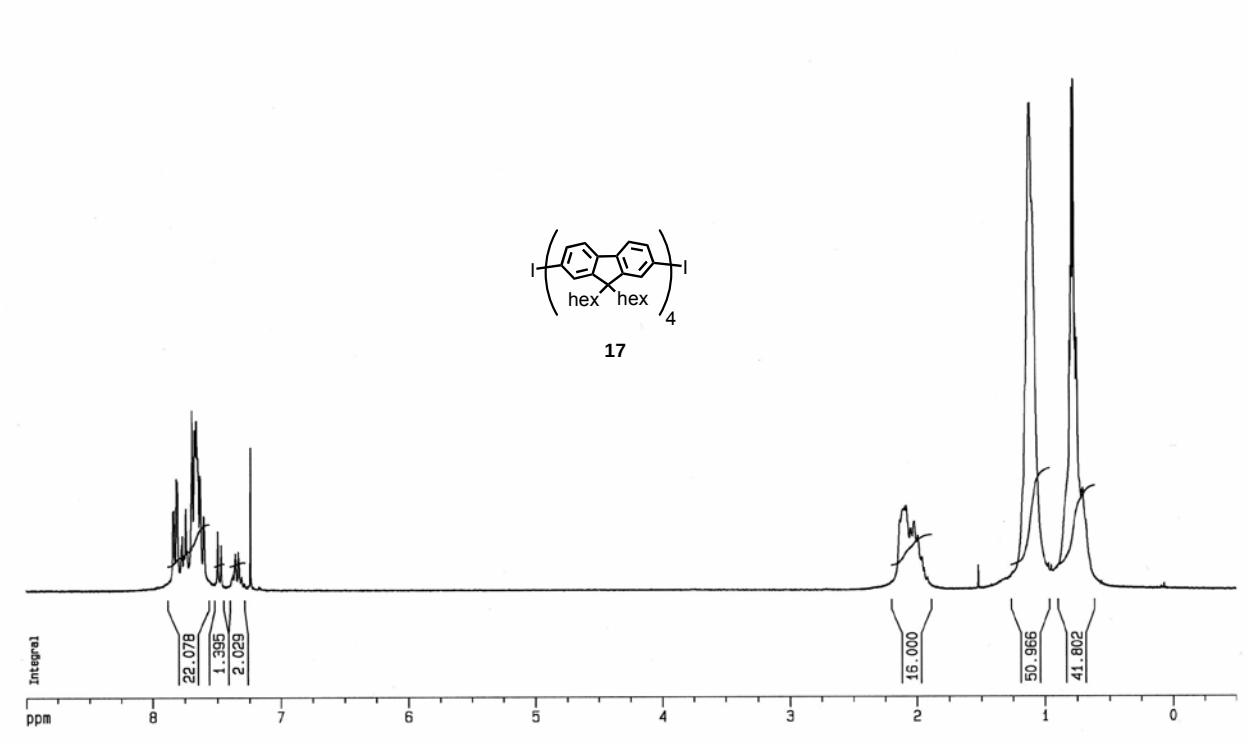

Figure A.8. The ^{1}H NMR spectrum of diiodo quaterfluorene **17**.

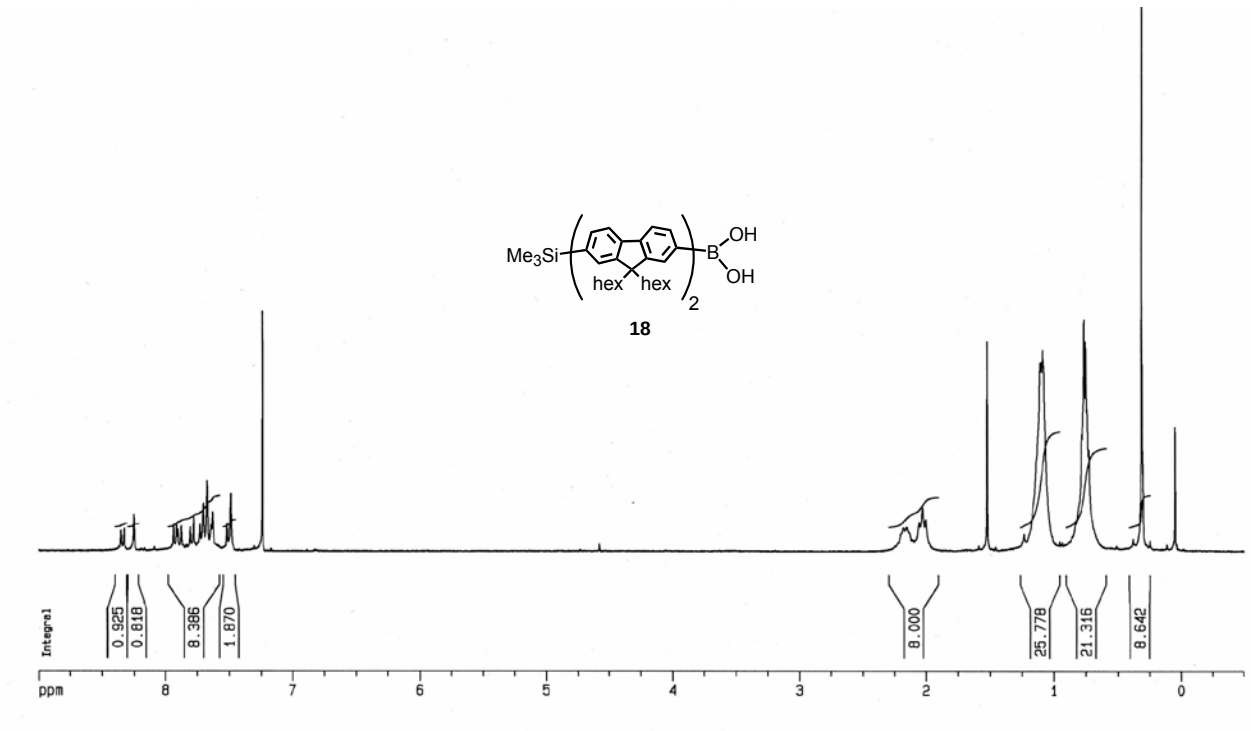

Figure A.9. The ^{1}H NMR spectrum of boronic acid **18**.

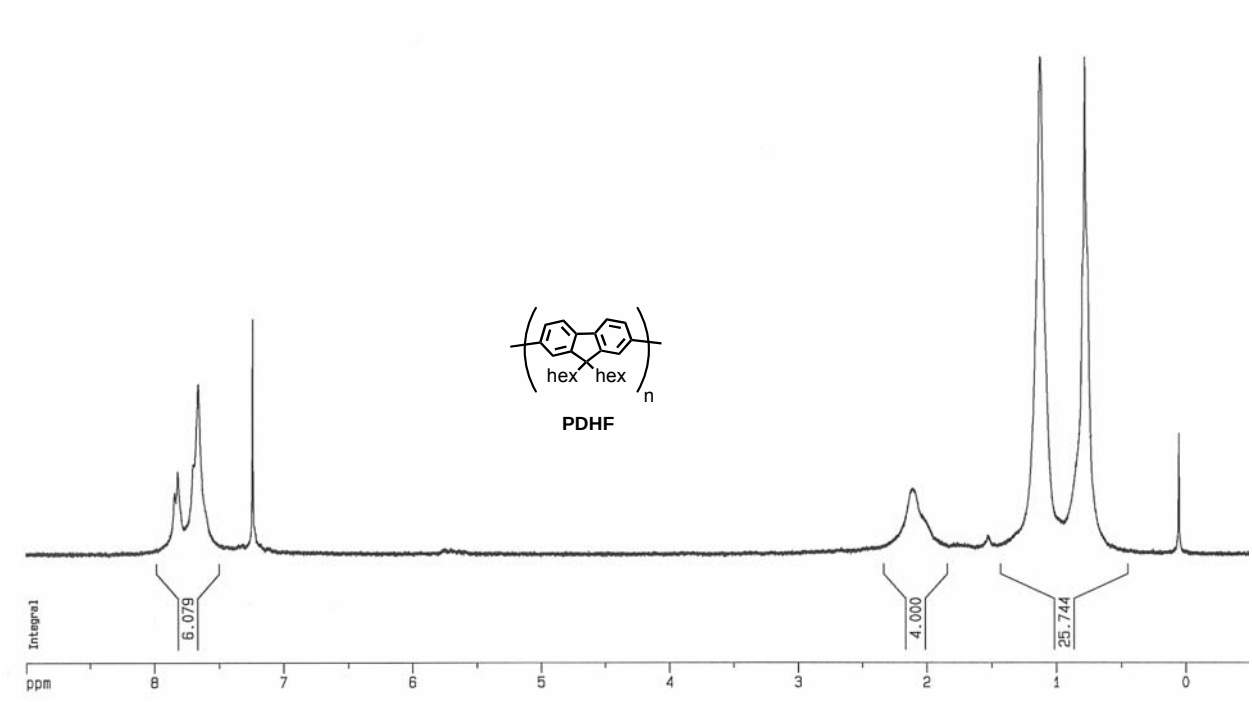

Figure A.10. The ^{1}H NMR spectrum of **PDHF-new**.

APPENDIX B

X-Ray Structure Refinement Data for Bifluorene 10

Table B.1. Crystal data and structure refinement for jc0630s.		
Identification code	jc0630s	
Empirical formula	C56 H82 Si2	
Formula weight	811.40	
Temperature	150(2) K	
Wavelength	0.71073 Å	
Crystal system	Monoclinic	
Space group	P2(1)/c	
Unit cell dimensions	a = 11.7999(8) Å	α= 90°.
	b = 18.8966(13) Å	β= 95.823(2)°.
	c = 24.6741(16) Å	γ = 90°.
Volume	5473.4(6) $Å^3$	
Z	4	
Density (calculated)	0.985 Mg/m^3	
Absorption coefficient	0.096 mm^{-1}	
F(000)	1784	
Crystal size	0.29 x 0.14 x 0.13 mm^3	
Theta range for data collection	1.66 to 25.00°.	
Index ranges	-14<=h<=14, -22<=k<=22, -29<=l<=29	
Reflections collected	43683	
Independent reflections	9625 [R(int) = 0.0640]	
Completeness to theta = 25.00°	99.9 %	
Absorption correction	None	
Max. and min. transmission	0.9876 and 0.9727	
Refinement method	Full-matrix least-squares on F^2	
Data / restraints / parameters	9625 / 0 / 523	
Goodness-of-fit on F^2	1.052	
Final R indices [I>2sigma(I)]	R1 = 0.1010, wR2 = 0.2286	
R indices (all data)	R1 = 0.1792, wR2 = 0.2658	
Largest diff. peak and hole	0.413 and -0.190 $e.Å^{-3}$	

Table B.2. Atomic coordinates (x 10^4) and equivalent isotropic displacement parameters ($Å^2$x 10^3) for jc0630s. U(eq) is defined as one third of the trace of the orthogonalized U^{ij} tensor.

	x	y	z	U(eq)
Si(1)	6989(1)	6438(2)	2535(1)	164(1)
C(1)	2818(4)	6877(3)	3290(2)	96(2)
Si(2)	-6469(1)	7194(1)	5910(1)	98(1)
C(2)	3920(3)	6480(3)	3239(2)	89(1)
C(3)	4820(4)	6667(3)	2943(2)	111(2)
C(4)	5764(4)	6220(4)	2930(2)	116(2)
C(5)	5756(4)	5600(4)	3222(2)	123(2)
C(6)	4871(4)	5388(3)	3519(2)	103(2)
C(7)	3955(3)	5848(3)	3523(2)	83(1)
C(8)	2893(3)	5784(2)	3791(2)	71(1)
C(9)	2504(3)	5253(2)	4109(2)	77(1)
C(10)	1440(3)	5334(2)	4296(2)	73(1)
C(11)	777(3)	5925(2)	4175(1)	63(1)
C(12)	1194(3)	6457(2)	3857(2)	74(1)
C(13)	2248(3)	6380(2)	3666(2)	75(1)
C(14)	-2226(3)	7219(2)	5164(2)	73(1)
C(15)	-1742(3)	6639(2)	4824(2)	63(1)
C(16)	-667(3)	6582(2)	4650(2)	69(1)
C(17)	-368(3)	5990(2)	4369(1)	63(1)
C(18)	-1165(3)	5450(2)	4271(2)	68(1)
C(19)	-2250(3)	5508(2)	4428(2)	69(1)
C(20)	-2542(3)	6101(2)	4705(1)	60(1)
C(21)	-3597(3)	6297(2)	4939(1)	62(1)
C(22)	-4631(3)	5947(2)	4927(2)	72(1)
C(23)	-5466(3)	6243(2)	5205(2)	81(1)
C(24)	-5318(3)	6871(2)	5497(2)	74(1)
C(25)	-4266(3)	7215(2)	5495(2)	79(1)
C(39)	-2254(4)	7935(2)	4876(2)	97(2)
C(26)	-3419(3)	6927(2)	5215(2)	68(1)
C(27)	2105(5)	6962(3)	2744(3)	118(2)
C(28)	1842(5)	6304(4)	2434(2)	119(2)

C(29)	1060(5)	6409(4)	1915(3)	147(2)
C(30)	865(7)	5767(5)	1573(4)	184(3)
C(31)	100(9)	5859(7)	1034(5)	242(5)
C(32)	163(15)	5373(12)	689(6)	458(16)
C(33)	2991(6)	7632(4)	3527(3)	146(2)
C(34)	3536(7)	7676(4)	4040(4)	173(3)
C(35)	3683(12)	8483(8)	4296(7)	254(7)
C(36)	2871(15)	8843(9)	4384(8)	320(8)
C(37)	3172(15)	9608(7)	4755(6)	294(7)
C(38)	3590(16)	10118(8)	4427(6)	333(8)
C(40)	-2855(4)	7952(3)	4311(3)	111(2)
C(41)	-2899(6)	8666(3)	4038(3)	157(3)
C(42)	-3461(7)	8682(4)	3479(4)	190(3)
C(43)	-3590(10)	9422(7)	3246(6)	311(8)
C(44)	-4174(12)	9523(9)	2816(6)	392(11)
C(45)	-1525(3)	7289(3)	5725(2)	92(2)
C(46)	-1410(5)	6637(3)	6070(2)	112(2)
C(47)	-632(5)	6715(4)	6595(3)	135(2)
C(48)	-530(9)	6046(6)	6922(3)	228(5)
C(49)	520(30)	5960(20)	7425(12)	460(20)
C(50)	-12(19)	6244(14)	7726(10)	420(20)
C(51)	6667(6)	7258(8)	2110(3)	331(9)
C(52)	7132(10)	5768(9)	2045(5)	422(12)
C(53)	8243(5)	6650(5)	2981(3)	201(4)
C(54)	-6421(6)	6661(4)	6535(2)	165(3)
C(55)	-6227(5)	8134(3)	6101(3)	136(2)
C(56)	-7883(4)	7080(4)	5507(3)	166(3)

Table B.3. Bond lengths [Å] and angles [°] for jc0630s.

Si(1)-C(52)	1.771(10)
Si(1)-C(53)	1.798(6)
Si(1)-C(4)	1.870(5)
Si(1)-C(51)	1.886(11)
C(1)-C(2)	1.517(6)
C(1)-C(27)	1.523(7)
C(1)-C(13)	1.523(6)
C(1)-C(33)	1.549(8)
Si(2)-C(54)	1.836(6)
Si(2)-C(55)	1.853(6)
Si(2)-C(56)	1.867(5)
Si(2)-C(24)	1.882(4)
C(2)-C(7)	1.383(6)
C(2)-C(3)	1.395(5)
C(3)-C(4)	1.401(7)
C(3)-H(3A)	0.9500
C(4)-C(5)	1.377(8)
C(5)-C(6)	1.393(6)
C(5)-H(5A)	0.9500
C(6)-C(7)	1.388(6)
C(6)-H(6A)	0.9500
C(7)-C(8)	1.480(5)
C(8)-C(13)	1.377(5)
C(8)-C(9)	1.379(5)
C(9)-C(10)	1.390(5)
C(9)-H(9A)	0.9500
C(10)-C(11)	1.380(5)
C(10)-H(10A)	0.9500
C(11)-C(12)	1.396(5)
C(11)-C(17)	1.483(5)
C(12)-C(13)	1.381(5)
C(12)-H(12A)	0.9500
C(14)-C(15)	1.527(5)
C(14)-C(26)	1.528(5)

C(14)-C(39)	1.528(6)
C(14)-C(45)	1.544(6)
C(15)-C(16)	1.383(4)
C(15)-C(20)	1.398(5)
C(16)-C(17)	1.381(5)
C(16)-H(16A)	0.9500
C(17)-C(18)	1.392(5)
C(18)-C(19)	1.379(5)
C(18)-H(18A)	0.9500
C(19)-C(20)	1.376(5)
C(19)-H(19A)	0.9500
C(20)-C(21)	1.472(4)
C(21)-C(26)	1.378(5)
C(21)-C(22)	1.385(5)
C(22)-C(23)	1.376(5)
C(22)-H(22A)	0.9500
C(23)-C(24)	1.388(5)
C(23)-H(23A)	0.9500
C(24)-C(25)	1.402(5)
C(25)-C(26)	1.383(5)
C(25)-H(25A)	0.9500
C(39)-C(40)	1.497(7)
C(39)-H(39A)	0.9900
C(39)-H(39B)	0.9900
C(27)-C(28)	1.477(7)
C(27)-H(27A)	0.9900
C(27)-H(27B)	0.9900
C(28)-C(29)	1.513(8)
C(28)-H(28A)	0.9900
C(28)-H(28B)	0.9900
C(29)-C(30)	1.483(9)
C(29)-H(29A)	0.9900
C(29)-H(29B)	0.9900
C(30)-C(31)	1.538(11)
C(30)-H(30A)	0.9900
C(30)-H(30B)	0.9900

C(31)-C(32)	1.260(14)
C(31)-H(31A)	0.9900
C(31)-H(31B)	0.9900
C(32)-H(32A)	0.9800
C(32)-H(32B)	0.9800
C(32)-H(32C)	0.9800
C(33)-C(34)	1.363(9)
C(33)-H(33A)	0.9900
C(33)-H(33B)	0.9900
C(34)-C(35)	1.654(14)
C(34)-H(34A)	0.9900
C(34)-H(34B)	0.9900
C(35)-C(36)	1.212(17)
C(35)-H(35A)	0.9900
C(35)-H(35B)	0.9900
C(36)-C(37)	1.729(19)
C(36)-H(36A)	0.9900
C(36)-H(36B)	0.9900
C(37)-C(38)	1.382(13)
C(37)-H(37A)	0.9900
C(37)-H(37B)	0.9900
C(38)-H(38A)	0.9800
C(38)-H(38B)	0.9800
C(38)-H(38C)	0.9800
C(40)-C(41)	1.507(7)
C(40)-H(40A)	0.9900
C(40)-H(40B)	0.9900
C(41)-C(42)	1.469(9)
C(41)-H(41A)	0.9900
C(41)-H(41B)	0.9900
C(42)-C(43)	1.513(11)
C(42)-H(42A)	0.9900
C(42)-H(42B)	0.9900
C(43)-C(44)	1.220(14)
C(43)-H(43A)	0.9900
C(43)-H(43B)	0.9900

C(44)-H(44A)	0.9800
C(44)-H(44B)	0.9800
C(44)-H(44C)	0.9800
C(45)-C(46)	1.497(6)
C(45)-H(45A)	0.9900
C(45)-H(45B)	0.9900
C(46)-C(47)	1.516(7)
C(46)-H(46A)	0.9900
C(46)-H(46B)	0.9900
C(47)-C(48)	1.498(10)
C(47)-H(47A)	0.9900
C(47)-H(47B)	0.9900
C(48)-C(49)	1.67(4)
C(48)-H(48A)	0.9900
C(48)-H(48B)	0.9900
C(49)-C(50)	1.15(5)
C(49)-H(49A)	0.9900
C(49)-H(49B)	0.9900
C(50)-H(50A)	0.9800
C(50)-H(50B)	0.9800
C(50)-H(50C)	0.9800
C(51)-H(51A)	0.9800
C(51)-H(51B)	0.9800
C(51)-H(51C)	0.9800
C(52)-H(52A)	0.9800
C(52)-H(52B)	0.9800
C(52)-H(52C)	0.9800
C(53)-H(53A)	0.9800
C(53)-H(53B)	0.9800
C(53)-H(53C)	0.9800
C(54)-H(54A)	0.9800
C(54)-H(54B)	0.9800
C(54)-H(54C)	0.9800
C(55)-H(55A)	0.9800
C(55)-H(55B)	0.9800
C(55)-H(55C)	0.9800

C(56)-H(56A)	0.9800
C(56)-H(56B)	0.9800
C(56)-H(56C)	0.9800

C(52)-Si(1)-C(53)	116.6(6)
C(52)-Si(1)-C(4)	109.3(4)
C(53)-Si(1)-C(4)	111.2(3)
C(52)-Si(1)-C(51)	103.7(7)
C(53)-Si(1)-C(51)	105.3(4)
C(4)-Si(1)-C(51)	110.4(3)
C(2)-C(1)-C(27)	112.4(4)
C(2)-C(1)-C(13)	100.4(4)
C(27)-C(1)-C(13)	111.5(4)
C(2)-C(1)-C(33)	113.8(4)
C(27)-C(1)-C(33)	106.1(5)
C(13)-C(1)-C(33)	112.8(4)
C(54)-Si(2)-C(55)	108.8(3)
C(54)-Si(2)-C(56)	109.5(3)
C(55)-Si(2)-C(56)	110.6(3)
C(54)-Si(2)-C(24)	108.3(2)
C(55)-Si(2)-C(24)	110.4(2)
C(56)-Si(2)-C(24)	109.2(2)
C(7)-C(2)-C(3)	119.9(4)
C(7)-C(2)-C(1)	111.5(3)
C(3)-C(2)-C(1)	128.5(5)
C(2)-C(3)-C(4)	120.6(5)
C(2)-C(3)-H(3A)	119.7
C(4)-C(3)-H(3A)	119.7
C(5)-C(4)-C(3)	117.0(4)
C(5)-C(4)-Si(1)	120.5(5)
C(3)-C(4)-Si(1)	122.5(5)
C(4)-C(5)-C(6)	124.4(5)
C(4)-C(5)-H(5A)	117.8
C(6)-C(5)-H(5A)	117.8
C(7)-C(6)-C(5)	116.7(5)
C(7)-C(6)-H(6A)	121.6

C(5)-C(6)-H(6A)	121.6
C(2)-C(7)-C(6)	121.4(4)
C(2)-C(7)-C(8)	108.3(4)
C(6)-C(7)-C(8)	130.3(5)
C(13)-C(8)-C(9)	120.9(3)
C(13)-C(8)-C(7)	107.9(4)
C(9)-C(8)-C(7)	131.2(4)
C(8)-C(9)-C(10)	118.3(4)
C(8)-C(9)-H(9A)	120.9
C(10)-C(9)-H(9A)	120.9
C(11)-C(10)-C(9)	121.9(4)
C(11)-C(10)-H(10A)	119.1
C(9)-C(10)-H(10A)	119.1
C(10)-C(11)-C(12)	118.7(3)
C(10)-C(11)-C(17)	120.8(3)
C(12)-C(11)-C(17)	120.5(3)
C(13)-C(12)-C(11)	119.8(4)
C(13)-C(12)-H(12A)	120.1
C(11)-C(12)-H(12A)	120.1
C(8)-C(13)-C(12)	120.4(4)
C(8)-C(13)-C(1)	111.8(3)
C(12)-C(13)-C(1)	127.7(4)
C(15)-C(14)-C(26)	100.7(3)
C(15)-C(14)-C(39)	111.8(3)
C(26)-C(14)-C(39)	112.4(3)
C(15)-C(14)-C(45)	111.0(3)
C(26)-C(14)-C(45)	111.8(3)
C(39)-C(14)-C(45)	109.0(4)
C(16)-C(15)-C(20)	120.0(3)
C(16)-C(15)-C(14)	129.2(3)
C(20)-C(15)-C(14)	110.8(3)
C(17)-C(16)-C(15)	120.5(3)
C(17)-C(16)-H(16A)	119.7
C(15)-C(16)-H(16A)	119.7
C(16)-C(17)-C(18)	118.6(3)
C(16)-C(17)-C(11)	121.1(3)

C(18)-C(17)-C(11)	120.3(3)
C(19)-C(18)-C(17)	121.6(3)
C(19)-C(18)-H(18A)	119.2
C(17)-C(18)-H(18A)	119.2
C(20)-C(19)-C(18)	119.3(3)
C(20)-C(19)-H(19A)	120.3
C(18)-C(19)-H(19A)	120.3
C(19)-C(20)-C(15)	119.9(3)
C(19)-C(20)-C(21)	131.6(3)
C(15)-C(20)-C(21)	108.4(3)
C(26)-C(21)-C(22)	120.9(3)
C(26)-C(21)-C(20)	108.6(3)
C(22)-C(21)-C(20)	130.5(3)
C(23)-C(22)-C(21)	118.0(4)
C(23)-C(22)-H(22A)	121.0
C(21)-C(22)-H(22A)	121.0
C(22)-C(23)-C(24)	123.1(3)
C(22)-C(23)-H(23A)	118.4
C(24)-C(23)-H(23A)	118.4
C(23)-C(24)-C(25)	117.4(3)
C(23)-C(24)-Si(2)	119.9(3)
C(25)-C(24)-Si(2)	122.6(3)
C(26)-C(25)-C(24)	120.3(4)
C(26)-C(25)-H(25A)	119.9
C(24)-C(25)-H(25A)	119.9
C(40)-C(39)-C(14)	116.0(4)
C(40)-C(39)-H(39A)	108.3
C(14)-C(39)-H(39A)	108.3
C(40)-C(39)-H(39B)	108.3
C(14)-C(39)-H(39B)	108.3
H(39A)-C(39)-H(39B)	107.4
C(21)-C(26)-C(25)	120.3(3)
C(21)-C(26)-C(14)	111.5(3)
C(25)-C(26)-C(14)	128.2(3)
C(28)-C(27)-C(1)	115.9(5)
C(28)-C(27)-H(27A)	108.3

C(1)-C(27)-H(27A)	108.3
C(28)-C(27)-H(27B)	108.3
C(1)-C(27)-H(27B)	108.3
H(27A)-C(27)-H(27B)	107.4
C(27)-C(28)-C(29)	113.9(6)
C(27)-C(28)-H(28A)	108.8
C(29)-C(28)-H(28A)	108.8
C(27)-C(28)-H(28B)	108.8
C(29)-C(28)-H(28B)	108.8
H(28A)-C(28)-H(28B)	107.7
C(30)-C(29)-C(28)	114.8(7)
C(30)-C(29)-H(29A)	108.6
C(28)-C(29)-H(29A)	108.6
C(30)-C(29)-H(29B)	108.6
C(28)-C(29)-H(29B)	108.6
H(29A)-C(29)-H(29B)	107.5
C(29)-C(30)-C(31)	116.3(8)
C(29)-C(30)-H(30A)	108.2
C(31)-C(30)-H(30A)	108.2
C(29)-C(30)-H(30B)	108.2
C(31)-C(30)-H(30B)	108.2
H(30A)-C(30)-H(30B)	107.4
C(32)-C(31)-C(30)	115.7(13)
C(32)-C(31)-H(31A)	108.4
C(30)-C(31)-H(31A)	108.4
C(32)-C(31)-H(31B)	108.4
C(30)-C(31)-H(31B)	108.4
H(31A)-C(31)-H(31B)	107.4
C(31)-C(32)-H(32A)	109.5
C(31)-C(32)-H(32B)	109.5
H(32A)-C(32)-H(32B)	109.5
C(31)-C(32)-H(32C)	109.5
H(32A)-C(32)-H(32C)	109.5
H(32B)-C(32)-H(32C)	109.5
C(34)-C(33)-C(1)	116.1(7)
C(34)-C(33)-H(33A)	108.3

C(1)-C(33)-H(33A)	108.3
C(34)-C(33)-H(33B)	108.3
C(1)-C(33)-H(33B)	108.3
H(33A)-C(33)-H(33B)	107.4
C(33)-C(34)-C(35)	115.7(9)
C(33)-C(34)-H(34A)	108.4
C(35)-C(34)-H(34A)	108.4
C(33)-C(34)-H(34B)	108.4
C(35)-C(34)-H(34B)	108.4
H(34A)-C(34)-H(34B)	107.4
C(36)-C(35)-C(34)	122.1(17)
C(36)-C(35)-H(35A)	106.8
C(34)-C(35)-H(35A)	106.8
C(36)-C(35)-H(35B)	106.8
C(34)-C(35)-H(35B)	106.8
H(35A)-C(35)-H(35B)	106.7
C(35)-C(36)-C(37)	116.1(18)
C(35)-C(36)-H(36A)	108.3
C(37)-C(36)-H(36A)	108.3
C(35)-C(36)-H(36B)	108.3
C(37)-C(36)-H(36B)	108.3
H(36A)-C(36)-H(36B)	107.4
C(38)-C(37)-C(36)	109.8(13)
C(38)-C(37)-H(37A)	109.7
C(36)-C(37)-H(37A)	109.7
C(38)-C(37)-H(37B)	109.7
C(36)-C(37)-H(37B)	109.7
H(37A)-C(37)-H(37B)	108.2
C(37)-C(38)-H(38A)	109.5
C(37)-C(38)-H(38B)	109.5
H(38A)-C(38)-H(38B)	109.5
C(37)-C(38)-H(38C)	109.5
H(38A)-C(38)-H(38C)	109.5
H(38B)-C(38)-H(38C)	109.5
C(39)-C(40)-C(41)	115.3(5)
C(39)-C(40)-H(40A)	108.4

C(41)-C(40)-H(40A)	108.4
C(39)-C(40)-H(40B)	108.4
C(41)-C(40)-H(40B)	108.4
H(40A)-C(40)-H(40B)	107.5
C(42)-C(41)-C(40)	115.6(6)
C(42)-C(41)-H(41A)	108.4
C(40)-C(41)-H(41A)	108.4
C(42)-C(41)-H(41B)	108.4
C(40)-C(41)-H(41B)	108.4
H(41A)-C(41)-H(41B)	107.4
C(41)-C(42)-C(43)	113.2(9)
C(41)-C(42)-H(42A)	108.9
C(43)-C(42)-H(42A)	108.9
C(41)-C(42)-H(42B)	108.9
C(43)-C(42)-H(42B)	108.9
H(42A)-C(42)-H(42B)	107.7
C(44)-C(43)-C(42)	120.1(15)
C(44)-C(43)-H(43A)	107.3
C(42)-C(43)-H(43A)	107.3
C(44)-C(43)-H(43B)	107.3
C(42)-C(43)-H(43B)	107.3
H(43A)-C(43)-H(43B)	106.9
C(43)-C(44)-H(44A)	109.5
C(43)-C(44)-H(44B)	109.5
H(44A)-C(44)-H(44B)	109.5
C(43)-C(44)-H(44C)	109.5
H(44A)-C(44)-H(44C)	109.5
H(44B)-C(44)-H(44C)	109.5
C(46)-C(45)-C(14)	116.7(4)
C(46)-C(45)-H(45A)	108.1
C(14)-C(45)-H(45A)	108.1
C(46)-C(45)-H(45B)	108.1
C(14)-C(45)-H(45B)	108.1
H(45A)-C(45)-H(45B)	107.3
C(45)-C(46)-C(47)	114.7(5)
C(45)-C(46)-H(46A)	108.6

C(47)-C(46)-H(46A)	108.6
C(45)-C(46)-H(46B)	108.6
C(47)-C(46)-H(46B)	108.6
H(46A)-C(46)-H(46B)	107.6
C(48)-C(47)-C(46)	112.8(6)
C(48)-C(47)-H(47A)	109.0
C(46)-C(47)-H(47A)	109.0
C(48)-C(47)-H(47B)	109.0
C(46)-C(47)-H(47B)	109.0
H(47A)-C(47)-H(47B)	107.8
C(47)-C(48)-C(49)	119.5(16)
C(47)-C(48)-H(48A)	107.5
C(49)-C(48)-H(48A)	107.5
C(47)-C(48)-H(48B)	107.5
C(49)-C(48)-H(48B)	107.5
H(48A)-C(48)-H(48B)	107.0
C(50)-C(49)-C(48)	91(3)
C(50)-C(49)-H(49A)	113.5
C(48)-C(49)-H(49A)	113.5
C(50)-C(49)-H(49B)	113.5
C(48)-C(49)-H(49B)	113.5
H(49A)-C(49)-H(49B)	110.8
C(49)-C(50)-H(50A)	109.5
C(49)-C(50)-H(50B)	109.5
H(50A)-C(50)-H(50B)	109.5
C(49)-C(50)-H(50C)	109.5
H(50A)-C(50)-H(50C)	109.5
H(50B)-C(50)-H(50C)	109.5
Si(1)-C(51)-H(51A)	109.5
Si(1)-C(51)-H(51B)	109.5
H(51A)-C(51)-H(51B)	109.5
Si(1)-C(51)-H(51C)	109.5
H(51A)-C(51)-H(51C)	109.5
H(51B)-C(51)-H(51C)	109.5
Si(1)-C(52)-H(52A)	109.5
Si(1)-C(52)-H(52B)	109.5

H(52A)-C(52)-H(52B)	109.5
Si(1)-C(52)-H(52C)	109.5
H(52A)-C(52)-H(52C)	109.5
H(52B)-C(52)-H(52C)	109.5
Si(1)-C(53)-H(53A)	109.5
Si(1)-C(53)-H(53B)	109.5
H(53A)-C(53)-H(53B)	109.5
Si(1)-C(53)-H(53C)	109.5
H(53A)-C(53)-H(53C)	109.5
H(53B)-C(53)-H(53C)	109.5
Si(2)-C(54)-H(54A)	109.5
Si(2)-C(54)-H(54B)	109.5
H(54A)-C(54)-H(54B)	109.5
Si(2)-C(54)-H(54C)	109.5
H(54A)-C(54)-H(54C)	109.5
H(54B)-C(54)-H(54C)	109.5
Si(2)-C(55)-H(55A)	109.5
Si(2)-C(55)-H(55B)	109.5
H(55A)-C(55)-H(55B)	109.5
Si(2)-C(55)-H(55C)	109.5
H(55A)-C(55)-H(55C)	109.5
H(55B)-C(55)-H(55C)	109.5
Si(2)-C(56)-H(56A)	109.5
Si(2)-C(56)-H(56B)	109.5
H(56A)-C(56)-H(56B)	109.5
Si(2)-C(56)-H(56C)	109.5
H(56A)-C(56)-H(56C)	109.5
H(56B)-C(56)-H(56C)	109.5

Symmetry transformations used to generate equivalent atoms:

Table B.4. Anisotropic displacement parameters ($Å^2 x\ 10^3$) for jc0630s. The anisotropic displacement factor exponent takes the form: $-2\pi^2[\ h^2\ a^{*2}U^{11} + ...\ + 2\ h\ k\ a^*\ b^*\ U^{12}\ ]$

	U^{11}	U^{22}	U^{33}	U^{23}	U^{13}	U^{12}
Si(1)	68(1)	326(3)	106(1)	-25(2)	46(1)	-31(1)
C(1)	76(3)	93(4)	128(4)	3(3)	53(3)	-8(3)
Si(2)	57(1)	138(1)	106(1)	-25(1)	33(1)	2(1)
C(2)	60(3)	119(4)	93(3)	-3(3)	33(2)	-12(2)
C(3)	70(3)	168(5)	99(4)	-3(3)	36(3)	-21(3)
C(4)	58(3)	213(7)	83(4)	-17(4)	30(3)	-18(4)
C(5)	57(3)	220(7)	96(4)	-19(4)	32(3)	23(4)
C(6)	65(3)	150(4)	96(3)	-8(3)	24(2)	20(3)
C(7)	54(2)	120(4)	77(3)	-12(3)	20(2)	1(2)
C(8)	52(2)	90(3)	74(3)	-6(2)	18(2)	2(2)
C(9)	64(2)	86(3)	83(3)	6(2)	16(2)	14(2)
C(10)	59(2)	86(3)	79(3)	9(2)	26(2)	0(2)
C(11)	51(2)	74(3)	66(2)	0(2)	17(2)	4(2)
C(12)	63(2)	71(3)	92(3)	1(2)	30(2)	5(2)
C(13)	59(2)	81(3)	91(3)	0(2)	33(2)	4(2)
C(14)	51(2)	69(3)	101(3)	-24(2)	26(2)	-9(2)
C(15)	48(2)	69(2)	74(2)	-7(2)	15(2)	-6(2)
C(16)	49(2)	75(3)	86(3)	-3(2)	21(2)	-10(2)
C(17)	55(2)	68(2)	68(2)	1(2)	23(2)	1(2)
C(18)	64(2)	69(2)	77(3)	-10(2)	29(2)	-5(2)
C(19)	57(2)	77(3)	75(3)	-7(2)	23(2)	-14(2)
C(20)	48(2)	69(2)	64(2)	-5(2)	15(2)	-4(2)
C(21)	48(2)	73(3)	66(2)	-5(2)	16(2)	-7(2)
C(22)	58(2)	80(3)	80(3)	-15(2)	20(2)	-18(2)
C(23)	50(2)	110(3)	87(3)	-19(3)	26(2)	-23(2)
C(24)	46(2)	104(3)	74(3)	-14(2)	16(2)	-2(2)
C(25)	55(2)	88(3)	97(3)	-28(2)	25(2)	-9(2)
C(39)	70(3)	79(3)	147(5)	-18(3)	36(3)	-8(2)
C(26)	49(2)	75(3)	83(3)	-11(2)	18(2)	-6(2)
C(27)	96(4)	127(5)	141(5)	50(4)	56(4)	15(3)
C(28)	95(4)	156(6)	107(4)	38(4)	20(3)	22(4)

C(29)	95(4)	211(8)	139(6)	47(5)	34(4)	21(5)
C(30)	163(7)	221(9)	163(8)	27(7)	-7(6)	22(7)
C(31)	179(9)	350(16)	189(10)	20(10)	-20(8)	71(10)
C(32)	400(20)	670(40)	279(17)	-230(20)	-93(15)	230(20)
C(33)	135(6)	136(6)	178(7)	22(5)	72(5)	-38(4)
C(34)	182(8)	149(7)	192(8)	0(6)	40(7)	-68(6)
C(35)	258(16)	197(13)	328(15)	-47(11)	131(14)	-29(10)
C(36)	330(20)	280(20)	350(20)	-23(16)	-6(18)	-52(16)
C(37)	420(20)	203(12)	268(16)	-26(11)	69(14)	-8(13)
C(38)	470(20)	267(16)	269(16)	18(12)	86(15)	-23(16)
C(40)	91(4)	98(4)	148(5)	17(3)	29(4)	3(3)
C(41)	135(5)	117(5)	224(8)	50(6)	42(5)	-1(4)
C(42)	198(8)	172(7)	202(8)	92(7)	33(7)	14(6)
C(43)	238(12)	296(14)	375(18)	209(14)	-83(11)	-62(10)
C(44)	294(17)	440(20)	420(20)	274(19)	-78(15)	9(14)
C(45)	54(2)	110(4)	113(4)	-49(3)	18(2)	-16(2)
C(46)	104(4)	126(5)	105(4)	-29(4)	10(3)	-10(3)
C(47)	97(4)	198(7)	109(5)	-30(5)	-1(3)	-5(4)
C(48)	281(12)	268(12)	116(6)	12(7)	-63(7)	-28(9)
C(49)	560(50)	500(40)	310(20)	-70(20)	10(30)	-80(40)
C(50)	310(20)	390(30)	510(40)	110(30)	-200(30)	-140(20)
C(51)	118(6)	730(30)	153(7)	217(12)	33(5)	-30(10)
C(52)	310(14)	610(30)	398(17)	-304(18)	281(14)	-192(16)
C(53)	80(4)	385(12)	137(5)	60(6)	11(4)	-54(5)
C(54)	176(6)	196(7)	138(5)	13(5)	91(5)	30(5)
C(55)	104(4)	142(5)	171(5)	-40(4)	50(4)	17(3)
C(56)	54(3)	265(8)	182(6)	-73(6)	26(3)	1(4)

Table B.5. Hydrogen coordinates (x 10^4) and isotropic displacement parameters ($Å^2$x 10^3) for jc0630s.

	x	y	z	U(eq)
H(3A)	4792	7101	2748	133
H(5A)	6396	5295	3221	147
H(6A)	4894	4950	3709	123
H(9A)	2952	4844	4197	93
H(10A)	1162	4971	4514	88
H(12A)	755	6871	3772	89
H(16A)	-131	6953	4725	83
H(18A)	-957	5033	4090	82
H(19A)	-2791	5141	4345	82
H(22A)	-4759	5516	4733	86
H(23A)	-6178	6007	5197	97
H(25A)	-4135	7647	5687	95
H(39A)	-2626	8282	5101	117
H(39B)	-1460	8095	4858	117
H(27A)	1378	7193	2808	142
H(27B)	2513	7286	2515	142
H(28A)	1483	5964	2669	143
H(28B)	2564	6091	2340	143
H(29A)	315	6582	2013	176
H(29B)	1386	6783	1696	176
H(30A)	522	5399	1791	221
H(30B)	1614	5587	1487	221
H(31A)	-700	5894	1119	290
H(31B)	299	6312	867	290
H(32A)	-363	5475	365	687
H(32B)	-42	4921	846	687
H(32C)	943	5347	586	687
H(33A)	3430	7910	3280	175
H(33B)	2235	7858	3527	175
H(34A)	4303	7464	4038	207

H(34B)	3111	7387	4286	207
H(35A)	4170	8442	4646	305
H(35B)	4122	8759	4048	305
H(36A)	2351	8549	4581	384
H(36B)	2455	8975	4030	384
H(37A)	2472	9784	4900	353
H(37B)	3743	9506	5068	353
H(38A)	3757	10551	4639	499
H(38B)	3020	10220	4120	499
H(38C)	4289	9945	4289	499
H(40A)	-3645	7783	4327	133
H(40B)	-2472	7615	4082	133
H(41A)	-3301	8999	4262	188
H(41B)	-2110	8841	4032	188
H(42A)	-4225	8464	3475	228
H(42B)	-3013	8393	3242	228
H(43A)	-3900	9723	3524	373
H(43B)	-2816	9600	3202	373
H(44A)	-4167	10028	2726	588
H(44B)	-4958	9372	2850	588
H(44C)	-3866	9251	2526	588
H(45A)	-751	7453	5664	110
H(45B)	-1877	7663	5933	110
H(46A)	-1117	6249	5854	134
H(46B)	-2176	6496	6162	134
H(47A)	134	6859	6507	162
H(47B)	-930	7095	6818	162
H(48A)	-460	5649	6665	273
H(48B)	-1257	5978	7084	273
H(49A)	706	5465	7524	552
H(49B)	1223	6225	7358	552
H(50A)	435	6286	8081	628
H(50B)	-702	5968	7764	628
H(50C)	-225	6716	7587	628
H(51A)	7315	7366	1906	497
H(51B)	6530	7656	2349	497

H(51C)	5987	7176	1855	497
H(52A)	7307	5316	2231	634
H(52B)	7751	5892	1826	634
H(52C)	6418	5723	1808	634
H(53A)	8455	6243	3216	301
H(53B)	8087	7059	3207	301
H(53C)	8869	6764	2764	301
H(54A)	-7018	6821	6755	247
H(54B)	-5675	6716	6744	247
H(54C)	-6545	6162	6438	247
H(55A)	-6834	8296	6314	205
H(55B)	-6230	8422	5770	205
H(55C)	-5489	8182	6319	205
H(56A)	-8485	7248	5721	249
H(56B)	-8006	6579	5419	249
H(56C)	-7900	7355	5169	249

APPENDIX C

GPC Traces of PFMs

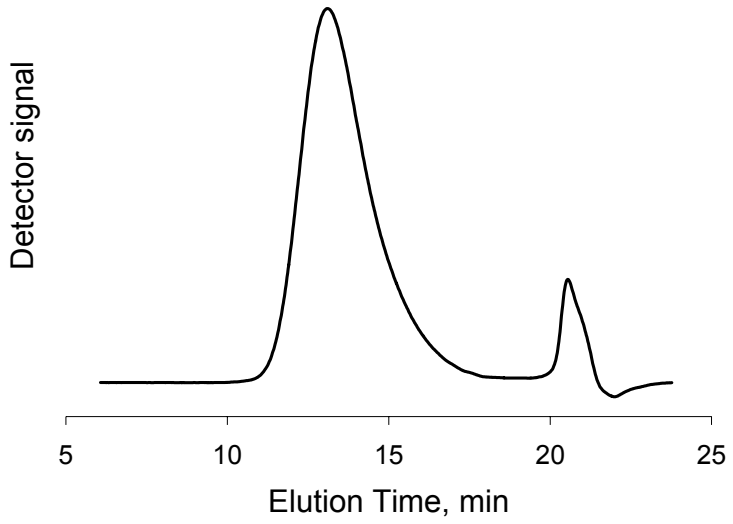

Figure C.1. GPC trace of **PF1M10**.

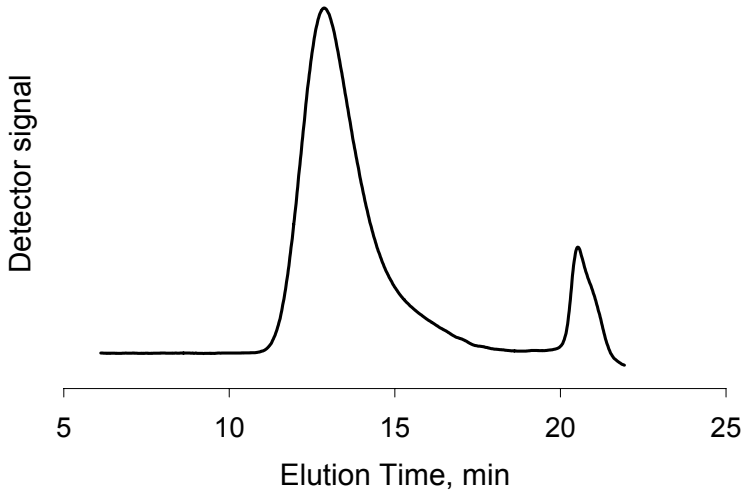

Figure C.2. GPC trace of **PF1M18**.

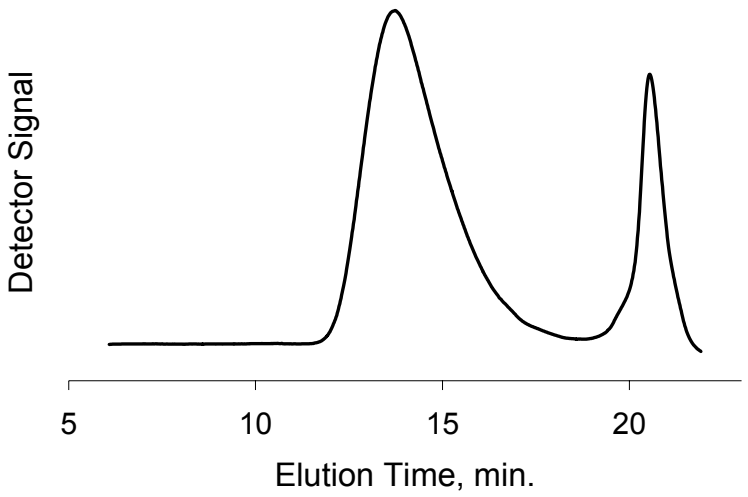

Figure C.3. GPC trace of **PF2M10**.

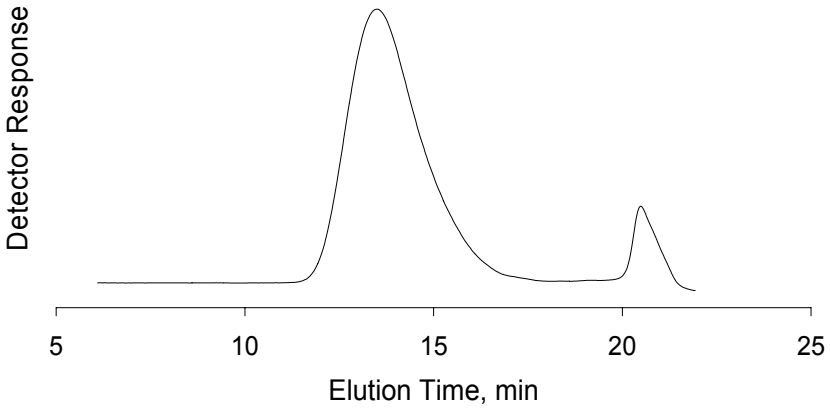

Figure C.4. GPC trace of **PF2M18**.

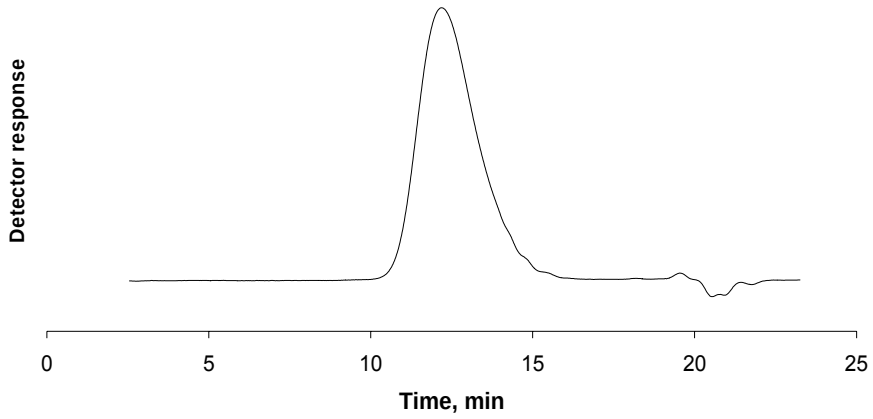

Figure C.5. GPC trace of **PF3M10**.

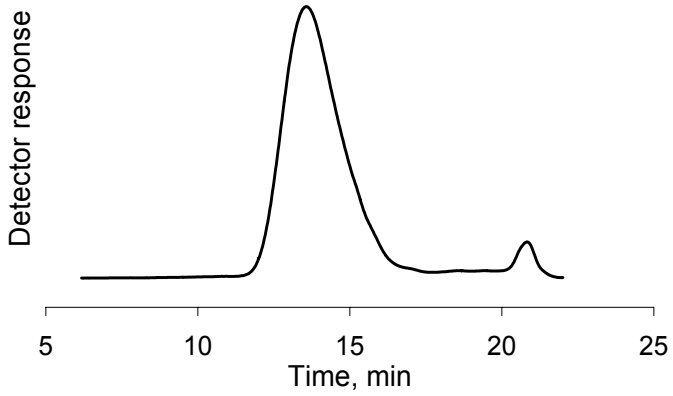

Figure C.6. GPC trace of **PF3M18**.

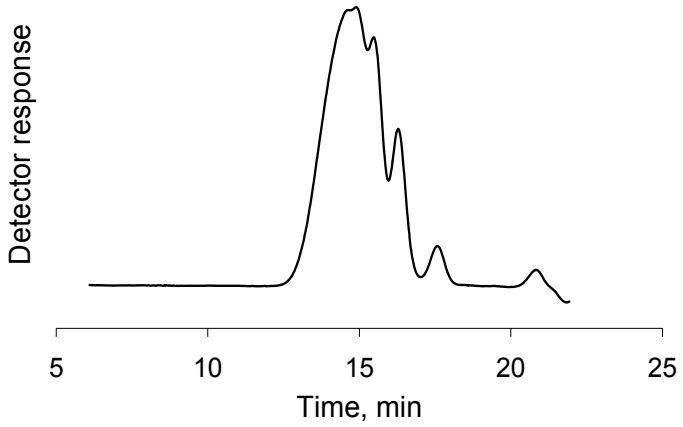

Figure C.7. GPC trace of **PF4M10**.

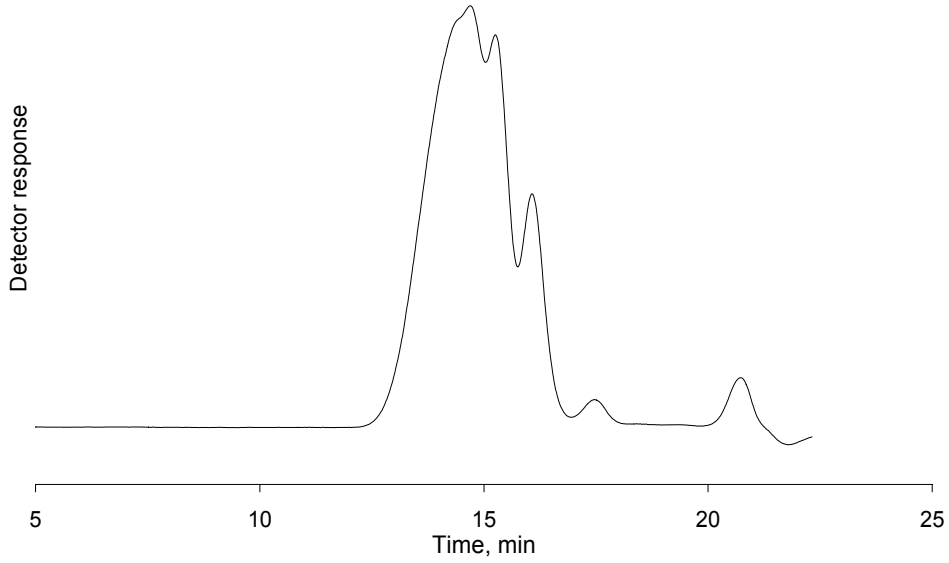

Figure C.8. GPC trace of **PF4M18**.

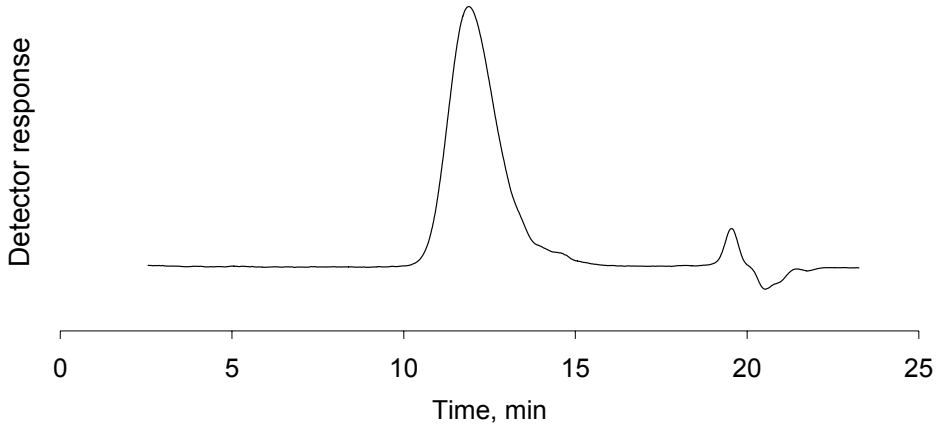

Figure C.9. The GPC trace of **PF7M18**.

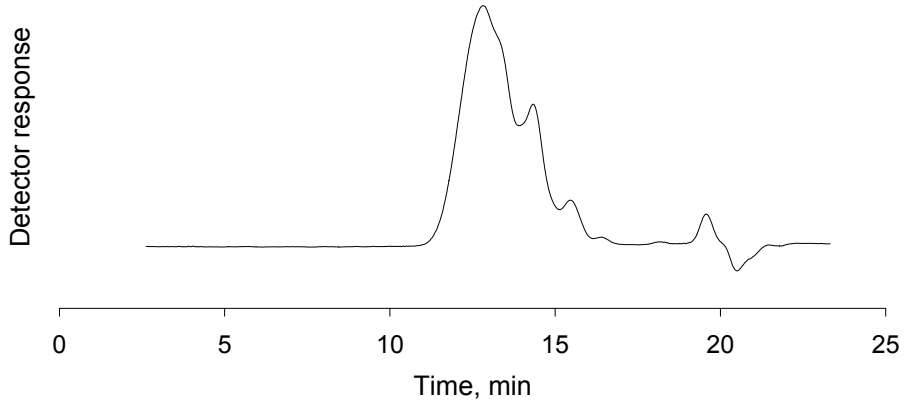

Figure C.10. The GPC trace of **PF8M18**.

APPENDIX D

UV-Induced Degradation Monitored by PL Spectroscopy

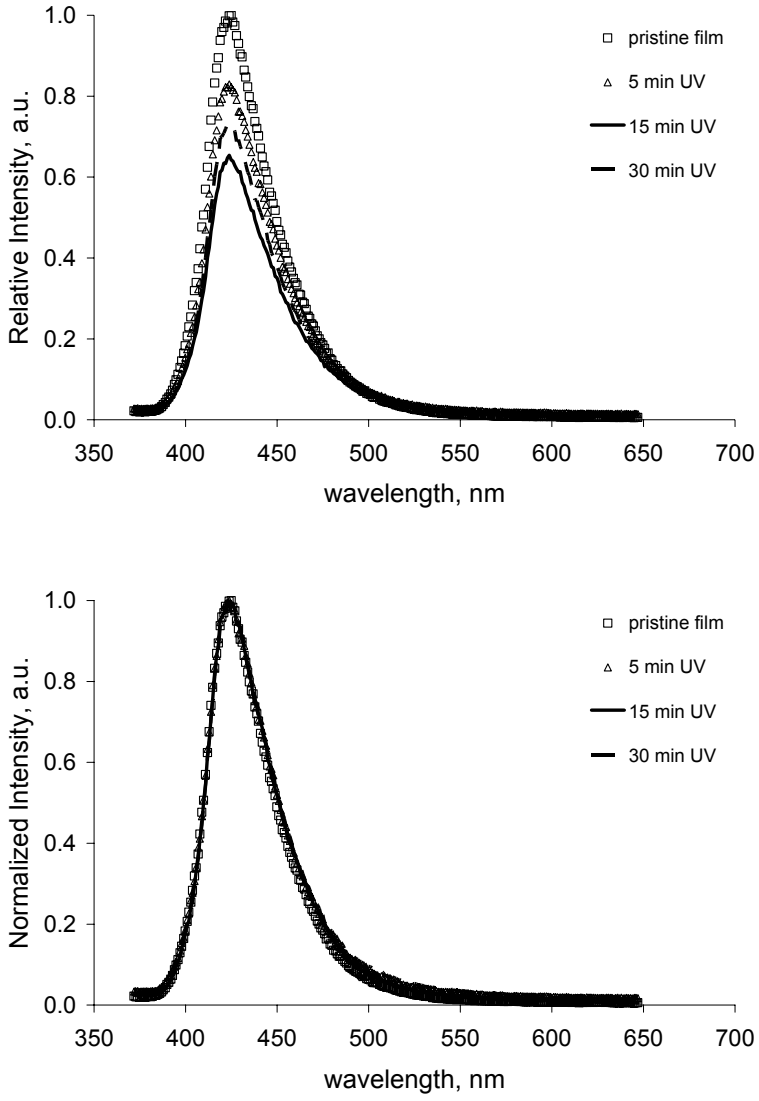

Figure D.1. PL spectra of relative (top, λ_{max} for pristine film = 1) and normalized (bottom, λ_{max} for all spectra = 1) intensities for a film of **PF3M10** irradiated by UV (λ = 366 nm) light.

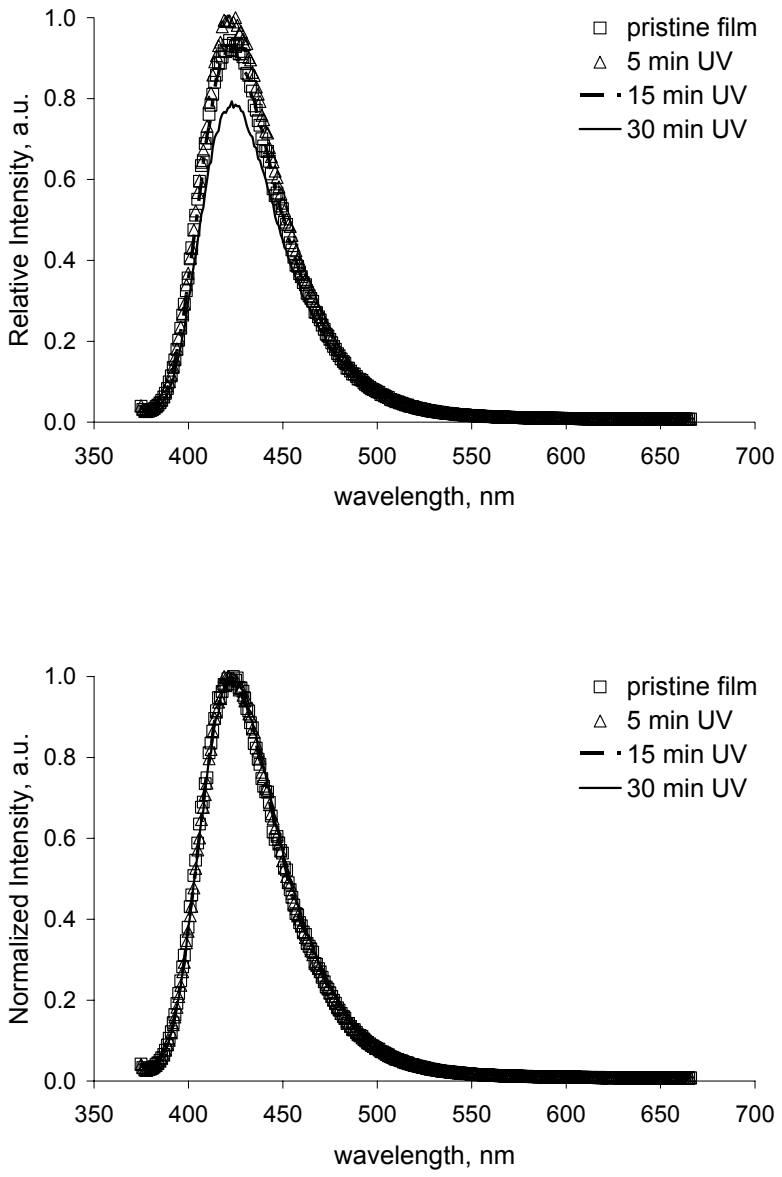

Figure D.2. PL spectra of relative (top, λ_{max} for pristine film = 1) and normalized (bottom, λ_{max} for all spectra = 1) intensities for a film of **PF3M18** irradiated by UV (λ = 366 nm) light.

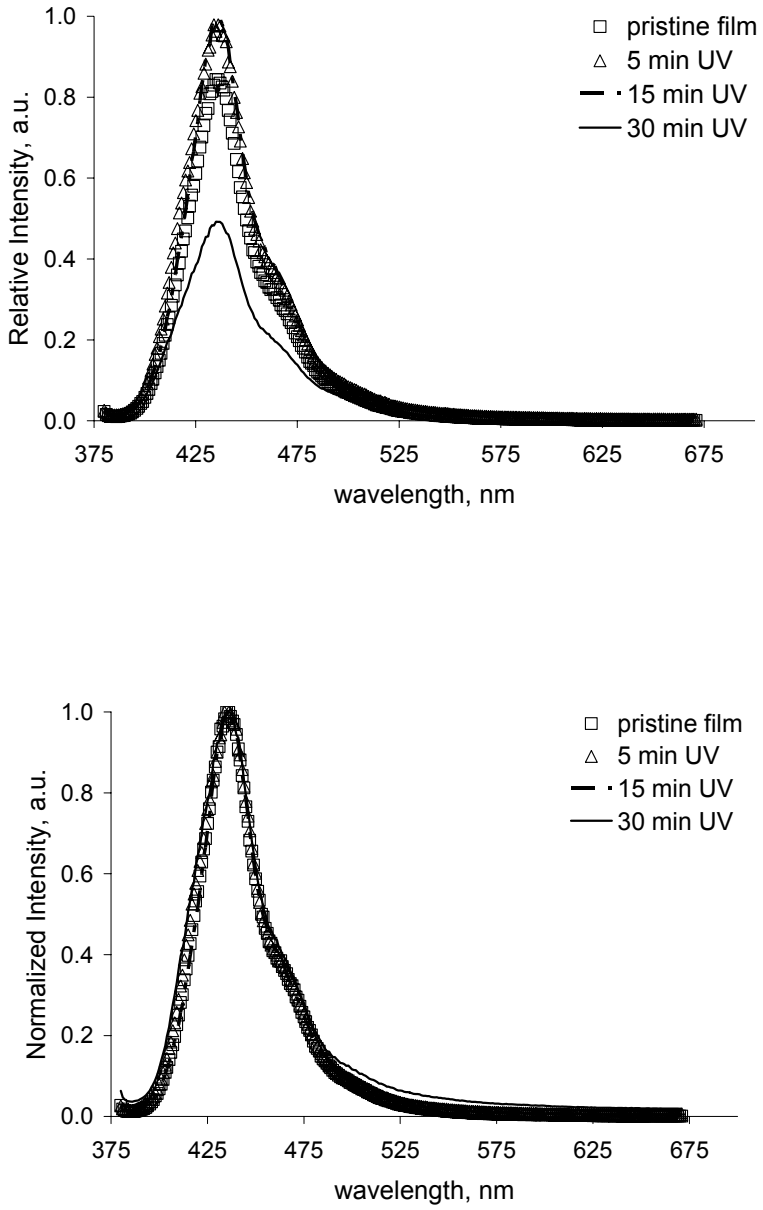

Figure D.3. PL spectra of relative (top, λ_{max} for pristine film = 1) and normalized (bottom, λ_{max} for all spectra = 1) intensities for a film of **PF4M10** irradiated by UV (λ = 366 nm) light.

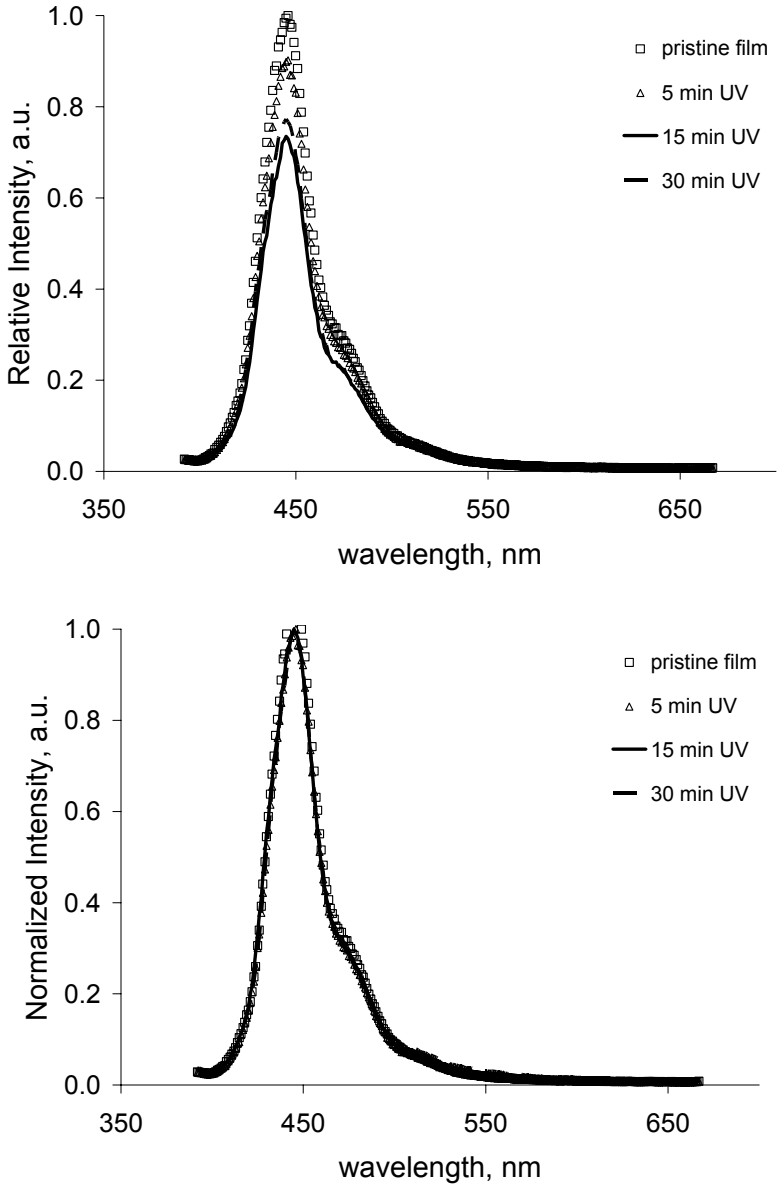

Figure D.4. PL spectra of relative (top, λ_{max} for pristine film = 1) and normalized (bottom, λ_{max} for all spectra = 1) intensities for a film of **PF7M18** irradiated by UV (λ = 366 nm) light.

APPENDIX E

UV-Induced Degradation Monitored by IR Spectroscopy

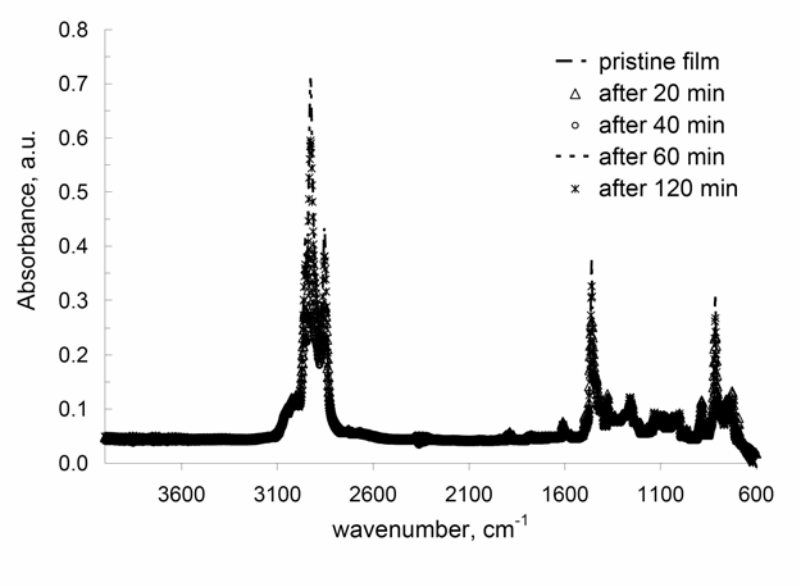

Figure E.1. IR spectra of **PF3M10** recorded after UV irradiation (λ = 366 nm) for 0, 20, 40, 60, and 120 min.

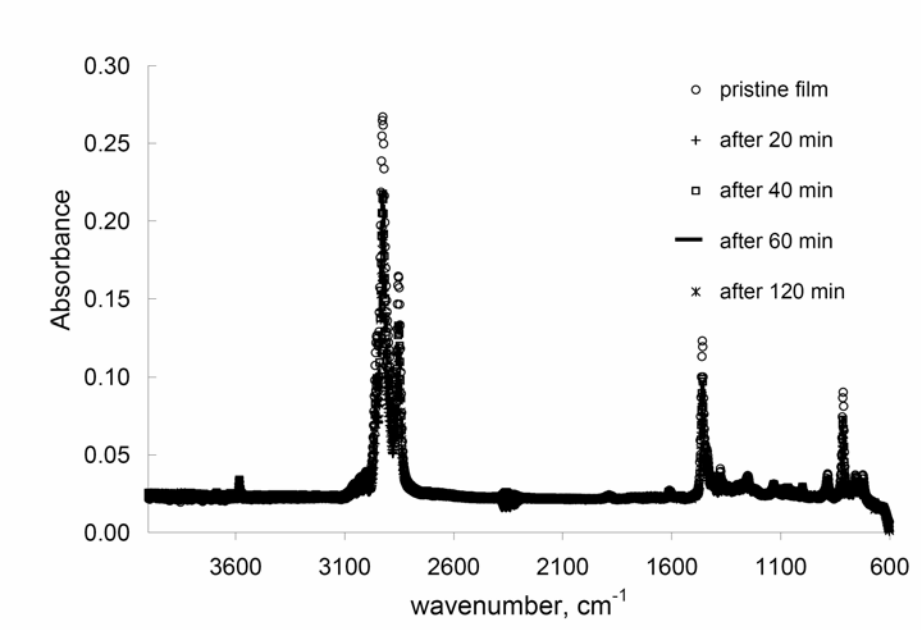

Figure E.2. IR spectra of **PF3M18** recorded after UV irradiation (λ = 366 nm) for 0, 20, 40, 60, and 120 min.

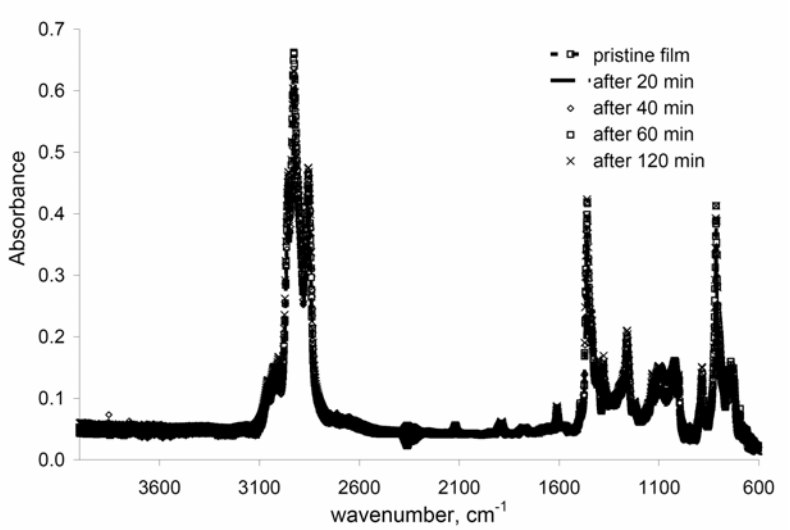

Figure E.3. IR spectra of **PF4M10** recorded after UV irradiation (λ = 366 nm) for 0, 20, 40, 60, and 120 min.

APPENDIX F

Thermally-Induced Degradation (160° C) Monitored by PL Spectroscopy

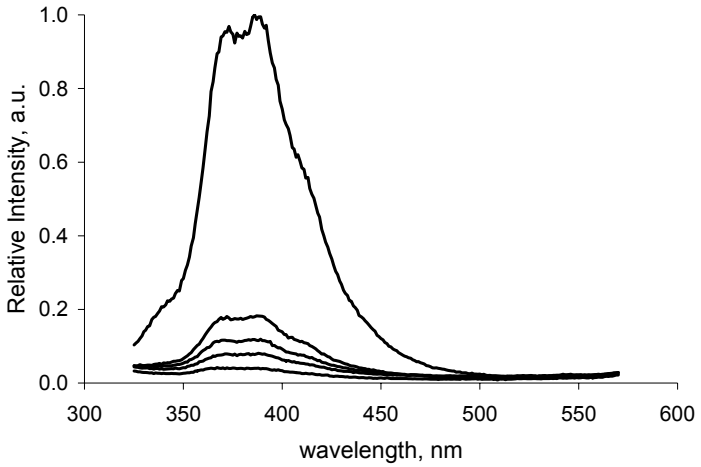

(a)

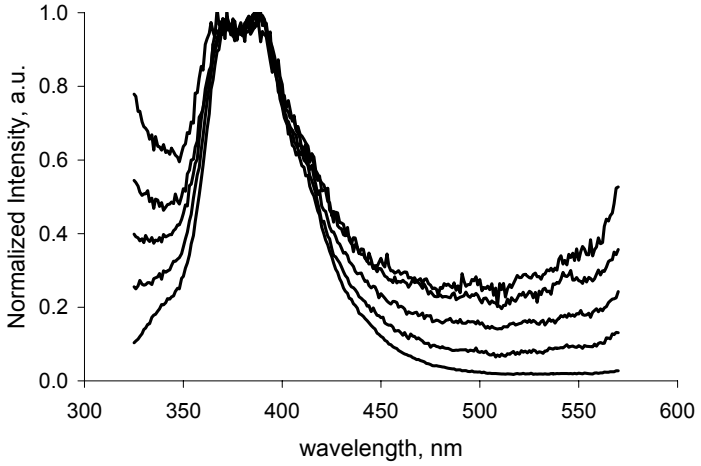

(b)

Figure F.1. Relative (a) and normalized (b) PL spectra of **PF1M10** (λ_{ex} = 300 nm) after heating at 160° C for (from top to bottom at 375 nm in left figure, bottom to top at 525 nm in right figure) 0, 0.5, 1, 2, and 4 h. (b) is normalized with respect to the 0-0 transition.

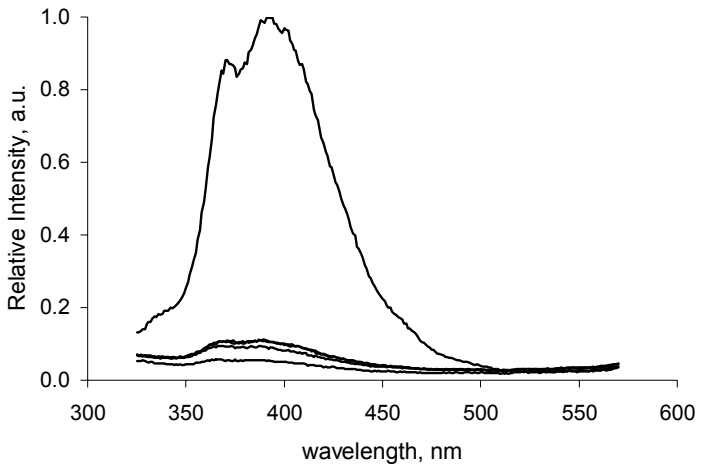

(a)

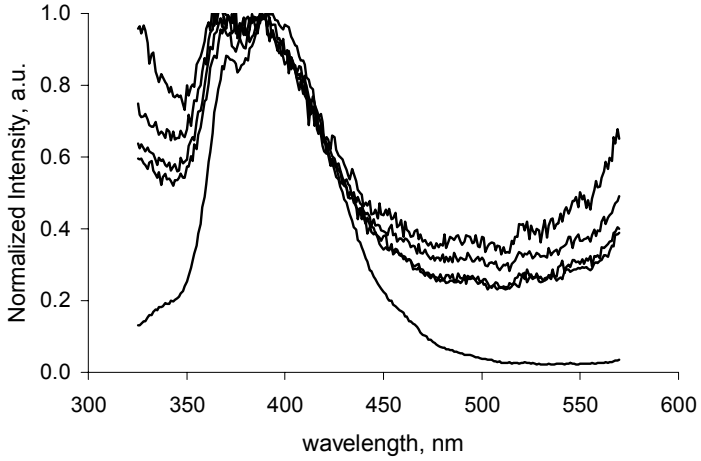

(b)

Figure F.2. Relative (a) and normalized (b) PL spectra of **PF1M18** (λ_{ex} = 300 nm) after heating at 160° C for (from top to bottom at 375 nm in left figure, bottom to top at 525 nm in right figure) 0, 0.5, 1, 2, and 4 h. (b) is normalized with respect to the 0-0 transition.

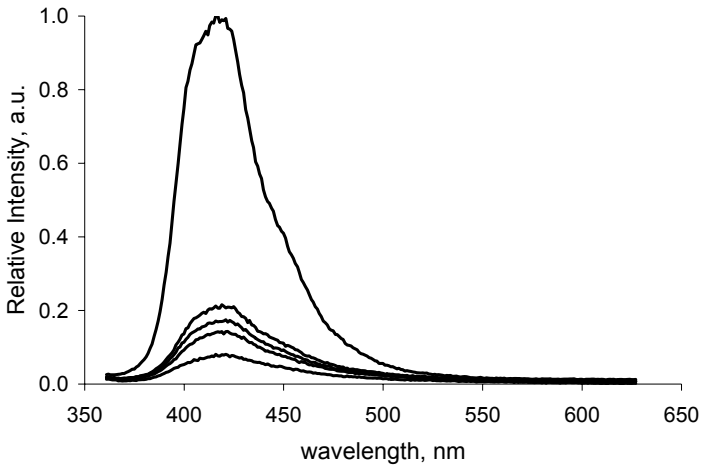

(a)

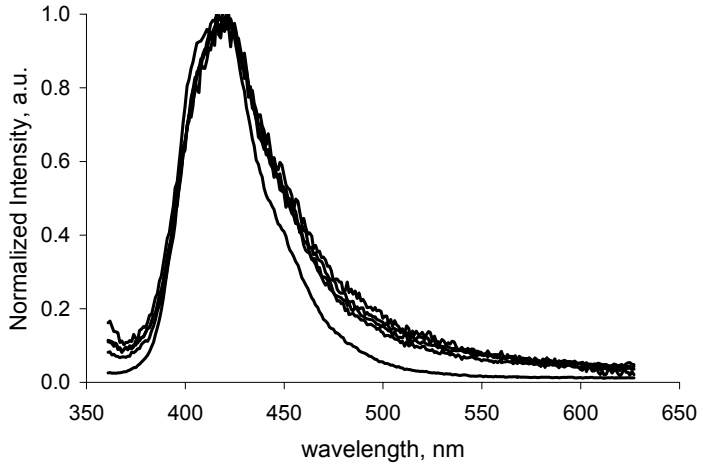

(b)

Figure F.3. Relative (a) and normalized (b) PL spectra of **PF2M10** (λ_{ex} = 335 nm) after heating at 160° C for (from top to bottom at 425 nm in left figure, bottom to top at 525 nm in right figure) 0, 0.5, 1, 2, and 4 h. (b) is normalized with respect to the 0-0 transition.

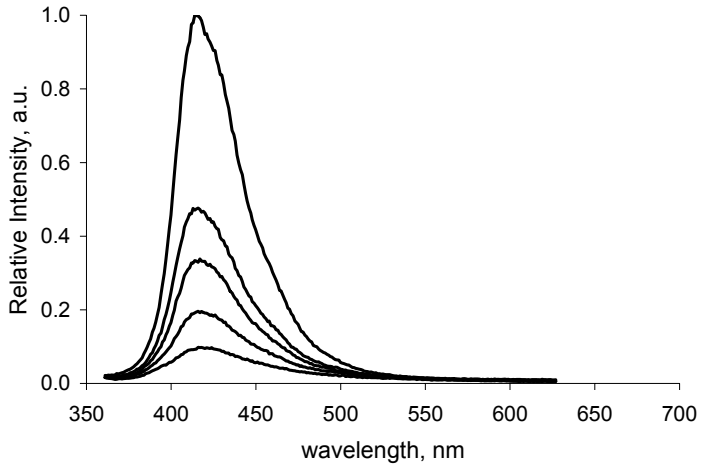

(a)

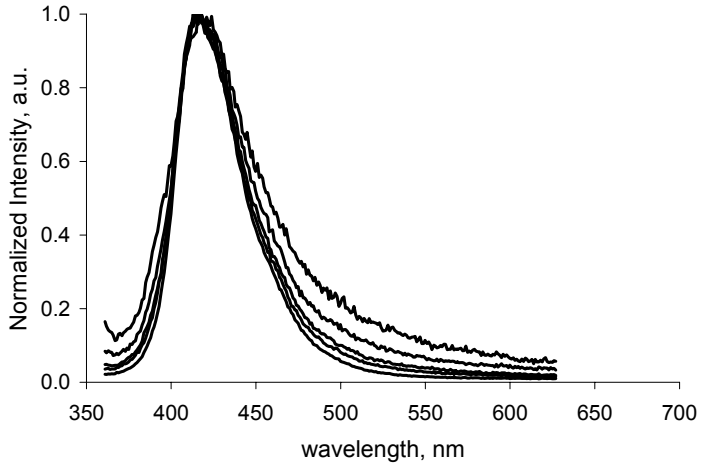

(b)

Figure F.4. Relative (a) and normalized (b) PL spectra of **PF2M18** (λ_{ex} = 335 nm) after heating at 160° C for (from top to bottom at 425 nm in left figure, bottom to top at 525 nm in right figure) 0, 0.5, 1, 2, and 4 h. (b) is normalized with respect to the 0-0 transition.

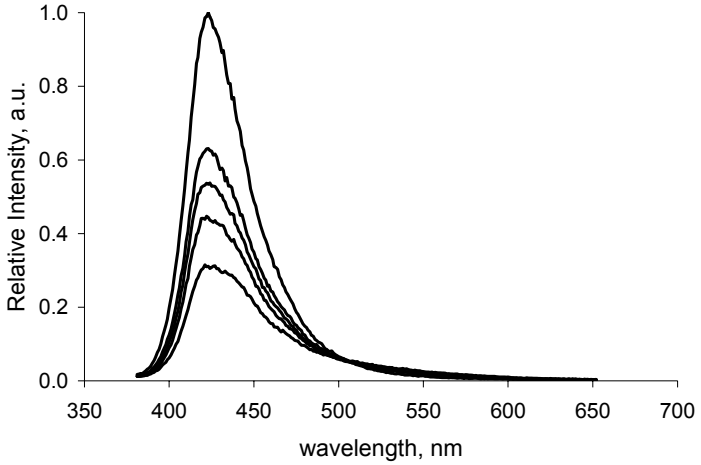

(a)

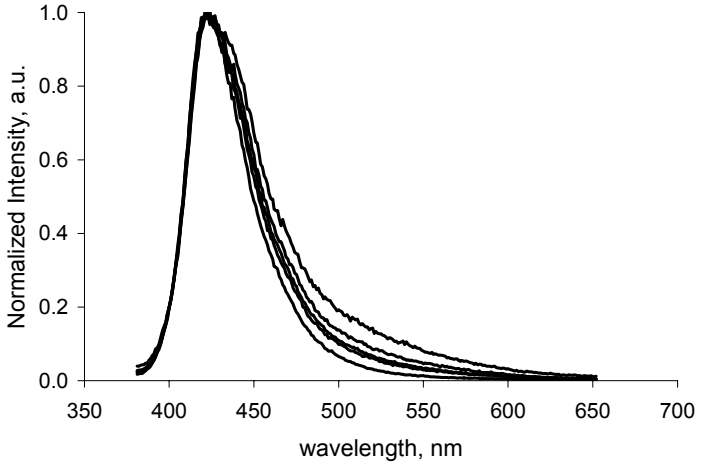

(b)

Figure F.5. Relative (a) and normalized (b) PL spectra of **PF3M10** (λ_{ex} = 355 nm) after heating at 160° C for (from top to bottom at 425 nm in left figure, bottom to top at 525 nm in right figure) 0, 0.5, 1, 2, and 4 h. (b) is normalized with respect to the 0-0 transition.

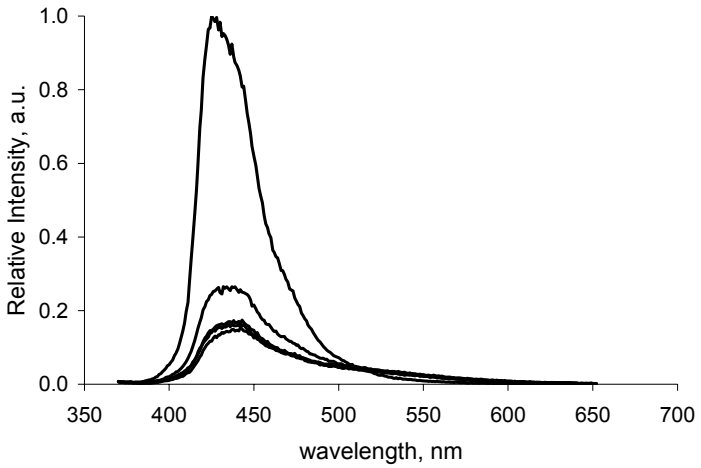

(a)

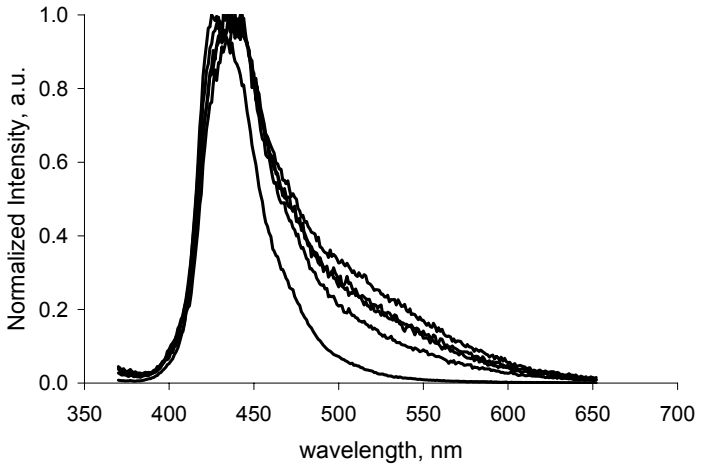

(b)

Figure F.6. Relative (a) and normalized (b) PL spectra of **PF3M10-2** (λ_{ex} = 355 nm) after heating at 160° C for (from top to bottom at 425 nm in left figure, bottom to top at 525 nm in right figure) 0, 0.5, 1, 2, and 4 h. (b) is normalized with respect to the 0-0 transition.

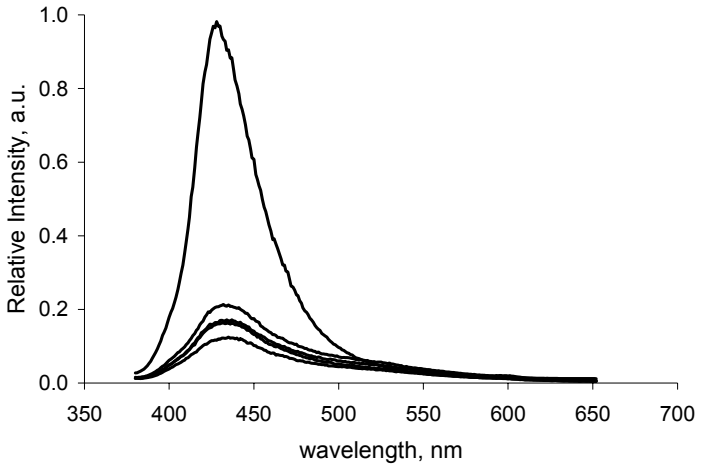

(a)

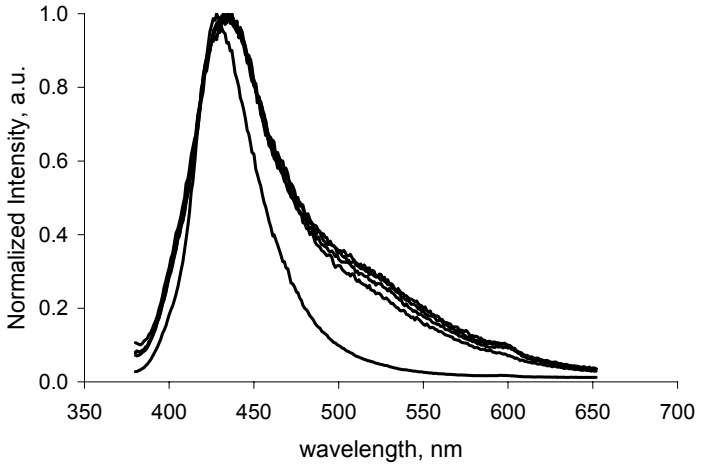

(b)

Figure F.7. Relative (a) and normalized (b) PL spectra of **PF3M18** (λ_{ex} = 355 nm) after heating at 160° C for (from top to bottom at 425 nm in left figure, bottom to top at 525 nm in right figure) 0, 0.5, 1, 2, and 4 h. (b) is normalized with respect to the 0-0 transition.

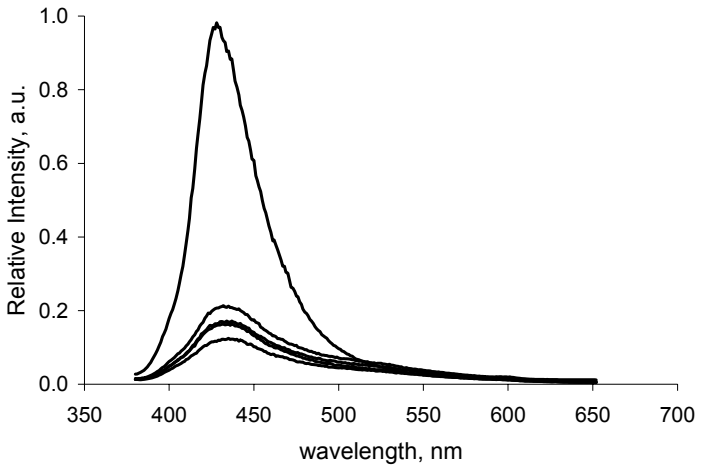

(a)

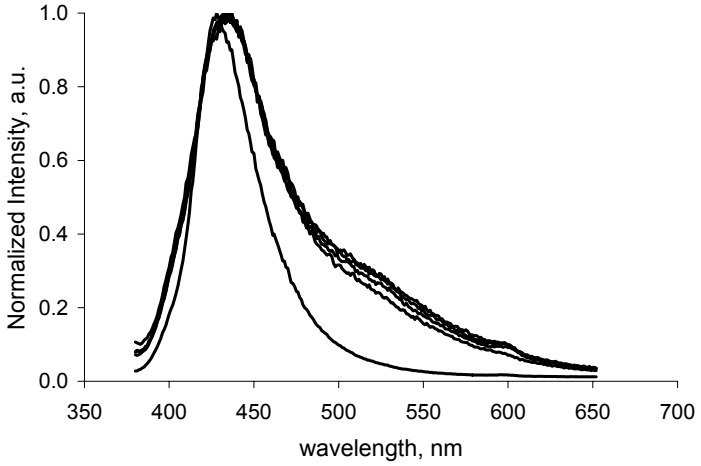

(b)

Figure F.8. Relative (a) and normalized (b) PL spectra of **PF4M10** (λ_{ex} = 365 nm) after heating at 160° C for (from top to bottom at 435 nm in left figure, bottom to top at 525 nm in right figure) 0, 0.5, 1, 2, and 4 h. (b) is normalized with respect to the 0-0 transition.

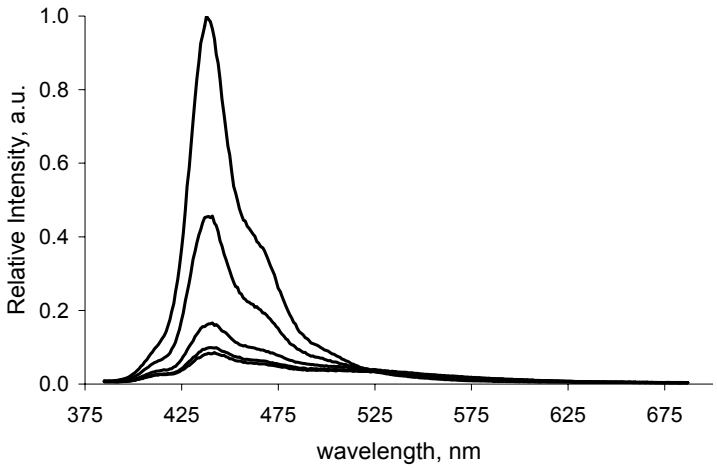

(a)

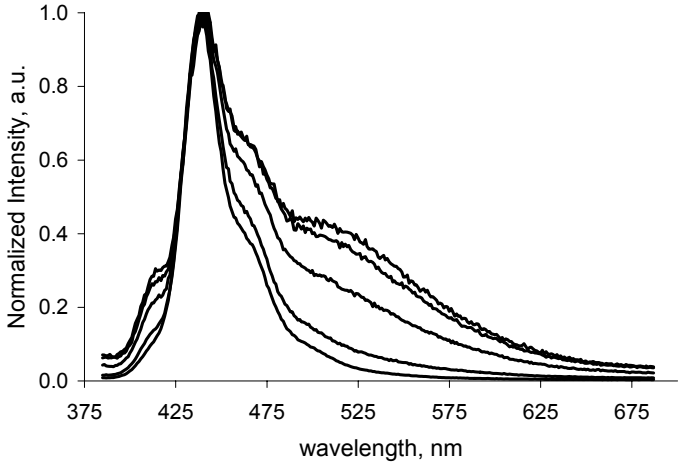

(b)

Figure F.9. Relative (a) and normalized (b) PL spectra of **PF4M18** (λ_{ex} = 365 nm) after heating at 160° C for (from top to bottom at 435 nm in left figure, bottom to top at 525 nm in right figure) 0, 0.5, 1, 2, and 4 h. (b) is normalized with respect to the 0-0 transition.

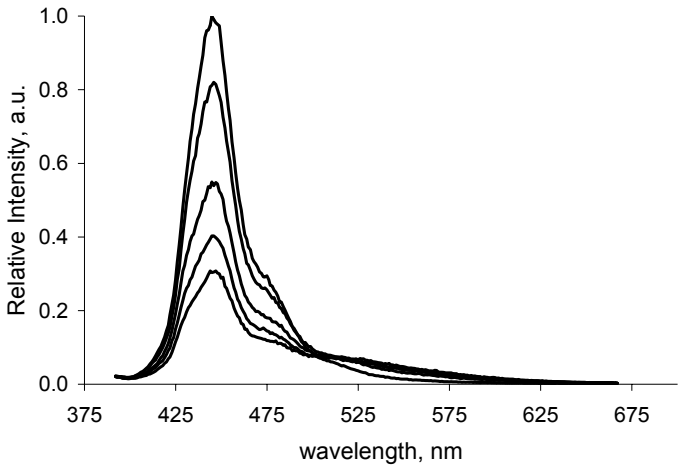

(a)

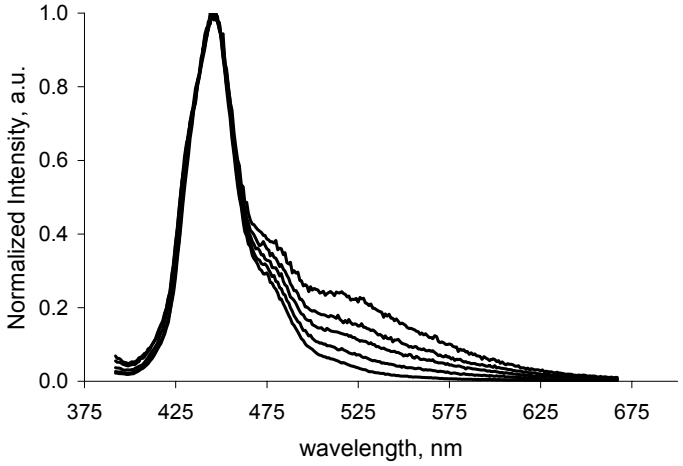

(b)

Figure F.10. Relative (a) and normalized (b) PL spectra of **PF7M18** (λ_{ex} = 375 nm) after heating at 160° C for (from top to bottom at 450 nm in left figure, bottom to top at 525 nm in right figure) 0, 0.5, 1, 2, and 4 h. (b) is normalized with respect to the 0-0 transition.

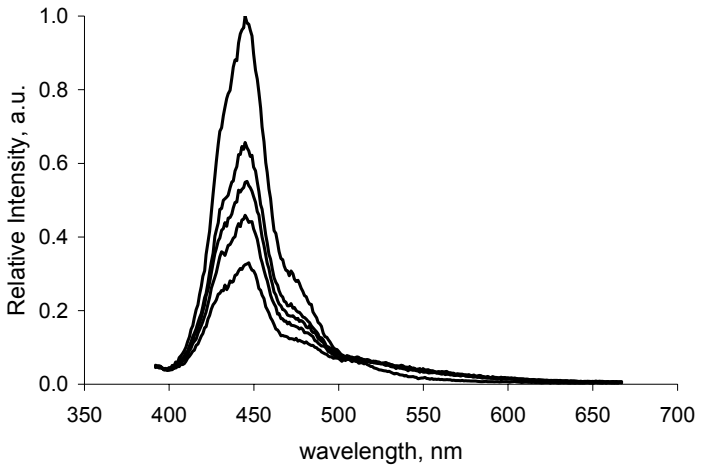

(a)

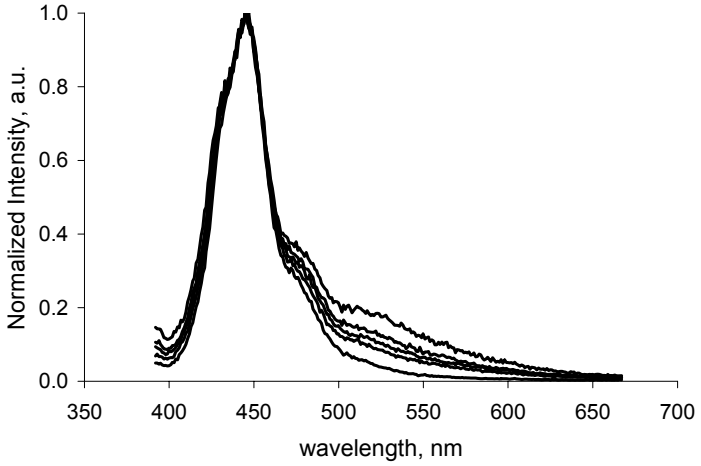

(b)

Figure F.11. Relative (a) and normalized (b) PL spectra of **PF8M18** (λ_{ex} = 375 nm) after heating at 160° C for (from top to bottom at 450 nm in left figure, bottom to top at 525 nm in right figure) 0, 0.5, 1, 2, and 4 h. (b) is normalized with respect to the 0-0 transition.

APPENDIX G

Thermally-Induced Degradation (200° C) Monitored by IR Spectroscopy

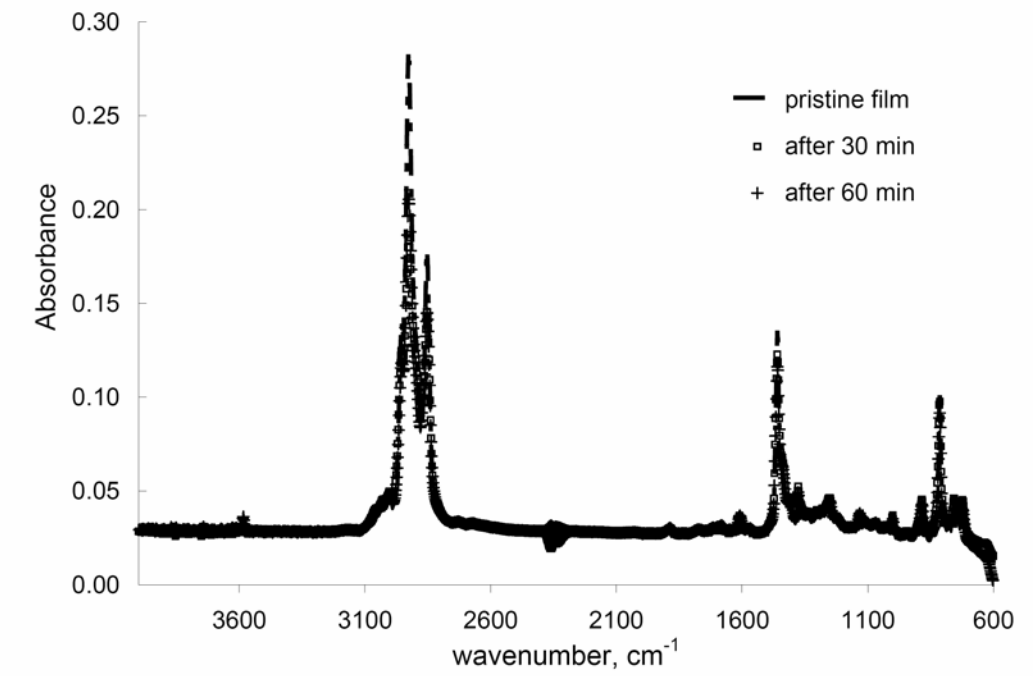

Figure G.1. IR spectra of **PF3M18** recorded after after heating at 200° C for 0, 0.5, and 1 h.

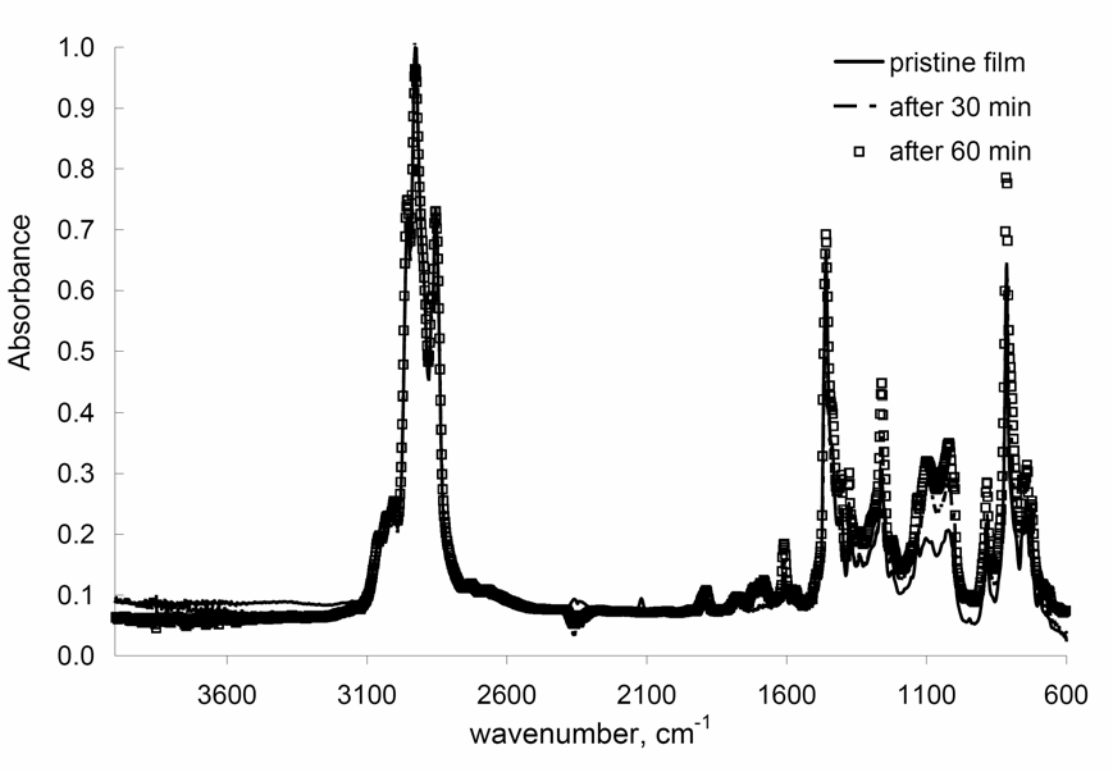

Figure G.2. IR spectra of **PF4M10** recorded after after heating at 200° C for 0, 0.5, and 1 h.

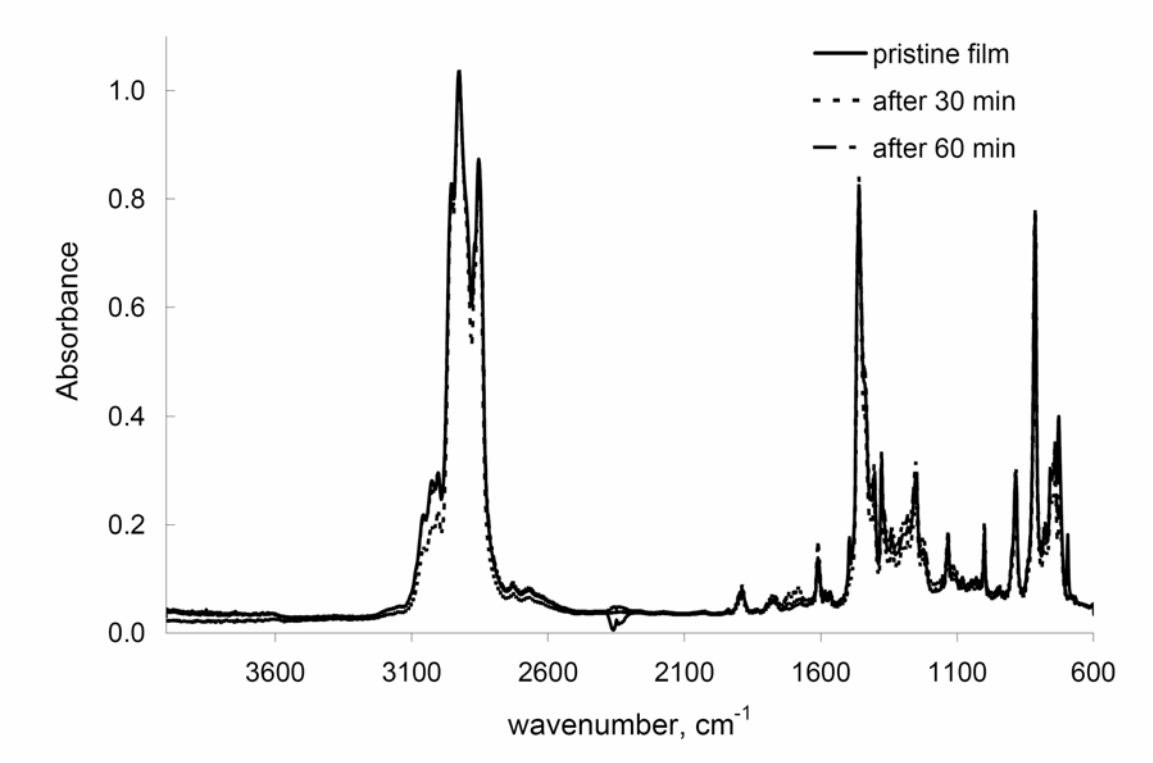

Figure G.3. IR spectra of **PF4M18** recorded after after heating at 200° C for 0, 0.5, and 1 h.

APPENDIX H

DSC Data

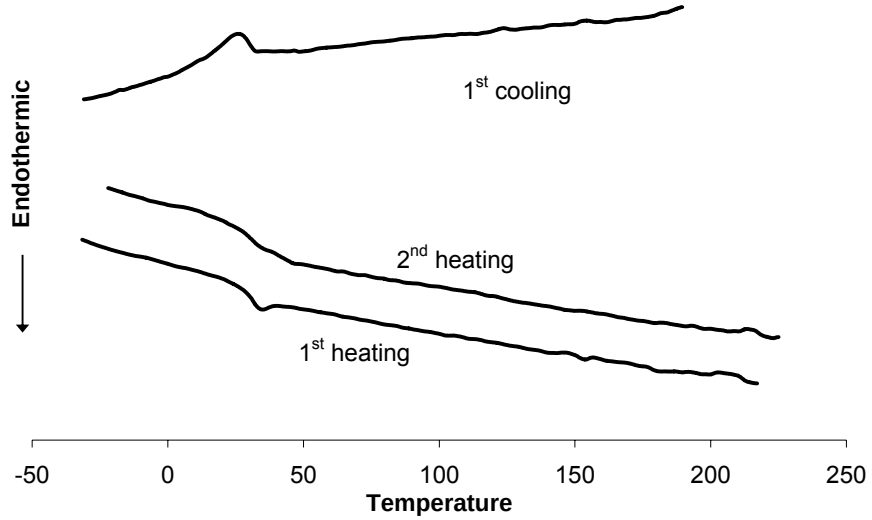

Figure H.1. DSC scan for **PF2M10**. Data was recorded at 20° C/min heating and cooling rates.

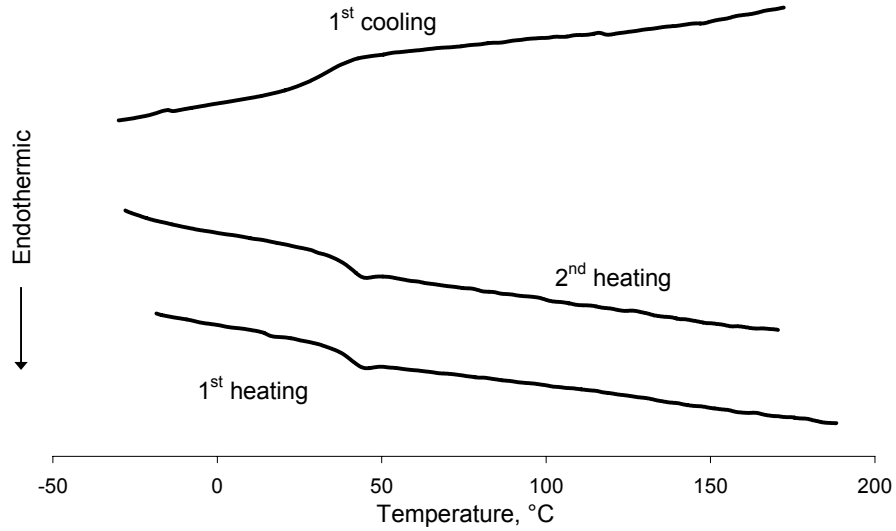

Figure H.2. DSC scan for **PF3M18**. Data was recorded at 20° C/min heating and cooling rates.

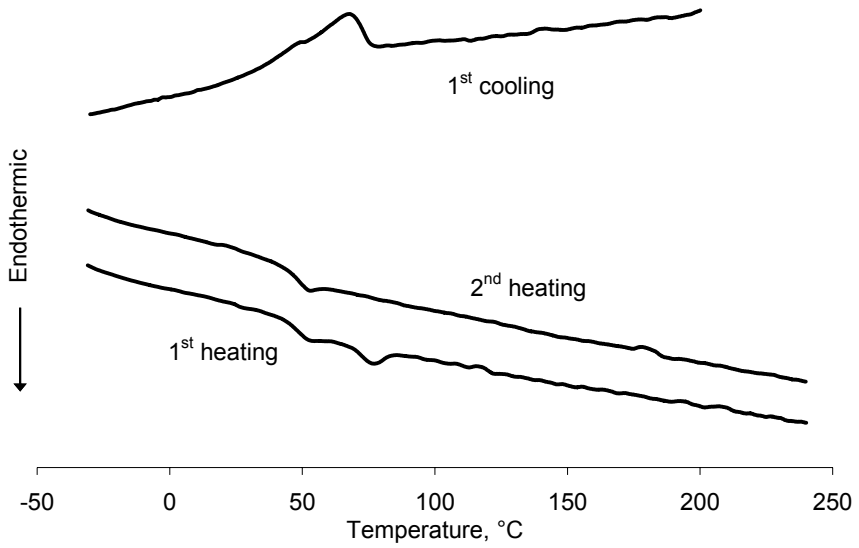

Figure H.3. DSC scan for **PF4M18**. Data was recorded at 20° C/min heating and cooling rates.

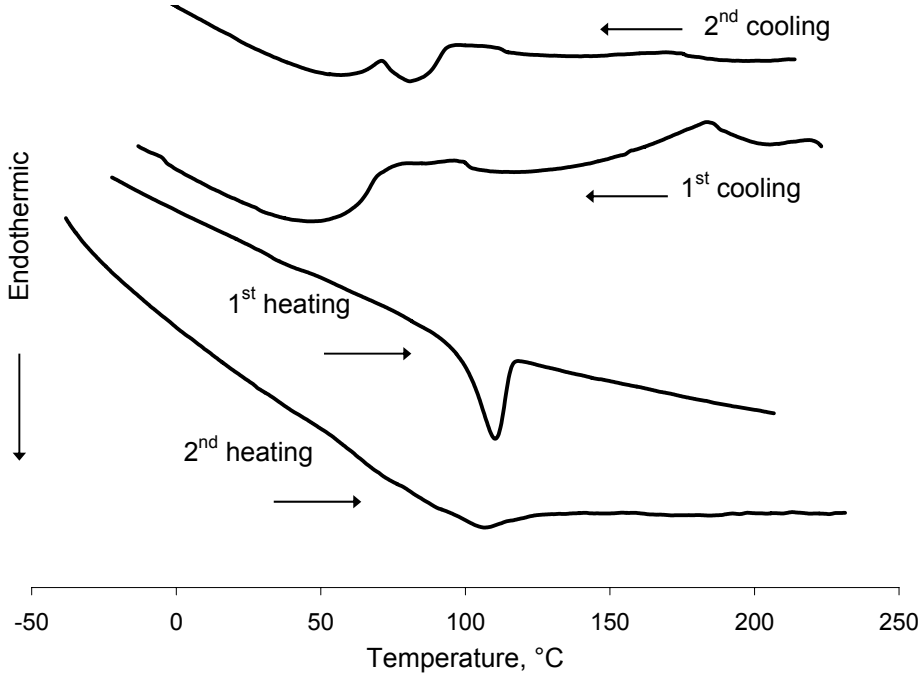

Figure H.4. DSC scan for **PF7M18**. Data was recorded at 20° C/min heating and cooling rates.

BIBLIOGRAPHY

1. McGrath, K. P.; Kaplan, D. L., *Protein-Based Materials*. Birkhaeuser: Cambridge, 1997.
2. Rathore, O.; Sogah, D. Y., "Self-assembly of beta-sheets into nanostructures by poly(alanine) segments incorporated in multiblock copolymers inspired by spider silk." *Journal of the American Chemical Society* **2001,** 123, (22), 5231-5239.
3. Kaplan, D.; Adams, W. W.; Farmer, B.; Viney, C., *Silk Polymers: Materials Science and Biotechnology*. American Chemical Society: Washington D.C., 1994.
4. Zhou, C.; Leng, B.; Yao, J.; Qian, J.; Chen, X.; Zhou, P.; Knight, D. P.; Shao, Z., "Synthesis and Characterization of Multiblock Copolymers Based on Spider Dragline Silk Proteins." *Biomacromolecules* **2006,** 7, (8), 2415-2419.
5. Krejchi, M. T.; Cooper, S. J.; Deguchi, Y.; Atkins, E. D. T.; Fournier, M. J.; Mason, T. L.; Tirrell, D. A., "Crystal Structures of Chain-Folded Antiparallel b-Sheet Assemblies from Sequence-Designed Periodic Polypeptides." *Macromolecules* **1997,** 30, (17), 5012-5024.
6. Fraser, R. D. B.; MacRae, T. P., *Conformation in Fibrous Proteins and Related Synthetic Polypeptides*. Academic Press: New York, 1973.
7. Urry, D. W., "Entropic elastic processes in protein mechanisms. I. Elastic structure due to an inverse temperature transition and elasticity due to internal chain dynamics." *Journal of Protein Chemistry* **1988,** 7, (1), 1-34.
8. Buchet, R.; Luan, C. H.; Prasad, K. U.; Harris, R. D.; Urry, D. W., "Dielectric relaxation studies on analogs of the polypentapeptide of elastin." *Journal of Physical Chemistry* **1988,** 92, (2), 511-17.

9. Bochicchio, B.; Jimenez-Oronoz, F.; Pepe, A.; Blanco, M.; Sandberg, L. B.; Tamburro, A. M., "Synthesis of and structural studies on repeating sequences of abductin." *Macromolecular Bioscience* **2005,** 5, (6), 502-511.

10. Martino, M.; Perri, T.; Tamburro, A. M., "Biopolymers and biomaterials based on elastomeric proteins." *Macromolecular Bioscience* **2002,** 2, (7), 319-328.

11. Renugopalakrishnan, V.; Pattabiraman, N.; Prabhakaran, M.; Strawich, E.; Glimcher, M. J., "Tooth enamel protein, amelogenin, has a probable b-spiral internal channel, Gln112-Leu138, within a single polypeptide chain: preliminary molecular mechanics and dynamics studies." *Biopolymers* **1989,** 28, (1), 297-303.

12. Termonia, Y., "Nanoscale Self-Assembly of Multiblock Copolymer Chains into Rods." *Biomacromolecules* **2004,** 5, (6), 2404-2407.

13. Fields, G. B.; Laurer-Fields, J. L.; Liu, R.-q.; Barany, G., "Principles and Practice of Solid-Phase Peptide Synthesis." In *Synthetic Peptides*, Grant, G. A., Ed. Oxford University Press: 2002; pp 93-219.

14. Yu, S. M.; Conticello, V. P.; Zhang, G.; Kayser, C.; Fournier, M. J.; Mason, T. L.; Tirrell, D. A., "Smectic ordering in solutions and films of a rod-like polymer owing to monodispersity of chain length." *Nature (London)* **1997,** 389, (6647), 167-170.

15. Link, A. J.; Mock, M. L.; Tirrell, D. A., "Non-canonical amino acids in protein engineering." *Current Opinion in Biotechnology* **2003,** 14, (6), 603-609.

16. Panitch, A.; Matsuki, K.; Cantor, E. J.; Cooper, S. J.; Atkins, E. D. T.; Fournier, M. J.; Mason, T. L.; Tirrell, D. A., "Poly(L-alanylglycine): Multigram-Scale Biosynthesis, Crystallization, and Structural Analysis of Chain-Folded Lamellae." *Macromolecules* **1997,** 30, (1), 42-49.

17. Dodge, J., "Polyurethanes and Polyureas." In *Synthetic Methods in Step Growth Polymers*, Rogers, M. E.; Long, T. E., Eds. John Wiley & Sons, Inc.: Hoboken, 2003; pp 197-263.

18. Velankar, S.; Cooper, S. L., "Microphase Separation and Rheological Properties of Polyurethane Melts. 2. Effect of Block Incompatibility on the Microstructure." *Macromolecules* **2000,** 33, (2), 382-394.

19. Velankar, S.; Cooper, S. L., "Microphase Separation and Rheological Properties of Polyurethane Melts. 3. Effect of Block Incompatibility on the Viscoelastic Properties." *Macromolecules* **2000,** 33, (2), 395-403.

20. Velankar, S.; Cooper, S. L., "Microphase Separation and Rheological Properties of Polyurethane Melts. 1. Effect of Block Length." *Macromolecules* **1998,** 31, (26), 9181-9192.

21. Versteegen, R. M.; Sijbesma, R. P.; Meijer, E. W., "Synthesis and characterization of segmented copoly(ether urea)s with uniform hard segments." *Macromolecules* **2005,** 38, (8), 3176-3184.

22. Sirigu, A., "Segmented -Chain Liquid Crystal Polymers." In *Liquid Crystallinity in Polymers*, Ciferri, A., Ed. VCH Publishers, Inc.: New York, 1991; pp 261-313.

23. Skorokhodov, S. S., "Thermotropic Liquid Crystal Polymers with Mesogenic Groups in the Main Chain." In *Liquid-Crystal Polymers*, Platé, N. A., Ed. Plenum Press: New York, 1993; pp 163-192.

24. Meurisse, P.; Noel, C.; Monnerie, L.; Fayolle, B., "Polymers with mesogenic elements and flexible spacers in the main chain. Aromatic-aliphatic polyesters." *British Polymer Journal* **1981,** 13, (2), 55-63.

25. Watanabe, J.; Hayashi, M., "Thermotropic liquid crystals of polyesters having a mesogenic p,p'-bibenzoate unit. 2. X-ray study on smectic mesophase structures of BB-5 and BB-6." *Macromolecules* **1989,** 22, (10), 4083-8.

26. Choe, E. W.; Borzo, M., "Synthesis and Randomization of Well-Defined Sequence, Wholly Aromatic Copolyester Esteramides." *Journal of Applied Polymer Science* **1994,** 53, (5), 621-632.

27. Alsunaidi, A.; Abu-Sharkh, B. F., "Influence of monomer sequence on microstructure of nonadditive hard chain copolymers: Simulation and equation of state." *Journal of Chemical Physics* **2003,** 119, (18), 9894-9902.

28. Chakraborty, A. K.; Fredrickson, G. H., "Elastic-Constants for Random Block-Copolymers in the Strong Segregation Limit - Effects of Sequence Distribution." *Macromolecules* **1994,** 27, (24), 7079-7084.

29. Vix, A.; Stocker, W.; Stamm, M.; Wilbert, G.; Zentel, R.; Rabe, J. P., "Chain Folding in Liquid-Crystalline Main-Chain Polymers with a Smectic Phase." *Macromolecules* **1998,** 31, (26), 9154-9159.

30. Tokita, M.; Takahashi, T.; Hayashi, M.; Inomata, K.; Watanabe, J., "Thermotropic Liquid Crystals of Polyesters Having a Mesogenic p,p'-Bibenzoate Unit. 7. Chain Folding in the Smectic Phase of BB-6." *Macromolecules* **1996,** 29, (4), 1345-8.

31. Joo, S. H.; Yun, Y. K.; Jin, J. I.; Kim, D. C.; Zin, W. C., "Synthesis of liquid crystalline polyesters of various types by acyclic diene metathesis polymerization." *Macromolecules* **2000,** 33, (18), 6704-6712.

32. Percec, V.; Asandei, A. D., "Monodisperse Linear Liquid Crystalline Polyethers via a Repetitive 2n Geometric Growth Algorithm." *Macromolecules* **1997,** 30, (25), 7701-7720.

33. Konstandakopoyloy, F. D.; Kallitsis, J. K., "Soluble rigid-flexible polyethers containing bis(biphenyl)anthracene or bis(styryl)anthracene units in the main chain for light-emitting applications." *Journal of Polymer Science, Part A: Polymer Chemistry* **1999,** 37, (20), 3826-3837.

34. Konstandakopoulou, F. D.; Gravalos, K. G.; Kallitsis, J. K., "Synthesis and Characterization of Processable Aromatic-Aliphatic Polyethers with Quinquephenyl Segments in the Main Chain for Light-Emitting Applications." *Macromolecules* **1998,** 31, (16), 5264-5271.

35. Chochos, C. L.; Papakonstandopoulou, D.; Economopoulos, S. P.; Gregoriou, V. G.; Kallitsis, J. K., "Synthesis and optical properties on a series of polyethers incorporating terfluorene segments and methylene spacers." *Journal of Macromolecular Science, Part A: Pure and Applied Chemistry* **2006,** 43, (3), 419-431.

36. Shirakawa, H.; Louis, E. J.; MacDiarmid, A. G.; Chiang, C. K.; Heeger, A. J., "Synthesis of electrically conducting organic polymers: halogen derivatives of polyacetylene, (CH)x." *Journal of the Chemical Society, Chemical Communications* **1977**, (16), 578-80.

37. Chiang, C. K.; Fincher, C. R., Jr.; Park, Y. W.; Heeger, A. J.; Shirakawa, H.; Louis, E. J.; Gau, S. C.; MacDiarmid, A. G., "Electrical conductivity in doped polyacetylene." *Physical Review Letters* **1977,** 39, (17), 1098-101.

38. Chiang, C. K.; Druy, M. A.; Gau, S. C.; Heeger, A. J.; Louis, E. J.; MacDiarmid, A. G.; Park, Y. W.; Shirakawa, H., "Synthesis of highly conducting films of derivatives of

polyacetylene, (CH)x." *Journal of the American Chemical Society* **1978,** 100, (3), 1013-15.

39. Service, R. F., "Chemistry nobel: Getting a charge out of plastics." *Science (Washington, D. C.)* **2000,** 290, (5491), 425, 427.

40. Tessler, N.; Denton, G. J.; Friend, R. H., "Lasing from conjugated-polymer microcavities." *Nature (London)* **1996,** 382, (6593), 695-697.

41. Zavelani-Rossi, M.; Lanzani, G.; Anni, M.; Gigli, G.; Cingolani, R.; Barbarella, G.; Favaretto, L., "Organic laser based on thiophene derivatives." *Synthetic Metals* **2003,** 139, (3), 901-903.

42. Horowitz, G., "Organic field-effect transistors." *Advanced Materials (Weinheim, Germany)* **1998,** 10, (5), 365-377.

43. Horowitz, G.; Hajlaoui, R.; Bourguiga, R.; Hajlaoui, M., "Theory of the organic field-effect transistor." *Synthetic Metals* **1999,** 101, (1-3), 401-404.

44. Heeney, M.; Bailey, C.; Giles, M.; Shkunov, M.; Sparrowe, D.; Tierney, S.; Zhang, W.; McCulloch, I., "Alkylidene Fluorene Liquid Crystalline Semiconducting Polymers for Organic Field Effect Transistor Devices." *Macromolecules* **2004,** 37, (14), 5250-5256.

45. Kraft, A.; Grimsdale, A. C.; Holmes, A. B., "Electroluminescent conjugated polymers-seeing polymers in a new light." *Angewandte Chemie, International Edition* **1998,** 37, (4), 403-428.

46. Marder, S. R.; Kippelen, B.; Jen, A. K. Y.; Peyghammbarian, N., "Design and synthesis of chromophores and polymers for electro-optic nd photorefractive applications." *Nature (London)* **1997,** 388, (6645), 845-851.

47. Marder, S. R.; Torruellas, W. E.; Blanchard-Desce, M.; Ricci, V.; Stegeman, G. I.; Gilmour, S.; Bredas, J.-L.; Li, J.; Bublitz, G. U.; Boxer, S. G., "Large molecular third-order optical nonlinearities in polarized carotenoids." *Science (Washington, D. C.)* **1997,** 276, (5316), 1233-1236.

48. Klaerner, G.; Miller, R. D., "Polyfluorene Derivatives: Effective Conjugation Lengths from Well-Defined Oligomers." *Macromolecules* **1998,** 31, (6), 2007-2009.

49. Berresheim, A. J.; Mueller, M.; Muellen, K., "Polyphenylene Nanostructures." *Chemical Reviews (Washington, D. C.)* **1999,** 99, (7), 1747-1785.

50. Chen, S. H.; Chou, H. L.; Su, A. C.; Chen, S. A., "Molecular Packing in Crystalline Poly(9,9-di-n-octyl-2,7-fluorene)." *Macromolecules* **2004,** 37, (18), 6833-6838.

51. Grell, M.; Bradley, D. D. C.; Long, X.; Chamberlain, T.; Inbasekaran, M.; Woo, E. P.; Soliman, M., "Chain geometry, solution aggregation, and enhanced dichroism in the liquid-crystalline conjugated polymer poly(9,9-dioctylfluorene)." *Acta Polymerica* **1998,** 49, (8), 439-444.

52. Watson, M. D.; Fechtenkoetter, A.; Muellen, K., "Big Is Beautiful-'Aromaticity' Revisited from the Viewpoint of Macromolecular and Supramolecular Benzene Chemistry." *Chemical Reviews (Washington, D. C.)* **2001,** 101, (5), 1267-1300.

53. Remmers, M.; Mueller, B.; Martin, K.; Raeder, H.-J.; Koehler, W., "Poly(p-phenylene)s. Synthesis, Optical Properties, and Quantitative Analysis with HPLC and MALDI-TOF Mass Spectrometry." *Macromolecules* **1999,** 32, (4), 1073-1079.

54. Izumi, T.; Kobashi, S.; Takimiya, K.; Aso, Y.; Otsubo, T., "Synthesis and spectroscopic properties of a series of b-blocked long oligothiophenes up to the 96-mer: re-evaluation

of effective conjugation length." *Journal of the American Chemical Society* **2003,** 125, (18), 5286-5287.

55. Ong, B. S.; Wu, Y.; Liu, P.; Gardner, S., "High-Performance Semiconducting Polythiophenes for Organic Thin-Film Transistors." *Journal of the American Chemical Society* **2004,** 126, (11), 3378-3379.

56. Cheon, C. H.; Joo, S.-H.; Kim, K.; Jin, J.-I.; Shin, H.-W.; Kim, Y.-R., "Synthesis and Luminescent Properties of Fluorene Copolymers Bearing DCM Pendants." *Macromolecules* **2005,** 38, (15), 6336-6345.

57. Yang, Y.; Pei, Q.; Heeger, A. J., "Efficient blue polymer light-emitting diodes from a series of soluble poly(para-phenylene)s." *Journal of Applied Physics* **1996,** 79, (2), 934-9.

58. Ranger, M.; Rondeau, D.; Leclerc, M., "New Well-Defined Poly(2,7-fluorene) Derivatives: Photoluminescence and Base Doping." *Macromolecules* **1997,** 30, (25), 7686-7691.

59. Lee, J.-I.; Zyung, T.; Miller, R. D.; Kim, Y. H.; Jeoung, S. C.; Kim, D., "Photoluminescence study on exciton migration and trapping in a copolymer based on poly(fluorene)." *Journal of Materials Chemistry* **2000,** 10, (7), 1547-1550.

60. Nothofer, H.-G.; Meisel, A.; Miteva, T.; Neher, D.; Forster, M.; Oda, M.; Lieser, G.; Sainova, D.; Yasuda, A.; Lupo, D.; Knoll, W.; Scherf, U., "Liquid crystalline polyfluorenes for blue polarized electroluminescence." *Macromolecular Symposia* **2000,** 154, (Polymers in Display Applications), 139-148.

61. Oda, M.; Nothofer, H. G.; Scherf, U.; Sunjic, V.; Richter, D.; Regenstein, W.; Neher, D., "Chiroptical properties of chiral substituted polyfluorenes." *Macromolecules* **2002,** 35, (18), 6792-6798.

62. Gamerith, S.; Gaal, M.; Romaner, L.; Nothofer, H.-G.; Guentner, R.; Scandiucci de Freitas, P.; Scherf, U.; List, E. J. W., "Comparison of thermal and electrical degradation effects in polyfluorenes." *Synthetic Metals* **2003,** 139, 855-858.

63. Wu, F.-I.; Dodda, R.; Jakka, K.; Huang, J.-H.; Hsu, C.-S.; Shu, C.-F., "Enhancing the thermal and spectral stabilities of polyfluorene-based blue-light-emitting materials by incorporating pendent spiro-cycloalkyl groups." *Polymer* **2004,** 45, (12), 4257-4263.

64. Pei, Q.; Yang, Y., "Efficient Photoluminescence and Electroluminescence from a Soluble Polyfluorene." *Journal of the American Chemical Society* **1996,** 118, (31), 7416-7417.

65. Chen, Y.; Araki, Y.; Doyle, J.; Strevens, A.; Ito, O.; Blau, W. J., "Synthesis, Characterization, and Optoelectronic Properties of a Novel Polyfluorene/Poly(p-Phenylenevinylene) Copolymer." *Chemistry of Materials* **2005,** 17, (7), 1661-1666.

66. Huang, F.; Hou, L.; Shen, H.; Jiang, J.; Wang, F.; Zhen, H.; Cao, Y., "Synthesis, photophysics, and electroluminescence of high-efficiency saturated red light-emitting polyfluorene-based polyelectrolytes and their neutral precursors." *Journal of Materials Chemistry* **2005,** 15, (25), 2499-2507.

67. Hong, J. W.; Hemme, W. L.; Keller, G. E.; Rinke, M. T.; Bazan, G. C., "Conjugated-polymer/DNA interpolyelectrolyte complexes for accurate DNA concentration determination." *Advanced Materials (Weinheim, Germany)* **2006,** 18, (7), 878-882.

68. Liu, B.; Bazan, G. C., "Optimization of the Molecular Orbital Energies of Conjugated Polymers for Optical Amplification of Fluorescent Sensors." *Journal of the American Chemical Society* **2006,** 128, (4), 1188-1196.

69. Zeng, G.; Yu, W.-L.; Chua, S.-J.; Huang, W., "Spectral and Thermal Spectral Stability Study for Fluorene-Based Conjugated Polymers." *Macromolecules* **2002,** 35, (18), 6907-6914.

70. Su, H.-J.; Wu, F.-I.; Tseng, Y.-H.; Shu, C.-F., "Color tuning of a light-emitting polymer: polyfluorene-containing pendant amino-substituted distyrylarylene units." *Advanced Functional Materials* **2005,** 15, (7), 1209-1216.

71. Ego, C.; Grimsdale, A. C.; Uckert, F.; Yu, G.; Srdanov, G.; Mullen, K., "Triphenylamine-substituted polyfluorene-a stable blue-emitter with improved charge injection for light-emitting diodes." *Advanced Materials (Weinheim, Germany)* **2002,** 14, (11), 809-811.

72. Setayesh, S.; Grimsdale, A. C.; Weil, T.; Enkelmann, V.; Muellen, K.; Meghdadi, F.; List, E. J. W.; Leising, G., "Polyfluorenes with Polyphenylene Dendron Side Chains: Toward Non-Aggregating, Light-Emitting Polymers." *Journal of the American Chemical Society* **2001,** 123, (5), 946-953.

73. Marsitzky, D.; Vestberg, R.; Blainey, P.; Tang, B. T.; Hawker, C. J.; Carter, K. R., "Self-Encapsulation of Poly-2,7-fluorenes in a Dendrimer Matrix." *Journal of the American Chemical Society* **2001,** 123, (29), 6965-6972.

74. Scherf, U.; List, E. J. W., "Semiconducting polyfluorenes - towards reliable structure-property relationships." *Advanced Materials (Weinheim, Germany)* **2002,** 14, (7), 477-487.

75. Wu, H.; Huang, F.; Mo, Y.; Yang, W.; Wang, D.; Peng, J.; Cao, Y., "Efficient electron injection from a bilayer cathode consisting of aluminum and alcohol-/water-soluble conjugated polymers." *Advanced Materials (Weinheim, Germany)* **2004,** 16, (20), 1826-1830.

76. Liu, B.; Gaylord, B. S.; Wang, S.; Bazan, G. C., "Effect of Chromophore-Charge Distance on the Energy Transfer Properties of Water-Soluble Conjugated Oligomers." *Journal of the American Chemical Society* **2003,** 125, (22), 6705-6714.

77. Grell, M.; Bradley, D. D. C.; Ungar, G.; Hill, J.; Whitehead, K. S., "Interplay of Physical Structure and Photophysics for a Liquid Crystalline Polyfluorene." *Macromolecules* **1999,** 32, (18), 5810-5817.

78. Ranger, M.; Leclerc, M., "Development of base-dopable polymers." *Synthetic Metals* **1999,** 101, (1-3), 48-51.

79. Ranger, M.; Leclerc, M., "New Base-Doped Polyfluorene Derivatives." *Macromolecules* **1999,** 32, (10), 3306-3313.

80. Gold, S.; Chu, K.-L.; Lu, C.; Shannon, M. A.; Masel, R. I., "Acid loaded porous silicon as a proton exchange membrane for micro-fuel cells." *Journal of Power Sources* **2004,** 135, (1-2), 198-203.

81. Neher, D., "Polyfluorene homopolymers: conjugated liquid-crystalline polymers for bright blue emission and polarized electroluminescence." *Macromolecular Rapid Communications* **2001,** 22, (17), 1365-1385.

82. Teetsov, J.; Fox, M. A., "Photophysical characterization of dilute solutions and ordered thin films of alkyl-substituted polyfluorenes." *Journal of Materials Chemistry* **1999,** 9, (9), 2117-2122.

83. Lieser, G.; Oda, M.; Miteva, T.; Meisel, A.; Nothofer, H.-G.; Scherf, U.; Neher, D., "Ordering, Graphoepitaxial Orientation, and Conformation of a Polyfluorene Derivative of the 'Hairy-Rod' Type on an Oriented Substrate of Polyimide." *Macromolecules* **2000,** 33, (12), 4490-4495.

84. Grell, M.; Bradley, D. D. C.; Inbasekaran, M.; Woo, E. P., "A glass-forming conjugated main-chain liquid crystal polymer for polarized electroluminescence applications." *Advanced Materials (Weinheim, Germany)* **1997,** 9, (10), 798-802.

85. Geng, Y.; Trajkovska, A.; Katsis, D.; Ou, J. J.; Culligan, S. W.; Chen, S. H., "Synthesis, Characterization, and Optical Properties of Monodisperse Chiral Oligofluorenes." *Journal of the American Chemical Society* **2002,** 124, (28), 8337-8347.

86. Fukuda, M.; Sawada, K.; Yoshino, K., "Synthesis of fusible and soluble conducting polyfluorene derivatives and their characteristics." *Journal of Polymer Science, Part A: Polymer Chemistry* **1993,** 31, (10), 2465-71.

87. Theander, M.; Inganaes, O.; Mammo, W.; Olinga, T.; Svensson, M.; Andersson, M. R., "Photophysics of Substituted Polythiophenes." *Journal of Physical Chemistry B* **1999,** 103, (37), 7771-7780.

88. Woo, E. P.; Inbasekaran, M.; Shiang, W. R.; Roof, G. R. "9-Substituted fluorenes and 9-substituted fluorene oligomers and polymers." 9705184, 1997.

89. Kreyenschmidt, M.; Klaerner, G.; Fuhrer, T.; Ashenhurst, J.; Karg, S.; Chen, W. D.; Lee, V. Y.; Scott, J. C.; Miller, R. D., "Thermally Stable Blue-Light-Emitting Copolymers of Poly(alkylfluorene)." *Macromolecules* **1998,** 31, (4), 1099-1103.

90. Wegner, G.; Muellen, K.; Editors, *Electronic Materials: The Oligomer Approach*. Wiley-VCH: New York, 1998; p 550 pp.

91. Lee, S. H.; Tsutsui, T., "Molecular design of fluorene-based polymers and oligomers for organic light-emitting diodes." *Thin Solid Films* **2000,** 363, (1,2), 76-80.

92. Culligan, S. W.; Geng, Y.; Chen, S. H.; Klubek, K.; Vaeth, K. M.; Tang, C. W., "Strongly polarized and efficient blue organic light-emitting diodes using monodisperse

glassy nematic oligo(fluorene)s." *Advanced Materials (Weinheim, Germany)* **2003,** 15, (14), 1176-1180.

93. Leclerc, M., "Polyfluorenes: twenty years of progress." *Journal of Polymer Science, Part A: Polymer Chemistry* **2001,** 39, (17), 2867-2873.

94. Schmitt, C.; Nothofer, H.-G.; Falcou, A.; Scherf, U., "Conjugated polyfluorene/polyaniline block copolymers." *Macromolecular Rapid Communications* **2001,** 22, (8), 624-628.

95. Asawapirom, U.; Guntner, R.; Forster, M.; Farrell, T.; Scherf, U., "Dialkylfluorene-oligothiophene and dialkylfluorene-dithienylvinylene alternating copolymers." *Synthesis* **2002**, (9), 1136-1142.

96. Cheng, Y.-J.; Luh, T.-Y., "Synthesizing optoelectronic heteroaromatic conjugated polymers by cross-coupling reactions." *Journal of Organometallic Chemistry* **2004,** 689, (24), 4137-4148.

97. Kulkarni, A. P.; Zhu, Y.; Jenekhe, S. A., "Quinoxaline-Containing Polyfluorenes: Synthesis, Photophysics, and Stable Blue Electroluminescence." *Macromolecules* **2005,** 38, (5), 1553-1563.

98. Sun, Q.; Zhan, X.; Yang, C.; Liu, Y.; Li, Y.; Zhu, D., "Photo- and electroluminescence properties of fluorene-based copolymers containing electron- or hole-transporting unit." *Thin Solid Films* **2003,** 440, (1,2), 247-254.

99. Liu, B.; Yu, W.-L.; Lai, Y.-H.; Huang, W., "Blue-Light-Emitting Fluorene-Based Polymers with Tunable Electronic Properties." *Chemistry of Materials* **2001,** 13, (6), 1984-1991.

100. Zhou, X.-H.; Zhang, Y.; Xie, Y.-Q.; Cao, Y.; Pei, J., "Effect of Fluorenone Units on the Property of Polyfluorene and Oligofluorene Derivatives: Synthesis, Structure-Properties Relationship, and Electroluminescence." *Macromolecules* **2006,** 39, (11), 3830-3840.

101. Cho, N. S.; Hwang, D.-H.; Lee, J.-I.; Jung, B.-J.; Shim, H.-K., "Synthesis and Color Tuning of New Fluorene-Based Copolymers." *Macromolecules* **2002,** 35, (4), 1224-1228.

102. Galbrecht, F.; Yang, X. H.; Nehls, B. S.; Neher, D.; Farrell, T.; Scherf, U., "Semiconducting polyfluorenes with electrophosphorescent on-chain platinum-salen chromophores." *Chemical Communications (Cambridge, United Kingdom)* **2005**, (18), 2378-2380.

103. Lim, S.-F.; Friend, R. H.; Rees, I. D.; Li, J.; Ma, Y.; Robinson, K.; Holmes, A. B.; Hennebicq, E.; Beljonne, D.; Cacialli, F., "Suppression of green emission in a new class of blue-emitting polyfluorene copolymers with twisted biphenyl moieties." *Advanced Functional Materials* **2005,** 15, (6), 981-988.

104. Vamvounis, G.; Schulz, G. L.; Holdcroft, S., "Enhanced Blue-Violet Emission from Poly(fluorene-co-thiophene) Host-Guest Systems." *Macromolecules* **2004,** 37, (24), 8897-8902.

105. Morin, J.-F.; Leclerc, M., "Syntheses of Conjugated Polymers Derived from N-Alkyl-2,7-carbazoles." *Macromolecules* **2001,** 34, (14), 4680-4682.

106. Charas, A.; Morgado, J.; Alcacer, L.; Brogueira, P.; Cacialli, F., "Synthesis and luminescence properties of a new polyfluorene copolymer with regulated solubility." *Synthetic Metals* **2004,** 147, (1-3), 275-279.

107. Chan, L.-H.; Lee, Y.-D.; Chen, C.-T., "Synthesis and Characterization of 3,4-Diphenylmaleimide Copolymers That Exhibit Orange to Red Photoluminescence and Electroluminescence." *Macromolecules* **2006,** 39, (9), 3262-3269.

108. Lee, S. K.; Hwang, D.-H.; Jung, B.-J.; Cho, N. S.; Lee, J.; Lee, J.-D.; Shim, H.-K., "The fabrication and characterization of single-component polymeric white-light-emitting diodes." *Advanced Functional Materials* **2005,** 15, (10), 1647-1655.

109. Cho, H. N.; Kim, D. Y.; Kim, J. K.; Kim, C. Y., "Control of band gaps of conjugated polymers by copolymerization." *Synthetic Metals* **1997,** 91, (1-3), 293-296.

110. Anuragudom, P.; Newaz, S. S.; Phanichphant, S.; Lee, T. R., "Facile Horner-Emmons Synthesis of Defect-Free Poly(9,9-dialkylfluorenyl-2,7-vinylene)." *Macromolecules* **2006,** 39, (10), 3494-3499.

111. Nomura, K.; Morimoto, H.; Imanishi, Y.; Ramhani, Z.; Geerts, Y., "Synthesis of high molecular weight trans-poly(9,9-di-n-octyl fluorene-2,7-vinylene) by the acyclic diene metathesis polymerization using molybdenum catalysts." *Journal of Polymer Science, Part A: Polymer Chemistry* **2001,** 39, (14), 2463-2470.

112. Pschirer, N. G.; Bunz, U. H. F., "Poly(fluorenylene ethynylene)s by Alkyne Metathesis: Optical Properties and Aggregation Behavior." *Macromolecules* **2000,** 33, (11), 3961-3963.

113. Brizius, G.; Pschirer, N. G.; Steffen, W.; Stitzer, K.; zur Loye, H.-C.; Bunz, U. H. F., "Alkyne Metathesis with Simple Catalyst Systems: Efficient Synthesis of Conjugated Polymers Containing Vinyl Groups in Main or Side Chain." *Journal of the American Chemical Society* **2000,** 122, (50), 12435-12440.

114. Asawapirom, U.; Guentner, R.; Forster, M.; Scherf, U., "Semiconducting block copolymers-synthesis and nanostructure formation." *Thin Solid Films* **2005,** 477, (1-2), 48-52.

115. Marsitzky, D.; Klapper, M.; Muellen, K., "End-Functionalization of Poly(2,7-fluorene): A Key Step toward Novel Luminescent Rod-Coil Block Copolymers." *Macromolecules* **1999,** 32, (25), 8685-8688.

116. Kong, X.; Jenekhe, S. A., "Block copolymers containing conjugated polymer and polypeptide sequences: synthesis and self-assembly of electroactive and photoactive nanostructures." *Macromolecules* **2004,** 37, (22), 8180-8183.

117. Tsolakis, P. K.; Kallitsis, J. K., "Synthesis and characterization of luminescent rod-coil block copolymers by atom transfer radical polymerization: Utilization of novel end-functionalized terfluorenes as macroinitiators." *Chemistry--A European Journal* **2003,** 9, (4), 936-943.

118. Chochos, C. L.; Kallitsis, J. K.; Keivanidis, P. E.; Baluschev, S.; Gregoriou, V. G., "Thermally Stable Blue Emitting Terfluorene Block Copolymers." *Journal of Physical Chemistry B* **2006,** 110, (10), 4657-4662.

119. Chochos, C. L.; Kallitsis, J. K.; Gregoriou, V. G., "Rod-Coil Block Copolymers Incorporating Terfluorene Segments for Stable Blue Light Emission." *Journal of Physical Chemistry B* **2005,** 109, (18), 8755-8760.

120. Chochos, C. L.; Tsolakis, P. K.; Gregoriou, V. G.; Kallitsis, J. K., "Influence of the Coil Block on the Properties of Rod-Coil Diblock Copolymers with Oligofluorene as the Rigid Segment." *Macromolecules* **2004,** 37, (7), 2502-2510.

121. Tirapattur, S.; Belletete, M.; Drolet, N.; Leclerc, M.; Durocher, G., Spectral and "Photophysical Properties of Fluorene-Based Polyesters in Solution and in the Solid State." *Macromolecules* **2002,** 35, (23), 8889-8895.

122. Lu, S.; Liu, T.; Ke, L.; Ma, D.-G.; Chua, S.-J.; Huang, W., "Polyfluorene-Based Light-Emitting Rod-Coil Block Copolymers." *Macromolecules* **2005,** 38, (20), 8494-8502.

123. McQuade, D. T.; Pullen, A. E.; Swager, T. M., "Conjugated Polymer-Based Chemical Sensors." *Chemical Reviews* **2000,** 100, 2537-2574.

124. Roncali, J.; Garreau, R.; Delabouglise, D.; Garnier, F.; Lemaire, M., "Modification of the structure and electrochemical properties of poly(thiophene) by ether groups." *Journal of the Chemical Society, Chemical Communications* **1989**, (11), 679-81.

125. Li, H. S.; Garnier, F.; Roncali, J., "Electroactivity of poly(thiophenes) containing oxyalkyl substituents." *Synthetic Metals* **1991,** 41, (1-2), 547-50.

126. Andre, J. J.; Bernard, M.; Francois, B.; Mathis, C., "Depinning of current carriers in n-type semiconducting polyacetylene." *Journal de Physique, Colloque* **1983**, (C3, Conf. Int. Phys. Chim. Polym. Conduct., 1982), 199-202.

127. Kolusheva, S.; Kafri, R.; Katz, M.; Jelinek, R., "Rapid Colorimetric Detection of Antibody-Epitope Recognition at a Biomimetic Membrane Interface." *Journal of the American Chemical Society* **2001,** 123, (3), 417-422.

128. Zhang, M.; Lu, P.; Ma, Y.; Shen, J., "Metal Ionochromic Effects of Conjugated Polymers: Effects of the Rigidity of Molecular Recognition Sites on Metal Ion Sensing." *Journal of Physical Chemistry B* **2003,** 107, (27), 6535-6538.

129. Zhou, X.-H.; Yan, J.-C.; Pei, J., "Exploiting an Imidazole-Functionalized Polyfluorene Derivative as a Chemosensory Material." *Macromolecules* **2004,** 37, (19), 7078-7080.

130. Zhou, G.; Qian, G.; Ma, L.; Cheng, Y.; Xie, Z.; Wang, L.; Jing, X.; Wang, F., "Polyfluorenes with Phosphonate Groups in the Side Chains as Chemosensors and Electroluminescent Materials." *Macromolecules* **2005,** 38, (13), 5416-5424.

131. Liu, B.; Bazan, G. C., "Interpolyelectrolyte complexes of conjugated copolymers and DNA: Platforms for multicolor biosensors." *Journal of the American Chemical Society* **2004,** 126, (7), 1942-1943.

132. Wang, Y.; Watson, M. D., "Transition-Metal-Free Synthesis of Alternating Thiophene-Perfluoroarene Copolymers." *Journal of the American Chemical Society* **2006,** 128, (8), 2536-2537.

133. Shi, L.; Chapman, T. M.; Beckman, E. J., "Poly(ethylene glycol)-block-poly(N-vinylformamide) Copolymers Synthesized by the RAFT Methodology." *Macromolecules* **2003,** 36, (7), 2563-2567.

134. Thomann, R.; Sernetz, F. G.; Heinemann, J.; Steinmann, S.; Muelhaupt, R.; Kressler, J., "Synthesis and Crystallization of Syndiotactic Random Copolymers of Styrene and p-n-Butylstyrene and of Syndiotactic Poly(p-n-butylstyrene)." *Macromolecules* **1997,** 30, (26), 8401-8409.

135. Radano, C. P.; Scherman, O. A.; Stingelin-Stutzmann, N.; Mueller, C.; Breiby, D. W.; Smith, P.; Janssen, R. A. J.; Meijer, E. W., "Crystalline-Crystalline Block Copolymers of Regioregular Poly(3-hexylthiophene) and Polyethylene by Ring-Opening Metathesis Polymerization." *Journal of the American Chemical Society* **2005,** 127, (36), 12502-12503.

136. Miyaura, N.; Suzuki, A., "Palladium-Catalyzed Cross-Coupling Reactions of Organoboron Compounds." *Chemical Reviews (Washington, D. C.)* **1995,** 95, (7), 2457-83.

137. Peifer, B.; Milius, W.; Alt, H. G., "Self-immobilized metallocene catalysts." *Journal of Organometallic Chemistry* **1998,** 553, (1-2), 205-220.

138. Wagener, K. B.; Patton, J. T., "Acyclic Diene Metathesis (Admet) Polymerization - Synthesis of Unsaturated Polycarbonates." *Macromolecules* **1993,** 26, (2), 249-253.

139. Wagener, K. B.; Valenti, D.; Hahn, S. F., "ADMET modeling of branching in polyethylene. The effect of a perfectly-spaced methyl group." *Macromolecules* **1997,** 30, (21), 6688-6690.

140. Lehman, S. E., Jr.; Wagener, K. B., "Comparison of the Kinetics of Acyclic Diene Metathesis Promoted by Grubbs Ruthenium Olefin Metathesis Catalysts." *Macromolecules* **2002,** 35, (1), 48-53.

141. Petkovska, V. I.; Hopkins, T. E.; Powell, D. H.; Wagener, K. B., "MALDI-TOF Detection of Olefin Structural Isomerization in Metathesis Chemistry." *Macromolecules* **2005,** 38, 5878-5885.

142. Schwendeman, J. E.; Church, A. C.; Wagener, K. B., "Synthesis and Catalyst Issues Associated with ADMET." *Adv. Synth. Catal.* **2002,** 344, 597-613.

143. Watson, M. D.; Wagener, K. B., "Tandem Homogeneous Metathesis/Heterogeneous Hydrogenation: Preparing Model Ethylene/CO2 and Ethylene/CO Copolymers." *Macromolecules* **2000,** 33, (9), 3196-3201.

144. Chung, T. C., "Synthesis of Polyalcohols via Ziegler-Natta Polymerization." *Macromolecules* **1988,** 21, 865-869.

145. Thiem, H.; Jandke, M.; Hanft, D.; Strohriegl, P., "Synthesis and Orientation of Fluorene Containing Reactive Mesogens." *Macromol. Chem. Phys.* **2006,** 207, 370-381.

146. Krysan, D. J.; Mackenzie, P. B., "A new, convenient preparation of bis(1,5-cyclooctadiene)nickel(0)." *Journal of Organic Chemistry* **1990,** 55, (13), 4229-30.

147. Kappaun, S.; Zelzer, M.; Bartl, K.; Saf, R.; Stelzer, F.; Slugovc, C., "Preparation of poly(fluorene)s using trans-bis(dicyclohexylamine)palladium diacetate as a catalyst: scope and limitations." *Journal of Polymer Science, Part A: Polymer Chemistry* **2006,** 44, (6), 2130-2138.

148. Navarro, O.; Kaur, H.; Mahjoor, P.; Nolan, S. P., "Cross-coupling and dehalogenation reactions catalyzed by (N-heterocyclic carbene)Pd(allyl)Cl complexes." *Journal of Organic Chemistry* **2004,** 69, (9), 3173-3180.

149. Alonso, F.; Beletskaya, I. P.; Yus, M., "Metal-Mediated Reductive Hydrodehalogenation of Organic Halides." *Chemical Reviews (Washington, DC, United States)* **2002,** 102, (11), 4009-4091.

150. Okumoto, K.; Shirota, Y., "New class of hole-blocking amorphous molecular materials and their application in blue-violet-emitting fluorescent and green-emitting phosphorescent organic electroluminescent devices." *Chemistry of Materials* **2003,** 15, (3), 699-707.

151. Price, D. W.; Tour, J. M., "Biphenyl- and fluorenyl-based potential molecular electronic devices." *Tetrahedron* **2003,** 59, (17), 3131-3156.

152. Thiem, H.; Jandke, M.; Hanft, D.; Strohriegl, P., "Synthesis and orientation of fluorene containing reactive mesogens." *Macromolecular Chemistry and Physics* **2006,** 207, (4), 370-381.

153. Wang, S.; Hong, J. W.; Bazan, G. C., "Synthesis of Cationic Water-Soluble Light-Harvesting Dendrimers." *Organic Letters* **2005,** 7, (10), 1907-1910.

154. Sims, M.; Bradley, D. D. C.; Ariu, M.; Koeberg, M.; Asimakis, A.; Grell, M.; Lidzey, D. G., "Understanding the origin of the 535 nm emission band in oxidized poly(9,9-dioctylfluorene): The essential role of inter-chain/inter-segment interactions." *Advanced Functional Materials* **2004,** 14, (8), 765-781.

155. Gong, X.; Iyer, P. K.; Moses, D.; Bazan, G. C.; Heeger, A. J.; Xiao, S. S., "Stabilized blue emission from polyfluorene-based light-emitting diodes: Elimination of fluorenone defects." *Advanced Functional Materials* **2003,** 13, (4), 325-330.

156. Tada, K.; Onoda, M., "Photooxidation study of polymer light-emitting devices." *Thin Solid Films* **2001,** 393, (1,2), 358-361.

157. Papadimitrakopoulos, F.; Konstadinidis, K.; Miller, T. M.; Opila, R.; Chandross, E. A.; Galvin, M. E., "The Role of Carbonyl Groups in the Photoluminescence of Poly(p-phenylenevinylene)." *Chemistry of Materials* **1994,** 6, (9), 1563-8.

158. Jenekhe, S. A.; Osaheni, J. A., "Excimers and exciplexes of conjugated polymers." *Science (Washington, DC, United States)* **1994,** 265, (5173), 765-8.

159. List, E. J. W.; Guentner, R.; Scanducci de Freitas, P.; Scherf, U., "The effect of keto defect sites on the emission properties of polyfluorene-type materials." *Advanced Materials (Weinheim, Germany)* **2002,** 14, (5), 374-378.

160. Liu, L.; Tang, S.; Liu, M.; Xie, Z.; Zhang, W.; Lu, P.; Hanif, M.; Ma, Y., "Photodegradation of Polyfluorene and Fluorene Oligomers with Alkyl and Aromatic Disubstitutions." *Journal of Physical Chemistry B* **2006,** 110, (28), 13734-13740.

161. Craig, M. R.; de Kok, M. M.; Hofstraat, J. W.; Schenning, A. P. H. J.; Meijer, E. W., "Improving color purity and stability in a blue emitting polyfluorene by monomer purification." *Journal of Materials Chemistry* **2003,** 13, (12), 2861-2862.

162. Bliznyuk, V. N.; Carter, S. A.; Scott, J. C.; Klaerner, G.; Miller, R. D.; Miller, D. C., "Electrical and Photoinduced Degradation of Polyfluorene Based Films and Light-Emitting Devices." *Macromolecules* **1999,** 32, (2), 361-369.

163. Yang, X. H.; Jaiser, F.; Neher, D.; Lawson, P. V.; Bredas, J.-L.; Zojer, E.; Guentner, R.; Scanduicci de Freitas, P.; Forster, M.; Scherf, U., "Suppression of the keto-emission in polyfluorene light-emitting diodes: Experiments and models." *Advanced Functional Materials* **2004,** 14, (11), 1097-1104.

164. Kulkarni, A. P.; Kong, X.; Jenekhe, S. A., "Fluorenone-Containing Polyfluorenes and Oligofluorenes: Photophysics, Origin of the Green Emission and Efficient Green Electroluminescence." *Journal of Physical Chemistry B* **2004,** 108, (25), 8689-8701.

165. Gong, X.; Moses, D.; Heeger, A. J.; Xiao, S., "White Light Electrophosphorescence from Polyfluorene-Based Light-Emitting Diodes: Utilization of Fluorenone Defects." *Journal of Physical Chemistry B* **2004,** 108, (25), 8601-8605.

166. Dias, F. B.; Maiti, M.; Hintschich, S. I.; Monkman, A. P., "Intramolecular fluorescence quenching in luminescent copolymers containing fluorenone and fluorene units: A direct measurement of intrachain exciton hopping rate." *Journal of Chemical Physics* **2005,** 122, (5), 054904/1-054904/11.

167. Chi, C.; Im, C.; Enkelmann, V.; Ziegler, A.; Lieser, G.; Wegner, G., "Monodisperse oligofluorenes with keto defect as models to investigate the origin of green emission from

polyfluorenes: Synthesis, self-assembly, and photophysical properties." *Chemistry--A European Journal* **2005,** 11, (23), 6833-6845.

168. Becker, K.; Lupton, J. M.; Feldmann, J.; Nehls, B. S.; Galbrecht, F.; Gao, D.; Scherf, U., "On-chain fluorenone defect emission from single polyfluorene molecules in the absence of intermolecular interactions." *Advanced Functional Materials* **2006,** 16, (3), 364-370.

169. Hintschich, S. I.; Rothe, C.; Sinha, S.; Monkman, A. P.; Scandiucci de Freitas, P.; Scherf, U., "Population and decay of keto states in conjugated polymers." *Journal of Chemical Physics* **2003,** 119, (22), 12017-12022.

170. Romaner, L.; Pogantsch, A.; Scandiucci de Freitas, P.; Scherf, U.; Gaal, M.; Zojer, E.; List, E. J. W., "The origin of green emission in polyfluorene-based conjugated polymers: On-chain defect fluorescence." *Advanced Functional Materials* **2003,** 13, (8), 597-601.

171. Lupton, J. M.; Craig, M. R.; Meijer, E. W., "On-chain defect emission in electroluminescent polyfluorenes." *Applied Physics Letters* **2002,** 80, (24), 4489-4491.

172. Sainova, D.; Neher, D.; Dobruchowska, E.; Luszczynska, B.; Glowacki, I.; Ulanski, J.; Nothofer, H.-G.; Scherf, U., "Thermoluminescence and electroluminescence of annealed polyfluorene layers." *Chemical Physics Letters* **2003,** 371, (1,2), 15-22.

173. Gaal, M.; List, E. J. W.; Scherf, U., "Excimers or Emissive On-Chain Defects?" *Macromolecules* **2003,** 36, (11), 4236-4237.

174. Prieto, I.; Teetsov, J.; Fox, M. A.; Vanden Bout, D. A.; Bard, A. J., "A Study of Excimer Emission in Solutions of Poly(9,9-dioctylfluorene) Using Electrogenerated Chemiluminescence." *Journal of Physical Chemistry A* **2001,** 105, (3), 520-523.

175. Ritchie, J.; Crayston, J. A.; Markham, J. P. J.; Samuel, I. D. W., "Effect of meta-linkages on the photoluminescence and electroluminescence properties of light-emitting

polyfluorene alternating copolymers." *Journal of Materials Chemistry* **2006,** 16, (17), 1651-1656.

176. Jo, J.; Chi, C.; Hoeger, S.; Wegner, G.; Yoon, D. Y., "Synthesis and characterization of monodisperse oligofluorenes." *Chemistry--A European Journal* **2004,** 10, (11), 2681-2688.

177. Chochos, C. L.; Papakonstandopoulou, D.; Economopolous, S. P.; Gregoriou, V. G.; Kallitsis, J. K., "Synthesis and optical properties on a series of polyethers incorporating terfluorene segments and methylene spacers." *Journal of Macromolecular Science, Part A: Pure and Applied Chemistry* **2006,** 43, (3), 419-431.

178. Grubbs, R. H.; Miller, S.J.; Fu, G.C., "Ring-Closing Metathesis and Related Processes in Organic Synthesis." *Acc. Chem. Res.* **1995,** 28, 446-452.

179. Wang, W.-D.; Espenson, J. H., "Metathesis Reactions of Tris(adamantylimido)methylrhenium and Aldehydes and Imines." *Organometallics* **1999,** 18, (24), 5170-5175.

180. Burland, M. C.; Pontz, T.W.; Meyer, T.Y., "Role of Trace Amine in the Metathesis of Imines by $CpTa(=NR)Cl_2$." *Organometallics* **2002,** 21, 1933-1941.

181. Bruno, J. W.; Xiu, J.L., "Use of Niobium(III) and Niobium(V) Compounds in Catalytic Imine Metathesis under Mild Conditions." *Organometallics* **2000,** 19, 4672-4674.

182. Wang, W.-D.; Espenson, J.H., "Metathesis Reactions of Tris(adamantylimido)methylrhenium and Aldehydes and Imines." *Organometallics* **1999,** 18, (24), 5170-5175.

183. Wang, W.-D.; Espenson, J.H., "Pairwise Exchanges of Oxo and Imido Groups in Rhenium(VII) Compounds." *Inorg. Chem.* **2002,** 41, (7), 1782-1787.

184. Meyer, K. E.; Walsh, P. J.; Bergman, R. G., "Zirconium-Mediated Imine Metathesis. Synthesis of 2,4-Diaza-1-zirconiacyclobutanes and the Mechanism of Their Reactions with Imines and Alkynes." *Journal of the American Chemical Society* **1994,** 116, (6), 2669-70.

185. Krska, S. W.; Zuckerman, R.L.; Bergman, R.G., "Use of Steric Hindrance and a Metallacyclobutene Resting State to Develop Robust and Kinetically Characterizable Zirconium-Based Imine Metathesis Catalysts." *J. Am. Chem. Soc.* **1998,** 120, 11828-11829.

186. McInnes, J. M.; Blake, A.J.; Mountford, P., "Reactions of Titanium Imido Complexes with α-Diimines: Complexation versus Ti=N/C=N Bond Metathesis." *J. Chem. Soc., Dalton Trans.* **1998**, 3623-3628.

187. McInnes, J. M.; Mountford, P., "Transition Metal Imide/Organic Imine Metathesis Reactions: Unexpected Observations." *Chem. Commun.* **1998**, 1669-1670.

188. Mountford, P., "New Titanium Imido Chemistry." *Chem. Commun.* **1997**, 2127-2134.

189. Cantrell, G. K.; Meyer, T.Y., "Catalytic C=N Bond Formation by Metal-Imide Mediated Imine Metathesis." *J. Am. Chem. Soc.* **1998,** 120, 8035-8042.

190. Cantrell, G. K.; Meyer, T.Y., "Transition-Metal-Catalyzed Imine Metathesis." *Organometallics* **1997,** 16, (25), 5381-5383.

191. Andes, C.; Harkins, S.B.; Murtuza, S.; Oyler, K.; Sen, A., "New Tantalum-based Catalyst System for the Selective Trimerization of Ethene to 1-Hexene." *J. Am. Chem. Soc.* **2001,** 123, 7423-7424.

192. Bielawski, C. W.; Benitez, D.; Grubbs, R.H., "An 'Endless' Route to Cyclic Polymers." *Science* **2002,** 297, 2041-2044.

193. Unpublished Results. Badawood, O.; Meyer., T.Y.

194. Cantrell, G. K.; Geib, S.J.; Meyer, T.Y., "Ring-Opening of a Cyclic Imine: The First Step of Imine ROMP." *Organometallics* **1999,** 18, 4250-4252.

195. Brumaghim, J. L.; Girolami, G.S., "Ring-Opening Metathesis Polymerization of Norbornene by $Cp^*_2Os_2Br_4$ and Related Compounds." *Organometallics* **1999,** 18, 1923-1929.

196. Arnauld, T.; Barrett, A.G.M.; Cramp, S.M.; Roberts, R.S.; Zecri, F.J., "ROMPGEL Scavengers: A High-Loading Supported Anhydride for Sequestering Amines and Hydrazines." *Org. Lett.* **2000,** 2, (17), 2663-2666.

197. Trnka, T. M.; Grubbs, R.H., "The Development of $L_2X_2Ru=CHR$ Olefin Metathesis Catalysts: An Organometallic Success Story." *Acc. Chem. Res.* **2001,** 34, 18-29.

198. Esteruelas, M. A.; Werner, H., "Five- and Six-Coordinate Hydrido(Carbonyl)-Ruthenium(II) and -Osmium(II) Complexes Containging Triisopropylphosphine as Ligand." *J. Organomet. Chem.* **1986,** 303, 221-231.

199. Yi, C. S.; He, Z.; Lee, D.W., "Hydrovinylation of Alkenes Catalyzed by the Ruthenium-Hydride Complex Formed in Situ from $(PCy_3)_2(CO)RuHCl$ and $HBF4{\cdot}OEt_2$." *Organometallics* **2001,** 20, 802-804.

200. Arcadi, A. M., F.; Bernocchi, E.; Cacchi, S.; Ortar, G., "Palladium-Catalyzed Preparation of *exo*-Aryl Derivatives of the Norbornane Skeleton." *J. Organomet. Chem.* **1989,** 368, 249-256.